INSTRUMENTED IMPACT TESTING

STP 563

AMERICAN SOCIETY FOR TESTING AND MATERIALS

INSTRUMENTED IMPACT TESTING

A symposium
presented at the
Seventy-sixth Annual Meeting
AMERICAN SOCIETY FOR
TESTING AND MATERIALS
Philadelphia, Pa., 24-29 June 1973

ASTM SPECIAL TECHNICAL PUBLICATION 563
T. S. DeSisto, symposium chairman

List Price $21.75
04-563000-23

AMERICAN SOCIETY FOR TESTING AND MATERIALS
1916 Race Street, Philadelphia, Pa. 19103

Library of Congress Catalog Card Number: 74-81158

NOTE

The Society is not responsible, as a body,
for the statements and opinions
advanced in this publication.

Printed in Tallahassee, Fla.
October 1974

Foreword

The symposium on Instrumented Impact Testing was presented at the Seventy-sixth Annual Meeting of the American Society for Testing and Materials held in Philadelphia, Pa. 24-29 June 1973. Committee E-28 on Mechanical Testing sponsored the symposium. T. S. DeSisto, Army Materials and Research Center, presided as symposium chairman.

Related
ASTM Publications

Impact Testing of Metals, STP 466 (1970), $21.25
(04-466000-23)

Contents

Introduction

Mechanical and design engineers, metallurgists, and aeronautical engineers have become increasingly interested in instrumented impact testing. This volume presents eleven papers covering procedures, testing techniques, analysis, and interpretation of force and time curves, as well as inertial load effects, and analysis and interpretation of data from instrumented impact tests.

This state-of-the-art volume makes available information from many of the leading laboratories, of the more than forty that currently use instrumented impact testing. This relatively new method is applicable not only to metals, but also to such other materials as composites and cemented carbides. It is expected that there will be far reaching implications as a result of future experimental work.

T. S. DeSisto

Army Materials and Research Center,
Watertown, Mass. 02172; symposium chairman.

D. R. Ireland[1]

Procedures and Problems Associated with Reliable Control of the Instrumented Impact Test

REFERENCE: Ireland, D. R., "Procedures and Problems Associated with Reliable Control of the Instrumented Impact Test," *Instrumented Impact Testing, ASTM STP 563,* American Society for Testing and Materials, 1974, pp. 3-29.

ABSTRACT: The inherent characteristics of the instrumented impact test are discussed. The hammer energy is reduced by deforming the test specimen, accelerating the specimen from rest, Brinell-type deformation at the load points, vibrations of the hammer assembly, and elastic deformation within the machine. The limitations of the electronic components can affect the test results. The superimposed oscillations on the apparent load-time signal derived from the instrumented tup are best controlled by varying the initial impact velocity. Dynamic load cells must be calibrated by dynamic loading and then be checked by comparisons of dynamic and static test results for a strain-rate insensitive material. The analysis of instrumented tup signals for determination of various energy, deflection, and load values must be done with a clear understanding of dissolution of hammer energy, electronic limitations, and superimposed oscillations.

KEY WORDS: impact tests, dynamic tests, instrumented impact, tests, procedures, problems, evaluation

The instrumented impact test is rapidly being accepted as a useful tool for evaluating the dynamic response of a wide range of materials. In the United States there were less than five laboratories actively using the instrumented impact test in 1970; in 1972 the number of laboratories was approximately 25; in 1973 the number was greater than 50. There is a definite requirement for standard procedures for instrumented impact testing, and several facilities have already initiated specialized test procedures [*1*].[2] Unfortunately, dynamic mechanical property data which have been derived from instrumented impact tests are beginning to appear in the open literature without reference to the experimental details [*2*].

It is vitally important that some general guidelines be employed for reliable use of the instrumented impact test. The discussion in this paper is intended to stimulate action for development of reliable procedures. The three most impor-

[1] Assistant director, Materials Engineering, Effects Technology, Inc., Santa Barbara, Calif. 93105.

[2] The italic numbers in brackets refer to the list of references appended to this paper.

tant factors for reliable instrumented impact testing are calibration of the dynamic load cell, control of the instrumented tup signal, and reduction of data. Each of these is briefly discussed. Also included as background information are discussions of some of the inherent characteristics of instrumented impact testing, which include dissolution of hammer energy, oscillations of the instrumented tup signal, and electronic frequency response.

Instrumentation Components

Instrumented impact testing involves a variety of different impact machines and test specimen designs; however, the basic instrumentation is essentially the same for each type of test. That is, each requires an impact machine, a load sensor, and a signal display component. The impact machines include both pendulum and drop tower types. The particular machine employed usually depends on what is most readily available and is not necessarily the optimum choice for dynamic testing. The general features of a typical instrumented impact system are illustrated in Fig. 1.

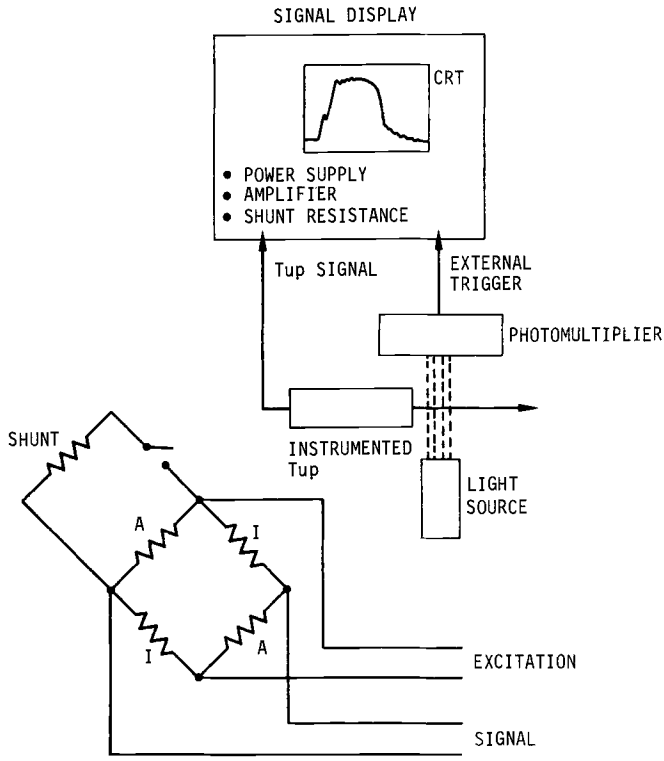

FIG. 1—*Schematic illustration of major components for instrumented impact testing and the circuit for an instrumented tup.*

The most commonly used load sensor is that obtained by cementing strain gages to the striker or specimen supports of the impact machine. These gages are positioned to sense the compressive force interaction between the impact machine and the test specimen. The gages are connected to form a Wheatstone bridge circuit as shown in Fig. 1. The strain-gaged striker is identified as the instrumented tup. Semiconductor strain gages provide the largest dynamic load measuring range for this type of load cell. To operate successfully as a load sensor, the instrumented tup requires a precision power supply which has a noise contribution to the output signal of the tup gages of less than 0.5 percent of full-scale output.

The most commonly used signal display component for instrumented impact testing is an oscilloscope system. The oscilloscope provides better signal resolution with respect to time than do any of the currently available fast writing strip charts or x, y recorders. It is convenient to have storage capability for the cathode ray tube (CRT) and thereby reduce photographic costs and ensure a permanent record of the instrumented tup signal.

Other components sometimes employed for signal display are high-speed tape recorders, transient signal recorders, and computers [*3,4*]. However, each of these usually involves intermediate use of a CRT-type device for final display of the signal.

The signal display component requires a command signal (external trigger) for coordination of the CRT sweep and the time when the tup makes initial contact with the specimen. Internal triggering of the sweep from the initial portion of the instrumented tup signal is not recommended when the zero load base line is not clearly defined. It is also convenient to have this external trigger signal constructed so that mechanical adjustments can be made for variations in specimen size or hammer velocity or both. A commonly employed technique for generation of the external trigger signal is one that employs a photoelectric device. This technique uses a high-intensity light source directed at a photomultiplier so that the hammer (instrumented tup assembly) intercepts the light beam just prior to making contact with the specimen (see Fig. 1) and thereby generates a signal for triggering of the recording system.

The signals generated by the instrumented tup usually require amplification before they can be displayed by the CRT. Included in the oscilloscope system is a module for signal amplification. This module should also include a means for precise balancing of the strain-gage circuit and control of signal amplification. The specific gain or amplification can be monitored by noting the signal produced when a known resistance is shunted across the strain-gage circuit (see Fig. 1).

Background

To implement reliable test procedures, one should have a general understanding of some of the inherent characteristics of instrumented impact testing. These characteristics include the dissolution of hammer energy, oscillations of the

instrumented tup signal, and electronic frequency response. Each of these is briefly discussed in the following.

Energy

The maximum energy E_o obtainable by the hammer or instrumented tup assembly (before impact with the specimen) can be found from

$$E_o = \frac{1}{2} I v_o^2 \tag{1}$$

where v_o is the hammer velocity immediately prior to impact and I is the moment of inertia of the assembly given by

$$I = \frac{\rho_w}{g} \tag{2}$$

where ρ_w is the effective hammer weight and g is the acceleration due to gravity. For drop tower testing, ρ_w is equivalent to the total weight of the hammer-tup assembly and $E_o = \rho_w h$. For pendulum impact testing [5]

$$\rho_w \simeq W_h + \frac{1}{3} W_b \tag{3}$$

where W_h is the hammer weight and W_b is the beam weight. However, ASTM Notched Bar Impact Testing of Metallic Materials (E 23-72) [6] describes a procedure for measuring ρ_w where the difference between this value and that obtained from Eq 3 is less than 2 percent [5]. If the hammer can be regarded as a free-falling object,

$$v_o = \sqrt{2gh_o} \tag{4}$$

where h_o is the drop height. Pendulum impact machines meeting the calibration requirements of ASTM Methods E 23 [6] have measured velocities within 2 percent of that calculated by Eq 4.

When the tup makes contact with a test specimen, the hammer energy is reduced by an amount ΔE_o and

$$\Delta E_o = E_I + E_{SD} + E_B + E_{MV} + E_{ME} \tag{5}$$

where

E_I = increment of energy required to accelerate the specimen from rest to the velocity of the hammer,

E_{SD} = total energy consumed by bending the specimen,

E_B = energy consumed by Brinell-type deformation at the specimen load points,

E_{MV} = energy absorbed by the impact machine through vibrations after initial contact with the specimen, and

E_{ME} = stored elastic energy absorbed by the machine as a result of the interactions at the specimen load points.

The reduction in hammer energy can be represented by the change in kinetic energy such that

$$\Delta E_o = E_o - E_f \tag{6}$$

where E_f is the kinetic energy at time τ after initial contact between specimen and tup. As for E_o in Eq 1, E_f can be represented in terms of the hammer velocity at time τ, and Eq 6 reduces to

$$\Delta E_o = \frac{1}{2} I (v_o^2 - v_f^2) \tag{7}$$

Starting from the basic relationship of force equals the product of mass and acceleration, it can be shown that the area under the force-time curve can be represented as

$$\int_o^\tau P dt = I (v_o - v_f) \tag{8}$$

where P is the force, t is time, and τ is the time elapsed after initial contact between specimen and tup. Equation 8 is simply a statement of the equivalence between impulse and change in momentum. Equations 7 and 8 can be combined to yield

$$\Delta E_o = E_a \left(1 - \frac{E_a}{4E_o} \right) \tag{9}$$

where, by definition,

$$E_a = v_o \int_o^\tau P dt \tag{10}$$

The relationship shown as Eq 9 has been attributed to Augland [7]; however, the first published derivation of this relationship was by Grumbach et al [8]. Equation 9 can be shown to be equivalent to [9]

$$\Delta E_o = \bar{v} \int_o^\tau P dt \tag{11}$$

where, by definition,

$$\bar{v} = \frac{1}{2} (v_o + v_f)$$

Frequency Response

When either performing instrumented impact tests or utilizing the results of such tests, it is vitally important to have a clear understanding of the effects of limited frequency response. All known instrumentation for instrumented impact testing has limited frequency response. Unfortunately, nearly all published discussions of this test technique, including all those in *Impact Testing of Metals* [*10*], *ASTM STP 466*, avoid discussion of the inherent electronic limitations.

The limited frequency response of a component is not usually the published frequency response value. The idealized and actual frequency responses of an arbitrary electronic or mechanical component are illustrated in Fig. 2. For the idealized case, f_R represents the highest frequency for which signals can be passed through the component without being totally attenuated. In the actual case, f_R is the frequency commonly specified by most manufacturers and electronic technicians and corresponds to that for a specific attenuation of the signal amplitude from A to A_R. The most commonly used value is the 3-dB attenuation frequency.

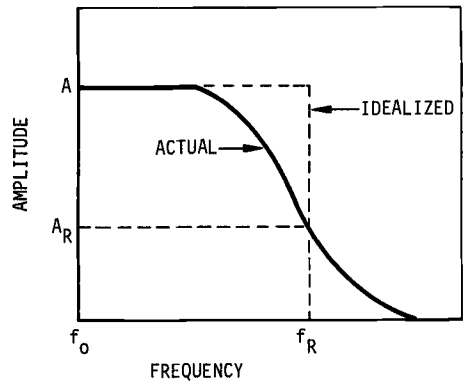

FIG. 2–*Schematic illustration of idealized and actual frequency response curves for mechanical and electrical components.*

The dB represents decibel or one tenth of the bel and is defined by

$$\text{dB} = 20 \log_{10}\left(\frac{\text{volts}_{in}}{\text{volts}_{out}}\right) \tag{12}$$

The 3-dB attenuation corresponds to the frequency for which

$$\text{volts}_{out} \simeq 0.7\ \text{volts}_{in}$$

or approximately a 30 percent reduction in the amplitude of the signal.

For most instrumented impact tests, assurance of a 10 percent or less amplitude reduction is sufficient. From the foregoing relationships this would correspond to the 0.915-dB attenuation. That is, the desired signal should be of a frequency less than or equal to that for which the electronic system has the 0.915-dB attenuation.

It is often easier to represent an electronic component in terms of rise time rather than frequency response. Rise time can be defined as the time required for a signal to increase from 10 to 90 percent of the full amplitude. The relationship between signal frequency f and rise time t_r for a sine wave is as follows

$$t_r \simeq \frac{0.35}{f} \tag{13}$$

For other wave forms, the constant 0.35 may vary between 0.34 and 0.39. The general form of the load signal obtained from an instrumented Charpy test is similar to a sine wave.

All components have a limiting response time. It is suggested that for instrumented impact test systems the 0.9-dB frequency response be determined for the total instrumentation system, and the corresponding rise time (Eq 13) be identified as T_R and used to set limits for dynamic signal analysis. Again, it should be noted that many electronic devices are specified in terms of the 3-dB attenuation, and published response times are usually those determined by Eq 13 for the frequency at a 3-dB attenuation.

The effects of impact velocity on the load-time record for a hypothetical material and the corresponding effects of rise time are illustrated in Fig. 3. In this example, the machine is assumed to be very stiff ($C_M \ll C_s$) and have sufficient kinetic energy with respect to that absorbed by the specimen, so that deflections d can be represented by

$$d = v \cdot t \tag{14}$$

where v is the impact velocity and t is time. The increase of impact velocity from v_a to v_c to v_u reduced the time to reach maximum load P_a with the results

$$v_u t_u = v_c t_c = v_a t_a$$

The test at velocity v_a is sufficiently long so that the signal is not distorted. The test at velocity v_u results in a large distortion of the signal by the limited frequency response. In addition to the signal amplitude being reduced, there is an increase in the apparent time to reach maximum load. However, it is not uncommon to find the impulse ($\int P \delta t$) for a signal distorted by frequency response to be equal to that for the undistorted signal.

The test at velocity v_c results in a load-time signal for which the apparent maximum load P_c is known to be within 10 percent of the actual value P_a. The

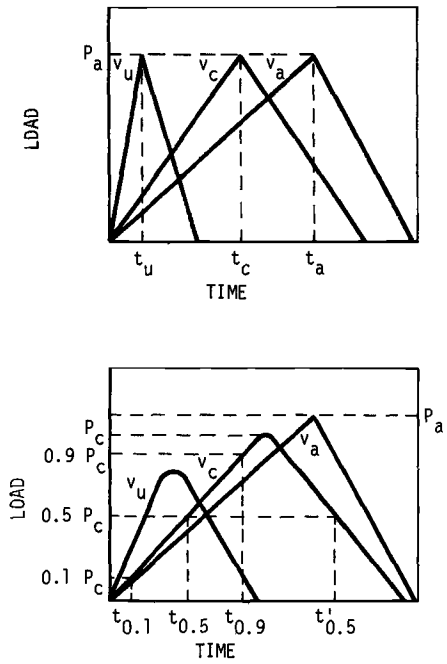

FIG. 3—*Schematic illustrations of the effects of impact velocity on specimen load-time behavior (*top*) and the effects of limited frequency response on the recorded load-time behavior (*bottom*).*

necessary condition for $P_c \simeq 0.9\ P_a$ has been determined by Fourier analysis of pulse shapes, and signal recording limitations, to be a pulse width (t_w) at half maximum load equal to or greater than twice the rise time [*11*];

$$t_w \equiv t'_{0.5} - t_{0.5}$$

$$t_w > 2t_r$$

This pulse width is characteristic of a system whose rise time is given by the following

$$t_r \equiv t_{0.9} - t_{0.1} \tag{15}$$

$$t_r \sim 0.35/f_{0.9\ \mathrm{dB}} \tag{16}$$

Care should be taken not to cut corners when determining the rise time of a specific signal. An example of a typical tup signal for a 4.5 ft/s (1.37 m/s) Charpy impact test of aluminum is shown in Fig. 4. The rise time for the first oscillation is determined by the relationship

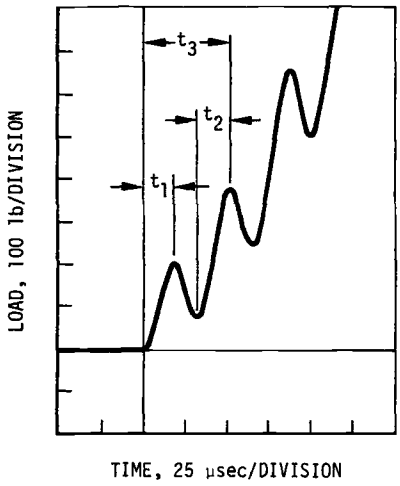

FIG. 4—*Typical instrumented tup signal for 4.5 ft/s impact test of aluminum Charpy specimens.* $T_R = 10$ *μs.*

$$t_r = t_{0.9} - t_{0.1} \tag{17}$$

where $t_{0.9}$ and $t_{0.1}$ are the time values defined by the fractions of the amplitude of the signal as shown in Fig. 3. If this signal had a distinct sawtooth shape,

$$t_r = 0.8t_1 \tag{18}$$

Most instrumented impact test records will have rounded peaks like that shown in Fig. 4, and the t_r value must be determined by the difference between $t_{0.9}$ and $t_{0.1}$. For the first oscillation in Fig. 4,

$$0.8t_1 > t_{0.9} - t_{0.1}$$

The rise time for the second oscillation of the signal shown in Fig. 4 is determined over the approximate time t_2 and not t_3 by the same procedure as used for the first oscillation.

Oscillations

The most commonly employed technique for determination of the load-time response of a specimen during impact loading is one which utilizes strain gages attached to the tup or striker portion of the impact hammer. The signal generated by the strain gages represents a complex combination of the following components:

1. The true mechanical response of the specimen.

2. Inertial loading of the tup as a result of acceleration of the specimen [*12-14*] from rest.

3. Low-frequency fluctuations caused by stored elastic energy [*13,15*] and reflected stress waves.

4. High-frequency noise in the K hertz range caused primarily by the amplification system [*3,16*].

The latter is usually minimized through use of high-gain strain gages (for example, semiconductor) to achieve a relatively large signal-to-noise ratio. In some instances, electronic filtering is employed to surpress the noise. Subsequent discussion in this paper assumes that the signal-to-noise ratio is sufficiently large to consider the signal generated by the strain gages on the tup to be composed of only the first three components. The first component is the obvious goal of the signal analysis; however, the second and third components can often overshadow the true mechanical response of the specimen.

The inertial loading on the tup can be viewed as the force caused by rigid-body acceleration of the specimen from a rest position to a velocity near that of the impacting hammer-tup assembly. This component dominates the initial 20 to 30 μs portion of the tup signal and is represented by the first load fluctuation (oscillation) of the load-time profile. The magnitude of this inertial oscillation is related to the acoustic impedances of the tup and specimen and the initial impact velocity. The inertial load is maximum at the moment of impact and rapidly decreases as the velocity of the specimen is increased. Because electronic components have limited frequency response, actual recordings of this inertia loading event have an appearance like that shown in Fig. 5. Recent work by Saxton et al [*12*] has yielded a rational understanding of the inertial oscillation and a model for predicting the apparent magnitude (P_I) of the oscillation. Their work has shown

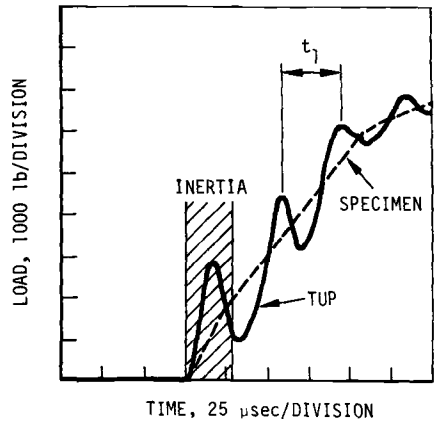

FIG. 5–*Comparison of typical oscillating tup signal to the expected specimen load-time behavior for an instrumented impact test.* T_R = *10* μs.

$$P_I \propto \frac{Z_1 Z_2}{Z_1 + Z_2} \quad v_0 \tag{19}$$

where $Z_i = C_{Di}\rho_i$ is the acoustic impedance of material i, C_{Di} is the dilation sound speed, ρ_i is the density, and v_0 is the impact velocity of the tup.

The period for which the inertia portion of the tup signal masks the load-time record of the specimen is primarily a function of the geometry of the specimen and the acoustic impedances of the tup and specimen. For aluminum or steel Charpy specimens, this period is on the order of 20 to 30 μs [*12-15*]. Variations in the impact velocity do not have much effect on this period (see Fig. 6).

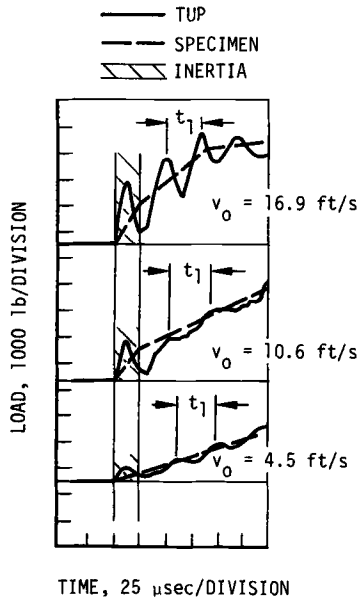

FIG. 6—*Effects of impact velocity on tup signal as compared with expected load-time records for mild steel Charpy specimens.* T_R = *10 μs.*

The superimposed oscillations caused by stored elastic energy and reflected stress waves have also been identified as inertial effects by Venzi et al [*13*] and Turner et al [*14,15*]. The discussion in this paper suggests that the first oscillation on the tup signal be considered primarily the result of inertial effects (as discussed in the foregoing) and the subsequent oscillations be treated as the result of the stored elastic energy and reflected stress waves.

The Saxton [*12*] work revealed a rational understanding of the magnitude of the first oscillation of the tup signal. The Venzi [*13*] and Turner [*14,15*] efforts yielded a rational understanding of the frequency of the subsequent oscillations.

This later work modeled the impact test as a vibrating mass on a spring system. The interaction force between the tup and the specimen results in energy being stored elastically in the machine. However, when the force is suddenly changed (for example, at initial impact, the elastic limit, and at brittle fracture) there is a corresponding sudden change in the stored energy. This energy change is transferred in a damped sinusoidal fashion, leading to oscillation in the force interaction between tup and specimen. The vibration mode of the specimen is a combination of Modes 1 and 3 shown in Fig. 7 [*13,17*].

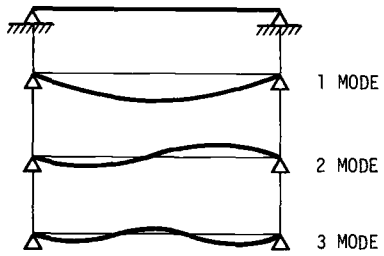

FIG. 7–*Free vibration of a beam.*

The sudden change in interaction force also generated reflected stress waves in the tup and the specimen. The frequency of a reflected stress wave is the ratio of the dilation sound speed (C_D) to the total path traversed by the wave. For a Charpy specimen of mild steel or aluminum, the frequency of reflected stress waves between the load points is approximately 100 kHz. The frequency for reflected stress waves in a typical instrumented Charpy tup is approximately 60 kHz.

The net effect of the reflected stress waves and the damping of suddenly released elastic energy is a signal oscillating at a frequency of approximately 30 kHz. As indicated in Fig. 6, the period, t_1, of these oscillations does not change appreciably for impact velocities between 4.5 and 16.9 ft/s (5.15 m/s). However, the amplitude of the oscillations is reduced significantly by the relatively small velocity decrease of 16.9 to 10.6 ft/s (3.23 m/s). The frequency and amplitude of these oscillations are apparently unaffected by changes in the compliance of the specimen [*15*].

For brittle fracture, the reaction of the specimen can be quite different than that of the supports (tup and anvil). Several investigators [*13-15,17,18*] have documented these differences through tests with strain gages appropriately positioned on the tup, anvil, and various locations on the specimen. The relationship of the specimen reaction (at midspan) to that for the tup and anvil is schematically shown in Fig. 8. As indicated, the reaction of the specimen is in phase with that for the anvil and approximately 180 deg out of phase with the tup reaction.

The amplitudes of the oscillations for the tup and anvil are larger than that for the specimen. However, there is a damping of these oscillations so that for times of 75 μs or greater the disparity between tup and specimen reactions has decreased significantly.

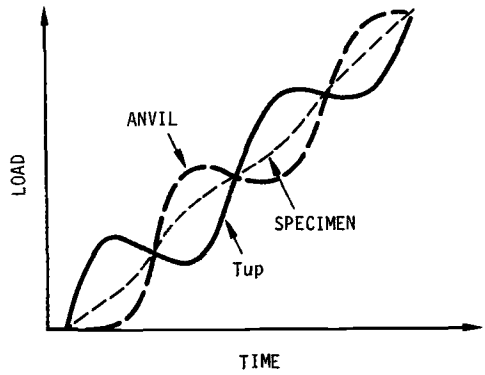

FIG. 8–*Relationship of specimen, tup, and anvil reactions during impact [13].*

Procedures

The preceeding extended background discussion is intended to be a guide for implementation of instrumented impact testing procedures. The three most important factors for reliable instrumented impact testing are calibration of the dynamic load cell, control of the instrumented tup signal, and reduction of data. Each of these is briefly discussed in the following.

Load Cell Calibrations

It is essential that the instrumented tup signal be a good analog of the time-dependent interaction force between the tup and the specimen. The instrumented tup is a dynamic load cell, and therefore the most applicable calibration procedure should be one utilizing dynamic loading techniques. It can be argued that because load is being equated to the results of strain-gage signals for elastic strains, and elastic properties are relatively strain-rate independent, static loads and dynamic loads will produce the same strain-gage signals. However, it is not uncommon to have strain gages respond differently for dynamic conditions than for static because of variations in the properties of the bonding materials which are holding the gages on the tup. It is also possible for the amplifier portion of the signal display system to have amplification characteristics that vary with the rate at which a signal is passed through the component. It is suggested that a

dynamic loading technique be used to calibrate the strain-gage output to the force interactions between tup and specimen for impact testing, and that test results for a strain rate-insensitive material be used to corroborate the agreement between static and impact loading. If a static calibration technique is employed for an instrumented tup, care should be taken to ensure that the loading geometry is exactly the same as that for the impact test.

Dynamic calibration of an instrumented tup can be done with the low-blow elastic impact test [*19*], by striking the tup with a known elastic impulse or by equating a secondary determination of specimen fracture energy to the area under the apparent load-time record. The latter is the most commonly employed technique for Charpy impact machines.

The pendulum impact machine has the distinct advantage (over a drop tower machine) of being able to supply a secondary determination of the energy consumed by fracturing a test specimen. This energy is the dial energy recorded by conventional Charpy and Izod impact machines. As discussed previously, the dial indication of energy is

$$\Delta E_o = E_I + E_{SD} + E_B + E_{ME} + E_{MV} \tag{5}$$

In this relationship, all but E_{MV} can be related to the force-time record of the tup, and this energy is small compared with ΔE_o when the impact machine is operated in accordance with ASTM Methods E 23 [*6*].

Calibration of the tup requires a determination of the specific amplifier gain; Eq 9 can be used to show

$$\Delta E_o \text{ (calculated)} = \Delta E_o \text{ (measured)}$$

Some instrumentation systems employ simultaneous integration of the tup signal so that energy-time, as defined by Eq 10, can be recorded as a second signal with the tup load-time signal. The maximum value of the energy-time signal (see Fig. 9) is the E_a value to be used in Eq 9 for calculating ΔE_o. The measured value of ΔE_o is that indicated by the pendulum dial energy.

Standard Charpy V-notch specimens [*6*] prepared from 6061-T6 aluminum plate will absorb total impact energies of approximately 10 ft·lb (13.6 J). Then, for an E_o of 240 ft·lb (325 J), Eq 9 reduces to

$$\Delta E_o = E_a \tag{20}$$

It is convenient to select a desired load sensitivity and change the gain adjustment of the amplifier of the tup signal until the E_a obtained from the energy-time signal agrees with the ΔE_o indicated by the pendulum dial.

For systems that do not directly record an energy-time signal, the E_a value is obtained by mechanical measurement of the area under the load-time profile. A polar planimeter is often used for these area measurements.

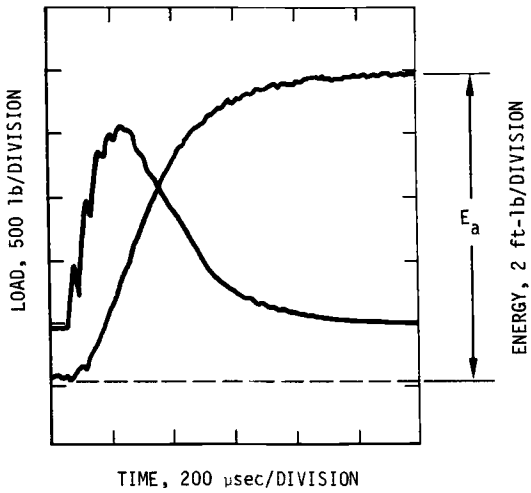

FIG. 9—*Load and energy records for standard Charpy V-notch specimen of 6061-T6 aluminum.* $T_R = 120\ \mu s$.

After the gain has been determined by the foregoing procedure, the load-time record for the impact test of the aluminum specimen should be compared with the similar data obtained by slow-bend tests of the same material. The slow-bend and impact load-time records should be identical. The maximum loads should agree within 3 percent. This, of course, assumes a uniform loading geometry for the two tests.

A typical maximum load value for the aluminum is approximately 1500 lb. The linearity of the calibrations should be checked by impact testing a specimen which has a limit load considerably greater than that for the aluminum. A standard Charpy specimen of 4340 at a hardness of HRC 52 will absorb approximately 10 ft·lb (13.6 J) and have a limit load greater than 6000 lb (26.7 kN). This material is not strain-rate insensitive, but if the machine capacity (E_o) is sufficiently large, Eq 20 can be used to compare the pendulum dial energy with that calculated by Eq 10 or displayed directly by an energy-time record.

This linearity check should include the load range of subsequent use with the instrumentation. Nonlinear behavior can be the result of amplifier characteristics, the geometry of the tup, or a fault in the bonding of the strain gage to the tup.

The performance of the tup calibration should be checked frequently by comparison of ΔE_o calculated by either Eq 9 or Eq 11 with that from the pendulum dial. If R is defined to be the ratio of these two energy values, then proper performance can be defined by $R = 1.0 \pm 0.04$. Mild steel bar stock with saw-cut notches of various depths can be conveniently used for these checks. A

typical plot of E_a (Eq 10) versus dial energy for a 240 ft·lb (325 J) capacity machine is shown in Fig. 10. When the calculated energy is determined by Eq 9 or 11, which account for the reduction in hammer velocity, a very good agreement with the dial energy is found; see Fig. 11.

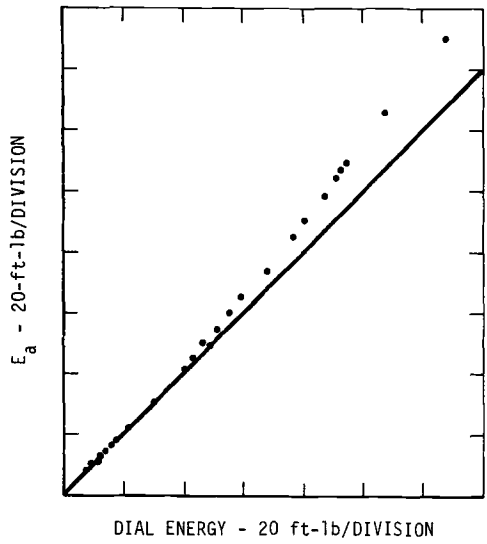

FIG. 10–*Comparison of pendulum dial energy with that calculated from the area under the instrumented tup signal record, where impact velocity is assumed to be constant.*

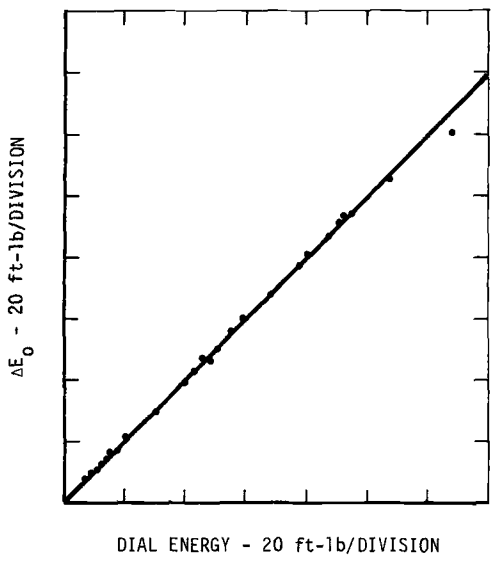

FIG. 11–*Comparison of pendulum dial energy with that calculated from the area under the instrumented tup signal record, where impact velocity is assumed to be the average value.*

When the energy absorbed by the specimen is greater than 0.5 E_o, the ΔE_o (calculated) should not be expected to match the dial indication of energy (that is, $R > 1.04$). Equations 9 or 11 are applicable to all ranges of energy absorption. The disparity in ΔE_o values occurs as a result of pendulum energy being consumed by factors such as E_{MV} (Eq 5) which are not represented in the load-time record. An example is shown in Fig. 11 for the dial value of 128 ft·lb (0.53 E_o) and ΔE_o of 121 ft·lb (164 J). Occasionally a similar disparity is observed when a brittle fracture results in the broken specimen halves rebounding from the sides of the hammer. This is a good illustration of the necessity for shrouds as specified in ASTM Method E 23 [6].

The other two techniques for dynamic calibration of an instrumented tup are quite similar. Both involve matching a calculated peak impulse load with that obtained from the instrumented tup signal. It is essential that the impact be entirely elastic because even small amounts of plastic deformation (E_B) will produce large reductions in the actual maximum load. The low-blow elastic impact technique requires a knowledge of the effective compliance C_M of the impact machine and the compliance C_S of the hard specimen being impacted. The maximum load to be expected by a low-blow impact is calculated from the following relationship [19] for elastic energy absorption:

$$P = \left(\frac{2E_o}{C_M + C_S} \right)^{1/2} \tag{21}$$

where E_o is the maximum available kinetic energy. These two techniques have an advantage over the energy equating technique in that the linearity of the dynamic load calibration can be easily checked by variations in E_o. However, care should be taken to avoid plastic deformation at the higher load values.

Dynamic Signal Control

The force-time signal obtained from strain gages on a tup during impact is not necessarily indicative of the reaction of the specimen [15,18,20]. The relationship of tup signal to that for the specimen is illustrated in Fig. 8 for the initial elastic portion of a Charpy-type test. It is not generally practical to experimentally separate the factors which cause the disparity between tup signal and specimen reaction. The experimenter has the following techniques available for determining the true mechanical response of a specimen tested by impact:

1. Monitor the response of strain gages or crack propagation gages or both attached directly to the specimen.

2. Reduce the amplitude of the oscillations of the tup signal by testing at a reduced velocity.

3. Electronically filter the tup signal without adversely distorting the signal with respect to the specimen reaction.

The first technique has been strongly recommended by Priest [20], and

unfortunately it has limited practical value. The specimen is assumed to have a linear relationship between load (P) and deflection (d_s) such that

$$P \cdot C_S = d_s \tag{22}$$

where C_S is the compliance of the specimen. The machine also has an elastic compliance (C_M) such that

$$P \cdot C_M = d_m \tag{23}$$

where d_m is the effective elastic deformation of the machine. When the tup velocity (v_o) is essentially constant during the time interval t,

$$v_o \cdot t = d_s + d_m \tag{24}$$

and the combining of Eqs 22, 23, and 24 yields

$$P = \frac{v_o t}{C_M + C_S} \tag{25}$$

The major experimental technique for determination of fracture load (P_F) by Eq 25 is the measurement of time to fracture t_f. Priest and May [*20*] used both strain gages attached across the specimen notch and measurements of voltage changes occurring in the plastic zone near the crack tip. Both techniques have large inherent errors not considered by the authors during subsequent fracture toughness calculations. Turner et al [*15*] employed a more accurate and reliable technique for detection of the onset of brittle fracture. This technique used a conducting paint grid such that the motion of the crack through the test piece would break successive grid lines and by appropriate instrumentation yield a t_f value. Determination of the constants C_M and C_S for use in relationships like that of Eq 25 is discussed later in the section on data reduction techniques.

Instrumentation of the specimen circumvents the dynamic signal control problem. The technique has distinct advantages for scientific studies of dynamic fracture properties. However, the technique does not comply with requirements for being cost effective and relatively simple. In particular, testing at various temperatures, like that for ASTM Methods E 23 [*6*] would be quite difficult.

The second technique for determining the mechanical response also circumvents the dynamic signal problem. This technique is simply a reduction of impact velocity to a level where the tup signal becomes a good representative of the specimen reaction. The signals obtained from an instrumented tup during an impact test are strongly dependent on the velocity of the impact test. As shown in Fig. 6, the amplitude of the superimposed oscillations on the specimen load-time curve is strongly dependent on the impact velocity. Please note, the load-time data shown in Fig. 6 are only the elastic loading portions of records for which the specimens fractured after general yielding. If the specimen tested at

16.9 ft/s (5.15 m/s) had fractured before general yielding, the large signal amplitudes could result in a substantial error for determination of the fracture load P_F. However, selection of a 10.6 ft/s (3.23 m/s) impact velocity would significantly decrease the amplitudes (see Fig. 6) and improve the accuracy of P_F determinations.

The reduction of impact velocity for certain tests was first proposed for control of the magnitude of the first oscillation, defined [*12*] as P_I in Eq 19. This suggestion was based on the concept that if P_F were greater than P_I, this apparent fracture load would be representative of the true mechanical response of the specimen.

The magnitude of P_I may vary for different impact machines and instrumentation systems. However, with the relationship shown in Eq 19 for the effects of impact velocity and acoustic impedance variations, the experimentalist can predict in advance the inertial loading of a new material based on the results of a few tests with mild steel specimens [*12*].

Assurance of $P_F > P_I$ can be too conservative, and a more practical criterion is one which separates the effects of the initial acceleration from the true mechanical response of the specimen. A critical test time can be selected for avoiding conflict with the inertia loading portion of the test. Unlike the apparent inertia load as predicted by Eq 19, this critical test time is not a strong function of the impact velocity. The interaction of reflected stress waves in the tup and specimen also distorts the initial appearance of the tup signal. The critical test time can be defined by this initial period of tup signal distortion; see the shaded areas in Fig. 6. As shown in the figure for Charpy tests of mild steel, velocity variations from 16.9 to 4.5 ft/s (5.15 to 1.37 m/s) cause the apparent inertia oscillation to occupy the first 20 to 30 μs of signal and that approximately 40 μs, from the initial impact, are required for the tup signal to return close to the actual specimen load-time behavior. These times will vary for different materials and test geometries.

The obvious disadvantage with the use of a reduced impact velocity is the loss of strain rate, which is often the driving force for performance of an impact test. The selection of a specific impact velocity or loading rate should be based on a fundamental understanding of the effects of strain rate on the mechanical properties of the material to be evaluated. For example, some of the most common strain rate-sensitive metals are the ferritic steels and at least a factor of 10 and very often a factor of 100 change in strain rate is required to produce measureable changes in mechanical properties [*14,18,20*]. Therefore, the <4 factor of change in impact velocity for the data shown in Fig. 6 should not be expected to produce a noticeable change in the properties of the mild steel, and the benefits in control of the signal oscillations are obvious.

A testing rate of 20 in./min (50.8 cm/min) is considered fast for the tension machines usually identified for so-called static tests. Comparison of this rate with the 4.5 ft/s (1.37 m/s) of the reduced velocity test in Fig. 6 reveals the strain rates differ by a factor of approximately 150. The reduced velocity test is

definitely a dynamic test as compared with conventional static test rates. The differential is magnified further when the more common static rate of 0.2 in./min is compared with the 4.5 ft/s (that is, a factor of 1.5×10^4).

The third technique which is sometimes employed for reducing the adverse effects of tup signal oscillations on the determination of the true mechanical reaction of the specimen is electronic filtering. However, the investigator should have a clear understanding of the overall effects of a limited rise time. That is, filtering can be as much of a problem as are the superimposed oscillations because of the possible signal distortion. The relationship between filtering and the true mechanical response of the specimen can be represented in terms of the signal rise time. Any instrumentation device has a finite response time (T_R), and it is suggested that this characteristic be identified as the signal rise time for an amplitude attenuation of 10 percent.

By superimposing a sine wave on the output of the strain-gage bridge (tup), T_R can be determined experimentally. Then, the frequency of the sine wave can be varied until the amplitude is attenuated and the response time for this attenuated signal is found from

$$T_R = \frac{0.35}{f_{0.9\ \mathrm{dB}}} \tag{26}$$

where $f_{0.9\ \mathrm{dB}}$ is the frequency corresponding to a 10 percent reduction of signal amplitude or the 0.915-dB attenuation.

When analyzing a dynamic signal with respect to system response time, T_R, the rise time of each oscillation should be evaluated. For example, consider the signal illustrated in Fig. 4. At time t the rise times of the signal during the indicated periods of t_2 and t_3 should each be compared with the system response T_R to determine if the signal has been attenuated. However, for sinusoidal signals like that obtained from strain gages on a tup during impact, the total time t_3 can be compared directly with T_R to determine the relative attenuation [*21*]. If $t_3 \geqslant T_R$, then the total signal attenuation $A \leqslant 10$ percent. When a relatively stiff specimen is to be tested and the expected time (t_f) to reach a critical load value is suspected to be adversely close to T_R, then the impact velocity should be reduced so as to increase t_f.

For brittle fracture, test data should be considered acceptable if $t_f > T_R$, and when $t_f \leqslant T_R$ the data should be considered suspect because of excessive attenuation. The t_f and T_R values should be included with all reports of dynamic test data.

Filtering should only be used for tests where the specimen is expected to fracture in a ductile manner. For example, the quality of the tup signal for an impact test of a standard [*6*] Charpy V-notch specimen of aluminum (6061-T6) is improved considerably by using a filter of $T_R = 120\ \mu s$ rather than a $T_R = 10\ \mu s$; see Fig. 12. Filtering is a useful technique for control of dynamic signal oscillations; however, it must by used judiciously and with a clear understanding of the overall effects of limiting signal response.

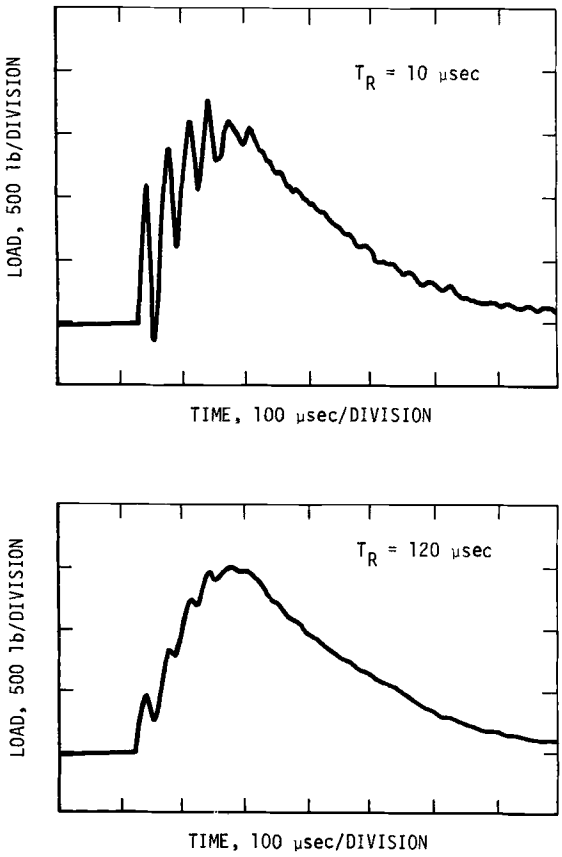

FIG. 12–*Comparison of tup signals for different system response times of a 16.9 ft/s impact of 6061-T6 aluminum standard Charpy specimens.*

Data Reduction

Techniques for reduction of dynamic test data usually vary with the specific goals of the investigator. The preceeding discussion of procedures for control of the dynamic signal indicated some general guidelines for analysis of oscillating instrumented tup signals. The following discussions of energy and deflection calculations are also intended only as general guidelines. Also included is a brief discussion of techniques for determination of machine compliance, which is required for much of the data reduction.

Energy–The instrumented tup signal provides a force-time record from which various load, energy, and deflection parameters can be determined. Within the limits discussed previously for response time T_R, the tup signal is indicative of the true mechanical response of the specimen. The exception to this statement is

the precise determination of the load at fracture for a brittle specimen. Instrumenting the specimen to determine the time to fracture t_f is not recommended for general use of the instrumented impact test. When $t_f \geqslant 60\ \mu s$ (for Charpy-type testing), the apparent indication of t_f by the tup signal is reasonably close to the true value [*14*]. However, the oscillations of the tup signal can cause an appreciable variance of apparent load from that indicative of the true mechanical response of the specimen. As shown in Fig. 6, minor reductions of impact velocity will sufficiently reduce the amplitude of the oscillations to that at $t > 60\ \mu s$ the apparent load (tup signal) will be within approximately 10 percent of the desired value. Additional work like that of Turner et al [*15*] should be performed so that rational procedures can be developed for determination of brittle fracture load from the tup signal. In the interim, extending the time to fracture t_f appears to be the most reasonable procedure for improving the accuracy of the tup signal for a brittle fracture. The elastic-plastic type of fracture does not present similar problems.

The energy absorbed at any time during the impact test can be determined by Eqs 9 or 11, where

$$\int_o^\tau P dt$$

is the area under the force-time curve. This calculated ΔE_o will be approximately equal to the energy (E_{SD}) required to deform the specimen when E_I, E_B, E_{MV} and E_{ME} are small; see Eq 5.

The E_B and E_{MV} are usually quite small compared with ΔE_o for brittle fractures, where E_I can be a significant fraction of ΔE_o. The E_I value can be estimated from the force-time record and Eq 10, where $\tau = \tau_i$ is the time associated with the inertia loading (approximately $\tau_i = t_3 - t_2$ in Fig. 4). The E_{ME} value is an elastic energy term, and from the relation in Eq 23 it can be shown

$$E_{ME} = \frac{1}{2} P_\tau d_{m\tau}$$

where P_τ and $d_{m\tau}$ are the specific values of load and effective machine elastic deformation at the time τ. This relationship reduces to

$$E_{ME} = \frac{1}{2} P_\tau^2 C_M \tag{27}$$

The energy consumed by bending of the specimen at time τ can then be found from

$$E_{SD} = \bar{v} \int_o^\tau P dt - v_o \int_o^{\tau_i} P dt - \frac{P_\tau^2}{2} C_M \tag{28}$$

For elastic-plastic fractures, E_I is usually a negligible contribution to ΔE_o. The plastic deformation of the specimen at the load points can be an accountable portion of the ΔE_o. Unfortunately, there is no simple technique for estimating E_B, and this value must be determined from the results of secondary experiments. The E_B must be related to the dynamic hardness of the specimen and the geometry of the load points. Preliminary work indicates that E_B is proportional to P^2. When E_B, E_I, and E_{MV} can be ignored, the energy consumed by bending the specimen at time τ can then be found from

$$E_{SD} = \bar{v} \int_o^\tau P dt - \frac{P_\tau^2}{2} C_M \tag{29}$$

The second term in this equation is E_{ME}, which by definition is an elastic energy term so that, when τ is the total duration of the impact event, the calculated energy for the specimen is found from

$$E_{SD} = \Delta E_o = \bar{v} \int_o^\tau P dt$$

For instrumentation systems which directly record an energy-time signal, it is convenient to express the foregoing relationship as

$$E_{SD} = E_a \left(1 - \frac{E_a}{4E_o} \right) \tag{30}$$

where E_a is obtained from the energy signal.

Deflection—The deflection d_τ at any time τ during the test can be conveniently determined from the force-time record and the known machine parameters. The force-time curve is used to calculate the effective velocity v and then

$$d_\tau = v\tau - d_{m\tau} \tag{31}$$

where $d_{m\tau}$ can be determined from Eq 23 and $v = v_o$ when ΔE_o is much smaller than E_o. For the general case $v = \bar{v}$, which is found by [9]

$$\bar{v} = \frac{v_o}{2} \left(1 + \left(1 - \frac{\Delta E_o}{E_o} \right)^{1/2} \right) \tag{32}$$

It can be shown that this equation is equivalent to

$$\overline{v} = v_0 \left(1 - \frac{E_a}{4E_0} \right) \tag{33}$$

Equation 31 can then be expressed as

$$d_T = \tau v_0 \left(1 - \frac{E_a}{4E_0} \right) - P_T C_M \tag{34}$$

where v_0, E_0, and C_M are the known machine parameters and τ, E_a, and P_T are obtained from the force-time curve.

Machine Compliance–There are several techniques for determining the compliance C_M of a Charpy impact machine. Each technique requires use of a test specimen for which the compliance C_s is accurately known for the specific loading conditions employed with the impact machine. This C_s value can be calculated from elastic beam theory; however, care must be taken to account for all contributions (tension, compression, and shear).

The low-blow impact test is a convenient method for using the instrumented impact system to determine C_M. In this test, the hammer is dropped from a height such that the maximum available energy E_0 is less than that required to produce any permanent damage in the specimen (including $E_B \simeq 0$). The force-time record for a typical low-blow impact test of a hardened 4340 steel Charpy V-notch specimen is shown in Fig. 13. There are three methods for determining C_M from this force-time record, and they are:

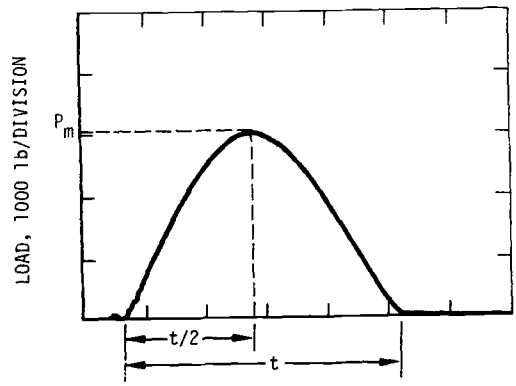

FIG. 13–*Low-blow (1.47 ft·lb) impact of standard Charpy V-notch specimen of 4340 steel (R_c 52).* T_R = *120 μs.*

1. Expand the scales so that the initial slope (C^{-1}) of the curve is essentially linear and then compare this slope with the theoretical slope (C_s^{-1}) to find C_M by [*22*]

$$C_M = C - C_s \tag{35}$$

2. Equate the sum of the elastic energy contributions (machine and specimen) to the low-blow energy E_o and solve for C_M as follows [*19*]

$$E_o = \frac{1}{2} P_m d_m + \frac{1}{2} P_m d_s$$

where P_m is the maximum load (see Fig. 13), and from Eqs 22 and 23

$$E_o = \frac{P_m^2}{2} (C_m + C_s)$$

which reduces to

$$C_M = \frac{2E_o}{P_m^2} - C_s \tag{36}$$

3. Consider the interaction between the hammer and specimen to be a vibrating mass on a spring so that the force-time record is a half oscillation of the system [*20*]. The time t for this half cycle is related to mass m and compliance C by

$$t = \pi (mC)^{1/2}$$

and

$$t = \pi (mC_M + mC_s)^{1/2}$$

which reduces to

$$C_M = \frac{g}{\rho_w} \left(\frac{t}{\pi}\right)^2 - C_s \tag{37}$$

where g is the acceleration of gravity and ρ_w is the effective hammer weight.

Typical values of C_M range from 1.5 to 2.0 × 10^{-6} in/lb (0.86 to 1.14 × 10^{-6} cm/N). For a specific machine, the foregoing three methods yield C_M values which agree within 10 percent [*15*]. Again, it should be noted that the resultant C_M value depends strongly on the accuracy of C_s.

Conclusions

When either performing instrumented impact tests or utilizing the results of this type of test, it is useful to have a general understanding of:

1. The various sources for dissolution of hammer energy which include the deformation of the specimen, the inertial acceleration of the specimen, Brinell-type deformation at the specimen load points, vibrational absorption by the machine, and elastic compliance-type deformation within the machine assembly.

2. The definitions for limited electronic frequency response and the effects of this limitation on the apparent load-time record.

3. The sources of the superimposed oscillations on the load-time record obtained from the instrumented tup and the effects of test variables on these oscillations.

The three most important factors for implementation of reliable procedures for the instrumented impact test are:

1. *Load Cell Calibration*—This should utilize dynamic loading and include comparison of dynamic and static test results for a strain rate-insensitive material.

2. *Dynamic Signal Control*—Electronic filtering can be used to reduce the amplitudes of superimposed oscillations; however, care must be taken to avoid abnormal distortion of the desired load-time record. Reduction of initial impact velocity is a useful technique for control of the superimposed oscillations.

3. *Data Reduction*—The analysis of instrumented tup signals for determination of various energy, deflection, and load values must be done with a clear understanding of dissolution of hammer energy, electronic limitations, and superimposed oscillations.

Acknowledgments

The author wishes to acknowledge the support and information received from his colleagues, R. A. Wullaert and W. L. Server. He is also grateful for the many helpful suggestions received from the Friends of Instrumented Impact Testing during the preparation of this manuscript.

References

[*1*] Mietz, A. F., Neil, G. T., and Conley, E. A., "Universal Test Procedure Instrumented Charpy Impact Test of Beryllium," Lockheed Missiles & Space Company, Inc., Report UTP No. 2, 30 Jan. 1973.

[*2*] Campbell, J. E., "Low Temperature Properties of Metals," *Review of Metals Technology*, 1 Dec. 1972.

[*3*] Oldfield, W., Bereda, J., Ireland, D. R., and Wullaert, R. A., *Materials Research and Standards*, Vol. 12, No. 2, Feb. 1972.

[*4*] Oldfield, W., Server, W. L., and Wullaert, R. A., "The Treatment of Data in Materials Testing—The Instrumented Charpy Impact Test," Presented at the Second Annual Cal Poly Measurement Science Conference, California Polytechnic State University, San Luis Obispo, Calif., Dec. 1972.

[*5*] Wullaert, R. A., Oldfield, W., Server, W. L., and Ireland, D. R., "Evaluation of Computerized Instrumented Charpy Systems," Effects Technology, Inc., Final Report No. CR-72-108 to Army Materials and Mechanics Research Center, Santa Barbara, Calif., 12 Dec. 1972.

[6] ASTM Methods E 23-72, "Notched Bar Impact Testing of Metallic Materials," *1972 Annual Book of ASTM Standards,* Part 31, American Society for Testing and Materials, 1972.
[7] Augland, B., *British Welding Journal,* Vol. 9, 1962, p. 434.
[8] Grumbach, M., Prudhomme, M., and Sanz, G., *Revue de Metallurgie,* April 1969, p. 271.
[9] Ireland, D. R., and Server, W. L., "Utilization of the DYNATUP Velocometer," Effects Technology, Inc., Technical Report 72-16, Santa Barbara, Calif., Oct. 1972.
[10] *Impact Testing of Metals, ASTM STP 466,* American Society for Testing and Materials, 1969.
[11] Naumann, W. J., unpublished results of studies at Effects Technology, Inc., Santa Barbara, Calif.
[12] Saxton, H. J., Ireland, D. R., and Server, W. L. in this symposium, pp. 50-73.
[13] Venzi, S., Priest, A. H., and May, M. J. in *Impact Testing of Metals, ASTM STP 466,* American Society for Testing and Materials, 1970, p. 165.
[14] Turner, C. E. in *Impact Testing of Metals, ASTM STP 466,* American Society for Testing and Materials, 1970, p. 93.
[15] Turner, C. E., Kennish, P., Culver, L. E., and Radon, J. C., "A Study of the Mechanics of Notched-Bar Impact Tests," Imperial College Department of Mechanical Engineering, Final report to Navy Department, Advisory Committee on Structural Steels, June 1970.
[16] Buys, E. C. J. and Cowan, A., "Interpretation of the Instrumented Impact Test," Document X-458-68, International Institute of Welding, July 1968.
[17] Leuth, R. C. in this symposium, pp. 166-179.
[18] Radon, J. C. and Turner, C. E., "Fracture Toughness Measurements by Instrumented Impact Test," *Engineering Fracture Mechanics,* Vol. 1, 1969.
[19] Server, W. L. and Ireland, D. R. in this symposium, pp. 74-91.
[20] Priest, A. H. and May, M. J., "Fracture Toughness Testing in Impact," NDACSS A86, 1969.
[21] Unpublished work in progress at Effects Technology, Inc., Santa Barbara, Calif.
[22] Iyer, K. R. and Miclot, R. B. in this symposium, pp. 146-165.

H. J. Saxton,[1] *A. T. Jones,*[1] *A. J. West,*[1] *and T. C. Mamaros*[1]

Load-Point Compliance of the Charpy Impact Specimen

REFERENCE: Saxton, H. J., Jones, A. T., West A. J., and Mamaros, T. C., "Load-Point Compliance of the Charpy Impact Specimen," *Instrumented Impact Testing, ASTM STP 563,* American Society for Testing and Materials, 1974, pp. 30-49.

ABSTRACT: To evaluate the instrumented impact test as a reliable way of collecting high strain rate, plane strain fracture toughness data, a detailed investigation of specimen mechanical performance and specimen-fixture interaction was undertaken. Finite element techniques were applied to calculate the compliance and stress intensity values for Charpy specimens subjected to both roller and pinned supporting conditions. For comparison, experimental compliances were gathered for 7075-T6 aluminum and 1018 steel Charpy specimens tested in slow and fast bending. The results indicate that both small specimen size and anvil friction can affect the interpretation of fracture load data used for K_{ID} calculations.

KEY WORDS: impact tests, fracture strength, toughness, bending, friction, impact strength, size effects

Nomenclature

a	Crack depth
B	Specimen thickness
C_V	Charpy total energy
E/A	Total impact energy per unit fracture area
E	Young's modulus
G_{IC}	Mode I energy release rate
K_{IC}	Mode I critical stress intensity, or fracture toughness measured in slow tests
K_{ID}	Mode I fracture-toughness measured in impact tests
K_{IQ}	Value assumed for K_{IC} prior to establishing validity of test
L	Specimen span length
P	Total load
v	Crack-mouth or load-point displacement

[1] Supervisor, Material Characterization Division, member of technical staff in the Experimental Mechanics Division, member of technical staff in the Exploratory Materials Division, and engineering staff assistant in the Experimental Mechanics Division respectively, Sandia Laboratories, Livermore, Calif. 94550.

W Specimen width

The Charpy impact test, primarily because of its simplicity, has been a useful screening test of toughness for many years. Recent improvements in instrumented impact testing have heightened interest in the technique, although many investigators have declared invalid the application of linear elastic fracture mechanics to, and subsequent calculation of K_{IC} from, Charpy impact tests. In order to establish the instrumented impact test as a reliable, quantitative method for collecting high rate, plane strain fracture toughness data, a detailed understanding of the specimen environment and performance is needed. During the past two years, in which the present investigation of this test has been underway, work has been focused as much as possible on specimen-fixture interaction and specimen performance. Goals in the study were:

1. To explain quantitatively the effects of small specimen size.
2. To determine the effects of fixture friction or brinelling or both on toughness data.
3. To assess the errors introduced by fixture compliance, alignment, and the location of the point of deflection measurement.

Since about 1962, a large amount of research has centered upon the instrumentation of the Charpy impact machine. With the aid of the additional information that Charpy instrumentation provides, the concepts of linear elastic fracture mechanics suggest that the Charpy test might produce high-strain-rate-toughness values (K_{ID}) as well as normally recorded total impact energies (C_V). The approaches to obtaining K_{ID} from Charpy tests have been numerous. They range from strictly empirical correlations to attempts to treat the Charpy impact test as a standard three-point bend fracture toughness test. The approaches are subject to criticism, ranging from applicability of empirical fits among differing materials and structures to the credibility of recorded load and deflection data.

Attempts have been made to use C_V as an independent variable [*1,2*][2] to predict K_{IC} and K_{ID} empirically. Although the empirical relationships may be proven valid for a single material or group of closely related materials, exceptions [*2,3*] to the relationships are common enough to prohibit reliance upon C_V data alone for evaluations of critical flaw sizes and structure integrity.

To estimate dynamic K_{IC} values as a function of temperature, Barsom and Rolfe [*3,4*] have shifted K_{IC} versus temperature data along the temperature axis by an increment BT equal to the shift in transition temperature observed for slow- and impact-loaded Charpy specimens. Significant scatter is observed in the correlation; and while not defined in the aforementioned references, the correspondence of strain rate in K_{IC} tests with that in impact tests must be explored for each material studied.

Beginning with the work of Orner and Hartbower [*5*], a series of studies has explored the possibility of equating the impact energy per unit fracture area

[2]The italic numbers in brackets refer to the list of references appended to this paper.

(E/A) with the critical crack-extension force (G_C). In the studies, fatigue-precracked Charpy specimens have been tested in slow bending and at impact rates. In slow-bend tests [*6*], the deflection as well as load can be directly measured, and the energy E is the area under the load-deflection curve. In standard impact tests, the fracture energy can be interpreted as the total impact energy [*7*] or it can be calculated from the load-time profiles recorded during instrumented impact tests [*8,9*]. During impact testing, the load-point displacement is often inferred from (1) the initial hammer velocity or (2) direct measurements of the hammer displacement [*10*]. Because of the difficulties in instrumentation, the actual displacement of the load point has not been measured experimentally. Ronald et al [*16*] have successfully predicted the K_{IC} of various titanium alloys using the E/A method in slow-bend testing of precracked bars.

The preceding approach to calculating G_C and arriving at K_C through the Irwin relation at impact rates has been criticized by Srawley and Brown [*11,12*] on the grounds that three assumptions about the test have to be made: (1) all of the energy loss has to be converted to fracture energy; (2) taking the projected fracture area corresponds to assuming uniform plane-strain fracture conditions across the entire bar; and (3) G must remain constant as the crack propagates.

As the research on inertial loading reported by Saxton, Ireland, and Server [*13*] indicates, it is very difficult to meet all three requirements simultaneously during an impact test. Only the testing of tougher materials ensures fairly complete energy conversion, and in these cases shear lips and mixed-mode fracture processes violate the final two requirements. While the testing of very brittle materials ensures a flat fracture surface and uniform plane-strain conditions, inertial loading, dynamic response, and imperfect system alignment prevent total energy conversion.

For noninstrumented systems, no reliable method is available to partition the energy between inertial, ringing, fracture-initiation, and fracture-propagation events; hence the possibility of deriving K_{IC} from total impact energy appears remote. The character of the load-time traces during an impact allows the experimentalist to identify the four contributions to the total energy before making toughness calculations. Recently, Ireland [*14*] and Hoover and Guess [*15*] have partitioned fracture propagation and inertial energies, respectively, to arrive at G calculations. Even with the aid of instrumentation, the foregoing discussion strongly indicates that only materials brittle enough to produce plane-strain fractures in small cross sections will produce values of E/A equivalent to $2G$ and hence convertible to K_{IC}.

To produce crack extension force data a valid ASTM plane-strain specimen is required. Then the Irwin relation promises convertibility between G and K, and the standard stress-intensity function for a three-point specimen would be equally valid for calculation. For the latter case, only a knowledge of the crack length and instability load is required to calculate K_{ID}. Many workers [*6,16-18*] are now using this technique to calculate the dynamic and static fracture toughness of alloys during impact and slow-bend Charpy tests. Without exception,

these experimentalists are using the standard ASTM three-point bend data provided in *ASTM STP 410* [*12*] as the best available approach even though it is widely understood that the small specimen size prevents most Charpy tests from giving valid K_{IC} data.

If the Charpy is to be used as a K_{IC} specimen, the following conditions must obtain:

1. The stress intensity relationships used must be valid for the test conditions imposed.
2. The experimental boundary conditions must be adequately known.

These are:

(*a*) Accurate knowledge of the loading, including anvil friction effects at any strain rate

(*b*) Test fixture compliance

(*c*) Specimen brinelling

(*d*) Alignment and machining tolerances

(*e*) Inertial effects at high strain rates

(*f*) Impact instrumentation response at high frequencies

Saxton et al [*13*] discuss the last two items in detail. Present study goals are the quantitative determination of: small specimen size effects, fixture friction, or brinelling effects on the performance of a Charpy specimen, and effects of specimen alignment.

All these factors must be known in advance of testing because the present capabilities for instrumenting impact do not include measurement of dynamic specimen compliance as a check on test performances.

Analytical Procedures

Finite Element Solutions

It is well known that no exact elasticity solution has been found for the Charpy configuration for either linear elastic or strain-hardening materials. Accordingly, approximate boundary collocation solutions have come to be the accepted stress analysis for this configuration. Srawley and Gross [*19*] and Bucci et al [*20*] have published stress intensity factors, load point, and crack-mouth compliances for the specimen. Because of the need to solve boundary conditions not discussed in the literature, the finite-element technique was adopted here. This method of solution permits examination of various displacement boundary conditions at the supports, and gives the displacements at any chosen location on the specimen. Only linear elastic materials are analyzed by this technique. The bar was meshed with 32 elements across the crack line and 40 elements longitudinally (only one half of the bar need be considered by symmetry). A procedure by Watwood [*21*] was adopted to compute the stress-intensity factors from the strain energy release rate during crack extension. A comparison between finite-element and collocation results shows agreement within a few percent over the entire range of crack lengths studied.

The major results of the stress analysis are presented as nondimensional stress intensity and nondimensional compliance. The specimen was assumed to be supported by rollers at the support points (to represent no support friction) and pinned at the support points (to represent high support friction). The compliances are for the plane-strain condition.

Dugdale Crack Model

To account for suspected size effects in a quantitative manner, a Dugdale crack model is used. Recent work by Hayes and Williams [*22*], using a numerical Green's function derived from finite-element results, gives Dugdale model solutions of pure bend specimens with a span-to-depth ratio of 6. Though this is not precisely the loading condition or size of the Charpy bar, the analyzed situation is near enough to use for estimates of plasticity effects in the form of plastic zone size and crack-opening displacements (at the rear of the plastic zone). These quantities were used to extrapolate crack-mouth displacements for both steel and aluminum bars. To execute the procedure, a straight line was first drawn from the intersection of the forward edge of the plastic zone with the crack line through the Dugdale crack-opening displacement at the rear edge of the plastic zone; then the line was extended to the crack mouth. The Dugdale model provides upper bounds to the actual crack-mouth displacement, and bounds derived in this manner are plotted in Fig. 4 for aluminum (σ_y= 75 000 psi) and steel (σ_y = 50 000 psi) alloys.

Experimental Procedures

Goals

Since most factors which affect the viability of the Charpy bar as a K_{IC} test specimen can be detected with compliance techniques, compliance tests were run on aluminum and steel Charpy bars at load-point displacement rates from 0.02 in./min (slow bend) to 6 in./s (in a servo-hydraulic machine) to record compliance both statically and dynamically.

Materials and Specimen Preparation

Standard ASTM Charpy specimens were machined from 7075-T651 aluminum and 1018 steel to provide examples of materials with widely different elastic moduli. From the bottoms of the machined notches, slots were electro-discharge machined to prescribed lengths. The widths of these slots were restricted to 0.010 in. or less. Large three-point bend specimens (0.50 in. thick) were machined to ASTM specification (L = 4W = 6 in.) from 7075-T651 aluminum for compliance testing also.

Test Fixtures

The bulk of the testing was conducted on a fixture which, though specially

designed to be installed in the load train of an Instron or MTS testing machine, was machined to the ASTM specifications for Charpy impact tups and anvils. Schematics of the experimental setup for crack-mouth and load-point testing are shown in Fig. 1. The crack-mouth measurements are taken between two razor blades glued to the specimen 0.150 in. apart. Previous experience [*23*] has shown that when absolute specimen dimensions are reduced, it is imperative that the clip gage be placed as close to the specimen surface as possible. For convenience, a displacement gage (LVDT) was placed below the notch instead of the load point. Both analytical and experimental results revealed differences of no greater than three percent in displacement between the two points for the range of crack lengths considered.

The compliance testing of the large aluminum three-point bend specimens was conducted on standard ASTM fixturing which included roller supports. Load-point as well as crack-mouth displacements were recorded.

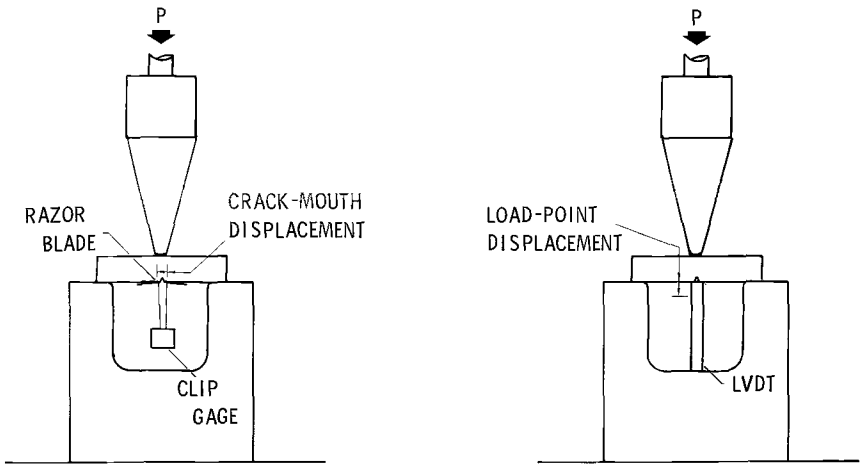

FIG. 1—*Schematic of experimental setups which measure either crack-mount or load-point-displacement.*

Test Procedures

Slow three-point bend tests on all Charpy specimens were conducted in a 20 000-lb-capacity Instron testing machine at crosshead rates of 0.02 in./min. Each sample was cycled a number of times to a load well below its gross yield point to establish its crack-mouth and load-point compliance.

High-rate three-point bend tests on the samples were conducted in a 100 000-lb-capacity servo-hydraulic machine, and each load-displacement curve was directly recorded by an oscilloscope camera. Crosshead rates of 0.05 and 6 in./s were achieved while load-point displacement was being measured. The high-

est rate achievable in the machine is still about one-half the slowest rate (10 in./s) used for instrumented impact testing in our laboratory. Full-blow tests conducted with our 128 ft·lb PhysMet impact machine develop displacement rates of about 160 in./s.

The fixture compliance correction was calculated by measuring the flexure of a 0.6 by 0.6-in. steel beam placed in the fixturing used for the compliance tests. Since the flexural displacement of the beam for a given load can be computed, the fixture displacement can be separated from the total displacement. In the simulated impact fixturing used for slow- and high-speed tests, tup compliance does not affect the load-point compliance and only "anvil" compliance is significant. During instrumented impact tests, elastic deformation of the tup and arm, as well as the anvil, influence effective specimen displacement rates.

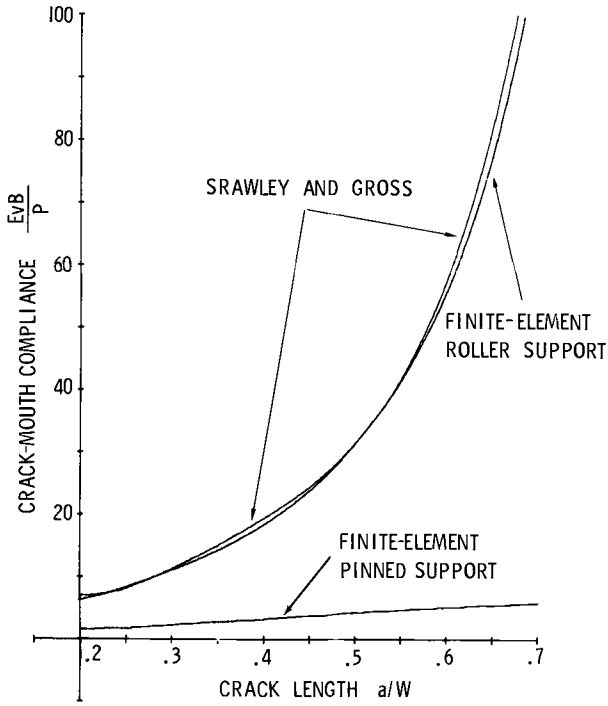

FIG. 2–*Comparison of boundary collocation and finite-element compliance calculations.*

Results

Analytical

Figure 2 compares the analytical results obtained from finite-element code calculation for a Charpy specimen with a published boundary collocation solu-

tion for three-point bend specimens with a span-to-width L/W ratio of 4. To approximate the forces generated by friction at the supports, two boundary conditions were considered: roller supports corresponding to no-support friction and pinned supports to infinite-support friction. On the figure, a dimensionless EvB/P (where E is the elastic modulus, v the crack-mouth or load-point displacement, B the specimen thickness, and P the total applied load) is plotted versus a/W (where a is the crack length and W the specimen width). Although the solutions agree within 5 percent, the boundary collocation solutions are slightly more complaint than the finite-element solutions. This result is consistent with the results of other similar studies [*24*]. Figure 3 presents nondimensional stress intensity for the two boundary cases. Two important findings can be drawn from Figs. 2 and 3. First, the finite-element code produces solutions for the roller condition which compare with those for other analytical techniques well enough to induce confidence in the pinned support solutions. Second, the differences between the roller and pinned solutions are significant, indicating that friction can substantially influence the stress intensity.

From the elastic stress analysis, the amount of specimen brinelling can be crudely estimated. At high loads the elastic indentation under the load can be as much as 5 percent, and this amount is a rough indication of the tup and anvil

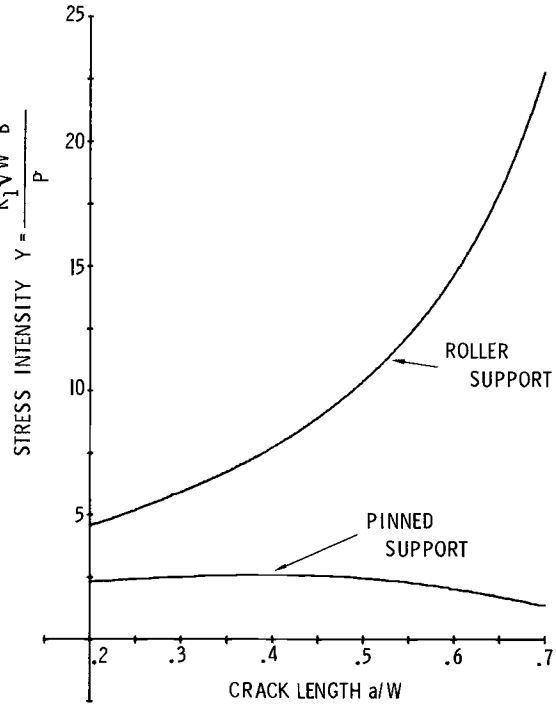

FIG. 3–*Stress intensity factor versus crack length for Charpy bars.*

indentation. Also, by examining code results, misalignment of measuring devices and load was determined to be an insignificant effect if reasonable care is taken to align these properly during testing.

One other comment should be made. For the pinned-end bar, the load deflection relation is nonlinear, the nonlinearity being caused by axial restraint. To determine if the latter effect should be considered, a check was performed on the Charpy geometry for an unnotched bar. The results indicated that the nonlinearity was slight and that, in the linear regime, sufficient axial force could be developed to cause slipping for the loads considered here. Nonlinearity was not considered in the pinned finite-element solutions plotted in this paper. These solutions were developed for loads of 400 lb and 1600 lb to include the range used in this study.

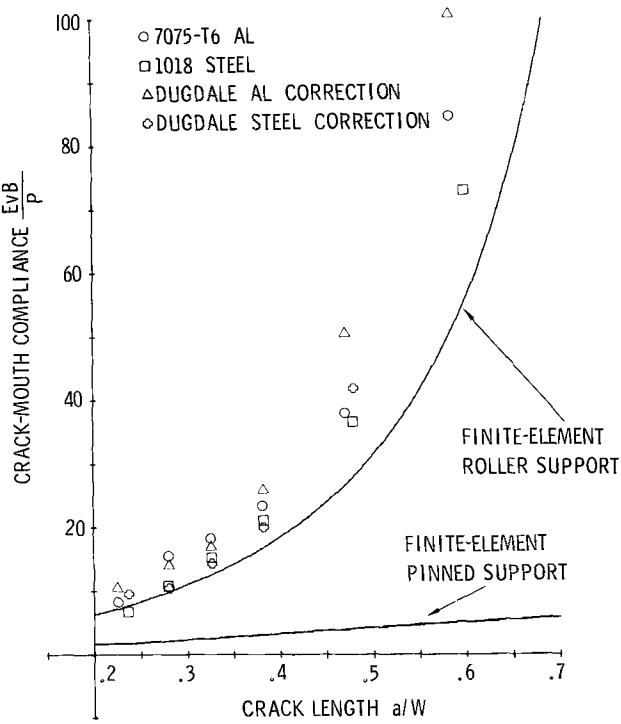

FIG. 4—*Experimental slow-bend crack-mouth compliance compared with finite-element and Dugdale models.*

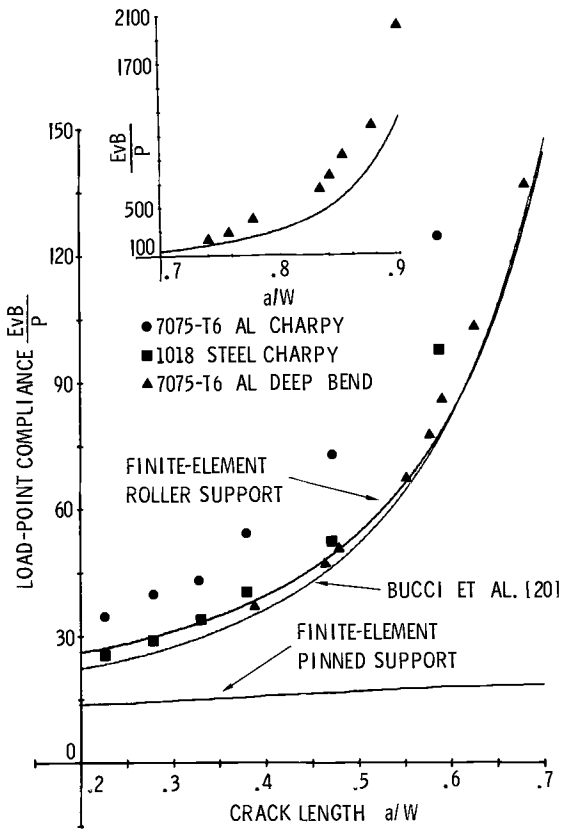

FIG. 5—*Experimental slow-bend load-point compliance data for Charpy and deep-bend (L = 6 in., W = 1.5 in., B = 0.5 in.) bars compared with finite-element model.*

Experimental

Figures 4 and 5 present the slow-bend compliance data gathered in crack-mouth and load-line experiments, respectively; and for correlation with experimental results, the plane-strain finite-element code results and Dugdale model estimates are also plotted. For the Dugdale model calculations, yield strengths were measured at 75 and 50 ksi for the aluminum and steel bars, respectively. Tabulated values of elastic moduli, 10.4 x 10^6 and 30 x 10^6 psi, were used for the aluminum and steel specimens, respectively.

A typical experimental compliance curve at a low loading rate is shown in Fig. 6. Upon loading, the specimen ends begin moving outward, restrained by in-plane frictional force which depends on the load. This increasing friction force causes the specimen to become stiffer as loading progresses. Between loading and unloading, as the specimen ends momentarily stop, static friction becomes oper-

ative and stiffens the specimen even further, causing the steep unloading slope. The compliances observed during initial unloading of the steel specimens are plotted as a function of a/W in Fig. 7. Eventually, the specimen breaks loose and resumes unloading, influenced by the dynamic friction.

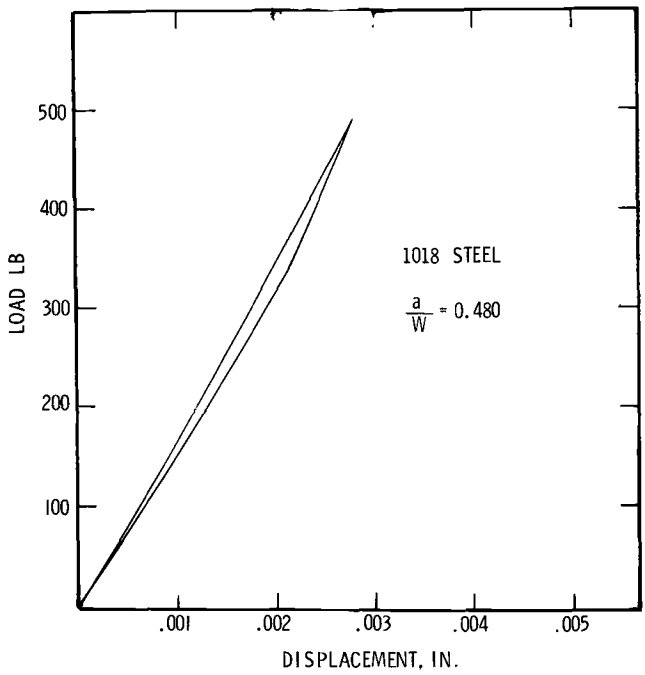

FIG.6–*Typical slow-bend load deflection record.*

Compliance data gathered in the present research is corrected for the anvil compliance, which was 1 x 10^{-6} in./lb. This value is about half that of the dynamic fixture compliances measured for actual impact machines, where tup as well as anvil deformation must be considered [*14,25*].

The load-point and crack-mouth compliances of the steel and aluminum data agree best at lower values of a/W and diverge increasingly as a/W increases. In addition, the aluminum specimens are consistently more compliant than the steel specimens. Although not plotted on Fig. 5, the slow-bend data gathered by Priest and May [*25*], using a PhysMet slow-bending machine and mild steel Charpv specimens, also follow the roller solution approximately and deviate increasingly at high a/W. Since their steel specimens appear more compliant, it is possible that these data were not corrected for machine compliance.

The deviation of experimental compliance above analytical predictions is believed to be a size effect since the Dugdale model predicts the same trends for

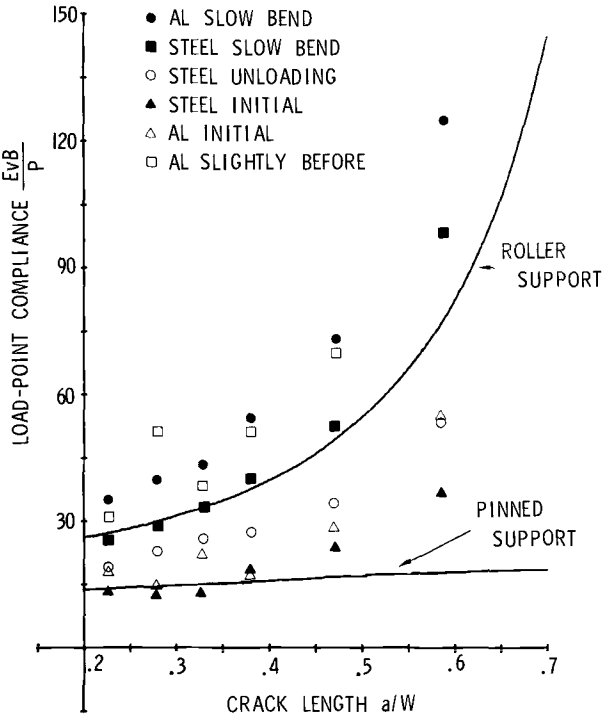

FIG. 7—*Experimental load-point compliances measured from slow-bend tests and at increasing times during high-speed tests compared with finite-element models.*

each alloy. The Dugdale solutions, which take account of specimen size, follow the experimental data quite closely. Agreement is especially good for the steel which has little strain-hardening capacity. To document further the size effect, a wide aluminum bend bar (L = 6 in., W = 1.5 in., B = 0.5 in.) was fatigue-cracked to similar a/W values, and agreement with the roller solution was excellent. The crack was then extended until the unbroken ligament was similar in absolute length to that of the Charpy bars. It is evident (Fig. 5) that compliance increases occurred exactly as for the Charpy bar.

While the slow-strain-rate data follow the roller solution except when unloaded, the high-strain-rate data (Fig. 7) initially appear to follow the pinned solution. Friction at the support points on the anvil appears sufficient during the first portion of the test to restrain lateral displacements. This initial pinning is shown in typical oscilloscope traces for both the aluminum and steel specimens (Figs. 8*a*,8*b*). The oscillation on the trace is caused by the load cell and tup fixture vibrating. During each vibratory cycle, slippage occurs on the supports and reduces the axial force due to end restraint present in the specimen. Reducing the axial force causes a corresponding increase in compliance; hence, the slope of the load deflection curves drops in increments. Since the effect is

present at loads lower than previous elastic preloads placed on the bars, yielding is not responsible for this compliance change. In Fig. 7, the compliances plotted represent those measured at increasing times on the load-displacement traces. The initial compliances are taken from the mean slope of the traces before the first ring (load-displacement discontinuity occurs). The compliance increases piecewise as the deflection increases until the linear portion close to fracture is reached. This linear portion of the load-deflection trace is within a few percent of the roller solution, thus indicating that friction is not a factor at the instant of fracture—at least for 7075-T6 aluminum at these strain rates.

A typical impact trace for A-286 stainless steel (Fig. 8*c*) demonstrates that compliance cannot be inferred easily from the load-time oscilloscope trace and the initial velocity. A-286 provides a linear trace until just before unstable crack propagation, and inertial effects play a negligible role in the test. The specimen was fatigue precracked to an a/W of 0.284 and tested at 203 in./s inital velocity. Even after correcting for the fixture compliance ($\sim 2 \times 10^{-6}$ in./lb) and average velocity loss, the trace still gives an EvB/P exceeding 70 while the load-point compliance plot (Fig. 5) predicts an EvB/P of about 30. Since in more brittle materials the occurrence of inertial effects increases the difficulty of making experimental compliance calculations, a direct measure of specimen compliance

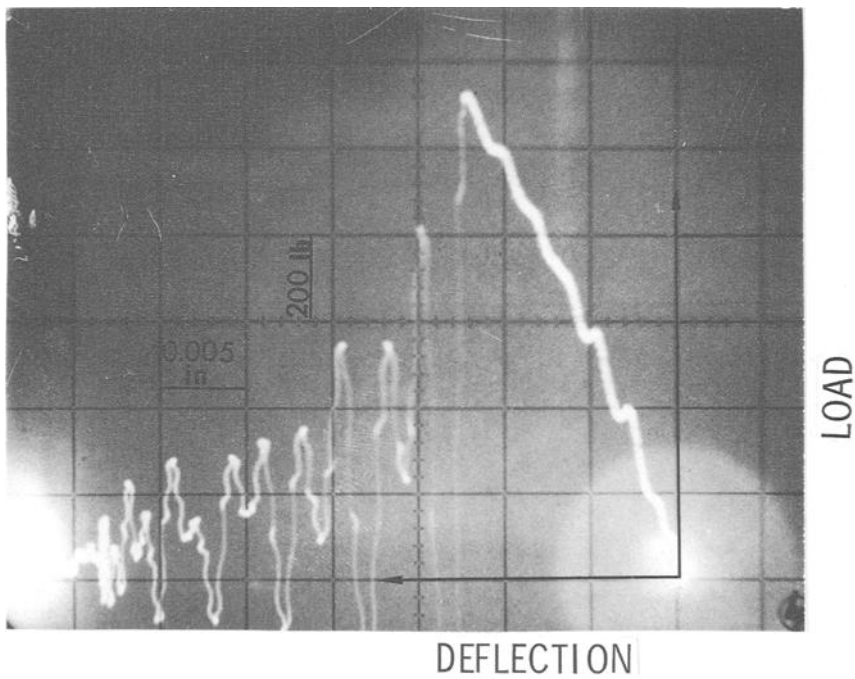

FIG. 8*a*—*Oscilloscope record of a high-speed 7075-T6 aluminum fracture in a servo-hydraulic machine test.*

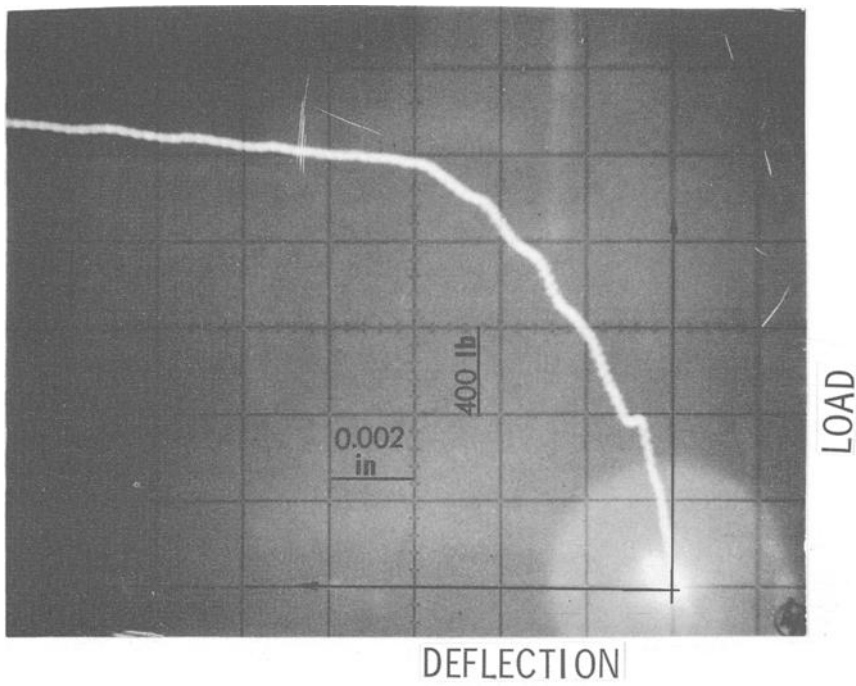

FIG. 8*b*—*Oscilloscope record of a high-speed 1018 steel fracture in a servo-hydraulic machine test.*

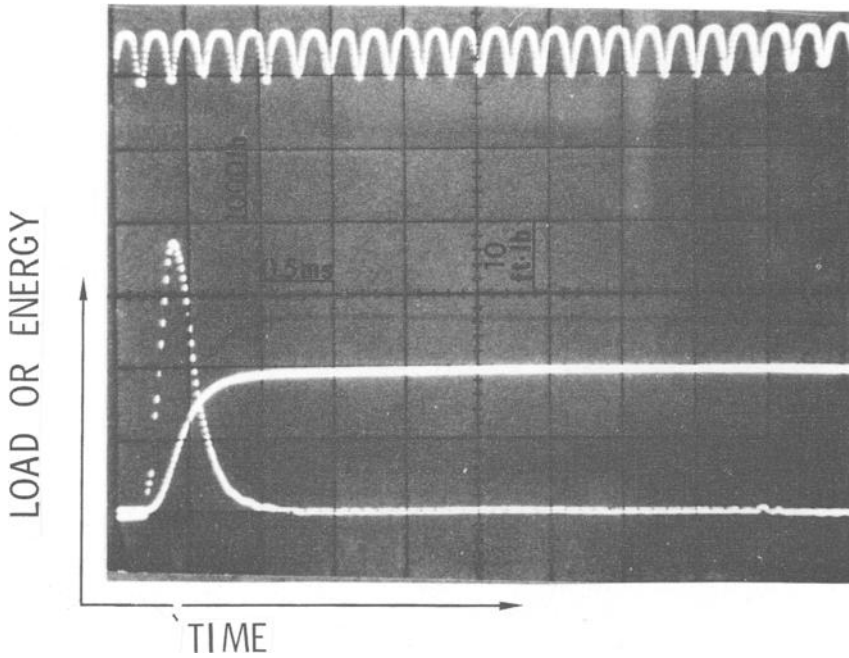

FIG. 8*c*—*Oscilloscope record of a high-speed A-286 steel fracture in an instrumented Charpy test.*

appears necessary. On the other hand, making these types of measurements detracts from the simplicity of the Charpy test.

Summarizing the analytical and experimental results clearly points out a number of areas calling for more detailed discussion. First, the small size of the Charpy specimen becomes a dominant factor of the compliance behavior as a/W increases. Second, the difficulty of measuring specimen compliance during actual impact testing (because of variable machine flexure, brinelling, and inertial effects) forces the experimentalist to assume the boundary conditions of his experiment without a test-to-test verification. Third, the compliance of the Charpy specimen appears to decrease as strain rate increases, and this change in compliance behavior will cause significant changes in stress intensity relationships.

Relation of Compliance Data to K_{IC} Testing

The previous discussion of Charpy specimen compliance has shown that support conditions and the small physical size of the specimen strongly affect stress and displacement levels during a test. It still remains to connect these effects with the calculation of K_{IC} or K_{ID}. Unless specifically mentioned, the influence of wave propagation and dynamics on specimen performance will be neglected when the effects of support conditions and specimen size are discussed.

Size Effects

When a K_{IC} test is performed, and yielding occurs on a moderate scale, the value of K_{IC} does not represent a true value of plane-strain fracture toughness since triaxiality of stresses near the crack tip is lost. Normally, in impact testing, such yielding is not accounted for; so it is appropriate here to discuss the data reduction procedure for a specimen that exhibits size effects.

Consider the application of linear elastic fracture mechanics to a Charpy bar where the optically observed flaw size and the fracture load are known. Figure 9 shows the method most investigators use to calculate K_{IC}, and the source of error which results from this method when Charpy specimens are tested in slow three-point bending. Path I shows how stress intensity is calculated with only the analytically derived K relationship and the optically observed flaw depth. Only specimen compliances near the analytical solution signify plane-strain behavior and imply that conditions are suitable for calculating K_{IC}. As experimental measurements show, plasticity effects cause aluminum and steel Charpy specimens to be more compliant than theory predicts; and the experimental stress intensity factor (calculated from the slope of the compliance curve [*26*] is also found to exceed the analytical value of K for respective values of a/W.

In the strictest sense, when compliance performance deviates from the analytical curve, it is highly questionable (even if the experimental K versus a/W curve is used for calculation) that the K_{IQ} calculated can be used to determine

critical defect sizes. However, when plasticity effects are relatively small, certain corrective methods like the Irwin crack extension relation $1/2\pi(K_{IC}/\sigma_y)^2$ can be applied. To use these methods successfully, it must be assumed that the plastic zone simply provides an effective crack extension, and that far-field elastic stresses still dominate the conditions for unstable crack extension. In view of the nature of the Dugdale correction, which considers finite specimen size, it is not clear that the foregoing two assumptions are met for the Charpy specimen.

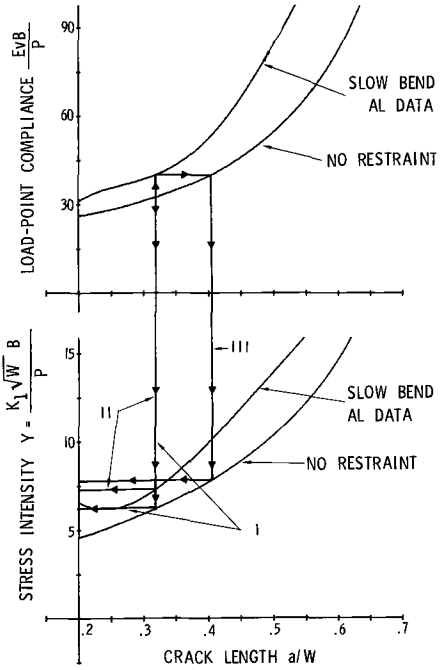

FIG. 9—*Alternate methods of calculating* K_Q *from a test which exhibits size effects.*

For purposes of discussion, however, a plasticity-corrected K_{IQ} can be calculated from Paths II or III in Fig. 9. Along Path II, an effective crack extension is calculated by horizontal translation between compliance curves, and I_{IQ} is calculated from the analytical K curve. Along Path III, the optical crack length is used with the experimentally determined K curve. If the smoothing and differentation needed to derive the experimental stress intensity are done properly, the two corrected K_{IQ} values should be nearly the same. With these corrections, Path I yields a value of K_{IQ} that is consistently low, the amount of lowering being dependent on the material and notch depth. Data for three-point bend specimens made of 7075-T651 recently published by Nelson et al [*27*] show that the size effect tends to lower apparent K_{IC} for small unbroken ligaments.

To summarize this discussion on size effects, the use of the Dugdale model appears valid for predicting compliance changes caused by plastic zone growth, but the results published by Hayes and Williams [*22*] indicate too much yielding to permit prediction of K_{IC} values from the plastic zone size of the specimen. Therefore, size effects introduce into K_{IC} measurements based on Charpy experiments an uncertainty which cannot be systematically corrected with theories or experimental models now available for fracture mechanics.

Friction Effects

If the effects of small size are neglected for the moment, the error in K_{IC} calculations introduced by friction (pinned support) can also be dealt with conceptually (Fig. 10). In this case, Charpy specimens with both roller and

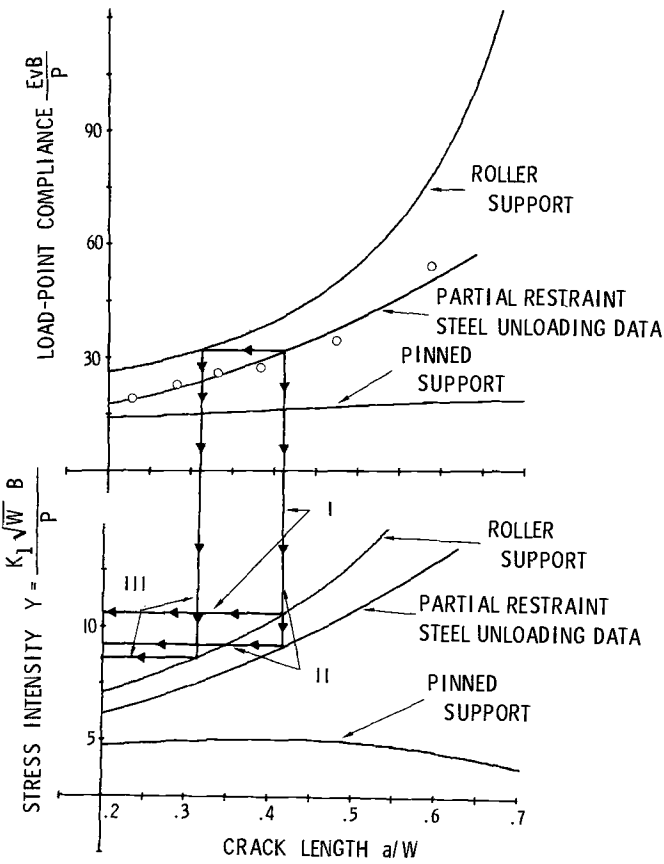

FIG. 10–*Alternate methods of calculating* K_Q *from a test which exhibits friction effects.*

pinned support provide stress intensity factors. However, any experimental compliance performance between the two theoretical curves can represent some loss of axial restraint without precluding Charpy bar deformation in a plane-strain condition. A specimen influenced by support friction will display the behavior like a roller-supported specimen with a much shorter crack length. It should be noted that friction and small size effects on compliance tend to cancel when simultaneously present. However, any performance below the theoretical roller compliance curve indicates that friction effects are dominant.

Also plotted in Fig. 10, for discussion purposes, are the least-squares fit of experimental compliance and experimentally derived stress intensity behavior of the steel Charpy bars during slow-bend unloading. Stress intensity can be calculated from Paths I, II, or III, and while Path I is the method used by most investigators, more nearly correct calculations are made from Paths II or III. For example, Paths II or III give similar values of K_{IQ} for an $a/W \approx 0.5$, while Path I makes K_{IQ} too high, thus illustrating the dangerous tendency of frictional effects to cause an apparent increase in fracture toughness.

Data taken from aluminum in this study indicated that friction was unimportant at the fracture load. The steel did not fracture, but reached a limit load within 10 percent of that predicted by Bucci et al [*29*], which neglects friction effects, thus indicating that for steel also, friction forces were not operative near the peak loads. It is hypothesized that vibration in the load cell tup fixture allowed slippage at the support points. If the material had been more brittle, and had broken earlier as the load was applied, friction would probably have been very important since insufficient release occurred at very early times (Fig. 8) and the same thing may be true at the higher load rates in impact testing.

Data Comparison

Enough data exist in the literature concerning K_{IC}, K_{ID}, G_{IC}, and G_{ID} to encourage its use as circumstantial evidence when evaluating the relative importance of small size and friction effects. However, close inspection of the materials being tested and the tests being performed reveals the limited utility of the data. First, K_{ID} values calculated from instrumented Charpy tests (Ref *16*, for example) performed on various steels indicate that K_{ID} is lower than K_{IC} measured in static tests on standard-size specimens. Since these steels are strain-rate sensitive, this decrease in fracture toughness with increases in strain rate can reflect changes in material behavior as well as specimen size effects. Second, a large body of data (for example, Ref *7*) indicates that G_{ID} collected in Charpy impact tests is larger than G_{IC} collected from Charpy specimens tested in slow bending. However, the materials being tested exhibit very brittle behavior; hence the increase in fracture toughness can reflect the presence of inertial effects as well as friction effects. Therefore, insufficient data exist in the literature to judge the relative importance of size, friction, and materials response.

Conclusions

Data gathered and analysis performed in our study of the Charpy impact specimen indicate that aside from specimen dynamics, two important factors must be considered before K_{IC} can be computed from an instrumented Charpy test. These factors, friction and specimen size, have opposing effects on K_{IC}, and the consequence of both must be ascertained near the fracture load during an impact rate test. However, the compliance data required are not normally available in a reliable and usable form. It seems that the friction problem is the most traceable, since size effects result directly from the specimen material properties and Charpy bar size.

References

[1] Barsom, J. M. and Rolfe, S. T. in *Impact Testing of Metals, ASTM STP 466,* American Society for Testing and Materials, 1970, p. 281.

[2] Sailors, R. H. and Corten, H. T., "Relationship Between Material Fracture Toughness Using Fracture Mechanics and Transition Temperature Tests," Heavy Section Steel Technology Program, 5th Annual Information Meeting, Paper No. 3, Oak Ridge National Laboratory, March 1971.

[3] Semar, D. J., Kallenberg, G. P., and Towner, R. J., "Fracture Toughness of Low Strength Steels," Report No. WAPD-TM-895, Bettis Atomic Power Laboratory, Pittsburgh, Pa. May 1971.

[4] Barsom, J. M. and Rolfe, S. T., *Engineering Fracture Mechanics,* Vol. 2, 1971, p. 341.

[5] Orner, G. M. and Hartbower, C. E., *The Welding Journal,* Vol. 40, No. 9, Sept. 1961, p. 405.

[6] Ronald, T. M. F., Hall, J. A., and Pierce, C. M., *Metallurgical Transactions,* Vol. 3, April 1972, p. 813.

[7] Hartbower, C. E. in *Impact Testing of Metals, ASTM STP 466,* American Society for Testing and Materials, 1970, p. 115.

[8] Tardif, H. P. and Marquis, H., *Canadian Metallurgical Quarterly,* Vol. 2, No. 4, Oct.-Dec. 1963, p. 373.

[9] Cotterill, B., *British Welding Journal,* Vol. 9, No. 2, 1962, p. 690.

[10] Radon, J. C. and Turner, C. E., *Engineering Fracture Mechanics,* Vol. 1, 1969, p. 411.

[11] Srawley, J. E. and Brown, W. F. in *Fracture Toughness Testing and Its Applications, ASTM STP 381,* American Society for Testing and Materials, 1965, p. 133.

[12] Brown, W. F. and Srawley, J. E. in *Plane Strain Crack Toughness Testing of High-Strength Metallic Materials, ASTM STP 410,* American Society for Testing and Materials, 1969, p. 1.

[13] Saxton, H. J., Ireland, D. R., and Server, W. L. in this symposium, pp. 50-73.

[14] Ireland, D. R., Effects Technology, Inc., Santa Barbara, Calif., private communication.

[15] Hoover, W. R. and Guess, T. R., "The Dynamic Fracture Toughness of CVD/FW and CVD/Felt Carbon-Carbon Composites and ATJ-S Graphite," Sandia Laboratories, Albuquerque, N. Mex., to be published.

[16] Server, W. L. and Tetelman, A. S., "The Use of Pre-Cracked Charpy Specimens to Determine Dynamic Fracture Toughness," UCLA Report ENG-7153, University of California, Los Angeles, July 1971.

[17] Greenfield, M. A. and Margolin, H., *Metallurgical Transactions,* Vol. 2, March 1971, p. 841.

[18] Thompson, A. W. and Saxton, H. J., "Structure, Strength, and Fracture of Electrodeposited Nickel and Nickel-Cobalt Alloys," Sandia Report No. SCL-DC-720058,

Sandia Laboratories, Livermore, Calif., Dec. 1972, to be published in *Metallurgical Transactions.*

[*19*] Srawley, J. E. and Gross, G., *Engineering Fracture Mechanics*, Vol. 4, No. 3, Sept. 1972, p. 587.

[*20*] Bucci, R. J., Paris, P. C., Landes, J. D., and Rice, J. R., "J-Integral Estimation Procedures," Scientific paper 71-IE7-FMPWR-P1, Westinghouse Electric Co., Pittsburgh, Pa., 1971.

[*21*] Watwood, V. G., *Nuclear Engineering and Design*, Vol. 11, 1969, pp. 323-332.

[*22*] Hayes, D. J. and Williams, J. G., *International Journal of Fracture Mechanics*, Vol. 8, No. 3, Sept. 1972, p. 239.

[*23*] Jones, A. T., *A Radially Cracked, Cylindrical Fracture Toughness Specimen*, SLL-73-5009, Sandia Laboratories, Livermore, Calif., 1973.

[*24*] Zienkiewicz, O. C., and Cheung, Y. K., *The Finite Element Method in Engineering Sciences*, McGraw-Hill, New York, 1971, p. 30.

[*25*] Priest, A. H. and May, M. J., BISRA Report No. MG/C/46169, The Inter-Group Laboratories of the British Steel Corporation, London, 1969.

[*26*] Paris, P. C. and Sih, G. C. in *Stress Analysis of Cracks, ASTM STP 381*, American Society for Testing and Materials, 1965, p. 59.

[*27*] Nelson, F. G., Schilling, P. E., and Kaufmann, J. G., *Engineering Fracture Mechanics*, Vol. 4, No. 1, March 1972, p. 33.

H. J. Saxton,[1] *D. R. Ireland,*[2] *and W. L. Server*[2]

Analysis and Control of Inertial Effects During Instrumented Impact Testing

REFERENCE: Saxton, H. J., Ireland, D. R., and Server, W. L., "Analysis and Control of Inertial Effects During Instrumented Impact Testing," *Instrumented Impact Testing, ASTM STP 563,* American Society for Testing and Materials, 1974, pp. 50-73.

ABSTRACT: To improve the understanding of load-time traces observed during instrumented impact testing, analytical and experimental studies have been conducted to determine the effects of inertial loading. The first load discontinuity in a load-time profile has been found to result from the interaction of a rapidly decreasing inertial load developed by Charpy specimens as they accelerate from rest and the finite ability of the instrumented tup to react to very rapid load transients. A model is developed which quantitatively correlates initial portions of load-time profiles for Al_2O_3 and U-3/4Ti with rigid-body accelerations of these materials. In addition, the magnitude of the initial load discontinuity is related to the acoustic impedances of the tup and specimen and the initial impact velocity in agreement with theory drawn from elastic wave mechanics. Successful correlation of this theory for a large variety of materials has allowed a semi-empirical relation to be developed for the prediction of inertial loads. Control procedures are suggested to both identify and reduce the role of inertial loads in instrumented impact testing.

KEY WORDS: impact tests, inertia effects, frequency response, fracture strength, crack propagation, transition temperature, stress waves, rigid body motion, toughness

When an instrumented impact test is conducted on a tough material,[3] frequently the load-time behavior detected by strain gages placed on the tup will contain features similar to those schematically illustrated in Fig. 1. During the initial loading of the tup, a discontinuity occurs before the load again increases. This study is concerned with: (1) the source and magnitude of the discontinuity and (2) the behavior of the load-time trace in its vicinity. For discussion purposes, the magnitude of the discontinuity is defined as the "inertial load", P_I, and this first discontinuity should be distinguished from later oscillations (Fig.

[1] Supervisor, Material Characterization Division, Sandia Laboratories, Livermore, Calif. 94550.

[2] Managers, Dynatup Operations and Services, respectively, Effects Technology, Inc., Santa Barbara, Calif. 93105.

[3] A tough material is defined as one which undergoes general yielding and work hardens prior to unstable crack propagation, while a brittle material is defined as one which fails prior to general yielding.

1) which appear most prominently following rapid changes in deflection rate (for example, at the onset of general yielding and following unstable crack propagation).

The presence of inertial loads in published oscilloscope traces of instrumented impact tests, beginning with the work of Cotterell [*1*][4] and frequently thereafter [*2-16*], has been the subject of several physical interpretations. Three

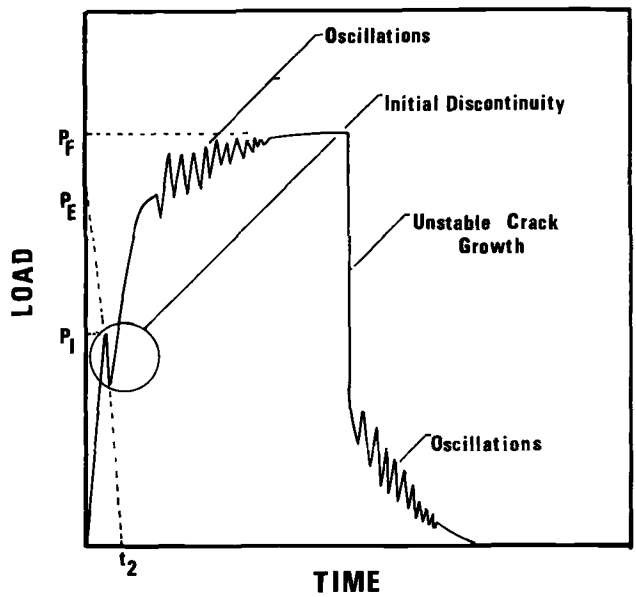

FIG. 1–*Schematic of load-time behavior frequently recorded for a tough material; time* t_2 *results from a linear extrapolation.*

possible interpretations include:

1. Treating the Charpy specimen as an accelerating and decelerating rigid body.
2. Treating the impact machine and specimen as an oscillating spring mass system.
3. Treating the impact event as a one- to three-dimensional dynamic wave propagation problem.

These interpretations are related in two ways. First, they each attempt to model the initial dynamic response of a Charpy specimen following the impact contact of the tup on the specimen. Second, in the order listed, each interpreta-

[4]The italic numbers in brackets refer to the list of references appended to this paper.

tion is successively a more general description of dynamic interactions. A complete wave propagation analysis can describe the motion of rigid bodies, but the application of rigid-body mechanics can be quite limited when applied to dynamic problems. Before discussing previous work leading to these interpretations, a clear definition of what the term "inertial loading" means in this study is necessary. Beginning with impact of the tup, the Charpy bar's response is governed by a complex interaction of tensile and compressive stress waves propagating throughout the specimen. The energy transferred to the specimen by these waves produces mechanical bending, system ringing, and acceleration of the specimen mass to the velocity of tup. All three load contributions are sensed by an instrumented tup. Inertial loading is defined as that portion of the load placed upon the tup resulting from specimen acceleration.

Cotterell [*1*] used elastic wave theory to account for the initial discontinuity in his load traces, and he suggested that the subsequent unloading following the discontinuity resulted from initial passage of reflected tension waves within the tup. His belief that dynamic wave propagation controlled the initial portion of the load-time trace was supported by the observation that the "initial impact load" for mild steel (he did not call it an inertial load) was directly proportional to the impact velocity. This proportionality has been verified for a number of materials in this study. Together with elastic wave propagation theory, the proportionality will be used to develop a semi-empirical relationship for predicting inertial loads.

Although Fearnehough and co-workers [*2,3*] agreed with Cotterell that the initial discontinuity resulted from a tensile reflection, Radon and Turner [*4-7*] disagreed. This decision was based upon the observation that similar load oscillations were found when specimens were struck with totally different forms of striker heads. In addition, these investigators believed that for the first brief period of impact, about 10 μ s, the measured load on the tup is caused by the specimen acting solely as a reacting mass. In fact, tests conducted without supporting anvils produce inertial loadings comparable to those measured with supports, and bending produced in the unsupported specimen produces fractures in steel tested at –196°C (–321°F) [*5*].

Based upon their findings, Radon and Turner developed a quantitative model for identifying inertial contributions to measured load-time traces. In their model, it is assumed that each particle in the specimen undergoes constant acceleration from the moment of impact until the instant of fracture. Upon reexamination, however, the authors concluded that this correction is inadequate because its magnitude depends upon the crack length-to-width ratio (a/W) for the impacted specimen. Experimental observations in this study suggest that the magnitude of the inertial loading may be independent of a/W (Fig. 11*b* and *c*). Radon and Turner's assumption that the acceleration during initial impact loading is constant also conflicts with the simple model presented in this study.

Venzi, Priest, and May [*8,9*] have treated inertial loading as a series of

oscillations whose performance may be modeled by a spring-mass system. These workers have thereby predicted system frequencies and specimen loads after initial impact. The method requires instrumentation of the anvil as well as tup; example traces presented in their studies, however, indicate that the inertial loading often completely subsides before the anvil registers its first load [*9*]. Therefore, events prior to the first load discontinuity recorded by the tup should be separated from the aforementioned spring-mass description because at the moment of impact the load is solely exchanged between the specimen and reacting tup. In the present study, the initial loading is treated as solely a tup-specimen interaction.

An excellent review of the measurement of fracture loads during instrumented impact tests has been presented by Man and Holzmann [*10*]. They point out that the inertial loading results from the impulse imparted from the tup to the specimen as it changes momentum from zero. They also note that the inertial load increased with impact velocity; in fact, their data (Fig. 7 in Ref *10*) support a linear relationship. In agreement with Radon and Turner [*5*], inertial loads exceeding fracture loads and inertial loading of nonsupported specimens were found.

In the present study, the effect of system frequency response upon measured inertial loads also will be discussed. Reduction in the measured amplitude of fast-changing loads has been noted by both Turner [*6*] and Man and Holzmann [*10*]. Later discussion will show that the existence of the inertial load discontinuity is a result of limited frequency response.

Inertial Loading Model

The first step in developing this model is to separate, for discussion purposes, the three major contributions to the loading of a tup observed during impact testing:

1. Mechanical bending loads.
2. Test system ringing.
3. Inertial acceleration loads.

In actual testing, all contributions assume varying degrees of importance depending on the toughness of the material tested, its acoustic impedance, and the portion of the test being studied. The test system ringing can be related to the vibrational bending of the specimen itself [*11*], and presents itself as an oscillating signal of about 20 kHz about the mean load path. Hence it can be often averaged out of the problem. At longer times ($> 50\,\mu$s for tougher materials) the mechanical bending response of the specimen clearly dominates the load being recorded. However, the load immediately following impact and certainly in the first 20 μs of the test is dominated by an inertial exchange between the tup and the specimen [*8,9*]. It is this portion of the test which will be treated in the model.

When the specimen is struck by the tup, it is accelerated rapidly from rest to an average velocity equal to the tup velocity. The maximum inertial load should

occur near the moment of impact and become zero when the specimen attains the tup velocity. At the same time, the specimen begins to respond mechanically, and finally that response dominates measured loads as the test progresses. The total process (without ringing) is schematically illustrated for a tough material in Fig. 2. As will be shown later, in brittle materials the entire mechanical performance including fracture can be completed while the specimen is still being accelerated. The fact that the actual behavior illustrated in Fig. 2 indicates a load near zero time, and oscilloscope-recorded traces indicate no load (Fig. 1), is related to the fact that electronic and strain-gage systems have finite response times. The maximum load at impact and hence the maximum acceleration of the specimen is governed by the dynamic properties, specifically the acoustic impedances, of the tup and the specimen being tested. An estimate of this load can be obtained by assuming that at the instant of impact, one-dimensional stress wave theory for planar impact applies. In particular, the magnitude of the initial elastic stress wave generated at the impact interface is given by [*17*]

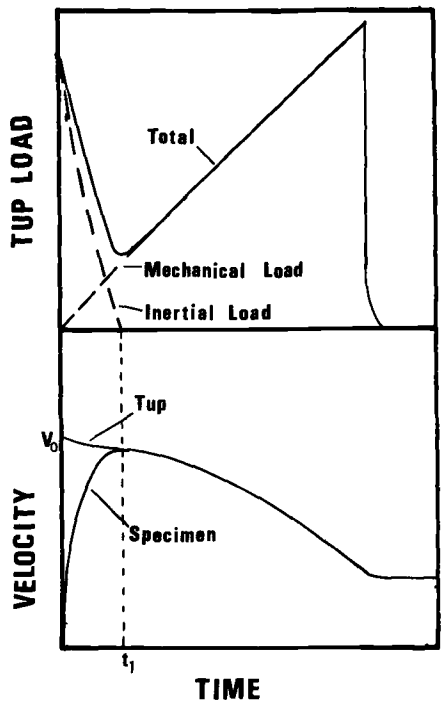

FIG. 2–*Schematic of the load-time and velocity-time behavior actually experienced by an impacting tup along with the velocity-time behavior of a tough material specimen being tested;* t_1 *is the time required for the specimen to reach velocity equilibrium with the tup.*

$$\sigma = \frac{Z_1 Z_2}{Z_1 + Z_2} V_0 \tag{1}$$

where

Z_i = $C_{Di}\rho_i$ acoustic impedance of material i,
C_{Di} = dilation sound speed,
ρ_i = density, and
V_0 = initial tup velocity.

This relation bounds the initial load and acceleration which can be imposed upon the specimen, and will be used in the following to analyze inertial load data. In addition, it will be assumed that a designated portion of the load-time profile at times earlier than t_2 (Fig. 1) contributes solely to rigid-body acceleration of the Charpy specimen. For calculation purposes, it will be assumed that this rigid-body motion can be described in one of the two ways idealized in Fig. 3. Pure rigid-body translation would qualitatively agree with the findings of Priest, May, and co-workers [*8,9*], which showed that the initial inertial transient measured at the impact tup fully decays to zero load before the supporting anvil detects initial loading and three-point bending begins. On the other hand, pure rigid-body rotation would qualitatively agree with findings that specimens virtually precracked through the specimen exhibit about the same inertial loads as normally precracked specimens. As later discussion will show, good correlations between experiment and analysis can be obtained using either assumption.

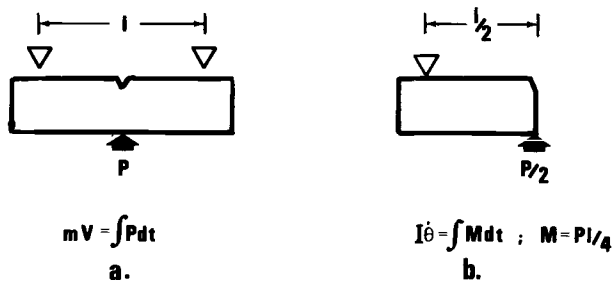

FIG. 3–*Models used for rigid-body acceleration calculations: (a) rigid-body acceleration leading to a translation velocity* V; *(b) rigid-body acceleration leading to a rotational velocity* $\dot{\theta}$.

The foregoing model is hypothesized to achieve the following goals in this study:

1. Verify that the initial loading discontinuity observed in impact traces is related to a simple rigid-body acceleration process and the limited frequency response of the instrumented system.

2. Using elementary elastic wave mechanics (Eq 1), develop a semi-empirical method for predicting inertial loads.

3. Develop a method for controlling inertial effects during impact testing.

Experiments

Procedures

The basic experimental procedure followed in this study was to gather values of the inertial load, P_I (Fig. 1), for a large variety of materials tested at different initial impact velocities. In all cases, except that for CVD/felt (carbon-carbon composite) specimens, the data were collected on a 325-J (240-ft·lb) Satec impact machine located at Effects Technology, Inc., or on a (128-ft·lb) PhysMet impact machine located at Sandia Laboratories, Livermore, Calif. Both machines are instrumented with the Dynatup System Model 500. With one exception, all the data were collected at system frequency response settings of 100[5] or 40 kHz; the CVD/felt data were collected at 20 kHz. Table 1 lists the test system, system frequency response setting, initial velocity range studied, dilatation sound speed, density, and acoustic impedance of materials tested. The data have been collected and presented without regard to a/W, which varies from machine-notched Charpy specimens ($a/W = 0.2$) to Charpy specimens precracked in excess of $a/W = 0.98$.

A special series of impact tests was performed at Sandia Laboratories, Livermore upon machine-notched specimens fabricated from Al_2O_3 and U-3/4Ti. While the U-3/4Ti specimens were machined to standard dimensions, the Al_2O_3 specimens were 2.900 in. (73.66 mm) long, 0.394 in. (10.00 mm) wide, and 0.500 in. (12.70 mm) thick. In these tests load and velocity information were recorded using 900 ± 300 kHz VCO's on an Ampex 1900 tape recorder running at 120 in./s (3.05 m/s) and providing a 2-MHz frequency response. The information was played back for digital data manipulation with an Ampex FR1600 providing a 1.5-MHz frequency response. During the playback, EMR universal tunable demodulators were used with a 32:1 tape speed reduction being used. The objective in those experiments was the collection of highly time-resolved data for rigid-body acceleration calculations. Al_2O_3 and U-3/4Ti represent interesting examples for inertial load testing because, while they both have large acoustic impedances, U-3/4Ti is about five times more dense than Al_2O_3. Tests were carried out at impact velocities of 159, 73.5, and 39.5 in./s (4.04, 1.87, and 1.00 m/s) while the system frequency response was maintained at 100 kHz.

Results

Figures 4 and 5 are plots of the inertial load as a function of initial impact velocity for Charpy specimens tested under system frequency responses of 40 and 100 Hz, respectively. The linear relationship between load and velocity is the most obvious feature of the two plots. This same relationship was noted by

[5]The 100-kHz setting for the Model 500 includes no electronic filters; however, system frequency response as a whole is about 100 kHz.

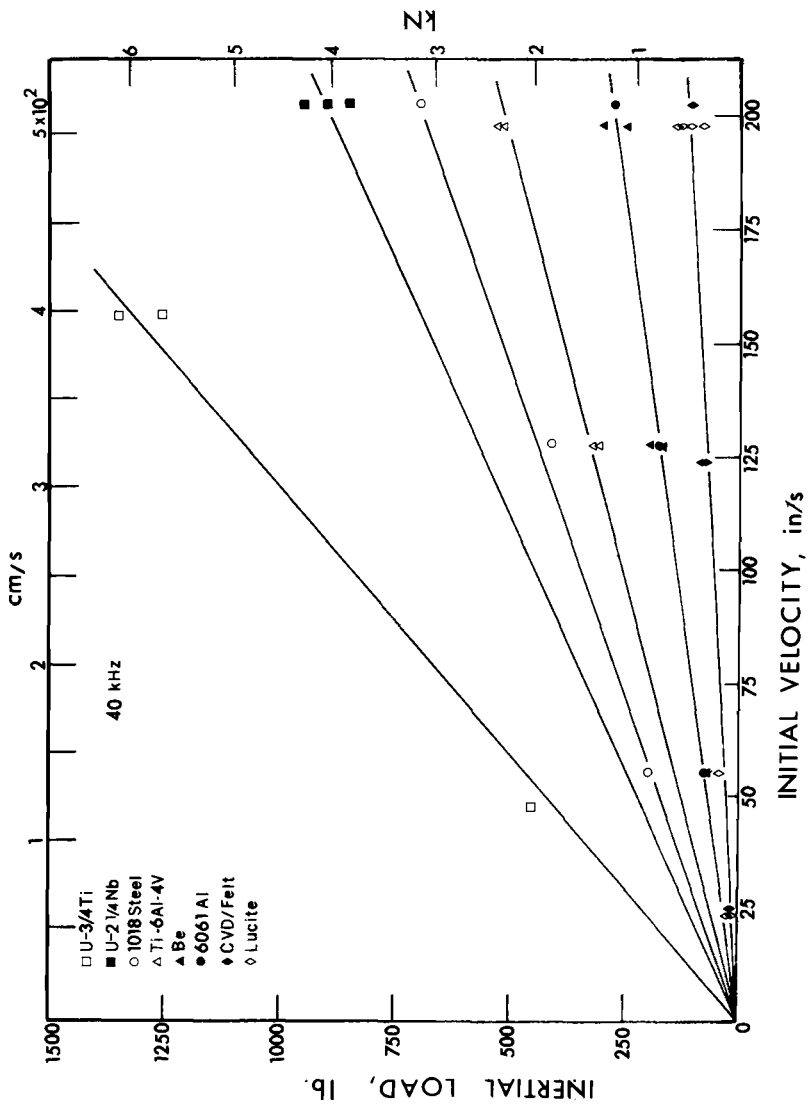

FIG. 4—*Inertial load versus initial impact velocity for a system frequency setting of 40 kHz.*

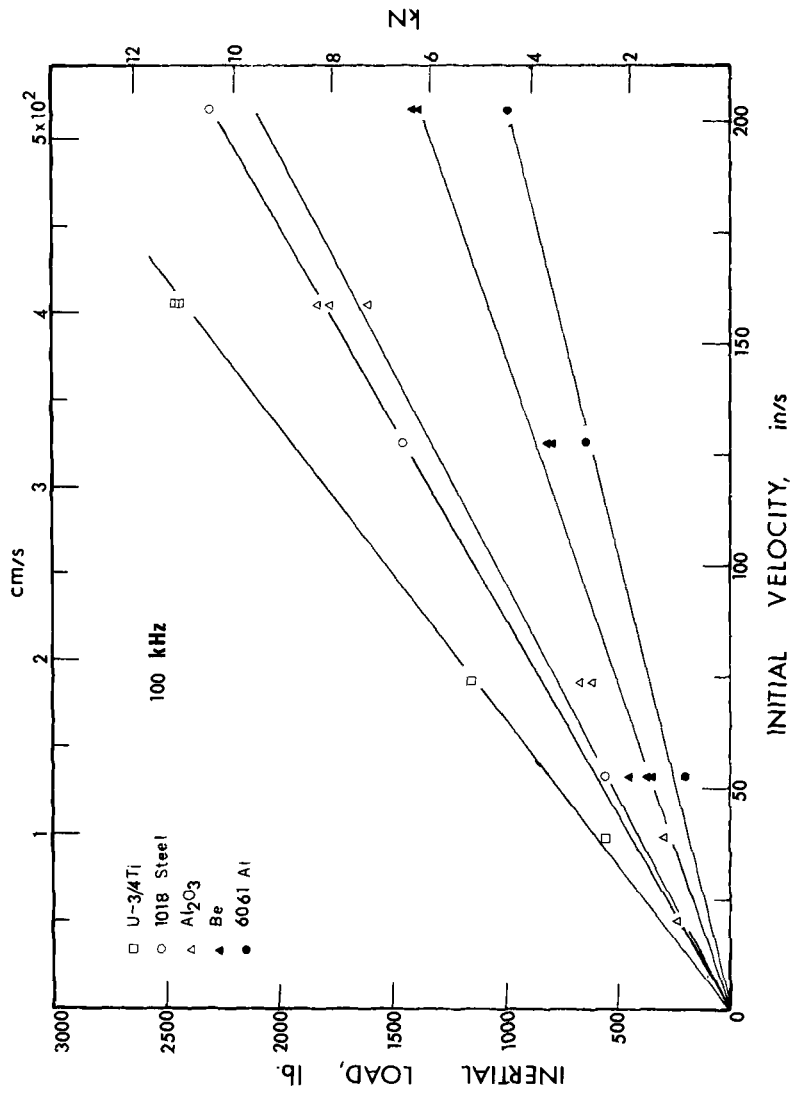

FIG. 5—*Inertial load versus initial impact velocity for a system frequency setting of 100 kHz.*

TABLE 1—*Test conditions and acoustic properties.*

	Material	Test System	System Frequency Response, kHz	V_o Range in./s	V_o Range cm/s	C_D cm/s	ρ, g/cm^3	Z, g/cm^2 s
1.	U2-1/4Cb	Satec	40	203	(516)	3.52×10^5	18.4	64.8×10^5
2.	1018 Steel	Satec	40	54-203	(137-516)	5.94	7.87	46.8
3.	Ti-6A1-4V	Satec	40	127-197	(323-500)	6.05	4.47	27.0
4.	Be	Satec	40	54-197	(137-500)	12.5	1.85	23.2
5.	6061 A1	Satec	40	54-203	(137-516)	6.31	2.70	17.0
6.	CVD/Felt	Satec	40	10-203	(25-516)	2.97	1.80	5.35
7.	Lucite	Satec	40	24-197	(61-500)	2.88	1.18	3.4
8.	U-3/4Ti	PhysMet	40	47-156	(119-396)	3.52	18.4	64.8
9.	U-3/4Ti	PhysMet	100	39.5-159	(100-404)	3.52	18.4	64.8
10.	1018 Steel	Satec	100	54-203	(137-516)	5.94	7.87	46.8
11.	$A1_2O_3$	PhysMet	100	21.7-159	(55-404)	10.55	3.67	38.7
12.	Be	Satec	100	54-203	(137-516)	12.5	1.85	23.2
13.	6061 A1	Satec	100	54-203	(137-516)	6.31	2.70	17.0

TABLE 2—*Rise time resulting in 10% reduction of input signal.*

System Frequency Setting, kHz	Critical Rise Time for 10% Reduction, μs
100	9
40	150
20	247
10	555

Cotterell [*1*] in impact tests on steel. Recently Man and Holzmann [*10*] presented without comment a number of example traces which exhibited the same linear relationship for another low-carbon steel. Second, consistently lower values for P_I are recorded at 40 kHz than at 100 kHz. Third, reference to Table 1 will show that the measured inertial loads increase with impedance of the material being tested.

Figures 6 and 7 exhibit example traces recorded for the special series of tests performed upon Al_2O_3 and U-3/4Ti. The changes in the shapes of these curves with initial impact velocity provide a useful illustration of the relative importance of inertial loading and mechanical loading during the progress of the total loading cycle. The traces indicate that inertial loading and mechanical loading contributions interacted less in the Al_2O_3 experiments, and hence rigid-body accelerations are expected to be more accurate for that material. These traces clearly illustrate the decrease of P_I with initial velocity, while U-3/4Ti exhibits a constant fracture load of about 3200 lb (14 kN).

Discussion

Frequency Response

As pointed out earlier, an inspection of the initial conditions of the impact indicate that the tup and specimen will undergo a near instantaneous load rise at time zero as illustrated in Fig. 2. However, because of the limited frequency response of the instrumentation, finite rise times (Figs. 6 and 7) are required to reach the maximum inertial load, P_I, measured in a test.

An analysis of the frequency response of the Dynatup instrumentation using Fourier techniques has revealed the limitations in response time caused by the inherent capabilities of the system and the additional limitations imposed when electronic filtering circuits are used to smooth rapidly oscillating signals. Table 2 lists the rise times which correspond to a 10 percent reduction in the actual signal when observed on the oscilloscope trace for each system setting. Longer or shorter rise times will produce respectively less or more attenuated recorded signals. Along with the reduction in amplitude of a fast rising signal on a recorded trace, another result of limited system frequency response is longer times to record maximum tup loads than the tup actually experiences. The total effect of attenuated magnitudes and extended times is demonstrated in Fig. 8, which displays how the Dynatup system responds to a square wave input at 100- and 40-kHz settings.

The inherent response time of the system is accurately reflected in the time of at least 10 μs necessary to reach maximum load in the load-time traces illustrated in Figs. 6 and 8. Priest and May [*8,9*] exhibit traces in their studies which display rise times between 5 and 6 μs. Because of the higher frequency response of their impact system, inertial loads exceeding 4000 lb (18 kN) were measured for steel at a V_o of 216 in./s (5.49 m/s). This inertial load can be compared to Dynatup values of about 2500 lb (11 kN) and 750 lb (3.3 kN),

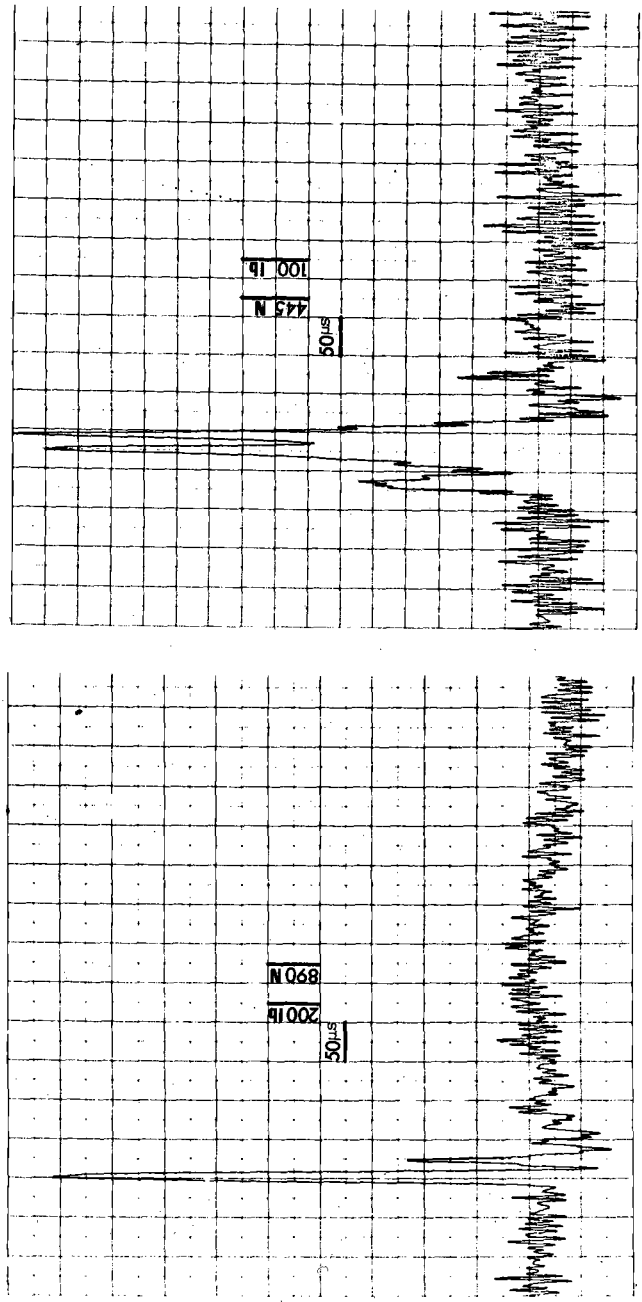

a. V_o = 159 in./s (4.04 m/s)

b. V_o = 39.5 in./s (1.00 m/s)

FIG. 6—*Load-time traces representative of special test series performed on machine-notched* Al_2O_3 *at 100 kHz: (a)* V_o = *159 in./s (4.04 m/s); (b)* V_o = *39.5 in./s (1.00 m/s).*

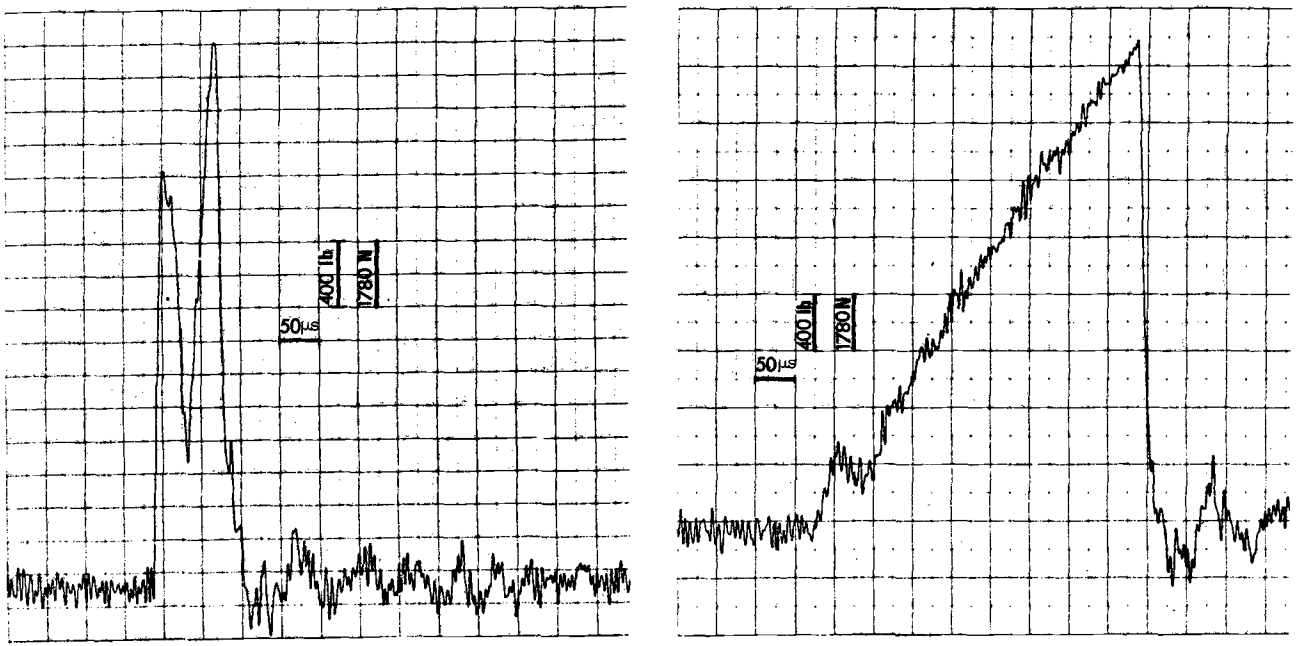

a. V_o = 159 in./s (4.04 m/s)

b. V_o = 39.5 in./s (1.00 m/s)

FIG. 7—*Load-time traces representative of special test series performed on machine-notched U-3/4Ti at 100 kHz: (a)* V_o *= 159 in./s (4.04 m/s); (b)* V_o *= 39.5 in./s (1.00 m/s).*

respectively, for tests run at 100 kHz (9-μs rise time) and 40 kHz (150-μs rise time). Therefore, ample experimental evidence exists that faster instrumentation places the maximum recorded inertial load closer to time zero.

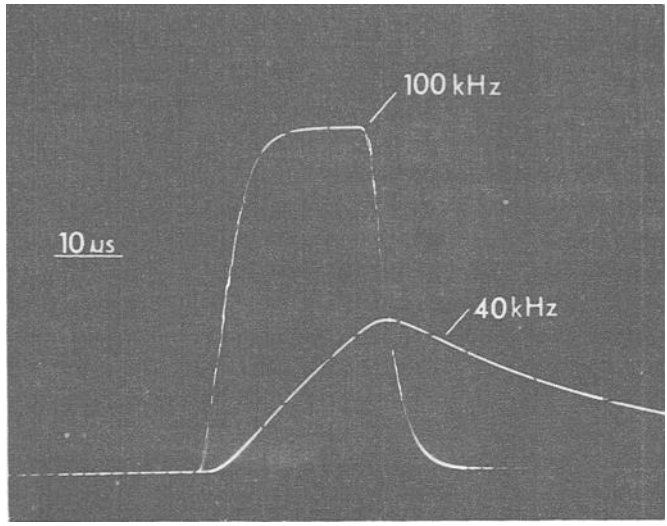

FIG. 8–*The response of the impact instrumentation to a square wave generator input at system frequency settings of 40 and 100 kHz.*

Given that the measured load-time traces used to calculate $\int Pdt$ (P = load) in the rigid-body analysis contain systematic errors, the following extrapolation schemes will be used. First, the time required for the specimen to reach tup velocity, t_2, will be defined by linearly extrapolating the inertial slope to the time axis (Fig. 1). A maximum inertial load, P_E, can be estimated by linearly extrapolating the inertial slope to the load axis. Referring to Fig. 6*a*, it can be seen that the approximately 10-μs response time also controls how fast the load decrease can be recorded since $t_2 \approx 20$ μs. The foregoing discussion has shown that actual inertial acceleration times (t_1 in Fig. 2) are smaller than the value estimated by linear extrapolation of a recorded trace (t_2 in Fig. 1). In addition, a smaller actual time means that the actual P_E should be higher than the extrapolated value. In light of these probable errors, two $\int Pdt$ areas (Fig. 1) have been selected for calculation:

1. The area, A_E, bounded by the origin, P_E, and t_2.
2. The area, A_I, bounded by the origin, P_I, and t_2.

Rigid-Body Acceleration

In Table 3 are listed the areas A_E and A_I for each of the impact tests

TABLE 3—*Comparison of actual masses and calculated masses.*

	Material	V_o in./s	A_E lb/s	A_I lb/s	Actual m', lb-mass/in.^{2}	m'_E, lb-mass/in.^{2}	m'_I, lb-mass/in.^{2}	Actual m, lb-mass	m_E, lb-mass	m_I, lb-mass
1.	Al_2O_3	159	3.8×10^{-2}	1.9×10^{-2}	1.73×10^{-4}	5.60×10^{-4}	2.80×10^{-4}	1.98×10^{-4}	2.39×10^{-4}	1.20×10^{-4}
2.	Al_2O_3	159	3.28	1.64	1.73	4.83	2.42	1.98	2.06	1.03
3.	Al_2O_3	73.5	1.82	0.870	1.73	5.80	2.77	1.98	2.47	1.26
4.	Al_2O_3	73.5	1.69	0.845	1.73	5.38	2.69	1.98	2.30	1.19
5.	Al_2O_3	39.5	0.990	0.499	1.73	5.86	2.95	1.98	2.51	1.15
6.	U-3/4Ti	159	12.97	7.42	6.78	28.82	16.15	5.78	8.16	4.67
7.	U-3/4Ti	159	12.97	7.42	6.78	28.82	16.15	5.78	8.16	4.67
8.	U-3/4Ti	73.5	6.80	3.30	6.78	32.03	15.55	5.78	9.26	4.45
9.	U-3/4Ti	39.5	3.33	2.55	6.78	29.16	22.33	5.78	8.43	6.42

conducted, along with the initial velocity (V_o), the actual mass/unit area m', and mass m for the Al_2O_3 and U-3/4Ti specimens tested. Assuming that the initial velocity is equal to the velocity at the end of inertial acceleration introduces an error of only 0.1 percent or less into the rigid-body calculations to follow. To show that inertial acceleration is responsible for the initial load transient, the following equations will be used to calculate the specimen mass and mass/unit area for comparison with the actual values, respectively, for Al_2O_3 and U-3/4Ti:

Rigid-body translation

$$m_E = \frac{A_E}{V_o} \tag{2}$$

$$m_I = \frac{A_I}{V_o} \tag{3}$$

Rigid-body rotation

$$m'_E = \frac{I^2}{8V_o} \quad \frac{A_E}{C} \tag{4}$$

$$m'_I = \frac{I^2}{8V_o} \quad \frac{A_I}{C} \tag{5}$$

where $I = Cm'$, and C is a dimensional constant equal to 0.1322 in.^{4} (5.503 cm^4) for the large Al_2O_3 specimens and 0.0895 in.^{4} (3.725 cm^4) for standard U-3/4Ti specimens. The results of these calculations are also listed in Table 3. In all cases, the predicted values agree with the actual values within a factor of five, and in general a larger error is found in predictions based upon rotation than those based on translation. With only one exception, the area A_E is found to predict a higher mass than actual while the area A_I is found to predict a lower mass than actual when calculations are based upon rigid-body translation. In the case of Al_2O_3, where the separation between inertial and mechanical loads is most pronounced, the actual mass is predicted within a factor of 2 or less. Because of the uncertainties introduced by frequency response of the system, it is difficult to pinpoint systematically the expected errors in the extrapolation schemes used to obtain A_E and A_I. Within these uncertainties of measurement, however, it appears that the initial load discontinuity results solely from an inertial reaction between the specimen and tup. Hence this discontinuity can be separated from later oscillations which result from system flexural response.

One source of error not yet discussed in detail is the $\int Pdt$ expended on the mechanical response of the Charpy bar during the acceleration period. Since the inertial impulse decreases as the initial velocity decreases, larger differences between calculated and actual specimen masses should occur because the mechanical response becomes important in comparison to the inertial loads. This hypothesis is verified by the Al_2O_3 data, which generally indicate that the calculated mass or mass/unit area increases with decreasing V_o. In addition, the shape of the load-time traces in Figs. 6 and 7 indicates that mechanical response plays a larger role in U-3/4Ti than in Al_2O_3, and this factor is reflected in larger positive errors.

Inertial Load Estimation

Referring to the plots of P_I versus V_o in Figs. 4 and 5, the linear dependence of these two variables leads to the conclusion that Eq 1 taken from one-dimensional wave propagation theory may control the value of P_I measured in impact tests. In addition, P_I appears to increase with specimen impedance in both plots. Even in view of the attenuation due to frequency response, and the fact that the total impact process is at least a two-dimensional problem, Eq 1 provides a guide for inertial load prediction.

To predict inertial loads, a semi-empirical approach can be devised by normalizing all the data taken at one frequency to the steel data. The normalization factor is derived in the following way (noting that a steel tup is used in all the experiments):

1. The initial impact stress for a steel specimen is given by

$$\sigma_1 = \frac{Z_1}{2} V_o$$

where Z_1 is the impedance of steel.

2. The initial impact stress for a specimen fabricated from Material 2 is given by

$$\sigma_2 = \frac{Z_1 Z_2}{Z_1 + Z_2} V_o$$

where Z_2 is the impedance of Material 2.

By assuming that the measured inertial load P_I is directly proportional to the initial stress generated at the impact interface, the normalization factor becomes

$$P_2/P_1 = \frac{2Z_2}{Z_1 + Z_2} \tag{6}$$

Using the data for Z_i given in Table 1, normalized inertial data are generated with Eq 6 and plotted in Figs. 9 and 10. The normalization process greatly reduces the spread of data observed in Figs. 6 and 7, and allows semi-empirical expressions to be developed for inertial testing in terms of pounds and inches per second:

For 100 kHz
$$P_I = \frac{22.80\, Z_2 V_o}{Z_1 + Z_2} \pm 20\% \tag{7}$$

For 40 kHz
$$P_I = \frac{7.34\, Z_2 V_o}{Z_1 + Z_2} \pm 40\% \tag{8}$$

The equations as written may be used to estimate the inertial load developed by a Satec or PhysMet impact machine equipped with Dynatup Model 500

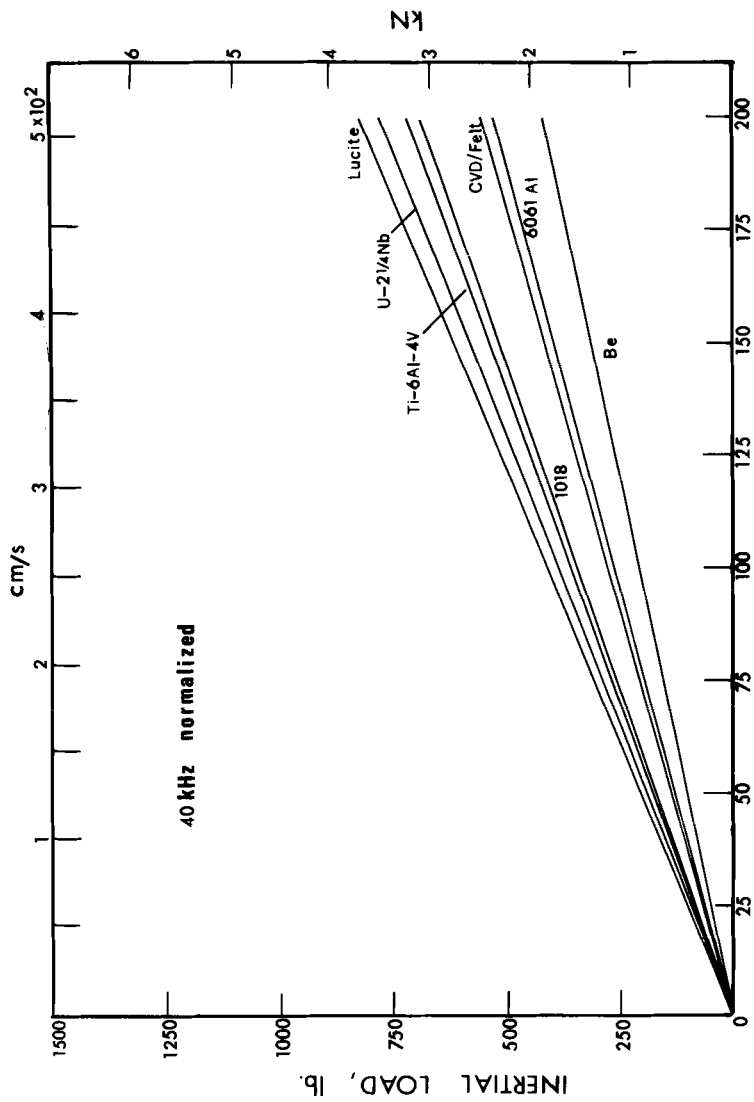

FIG. 9—*Normalized inertial load versus initial impact velocity for a system frequency setting of 40 kHz.*

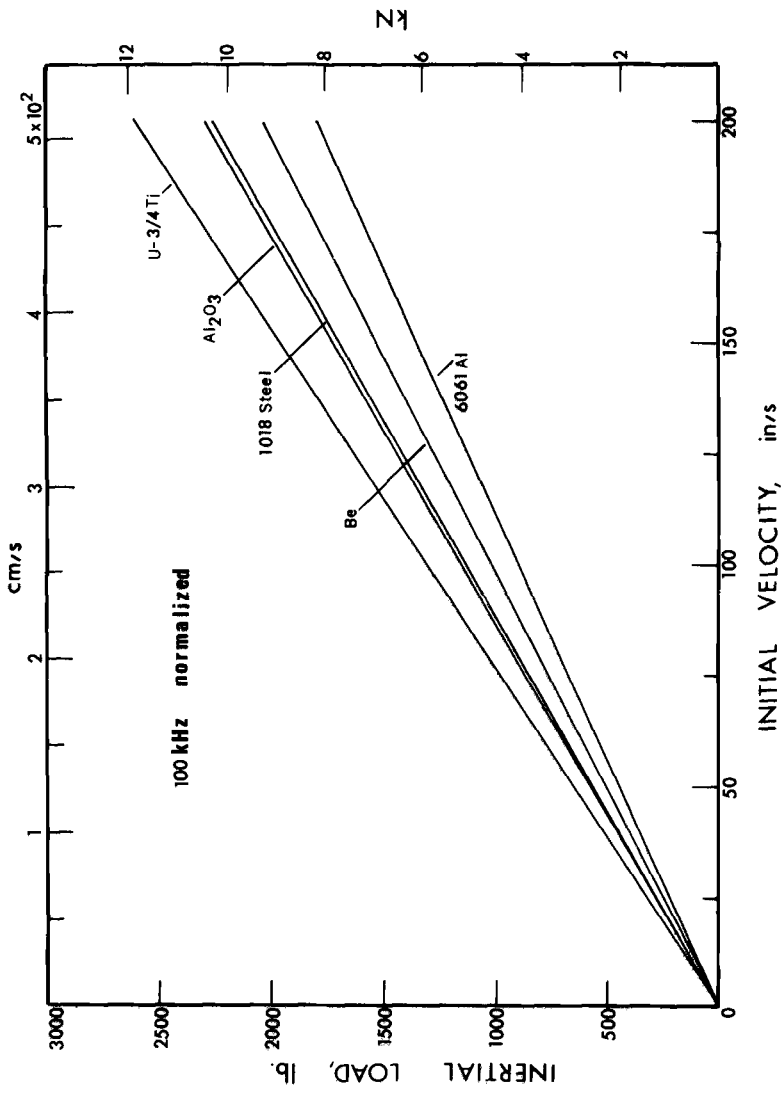

FIG. 10—*Normalized inertial load versus initial impact velocity for a system frequency setting of 100 kHz.*

instrumentation. Earlier discussion has shown that changes in instrumentation response due to differences in machine or electronics design can strongly affect measured inertial loads. An example is provided by the large difference in P_I recorded for U2-1/4 Cb on the Satec and U-3/4Ti on the PhysMet at 40 kHz (Fig. 4). Equations similar to Eqs 7 and 8 can be determined for any specific system by running a series of impact experiments on steel Charpy bars over a range of impact velocities, and then applying the impedance normalization factor given in Eq 6.

Therefore, use of these relationships allows the experimenter to predict both absolute values of inertial load for new materials being tested and the way the inertial load will vary with changes in V_0. It is interesting to note that while rigid-body mechanics adequately describe the total acceleration of the specimen to tup velocity, prediction of the initial acceleration requires the principles of elastic wave mechanics.

Inertial Load Control

With the understanding gained by the hypothesis and verification of the inertial model presented, methods for control of inertial effects during impact testing can be devised. First, the inertial load (P_I in Fig. 1) has been uniquely defined as the point of first-load discontinuity in recorded load-time traces. Depending upon the impedance, strength, and ductility of the material being impacted, the inertial load can assume varying degrees of importance. Several schematic examples are provided in Fig. 11. In the first three cases, the inertial and mechanical loading contributions can be easily identified, and hence confidence can be placed in choosing the correct value of P_F (Fig. 11*a,b,c*) for K_{Ic} calculations. If crack extension force, G, calculations are desired, it is possible to estimate the quantity E/A (E = energy expended in forming the fracture surface area A) by: (1) extrapolating the mechanical loading portion of the trace to zero time and (2) assuming that E can be calculated from the cross-hatched area in Fig. 11*a,b,c* [*16*]. The real danger arises when interpreting load-time traces of medium- to high-strength materials which are brittle and exhibit a medium to high impedance. Examples of such materials include Al_2O_3, precracked U-3/4Ti, and precracked mild steel tested at −196°C (−321°F). When impact is tested, the entire mechanical response curve can lie within the inertial loading curve (Fig. 11*d*). With this type of impact response, it is impossible to identify directly P_F or E. Radon and Turner [*4-7*] developed their inertial load correction model because they suspected the existence of this problem in the low-temperature testing of steels. This difficulty in obtaining unambiguous values of P_F and E/A from brittle specimens is disappointing because these very materials are candidates for valid K_{Ic} testing at high strain rates.

This problem was graphically demonstrated in a series of transition temperature tests from −196 to +130°C (−321 to +266°F) conducted on precracked U-3/4Ti specimens (Fig. 12). In these tests the apparent P_F remained

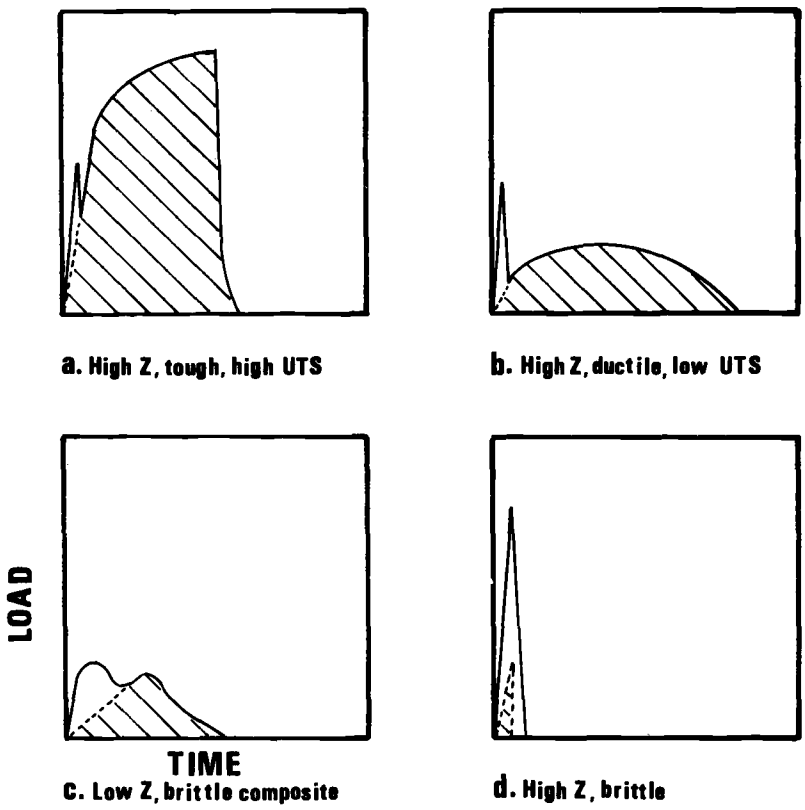

FIG. 11—*Schematic examples demonstrating the interrelationship of impedance (Z), and materials properties. Typical example materials for each figure include: (a) mild steel at room temperature, (b) copper, (c) CVD/felt, (d) mild steel at −196°C (−321°F) and precracked U-3/4Ti (see Fig. 12).*

constant in the vicinity of 1300 lb (5.8 kN) except for the 130°C (266°F) test, where a double peak was observed. Until temperature increases had sufficiently raised the toughness of the material so that $P_F > P_I$, the inertial load of 1300 lb had dominated the load-time trace and masked any transition temperature behavior which the material could be exhibiting.

As indicated by Eq 1 and the data presented in Figs. 6 and 7, inertial load effects can be controlled by varying the initial impact velocity. For both Al_2O_3 and U-3/4Ti, the inertial loads are reduced from a major to minor contribution as the impact velocity is reduced from 159 the 39.5 in./s. This reduction in velocity, equivalent to reducing the energy capacity of the PhysMet impact machine from 128 to 8 ft·lb (175 to 11 J), is still more than adequate to break Al_2O_3 and precracked U-3/4Ti Charpy specimens. Unless very high strain rates are a part of a system design requirement, the experimentalist should: (1) not

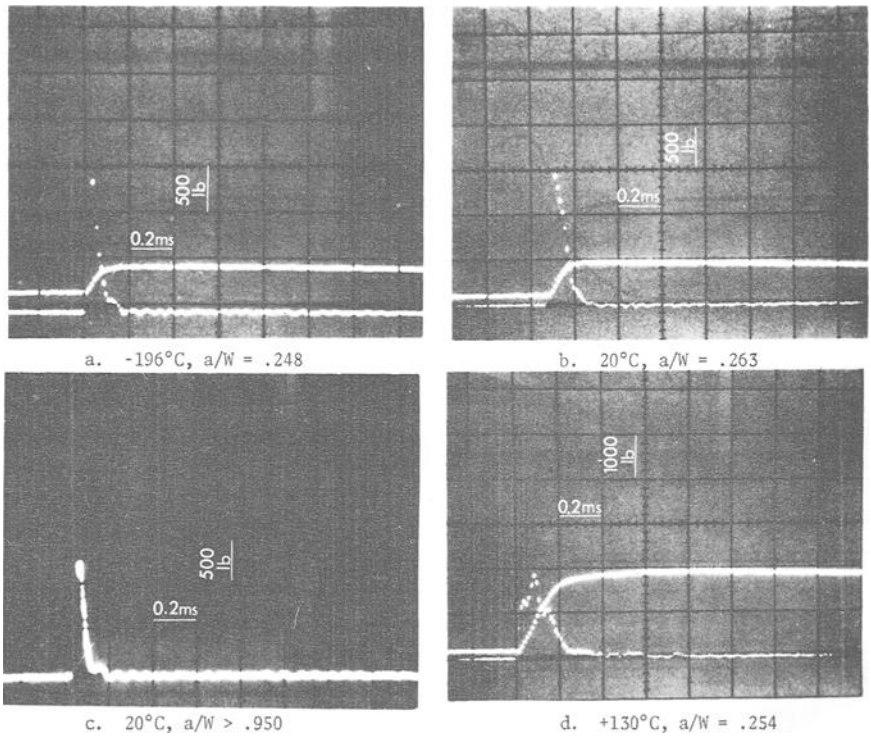

FIG. 12–*Typical load-time traces recorded during impact testing of precracked U-3/4Ti Charpy specimens using a* V_o *of 156 in./s (4.04 m/s) and a system frequency setting of 40 kHz: (a) –196°C (–321°F),* a/W = *0.248; (b) 20°C (68°F),* a/W = *0.263; (c) 20°C (68°F),* a/W > *0.950; (d) +130°C (+266°F),* a/W = *0.254.*

feel restricted to the preset hammer velocities provided by commercial machines and (2) change the hammer velocities to values consistent with obtaining valid performance loads and energies.

Equations 7 and 8 also indicate that changing the tup material will change the measured inertial load. Therefore, an aluminum tup should produce lower inertial loads than steep tups.

To summarize this discussion on inertial loading control, the following set of procedures is suggested. First, expected inertial loads can be predicted using the semi-empirical methods described. Second, a small number of tests can be performed over a range of hammer velocities, and if the impact instrumentation is adequately responsive, an inertial load discontinuity will be observed in every trace. Then an adequately small velocity can be chosen to reasonably separate the maximum mechanical load from the inertial load. With reasonable separation, more confidence can be placed in P_F as the maximum mechanical load the specimen can support. If a material is not strain-rate sensitive (like

U-3/4Ti in Fig. 7), the P_F will remain constant while impact velocities and inertial loads are reduced. A single sharp peak in a load trace is indicative of a test dominated by inertial loading.

Finally, it should be noted that when standard Charpy impact tests are performed without strain-gage instrumentation, the dial energy measured is the sum of all the contributions. Without load-time profiles, one must depend on experience alone to evaluate whether the energy values measured are representative of the fracture resistance of the material, or whether the fracture resistance is being masked by inertial effects.

Conclusions

During this study, the first load discontinuity in load-time profiles has been identified as a feature of inertial loading caused when the Charpy specimen is rapidly accelerated from rest to the tup velocity. The discontinuity itself results from the interaction of a rapidly decreasing inertial load (maximum inertial load is developed upon initial impact) and the finite ability of the instrumented tup to react to very rapid load transients (finite frequency response). The importance of understanding the systematic errors (lower measured loads and longer measured times) introduced by limited frequency response has been emphasized.

A quantitative correlation of extrapolated inertial load-time profiles shows that the loads recorded during the first stage of an impact are dominated by the rigid-body acceleration of the specimen by the impacting tup. During this time, the mechanical bending load plays a minor role. The flexural response of the system appears to be responsible for the oscillations which are recorded after the first load discontinuity.

The linear dependence of the inertial load, P_I, upon the initial impact velocity, V_o, coupled with the systematic increase of P_I with the acoustic impedance of the material, has led to the conclusion that the initial load imparted to the specimen is governed by elementary elastic wave mechanics. Use of Eq 6 allows a successful normalization of P_I data and leads to the development of two useful semi-empirical relations (Eqs 7 and 8). These relations allow the experimentalist to predict in advance the inertial loading of a new material when the test is being conducted upon a Satec or PhysMet impact machine equipped with Dynatup Model 500 instrumentation. When other systems are used, similar relations can be developed by performing a few tests on mild steel over a range of impact velocities.

With the understanding of inertial load-time profiles gained in this study, it is possible to institute control procedures which allow the experimentalist to: (1) unambiguously identify both the inertial load and maximum mechanical load, and (2) reduce (mainly through control of V_o) the inertial load contribution to load-time profiles.

Acknowledgments

The authors wish to thank T. Mamaros and W. M. Clift for fatigue precracking the specimens and for performance of the impact tests, J. J. Totten for the high-speed taping and computer data reduction of the special test series, R. Bertolotti for providing the Al_2O_3 specimens, and A. W. Thompson for reviewing the manuscript. This work was performed under the auspices of the United States Atomic Energy Commission, Contract AT-(29-1)-789, and Effects Technology, Inc.

References

[1] Cotterell, B., *British Welding Journal,* Vol. 9, No. 2, Feb. 1962, p. 690.
[2] Fearnehough, G. D. and Joy, C. J., *Journal of the Iron and Steel Institute*, Vol. 202, Nov. 1964, pp. 912.
[3] Fearnehough, G. D. and Nichols, R. W., "Fracture Mechanics Considerations in the Charpy Impact Test," Technical Report X-410-67E, United Kingdom Atomic Energy Authority, Reactor Materials Laboratory, Culcheth, United Kingdom, 1967.
[4] Radon, J. C. and Turner, C. E., "Fracture Toughness Measurements by Instrumented Impact Test," Mechanical Engineering Department Technical Report, Imperial College of Science and Technology, London, England, Nov. 1967.
[5] Radon, J. C. and Turner, C. E., *Engineering Fracture Mechanics*, Vol. 1, No. 3, 1969, p. 411.
[6] Turner, C. E. in *Impact Testing of Metals, ASTM STP 466,* American Society for Testing and Materials, 1970, p. 93.
[7] Turner, C. E., Culver, L. E., Radon, J. C., and Kennish, R., *Journal of Institution of Mechanical Engineers*, Vol. C6, 1971, p. 38.
[8] Venzi, S., Priest, A. H., and May, M. J. in *Impact Testing of Metals, ASTM STP 466*, American Society for Testing and Materials, 1970, p. 165.
[9] Priest, A. H. and May, M. J., "Fracture Toughness Testing in Impact," BISRA Open Report MG/C/46/69, The Inter-Group Laboratories of the British Steel Corporation, London, England, 1969.
[10] Man, J. and Holzmann, M., *Journal of the Iron and Steel Institute*, Vol. 208, Feb. 1970, p. 199.
[11] Tardif, H. P. and Marquis, H., *Canadian Metallurgical Quarterly*, Vol. 2, No. 4, Oct.-Dec. 1963, p. 373.
[12] Augland, B., *British Welding Journal*, Vol. 9, No. 7, July 1962, p. 434.
[13] Almond, E. A. and Embury, J. D., *Metal Science Journal*, Vol. 2, 1968, p. 194.
[14] "Interpretation of the Instrumented Impact Test," Document X-458-68 I.I.W., International Institute of Welding, Commission X, Jan. 1969.
[15] Taran, A. V., *Metallovedenie i Termicheskaya Obrabotka Metallov*, No. 6, June 1970, p. 37..
[16] Hoover, W. R. and Guess, T. R., "The Dynamic Fracture Toughness of CVD/FW and CVD/Felt Carbon-Carbon Composites and ATJ-S Graphite," Sandia Report No. 73-0449, Sandia Laboratories, Albuquerque, N. Mex., May 1973.
[17] Wasley, R. J., *Stress Wave Propagation in Solids*, Dekker, New York, 1973.

W. L. Server [1] *and D. R. Ireland*[1]

Nonstandard Test Techniques Utilizing the Instrumented Charpy and Izod Tests

REFERENCE: Server, W. L. and Ireland, D. R., "**Nonstandard Test Techniques Utilizing the Instrumented Charpy and Izod Tests,**" *Instrumented Impact Testing, ASTM STP 563,* American Society for Testing and Materials, 1974, pp. 74-91.

ABSTRACT: The Charpy impact test is rapidly being upgraded to include instrumentation for revealing the load history of the specimen while it is being fractured in three-point bending. Unfortunately, similar interest in upgrading the Izod test (cantilever bending) has been notably lacking. The first part of this paper discusses the results of a recent study of techniques for instrumenting the Izod test. Results from both standard and nonstandard Izod specimen tests are compared with similar results from instrumented Charpy tests. Also included are the results of instrumented Izod tests of tubular specimens of aluminum, steel, and composite materials.

Instrumented low-blow testing and three-point bend testing of ring-shaped specimens are typical variations of the instrumented Charpy impact test. These two test techniques are also discussed in this paper. There is hope that these and other variations in test techniques will lead to new inexpensive methods of evaluating material and small structure behavior under adverse loading conditions.

KEY WORDS: impact tests, dynamic tests, nonstandard tests, instrumented impact, tests, metals, composite materials

Since the work of Fearnehough and Hoy [*1*][2] in 1964, the electronics and techniques for use of the instrumented standard Charpy impact test have been upgraded and developed for many diverse applications. To meet the increasing need for reliable material performance under adverse conditions (for example, impact loading), economical and efficient test techniques are desired. Basic variations in instrumented Charpy testing and the application of instrumented three-point bend technology to cantilever bending (Izod) may help to implement these needs.

The first part of this paper deals with instrumented Izod testing. This study applied the major ingredients of the instrumented Charpy test to the Izod test. Results from both standard and unusual Izod samples are discussed and, in some

[1] Manager, Dynatup Services, and assistant director, Materials Engineering Technology, Inc., Santa Barbara, Calif. 93105.

[2] The italic numbers in brackets refer to the list of references appended to this paper.

cases, compared with results from instrumented Charpy tests. The paper also describes two variations in instrumented Charpy impact testing, low-blow testing, and three-point bend testing of ring-shaped samples. The former involves use of an impacting mass with maximum kinetic energy equal to or less than that required to completely fracture the test specimen.

Equipment

A standard Model 500 Dynatup System was used for the instrumented impact tests. The Dynatup System is essentially a three-component system for use with conventional impact testing machines to monitor the dynamic behavior and supply a precision analog output signal of the load-time history of the impacted test piece. The three components are the instrumented tup or dynamic load cell, an amplifier-oscilloscope system for signal display, and a reliable device for triggering the oscilloscope sweep. In this study, a Biomation Model 802 high-speed transient signal record was employed as a backup device to ensure the recording of the load-time record.

Impact tests were performed on a Satec 240-ft·lb-capacity machine and a Tinius Olsen 50-in·lb-capacity machine. The former met all requirements of ASTM Notched Bar Impact Testing of Metallic Materials (E 23) [*2*], and the latter met those for ASTM Tests for Impact Resistance of Plastics and Electrical Insulating Materials (D 256) [*3*].

Instrumented Izod

Although a cantilever bend test using a pendulum-type hammer is normally called an Izod test (after E. G. Izod), it is interesting to note that the Izod test, as well as the Charpy test, need not be performed solely with a pendulum machine; Mr. Izod himself [*4*] discusses cantilever bending in terms of both a pendulum machine and a vertical drop weight machine. However, all impact tests, including the Izod, should be updated with instrumentation to allow the dynamic load history of the test sample to be recorded. This additional information presents a more thorough knowledge of the total fracture process, which can aid in both materials selection and design.

The inherent differences in the shapes of the two tups make instrumentation of the Izod test quite different from that for the Charpy test. It is crucial for the strain gages to produce a signal which is a good analog of the response of the test specimen. An empirical approach to selection of the appropriate strain-gage position was employed by evaluation of three different locations on an Izod tup for a 240-ft·lb Satec machine (Fig. 1*a*). These positions sensed three strains: compression (similar to that normally used for the Charpy tup), shear, and compression bending. With the amplifier gain set at the same value for each of the strain-gage positions, low-blow tests (totally elastic) were performed by dropping the hammer from the same low height. The results from these tests are shown in Fig. 1*b*. The compression and shear gages produce distorted signals and

the outputs are less than one third that of the bending gages. It was also found that the output from the bending gages is linear with load up to approximately 10 000 lb. Therefore, the bending gages were selected for subsequent use in instrumented Izod testing.

Figure 2*a* shows the instrumented tup for the Tinius Olsen 50-in·lb-capacity machine. Because of the particular position of the tup in the impact head, the gages had to be placed in tension bending rather than compression bending. The output from this tup was also found to be linear with the applied load. A typical oscillograph record of the load-time and energy-time traces from an instrumented Izod test using this tup on a PMMA specimen is shown in Fig. 2*b*. The energy-time trace is an electronic integration of the load-time signal and is displayed directly in energy units by the Dynatup dynamic response module.

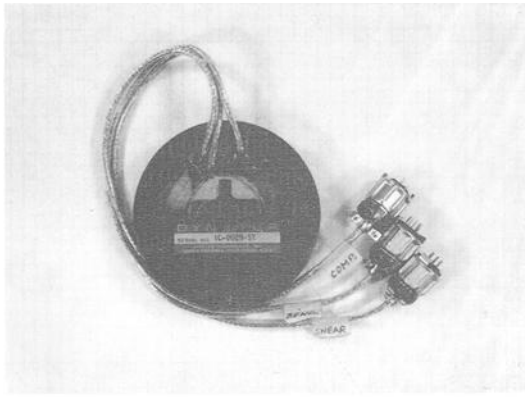

(a). Instrumented Izod Tup With Strain Gages in Three Different Positions

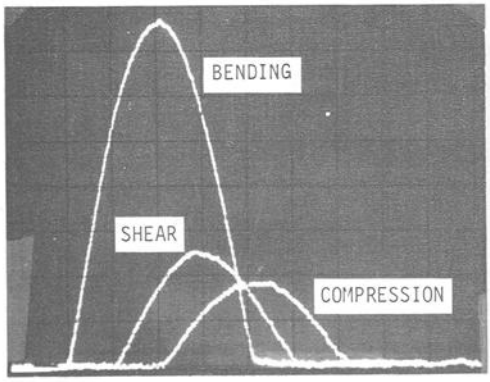

(b). The Output From the Three Sets of Gages

FIG. 1

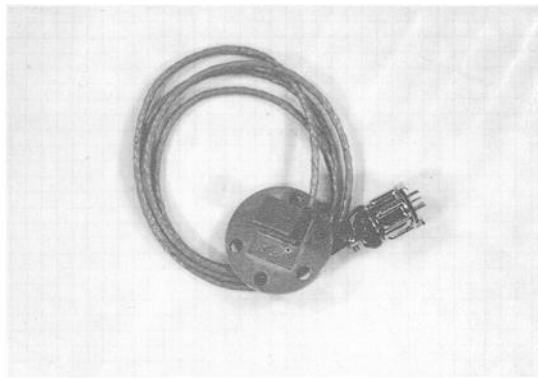

(a). Instrumented Izod Tup for a Tinius Olsen Plastics Machine - Strain Gages are in Tension Bending

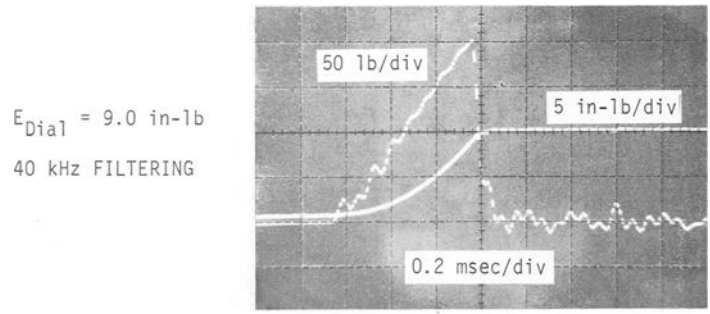

(b). Oscillograph from an Instrumented Izod Test on PMMA

FIG. 2

The test record for a standard Izod specimen is compared with that for a standard Charpy specimen in Fig. 3. For these specimens, most of the dimensions are the same, but the bending moments at the fracture area are different. The bending moment (M) for a Charpy specimen is $PL/4$, where P is the applied load at the center and L is the total support span. For units of lb·in., this reduces to $M \simeq 0.40P$. The corresponding bending moment for an Izod test is $P\ell$, where P is the applied load again and ℓ is the moment arm. Again for units of lb·in., this reduces to $M \simeq 0.87P$. To compare the Izod test with the Charpy test, two approaches were taken. The first approach employed tests of standard Izod and Charpy samples for a comparison of dynamic yield strengths as determined from the general yield loads. The second approach was to test precracked Izod and Charpy samples to compare dynamic plane-strain fracture toughness

values obtained from the fracture loads in tests where fractures occurred before general yield.

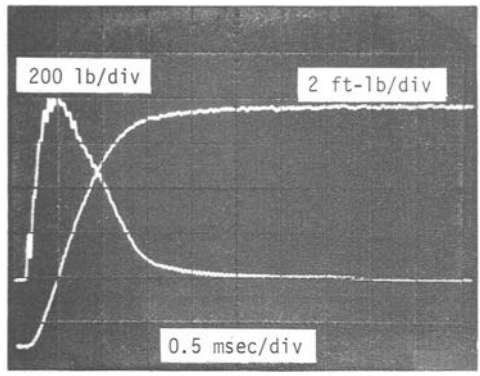

(a). Instrumented Izod

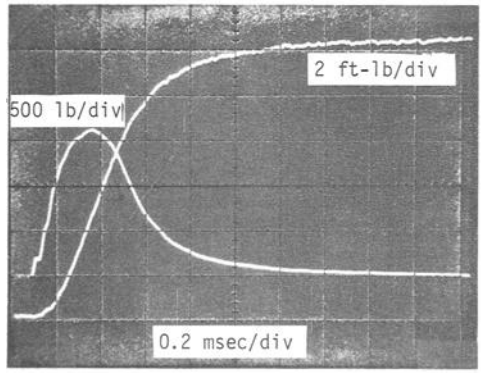

(b). Instrumented Charpy Test Records for 6061 T6 Aluminum

FIG. 3

A strain-rate independent aluminum alloy (6061-T6) was used for the general yield comparison, and typical test records are shown in Fig. 3. It is difficult to determine the general yield load in both cases since the yielding event is not as well-defined as in other materials. However, using a criterion of the first deviation from linearity, averages from three tests of each type of specimen give general yield loads of 650 lb and 1230 lb, respectively, for the Izod and Charpy tests. Conversion of these loads to yield strength values is a relatively simple

procedure for direct comparison, and in both cases these values should equal the static value of $\simeq$ 40 ksi. These calculations employed the slip-line field analysis of Green and Hundy [5] which has been reviewed by Server and Ireland [6] to adjust for specimen dimensional changes. For the dimensions of the standard Charpy specimen, the analysis reduces to

$$\sigma_y = 33.33\, P_{GY} \tag{1}$$

where P_{GY} is the general yield load in pounds and σ_y is the yield strength in psi. Using the Charpy test value of 1230 lb for P_{GY}, σ_y becomes 40.9 ksi, which is in very good agreement with the static value. For the Izod specimen and loading geometry, the slip-line field analysis reduced to

$$\sigma_y = 72.0\, P_{GY} \tag{2}$$

The yield strength value obtained from the Izod test of 6061-T6 aluminum is 46.8 ksi. This value is slightly higher than the static and that from the Charpy test; however, the difference may in part be due to the difficulty in accurately discerning the general yield load for the load-time record.

In the second comparison, fatigue precracked Izod and Charpy samples of 1014 steel were broken. Figure 4 shows typical oscillographs from each type of test. The fracture load data obtained from six Charpy tests were converted to dynamic fracture toughness [7] (K_{Id}) values, and the average of the six tests is 35.0 ksi-in.$^{1/2}$. Since there is no standard method of converting cantilever bend loads to fracture toughness, a comparison only utilizing the bending moments was used. The conventional three-point bend formula [7] for relating crack length variations to stress intensity factors was employed for the Izod test analysis with an adjustment made for the differences in bending moments. The average K_{Id} value obtained from three Izod tests was 34.4 ksi-in.$^{1/2}$. The values from three-point bend and cantilever bend are in excellent agreement.

It is interesting to note that the total fracture energy values obtained from Izod and Charpy tests are quite close for both the standard and precracked specimens (Figs. 3 and 4. Although the Izod maximum loads are about half the Charpy loads, the total fracture time for the Izod specimen is much longer. Thus, the load difference is compensated by the increased time and deflection to fracture.

Philpot Izod specimens (see Ref 2 for dimensions) of quenched and tempered 4145 steel were also broken and the results compared with those for standard Charpy tests of the same material. Figure 5 shows typical test records and the corresponding fracture surfaces. The Izod maximum loads are again about half the Charpy loads, but the total energies to fracture are approximately the same

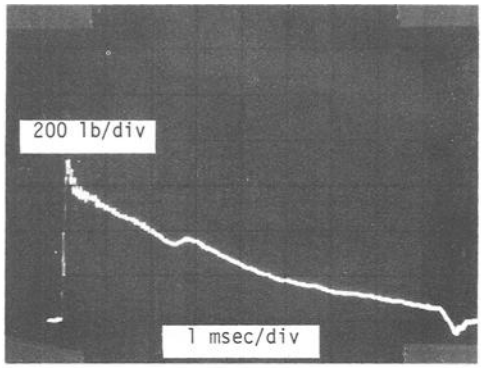

E_{Dial} = 22.5 ft-lb
a = 0.103 in
E/A = 236 in-lb/in^2
40 kHz FILTERING

(a). Instrumented Izod

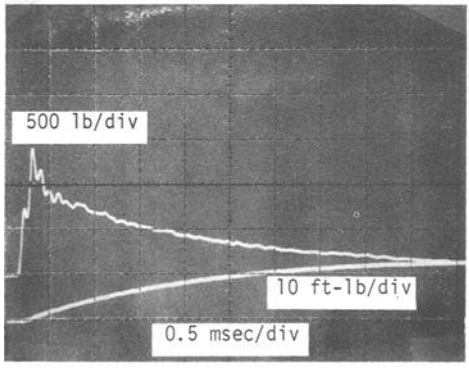

E_{Dial} = 18.0 ft-lb
a = 0.120 in
E/A = 200 in-lb/in^2
40 kHz FILTERING

(b). Instrumented Charpy Test Records for Precracked 1014 Steel

FIG. 4

(the total area, A, below the notch is approximately the same: Philpot A = 0.121 in.^{2} and Charpy A = 0.124 in.^{2}). The Philpot specimen is considered a nonstandard test by ASTM E 23 [*2*]. It is more difficult in this case to compare the fracture processes since the geometries are different; however, both tests reveal general yielding, exhibit fast fracture after reaching maximum load, and the fracture surfaces have about the same amount of flat fracture area.

Instrumented Izod tests of tube specimens of materials considered for golf club shafts were performed using a special anvil support designed to hold the curved specimens. Photographs of the broken specimens and the corresponding oscillographs are shown in Fig. 6. The fracture process for each type of material can be clearly identified from the load-time signal in the oscillograph. Table 1

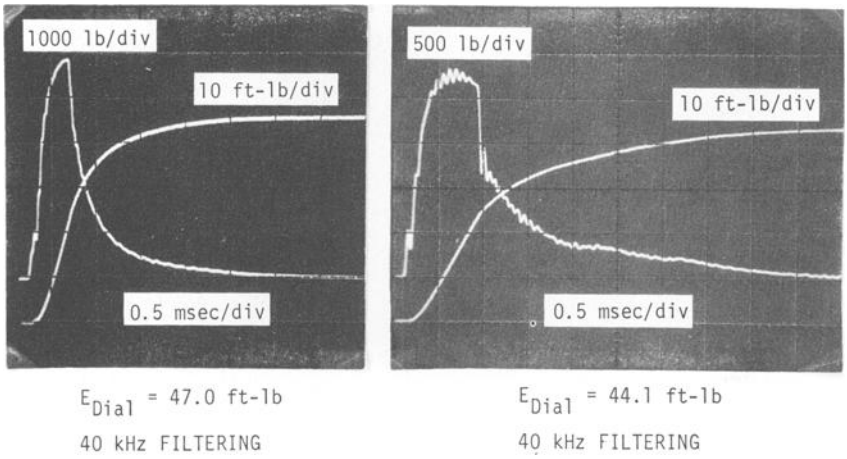

FIG. 5—*Comparison of instrumented Charpy and instrumented Izod (Philpot specimen) test records for 4145 quench and tempered steel.*

lists various parameters obtained from the oscillographs and a brief description of the fracture process. It is convenient to partition the loads and energies for a more complete understanding of how the fracture process progressed (that is, initiation energy is the energy consumed to reach maximum load and propagation energy is the subsequent energy expended to complete the fracture process). The compliance values were obtained from low-blow tests, which will be described in the following section. It is interesting to note the high compliance values for the steel samples; the high values are due to the thin wall thickness of these tubular specimens.

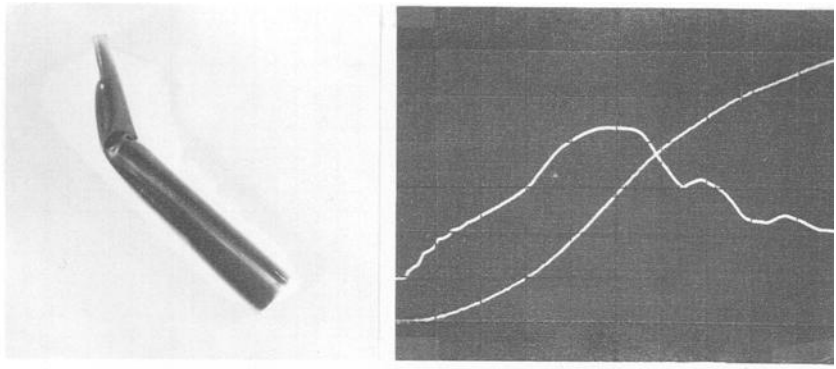

(a). Steel - E_{Dial} = 37.0 ft-lb

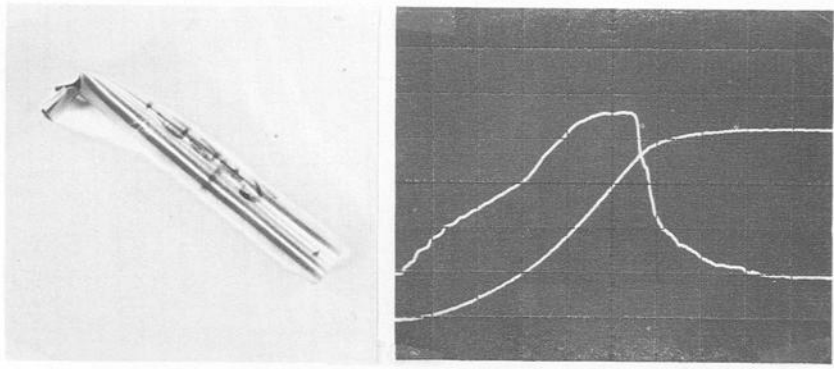

(b). Stainless Steel - E_{Dial} = 21.9 ft-lb

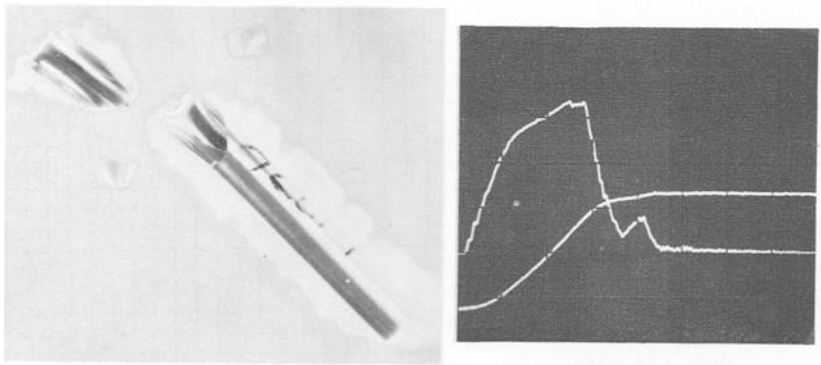

(c). Aluminum - E_{Dial} = 12.5 ft-lb

FIG. 6–*Instrumented Izod tests of tubular specimens. All test settings were: 200 lb/div, 5 ft·lb/div, 0.5 ms/div, 40 kHz filtering.*

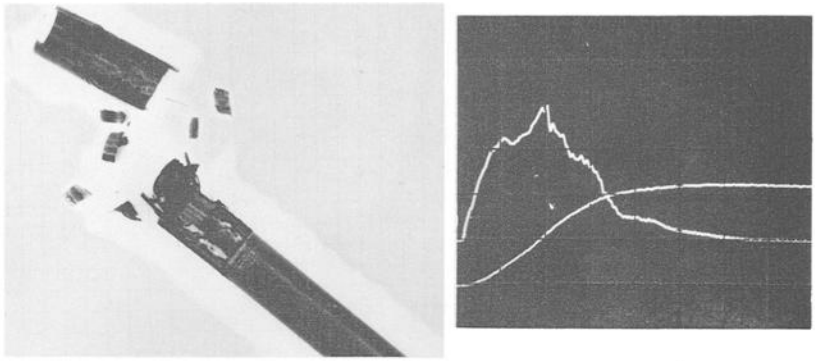

(d). Graphite Composite - E_{Dial} = 11.0 ft-lb

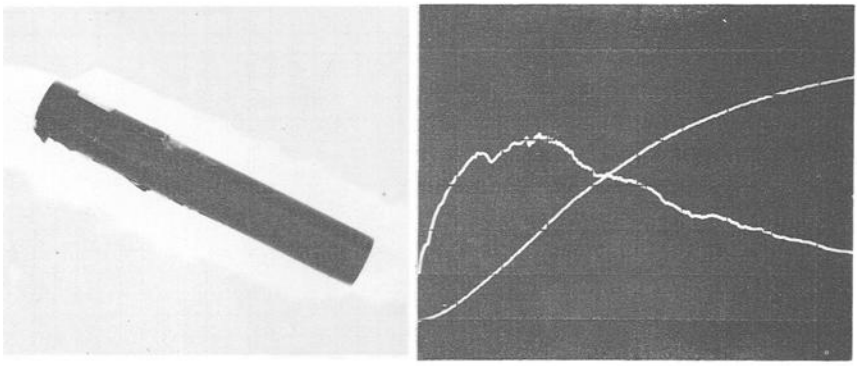

(e). Graphite/Fiberglass Composite - E_{Dial} = 31.8 ft-lb

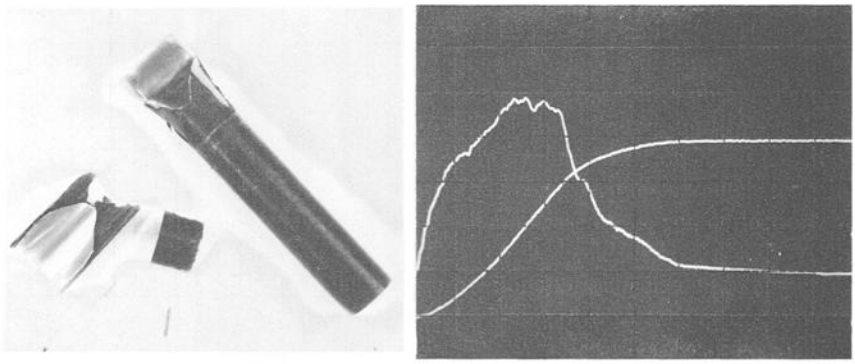

(f). Graphite/Aluminum Composite - E_{Dial} = 19.0 ft-lb

FIG. 6–*(Continued).*

TABLE 1–*Instrumented Izod testing of tubes.*

Material	Tube Wall Thickness, in.	Total Energy, ft·lb	Initiation Energy, ft·lb	Propagation Energy, ft·lb	Maximum Load, lb	Compliance, in./lb	Description of Fracture Process
Steel	0.03	37.0	17.0	20.0	660	21.0×10^{-4}	crushing at tup impact area, bending over at base support area
Stainless steel	0.03	21.9	16.8	5.1	720	20.0×10^{-4}	crushing at tup impact area, shearing at tup impact area
Aluminum	0.07	12.5	8.4	4.1	660	6.9×10^{-4}	initial yielding at tup impact area, brittle fracture at impact area
Graphite composite	0.11	11.0	5.9	5.1	590	6.0×10^{-4}	shattering at impact area, delamination at compressive surface near the base support
Graphite-fiberglass composite	0.12	31.8	9.9	21.9	610	6.0×10^{-4}	bending over at base support and springing back
Graphite-aluminum composite	0.11	19.0	10.0	9.0	760	4.5×10^{-4}	delamination and yielding at tup impact area, fast fracture of aluminum opposite tup impact partially contained by composite layer

Instrumented Low Blow

Low-blow testing originally meant hitting the test specimen with two successive blows; the first blow does not have enough energy to fracture the specimen, and the second blow is a full impact using the total available energy. Low-blow testing has been performed for various purposes since the Charpy test has been in existence; for instance, Orner and Hartbower [*8*] used low-blow testing to induce a type of "precrack" in Charpy specimens. Tardif and Marquis [*9*] extended the low-blow technique to instrumented impact testing. By further extending these initial ideas, a new connotation for low-blow testing can be achieved. Beginning with a very low impact energy, successive tests can be performed at increasing levels of energy until the first amount of damage is observed by the appearance of the load-time signal (see Fig. 7). The energy level at which first damage is observed can be used as a threshold value and might later be used in design as a damage tolerance criteria.

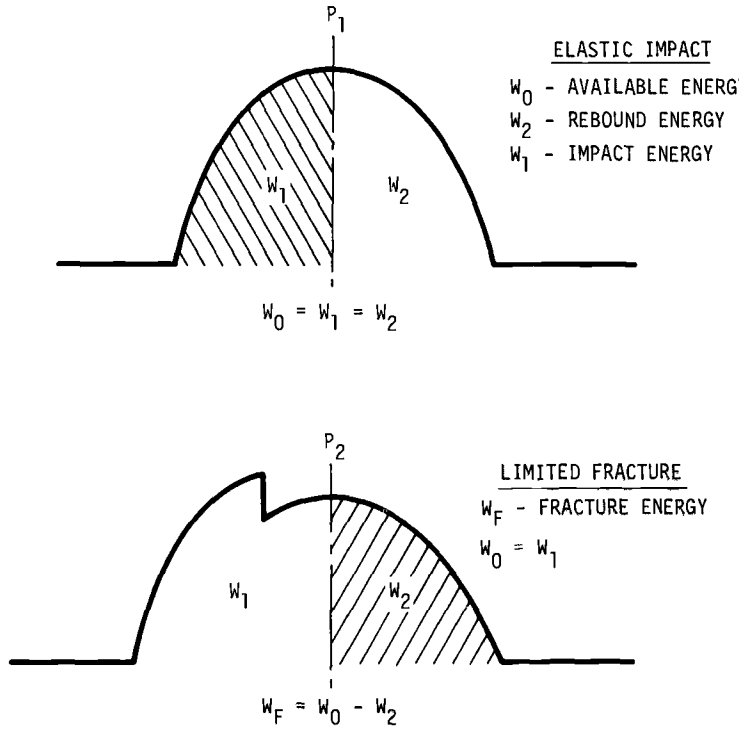

FIG. 7–*Schematic diagram of low-blow test records.*

Typical results from instrumented low-blow testing are shown in Figs. 8 and 9. The most common materials to which this approach has been applied are composites and surface-treated metals (namely, carburized bars, coatings). In Fig. 8 the velocity (and energy) were increased until the carbon-plastic composite began to delaminate. The initial blows before damage appears are totally elastic. The carburized bar test results shown in Fig. 9 illustrates initial elastic responses until the energy becomes great enough (~ 16 ft·lb) to cause limited plastic deformation. The highest level of impact (~ 20 ft·lb) eventually causes the outside carburized layer to crack, as can be seen in the oscillograph.

The low-blow test can also be used to determine the compliance of the test specimen. The load-time record for a totally elastic impulse is shown schematically in Fig. 7. The load-deflection record for linear elastic behavior has a

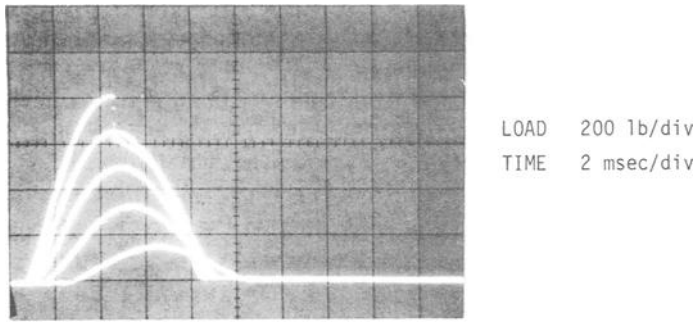

FIG. 8—*Low-blow test of a composite material.*

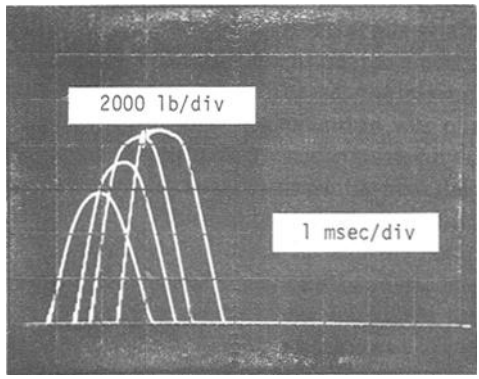

FIG. 9—*Low-blow test of a carburized steel bar.*

triangular shape rather than the curved appearance of the load-time record, and the impact energy (W_1) would be

$$W_1 = \frac{1}{2} P_1 d_1 \tag{3}$$

where P_1 is the maximum load and d_1 is the deflection to maximum load.

By definition, the specimen compliance, C is

$$C = \frac{d_1}{P_1} \tag{4}$$

Combining Eqs 3 and 4 gives

$$W_1 = \frac{C P_1^2}{2} \tag{5}$$

or

$$C = \frac{2W_1}{P_1^2} \tag{6}$$

Thus, by knowing the energy W_1, and measuring the load P_1, the compliance of the system can be calculated.

It is important to note that the system compliance is composed of the machine compliance, C_m, and the specimen compliance, C_s; that is, $C = C_s + C_m$. If it is assumed that the machine compliance is also totally elastic and linear, Eq 6 becomes

$$C_s + C_m = \frac{2W_1}{P_1^2} \tag{7}$$

Low blow tests of unnotched specimens of steel and aluminum, for which elastic beam theory is used to calculate C_s, can be used for determination of the machine compliance by Eq 7. For the Satec 240-ft·lb-capacity machine with a Charpy tup, the machine compliance was found to be approximately 2×10^{-6} in./lb. For resin composites, the specimen compliance is approximately 10^{-4} in./lb and the machine compliance is negligible. Equation 7 then reduces to

$$C_s = \frac{2W_1}{P_1^2} \tag{8}$$

and the load record for elastic impact (see Fig. 7) can be considered as a direct reflection of material response. For stiffer materials, however, the machine compliance becomes more important and needs to be considered. For example, an unnotched Charpy specimen of steel has a compliance of approximately 1.35×10^{-6} in./lb, which is nearly 70 percent of the machine compliance value. Then the elastic impact of this specimen results in approximately 40 percent of the available energy devoted to elastic deflection of the specimen and the balance of the energy is elastically absorbed by the machine. If energy is consumed by permanent deformation at the loading and support areas on the specimen, this reduction in energy must also be considered when analyzing the load-time record from an apparent elastic impact.

A further extension of the compliance technique is to measure the compliance for a series of low-blow tests until damage is observed by the appearance of the load-time curve (see Fig. 7). These values give the compliance of the specimen before any damage is created. After damage is recorded, a test at a sufficiently low-energy level allows the new compliance of the specimen to be determined. This new compliance, C' can now be used to calculate the amount of limited fracture energy, W_F, since

$$W_F = W_o - W_2 \tag{9}$$

where W_o is the total available impact energy and W_2 is the energy determined from Eq 6, the new compliance value C' and the load P_2 (Fig. 7). P_2 is the load at maximum deflection of the specimen with the remaining elastic energy of the system. This procedure for determination of W_F also applies to the case where

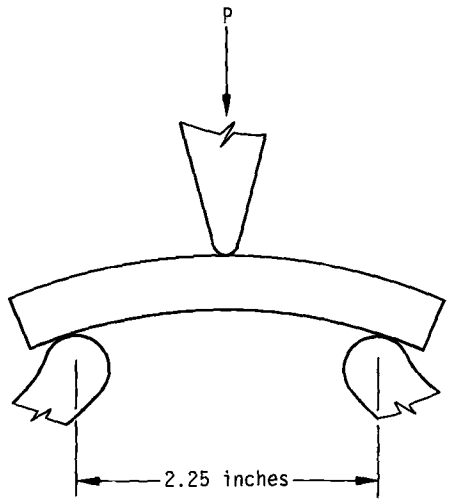

FIG. 10–*Schematic of the three-point bend test of ring-shaped specimens.*

the specimen consumes energy, W_F, by gross plastic deformation.

For some materials, the instrumented low-blow impact techniques may prove beneficial in evaluating the initiation process of fracture. A further extension of the low-blow technique is impact fatigue. In this application the available elastic energy W_o is kept constant and the number of impacts required to produce permanent damage as indicated by the load-time curve is recorded.

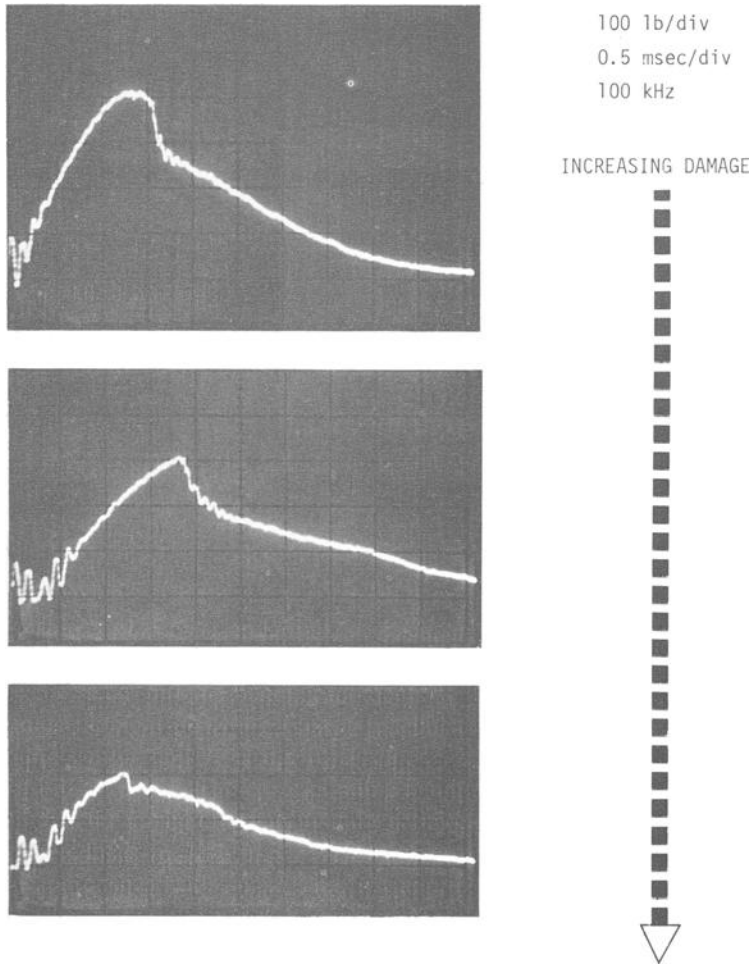

FIG. 11—*Test records from three point bend tests of ring-shaped specimens (carbon phenolic).*

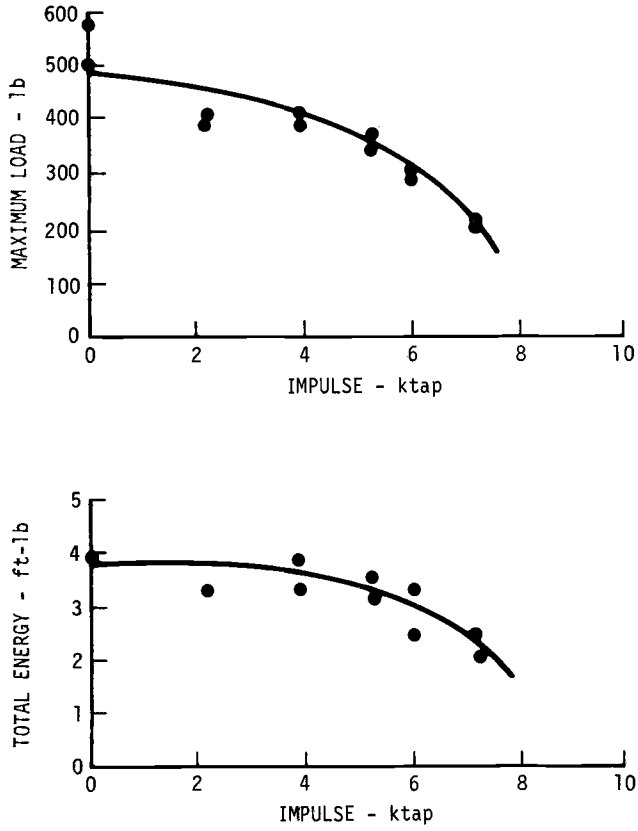

FIG. 12–*Results from impulsively loaded carbon phenolic ring-shaped specimens.*

Three-Point Bending of Ring-shaped specimens

By a simple modification of the anvils, a standard Charpy impact machine can be converted for three-point bend testing of ring-shaped specimens (arcs). The specimen loading geometry is illustrated in Fig. 10, where the tup impact face was kept parallel with the specimen face at contact. Typical test records from tests on carbon phenolic specimens [*10*] are shown in Fig. 11. The material was obtained from structures which had been subjected to various impulsive loads. The increasing amount of damage incurred during impulsive loading causes the compliance of the specimen to increase and the maximum load and energy to decrease. The results from the series of tests performed are shown graphically in Fig. 12. The instrumented impact test, in this application, may be a means of assessing shock damage to carbon phenolic structures.

Conclusions

Instrumented Izod, instrumented Charpy, instrumented low-blow (both Izod and Charpy), and variations of these techniques may lead to new inexpensive methods of evaluating materials and possibly even small structures. This study has attempted to show that the basics of conventional test techniques can be applied to newer tests to gain further information regarding material behavior under adverse loading conditions.

Acknowledgments

The authors wish to thank Hercules, Inc. for providing the tube specimens and Drilco, Inc. for providing the 4145 steel specimens.

References

[*1*] Fearnehough, G. D. and Hoy, C. J., *Journal, Iron and Steel Institute* Vol. 202, 1964, p. 912.

[*2*] E 23-72, "ASTM Standard Method for Notched Bar Testing of Metallic Materials," *1972 Annual Book of ASTM Standards,* American Society for Testing and Materials, 1972, pp. 276-292.

[*3*] D 256-70, "ASTM Standard Methods of Test for Impact Resistance of Plastics and Electrical Insulating Materials," *1972 Annual Book of Standards,* American Society for Testing and Materials, 1972, pp. 67-83.

[*4*] Izod, E. G. "Testing Brittleness of Steel," *Engineering, 25 Sept. 1903.*

[*5*] Green, A. P. and Hundy, B. B., *Journal of the Mechanics and Physics of Solids,* Vol. 4, 1956, pp. 128-144.

[*6*] Server, W. L. and Ireland, D. R., "General Yielding of Notched Three-Point Bend Specimens," Dynatup Technical Report TR72-19, Oct. 1972.

[*7*] Brown, W. F., Jr. and Srawley, J. E. in *Plane Strain Crack Toughness Testing of High-Strength Metallic Materials, ASTM STP 410,* American Society for Testing and Materials, 1966.

[*8*] Orner, G. M. and Hartbower, C. E., *The Welding Journal,* Vol. 40, Oct. 1961, p. 459-S.

[*9*] Tardif, H. P. and Marquis, H., *Canadian Metals Quarterly,* Vol. 2, 1963, p. 373.

[*10*] Tuler, F. R. and Server, W. L., to be published.

T. J. Koppenaal[1]

Dynamic Fracture Toughness Measurements of High-Strength Steels Using Precracked Charpy Specimens

REFERENCE: Koppenaal, T. J., "Dynamic Fracture Toughness Measurements of High-Strength Steels Using Precracked Charpy Specimens," *Instrumented Impact Testing, ASTM STP 563*, American Society for Testing and Materials, 1974, pp. 92-117.

ABSTRACT: The dynamic fracture toughness, K_{Id}, was measured in a number of ferrous alloys using precracked Charpy specimens and an instrumented impact machine. The alloys investigated included quenched and tempered steels (H-11, D6AC, and 4340), 18Ni maraging steels (grades 200, 250, and 300) and a high-temperature, stainless maraging steel (Pyromet X-15). Standard Charpy specimens were precracked in fatigue and tested at either 72° F (22°C) or −65°F (−54°C). Values of K_{Id} were determined as a function of yield strength and microstructure, and correlations were established between K_{Id} and both the energy to initiate fracture, W_m/A, and the total energy of fracture, W/A. The instrumented, precracked Charpy test is shown to be a convenient method of determining relative fracture toughness; under proper conditions this test procedure can be used to determine the dynamic plane-strain fracture toughness.

KEY WORDS: impact tests, dynamic tests, toughness, fracturing, ferrous alloys, strain rate, low temperature tests, evaluation tests

Impact testing with Charpy V-notch specimens has been used for several decades as a standard toughness test for many types of alloys. More recently, two important features related to fracture toughness testing have been established or developed that contribute significantly to the type of data that can be generated by the Charpy impact test. One of the improvements relates to the use of precracked specimens, which became necessary for measuring the toughness of higher-strength alloys developed for the aerospace and defense industry. Even with precracking, however, the only quantitative datum that could be determined from an impact test was the total energy per unit area, W/A, involved in fracture. The second improvement was to instrument the impact machine such that the load could be measured *during* an impact test. Using the load-displacement curves, dynamic fracture toughness values, K_{Id}, could be determined by methods already in practice for testing at slower (static) strain rates.

[1] Supervisor, Physical Metallurgy, Aeronutronic Division, Philco-Ford Corporation, Newport Beach, Calif. 92663.

During various ordnance programs that were conducted in our laboratory to establish relative toughness of alloys operating under dynamic strain-rate conditions, the use of the instrumented, precracked Charpy test was evaluated as a procedure for measuring fracture toughness. These tests were made with commercial alloys that were of interest because of their possible use in ordnance systems. The results presented in this report are directed at evaluating three general types of behavior related to the instrumented, precracked Charpy impact test:

1. Can this testing procedure be used as a materials evaluation and screening test to determine relative toughness values?
2. Can this type of testing be used to measure the dynamic *plane-strain* fracture toughness of high-strength metallic alloys.
3. Is there a unique relationship between dynamic fracture toughness (K_{Id}) of a material and the energy (W/A) involved in fracture during impact testing?

The report that follows will emphasize these factors.

Experimental Procedure

All of the specimens used in this investigation were taken from round or square cross-sectioned billets of sizes varying from 2 to 4 in. (diameter or square width). The heat treatments used for the various alloys are given in Table 1. Following heat treatment, standard Charpy specimens ($B = W = 0.394$ in.) were machined from either the WT or RT orientations; see Fig. 1. Except as noted, all results are for specimens in the WT orientation.

TABLE 1–*Heat treatment of various alloys.*

Alloy	Austenitizing or Solution Heat Treatment[a]	Tempering or Aging Treatment
H-11	1860°F, 1 h, AC (1016°C)	triple tempered at 1180° to 1250°F 2 h (638 to 677°C)
D6AC	1650°F, 1 h, AC (899°C)	double tempered at 1159 to 1275°F 2 h (626 to 691°C)
4340	1575°F, 1/2 h, OQ (857°C)	double tempered at 950 to 1100°F 4 h (510 to 593°C)
200 Maraging	1500°F, 1 h, AC (816°C)	900°F, 3 h (482°C)
250 Maraging	1500°F, 1 h, AC (816°C)	900°F, 6 h (482°C)
300 Maraging	1700°F, 1 h AC (917°C) + 1475°F, 1 h AC (802°C)	900°F, 6 h (482°C)
Pyromet X-15	1700°F, 1 h OQ (927°C)	1025 to 1250°F, 4 h (552 to 677°C)

[a] AC - air cooled.
OQ = oil quenched.

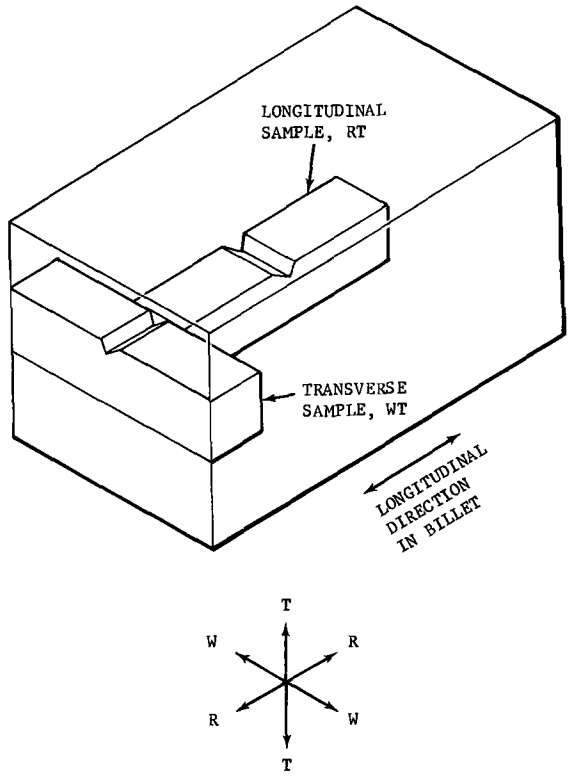

FIG. 1–*Test specimen orientations.*

The Charpy specimens were precracked by fatigue cycling to a total depth (including the V-notch) of 0.12 ± 0.01 in., using tension-zero loading with cantilever beam loading. Generally, about 30 000 to 60 000 cycles were necessary to produce the desired crack length; the rate of cycling was about 1500 to 2000 cpm. Early in the program, the standard Charpy specimen with a 10-mil root radius was used. It was later established that precracking could be accomplished in about one half as many fatique cycles when a sharp root radius (~ 0.5 mil) was used.

All testing was done at either room temperature (72°F (22°C) or –65°F (–54°C). A dry-ice and alcohol bath controlled to ± 1°F was used for the –65°F (–54°C) testing; the impact tests were completed within five seconds after withdrawing the specimens from the bath.

The impact testing was done with a Riehle Impact Machine using a 60-lb

hammer dropped from 48 in. (240 ft·lb of kinetic energy available at impact). This machine was certified to the Watertown Arsenal Specification for Charpy V-notch testing. The speed of the hammer at impact was measured to be 16.1 ft/s. The impact machine was instrumented with a Dynatup System such that load, integrated energy, and displacement of a specimen during impacting were displayed on an oscilloscope. The details concerning the nature of the instrumentation can be found elsewhere [*1,2*].[2] The load output was calibrated and checked daily using Standard Charpy V-notch specimens of 6061-T651 aluminum alloy; this particular alloy is recommended because the fracture load is strain-rate insensitive over the strain rates of interest. Where applicable, the testing procedure specified in ASTM Notched Bar Impact Testing of Metallic Materials (E 23-72) was followed. Triplicate fracture toughness tests were made in this investigation (except as noted).

Tension testing was done with an Instron Testing Machine at a crosshead speed of 0.01 in./min. The specimens had a reduced gage length of one inch and a diameter of 3/16 to 1/4 in. Duplicate tension specimens were used throughout this study.

Results

General Observations

An example of an oscilloscope recording for an impact test of a 300 maraging steel precracked Charpy specimen at −65°F (−54°C) is shown in Fig. 2. The load is seen to increase linearly until the maximum load is reached where frac-

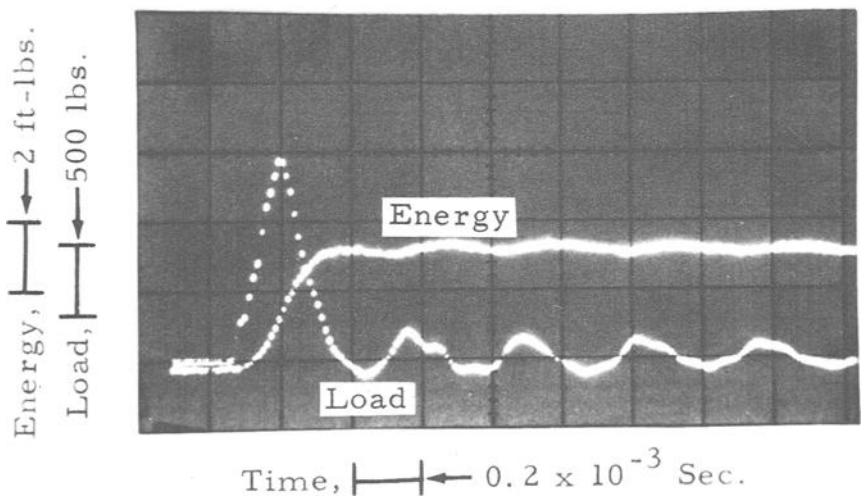

FIG. 2–*Oscilloscope recording of load and integrated energy as a function of time for a test of a 300 maraging steel specimen tested at −65°F (−54°C).*

[2]The italic numbers in brackets refer to the list of references appended to this paper.

ture is initiated. For those cases where fracture occurs before general yielding, the dynamic fracture toughness, K_{Id}, can be determined from linear elastic fracture mechanics [*3*] as

$$K_{Id} = \frac{6\,YM}{BW^2}\,a^{1/2} \tag{1}$$

where

$$Y = 1.93 - 3.07\left(\frac{a}{W}\right) + 14.53\left(\frac{a}{W}\right)^2 - 25.11\left(\frac{a}{W}\right)^3 + 25.8\left(\frac{a}{W}\right)^4 \tag{2}$$

and

M = applied moment at fracture,
B = specimen width,
W = thickness, and
a = total crack length.

Since a constant geometry is involved with the standard Charpy specimens, Eq 1 can be expressed as

$$K_{Id} = ZP_m \tag{3}$$

where P_m is the maximum load and Z a constant that depends only upon the crack length, a. Server [*4*] calculated Z as a function of a, and his results are shown in Table 2. For the test shown in Fig. 2, the K_{Id} is calculated to be 33.5 ksi-in.$^{1/2}$ using the crack length of 0.109 in.

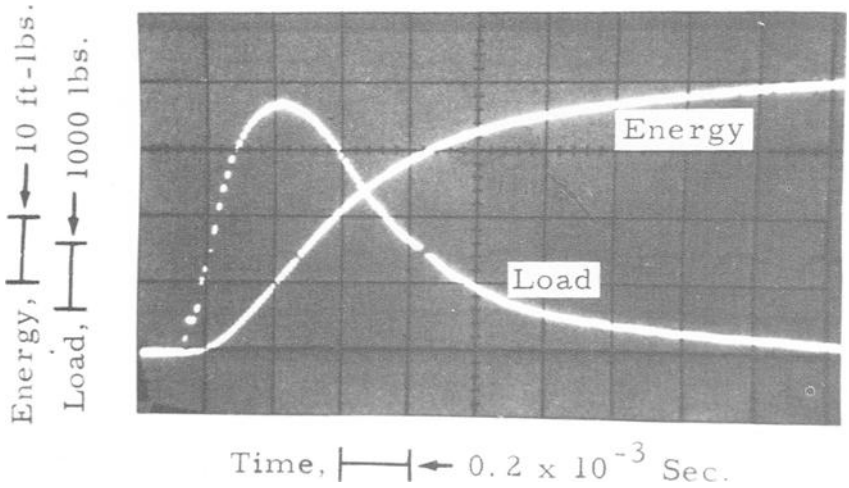

FIG. 3–*Oscilloscope recording of load and integrated energy as a function of time for a room temperature test of a Pyromet X-15 specimen heat treated for high toughness.*

TABLE 2–*Values of* Z *in Eq 3 as a function of crack length,* a *After Server [4]*

a	Z	a	Z	a	Z
0.079	18.880	0.119	24.681	0.158	32.008
0.080	19.015	0.120	24.842	0.159	32.232
0.081	19.150	0.121	25.004	0.160	32.459
0.082	19.286	0.122	25.167	0.161	32.688
0.083	19.421	0.123	25.332	0.162	32.919
0.084	19.558	0.124	25.497	0.163	33.153
0.085	19.694	0.125	25.664	0.164	33.389
0.086	19.831	0.126	25.832	0.165	33.628
0.087	19.968	0.127	26.001	0.166	33.870
0.088	20.106	0.128	26.171	0.167	34.114
0.089	20.244	0.129	26.343	0.168	34.360
0.090	20.383	0.130	26.516	0.169	34.610
0.091	20.522	0.131	26.690	0.170	34.862
0.092	20.661	0.132	26.865	0.171	35.117
0.093	20.801	0.133	27.042	0.172	35.375
0.094	20.942	0.134	27.221	0.173	35.636
0.095	21.083	0.135	27.401	0.174	35.899
0.096	21.224	0.136	27.582	0.175	36.166
0.097	21.336	0.137	27.765	0.176	36.436
0.098	21.509	0.138	27.949	0.177	36.709
0.099	21.653	0.139	28.135	0.178	36.985
0.100	21.797	0.140	28.323	0.179	37.264
0.101	21.941	0.141	28.512	0.180	37.547
0.102	22.087	0.142	28.703	0.181	37.833
0.103	22.233	0.143	28.895	0.182	38.122
0.104	22.380	0.144	29.089	0.183	38.415
0.105	22.527	0.145	29.285	0.184	38.711
0.106	22.675	0.146	29.483	0.185	39.011
0.107	22.824	0.147	29.683	0.186	39.314
0.108	22.974	0.148	29.884	0.187	39.622
0.109	23.125	0.149	30.087	0.188	39.932
0.110	23.276	0.150	30.292	0.189	40.247
0.111	23.429	0.151	30.500	0.190	40.566
0.112	23.582	0.152	30.709	0.191	40.888
0.113	23.736	0.153	30.920	0.192	41.215
0.114	23.891	0.154	31.133	0.193	41.545
0.115	24.047	0.155	31.349	0.194	41.880
0.116	24.204	0.156	31.566	0.195	42.219
0.117	24.362	0.157	31.786	0.196	42.562
0.118	24.521				

The other general type of behavior that can be observed is shown in Fig. 3. This was a room temperature test with a specimen of Pyromet X-15 heat treated for high toughness. It is evident that general yielding has occurred prior to reaching maximum load, and as a result, linear elastic fracture mechanics cannot be used to determine K_{Id}. For these types of behavior, K_{Id} was calculated using the equivalent energy method developed by Witt [5]. Briefly, this concept states that an equivalent amount of energy would have been necessary to reach maximum load had the specimen been thick enough to avoid general yielding prior to fracture (that is, had the specimen been thick enough for plane-strain conditions

to have existed). Referring to the schematic load-deflection curve shown in Fig. 4, it is necessary to determine the load, P^*, such that the energy (area under the load curve) up to P^* is equivalent to the energy of the experimental curve up to P_m. The most convenient method of determining P^* was to use the relationship

$$P^* = C\ (2A_m \tan\theta) \tag{4}$$

where

$$A_m = \int_0^{d_m} P\, d\,(d) \tag{5}$$

and C is a constant relating to the conversion of chart distance to load. Experimentally, the area under the load curve up to P_m is measured with a planimeter and θ is measured with a protractor. For the test shown in Fig. 3, P^* was

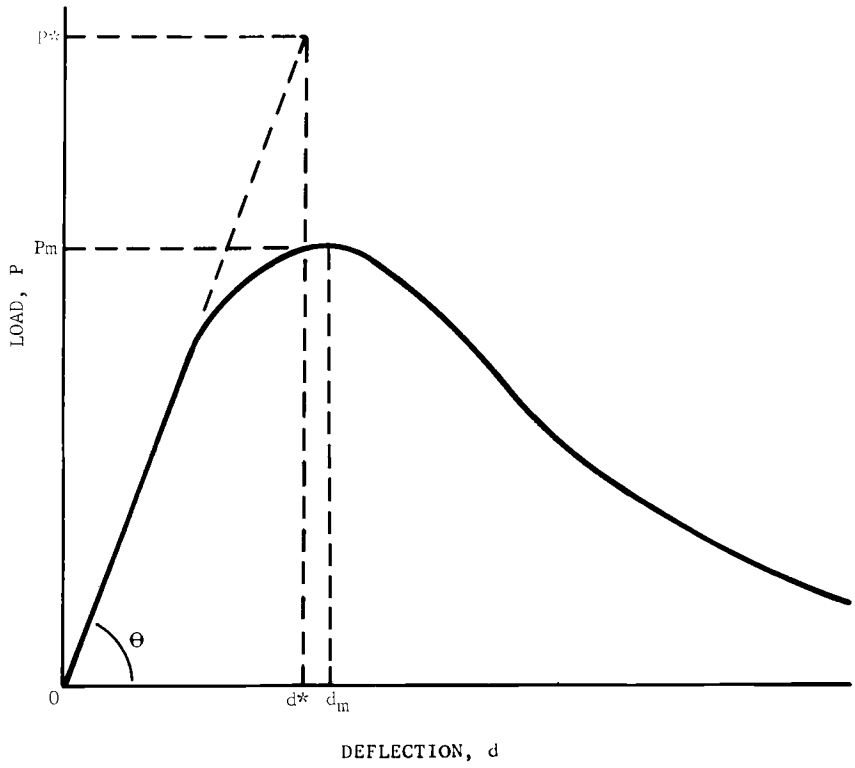

FIG. 4—*Schematic load-deflection curve of a specimen where plastic yielding occurs prior to reaching maximum load.*

calculated to be 5260 lb, which is appreciably larger than the P_m value of 3720 lb. Using the precrack length of 0.115 in., K_{Id} was calculated to be 126.5 ksi-in.$^{1/2}$. There has been recent experimental evidence [6] indicating that fracture is initiated before maximum load is reached in samples with load-deflection curves similar to that shown in Fig. 3. With this consideration, the calculated value of K_{Id} using the equivalent energy approach is probably an upper boundary value.

A few additional features in Fig. 3 are of interest. The total integrated energy, W, from the oscilloscope recording was about 40.5 ft·lb, and this agreed with the energy reading on the machine dial of 41 ft·lb for this test. The energy to maximum load, W_m, can also be measured from the oscilloscope recording and a value of 11.6 ft·lb is obtained for this particular test. Thus, about 28 percent of the total energy was expended in reaching the maximum load.

In order to evaluate the validity of the oscilloscope recordings, the integrated and dial energies that were obtained with a number of tests with H-11, D6AC, and 4340 were compared. The results are shown in Fig. 5, and good agreement between the two values is seen to exist. Since the energy reading from the oscilloscope recording is merely an integrated value of the load-deflection (time)

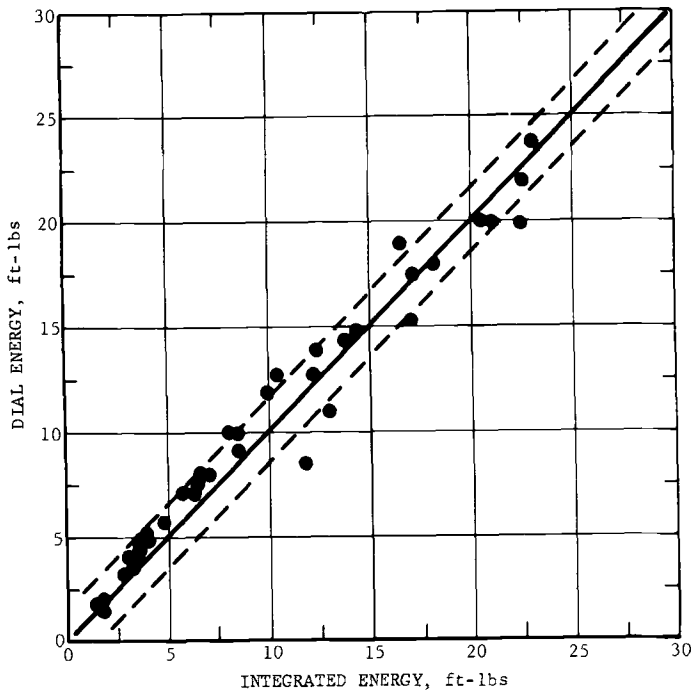

FIG. 5—*Dial energy versus integrator energy for tests with quenched and tempered steels. The solid line is drawn with a slope of unity and the dotted lines are at ± 1 ft·lb.*

curve, the good agreement between the integrated and dial energies substantiates the validity of the load data.

Quenched and Tempered Steels

Figure 6 shows the hardness and room temperature yield strength as a function of tempering temperature for the H-11, D6AC, and 4340 specimens. The yield strength levels investigated here are seen to be lower than usually evaluated for these alloys; this is a reflection of the specific application for which the allows were being considered.

Values of K_{Id} at −65°F (−54°C) are shown as a function of the static yield strength at −65°F in Fig. 7. At equivalent yield strengths the value of K_{Id} increases in the order of H-11, D6AC, and 4340 with more than a factor of two separating the K_{Id} values for H-11 and 4340. The value of W/A (total energy per unit area) observed in these −65°F tests is shown in Fig. 8 as a function of the yield strength at −65°F, and the same relative behavior is observed. Thus a materials screening and selection program based upon impact energy measurements alone with precracked specimens would have established the same relative degree of toughness as did the K_{Id} analysis.

The values of K_{Id} observed at −65°F (−54°C) and 72°F (22°C) (duplicate specimens for these tests at 72°F) are shown versus $(W/A)^{1/2}$ in Fig. 9 for the three temper conditions of each steel. This particular method of presenting the data is made to illustrate a number of features; the theoretical basis of this relationship is discussed later. For those cases where K_{Id} was calculated by the equivalent energy relationship, Eq 4, the value of K_{Id} that would have been calculated based upon the maximum load (P_m) and linear elastic fracture mechanics is shown by a cross (X) in Fig. 9. The value of K_{Id} based upon the equivalent energy calculations using P^* is shown by the arrows to the normal data points. The dotted line in Fig. 9 has been constructed such that all of the data to the left of the line satisfy the ASTM thickness requirement for a valid (static) plane-strain fracture toughness test [3]. This requirement for the thickness, T is

$$T \geqslant 2.5 \left(\frac{K_{Ic}}{\sigma_y} \right)^2 \tag{6}$$

where σ_y is the yield strength. Although no such requirement has as yet been established for K_{Id} testing, the data to the left of the dotted line in Fig. 9 can be considered as having been obtained under plane-strain conditions. With these explanations for the data in Fig. 9, two important features can be established. First, for each of those K_{Id} tests that satisfied the thickness requirement for a valid static test, maximum load occurred prior to general yielding and K_{Id} could be calculated by linear elastic fracture mechanics. This result was also true for all the other alloys being reported upon in this paper. The second feature

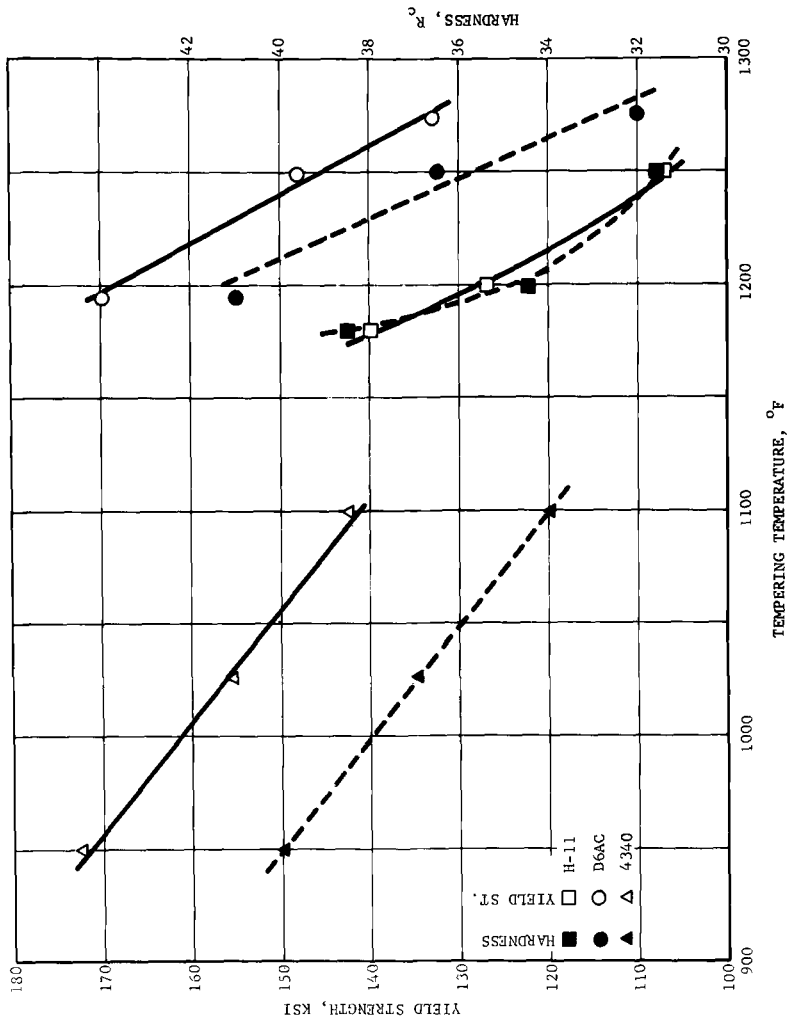

FIG. 6—*Room temperature yield strength and hardness of H-11, D6AC, and 4340 as a function of tempering temperature.*

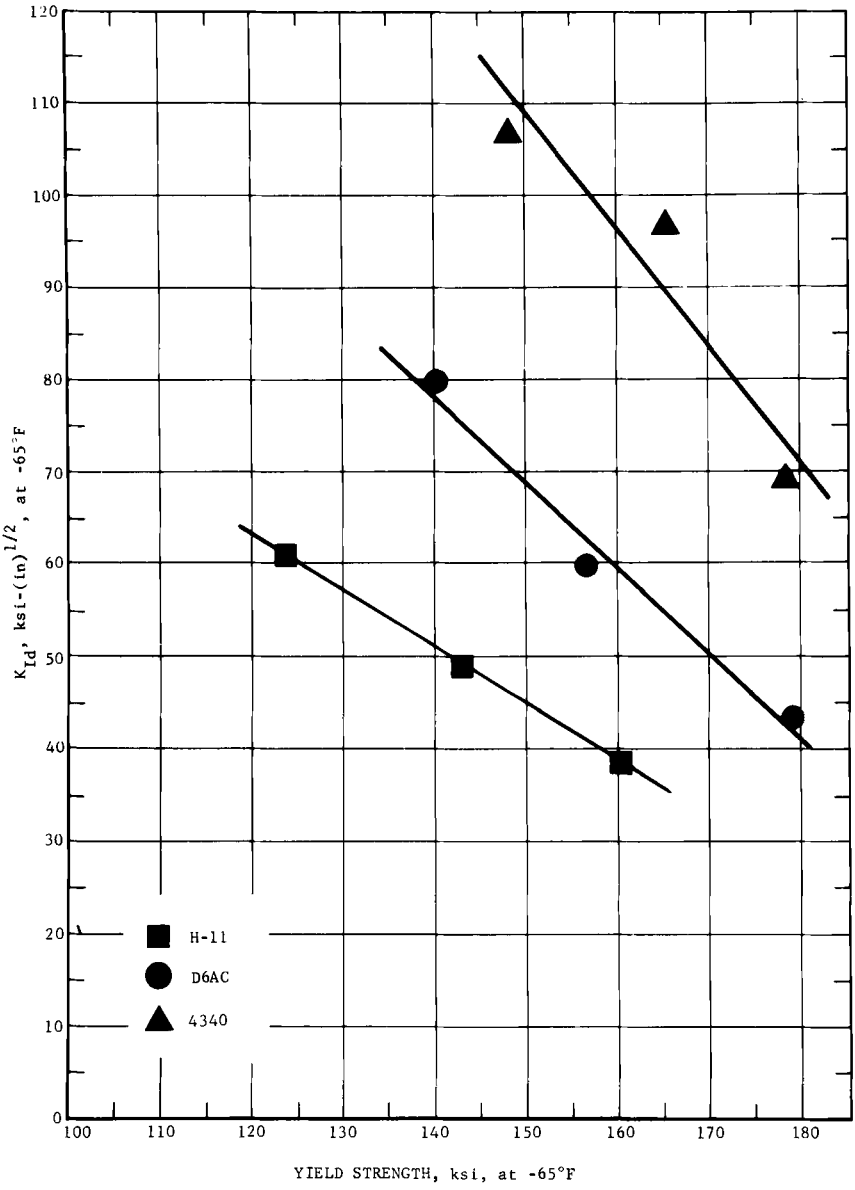

FIG. 7–K_{Id} *at −65°F (−54°C) as a function of the static yield strength at −65°F (−54°C).*

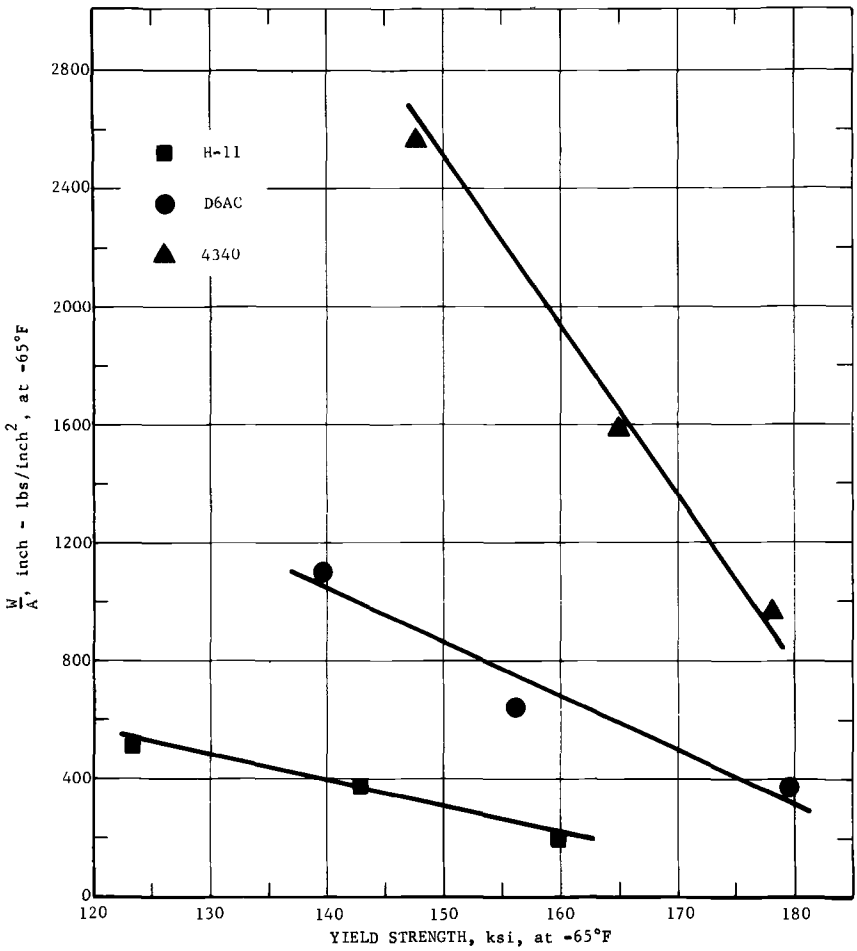

FIG. 8–W/A *at −65°F (−54°C) as a function of the static yield strength at −65°F (−54°C).*

established in Fig. 9 is that the values of K_{Id} calculated by the equivalent energy concept are a linear extrapolation of the K_{Id} data calculated by linear elastic fracture mechanics.

Since the raw data from these instrumented tests include a recording of integrated energy as a function of time, it is also possible to examine the relationship between the energy to maximum load per unit area, W_m/A, and K_{Id}. In Fig. 10, both W/A and W_m/A are plotted versus $K_{Id}{}^2/E$, where E is Young's modulus. In each case, a linear relationship can be used to describe the data.

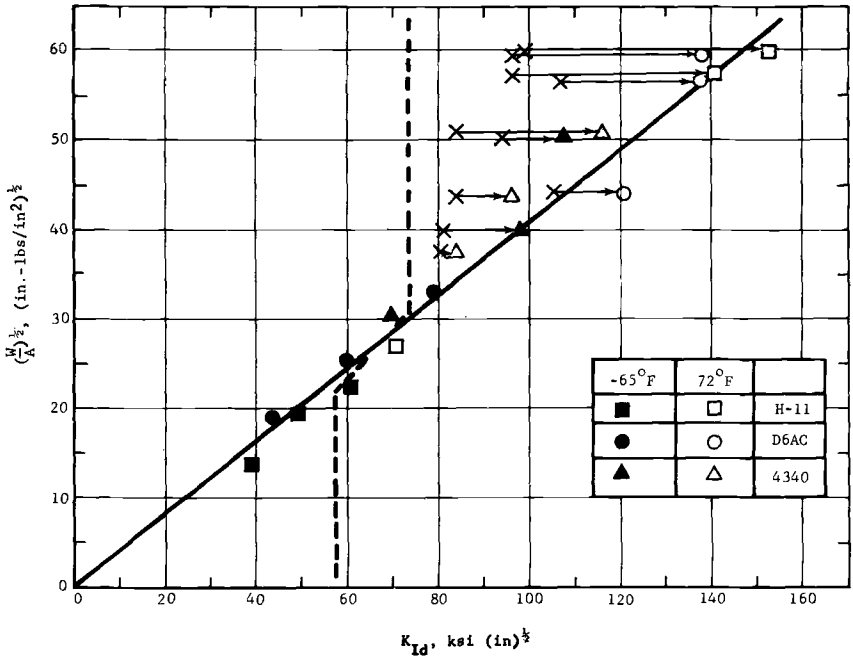

FIG. 9–$(W/A)^{1/2}$ *versus* K_{Id} *for quenched and tempered steels. (See text for explanation.)*

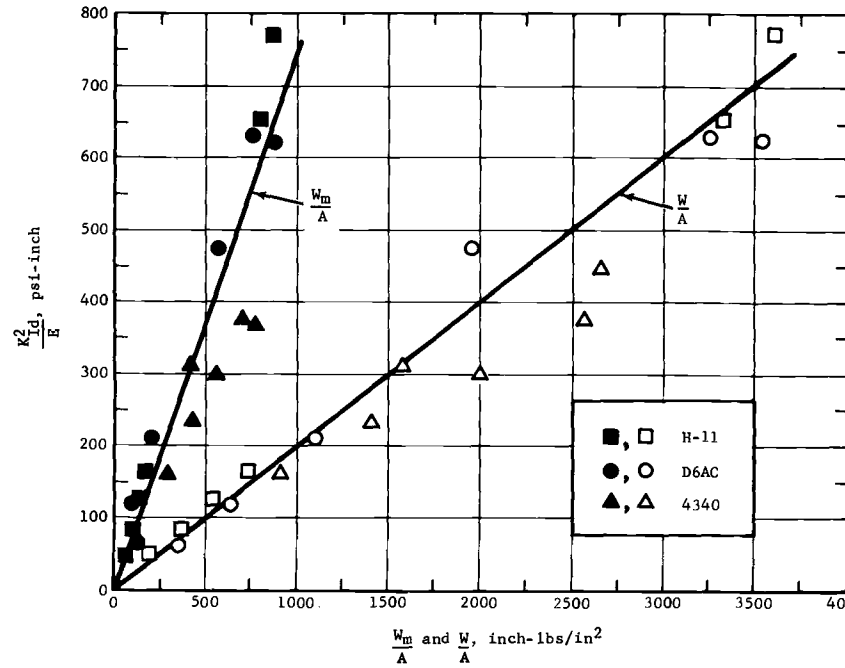

FIG. 10–$K_{Id}{}^2/E$ *versus* W_m/A *and* W/A *for quenched and tempered steels.*

Maraging Steels

Specimens of 200, 250, and 300 maraging steel were tested at –65°F (–54°C) and 72°F (22°C); specimens from both the WT and RT orientations were included in this evaluation. The values of K_{Id} are shown in Fig. 11 as a function of the static yield strength. All of the K_{Id} data shown in Fig. 11 were obtained by linear elastic fracture mechanics, Eq 3, and, with the exception of the data for 200 maraging steel in the RT orientation, all of the data satisfy the thickness requirement specified by Eq 6. The variation of K_{Id} with yield strength appears to be normal for these alloys. The dotted areas in Fig. 11 represent the behavior reported [*3,7,8*] for static K_{Ic} data of commercial-purity maraging steels. Considering that both the plane-strain fracture toughness and the yield strength of maraging steels are known to be relatively strain-rate insensitive, the K_{Id} data observed here are in good agreement with existing K_{Ic} data.

The K_{Id} data exhibit little temperature dependency in 200 maraging steel, a modest temperature dependency in 250 maraging steel, and a significant temperature dependency in 300 maraging steel. The K_{Id} data of the 300 maraging steel specimens indicate a 29 to 30 percent decrease in a change of testing temperature from 72°F (22°C) to –65°F (–54°C). This again compares favorably with the results reported for static K_{Ic} tests; Carter [*7*] observed a 20 percent reduction in the K_{Ic} value of 300 maraging between room temperature and –65°F (–54°C). The temperature dependency of K_{Id} in the 250 maraging steel samples is also about the same as Kendall [*8*] reported for K_{Ic} tests in that alloy. Therefore, K_{Id} varies with both the yield strength and the testing temperature in a manner that is quantitatively similar to static K_{Ic} observations.

The fractured surfaces for one specimen of each type of maraging steel in both orientations tested at 72 and –65°F (22 and –54°C) are shown in Fig. 12; the number below each specimen is the observed average value of K_{Id} in units of ksi-in.$^{1/2}$. The amount of shear lip varies from about 5 percent in one of the 300 maraging specimens to about 36 percent in one of the 200 maraging specimens. This is significant since *all* of the K_{Id} values were calculated using linear elastic fracture mechanics.

The relationship between K_{Id} and W/A for the maraging steels is shown in Fig. 13 with K_{Id}^2/E plotted as a function of both W/A and W_m/A. As in the case of the quenched and tempered steels, the experimental data can be adequately described by linear relationships.

Pyromet X-15

Pyromet X-15 is stainless maraging-type alloy that has a higher solution heat treating temperature (1700°F) (927°C) and higher aging temperatures (> 1025°F) (> 522°C) than the normal 18Ni maraging steels. The maximum yield strength of Pyromet X-15 is about 204 ksi following the 1025°F (552°C) aging

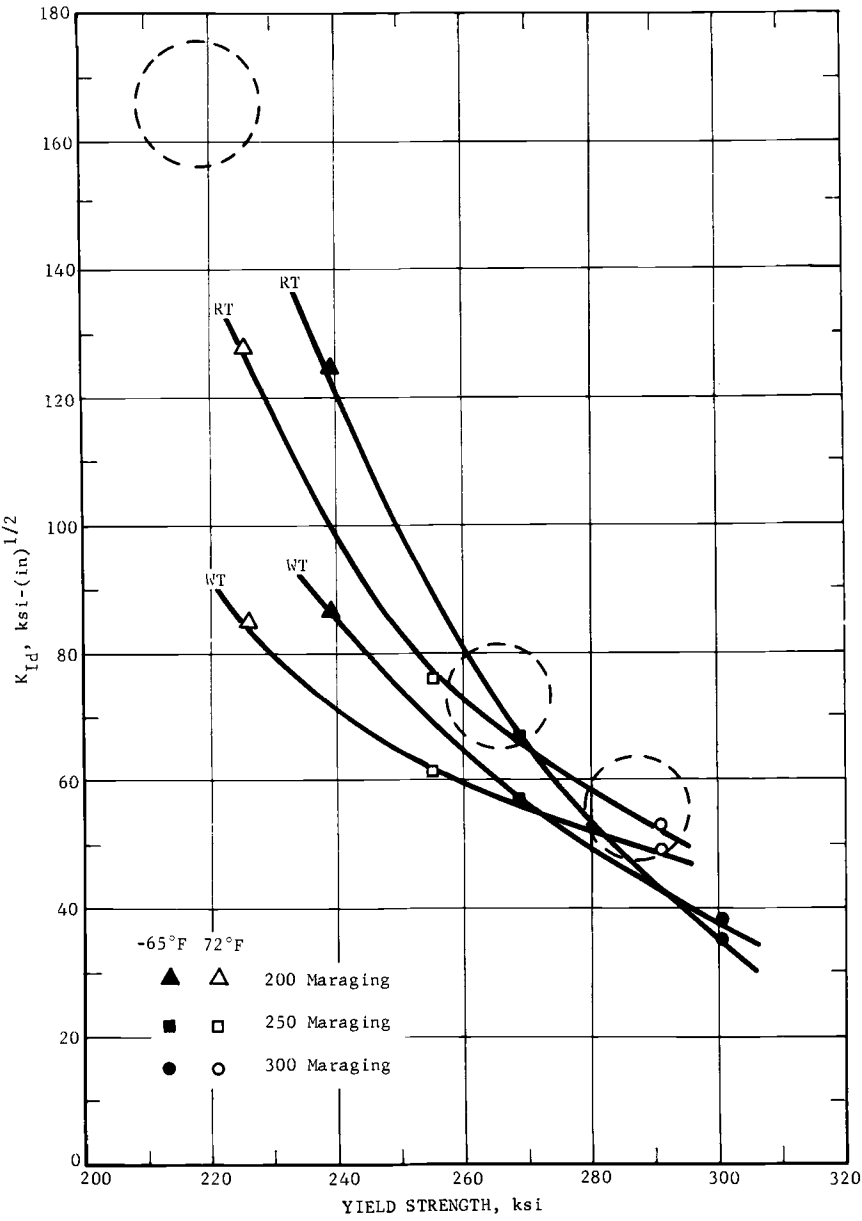

FIG. 11–K_{Id} *versus static yield strength of maraging steels.*

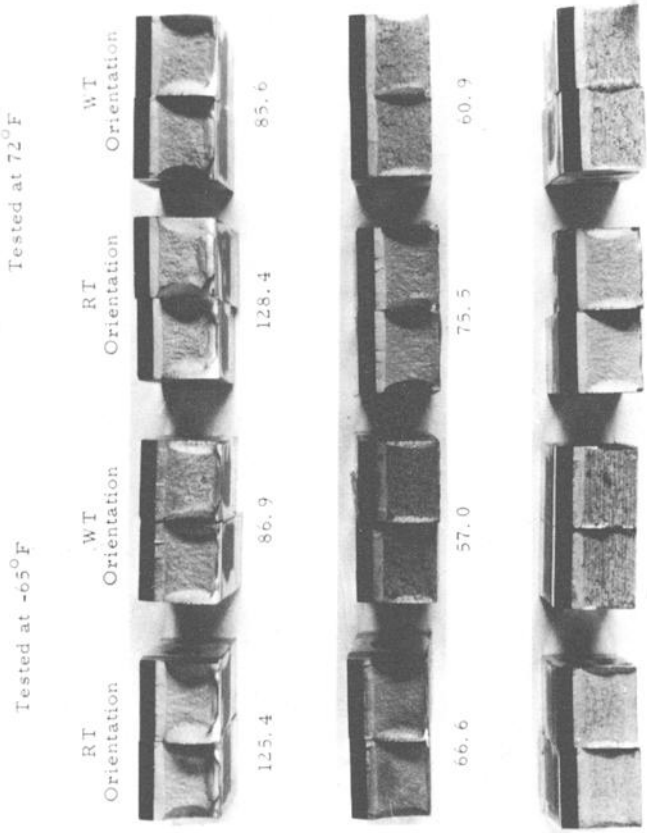

FIG. 12—*Fractured surfaces of maraging steel specimens. The numbers below each specimen are the average* K_{Id} *values in units of ksi-in.*$^{1/2}$

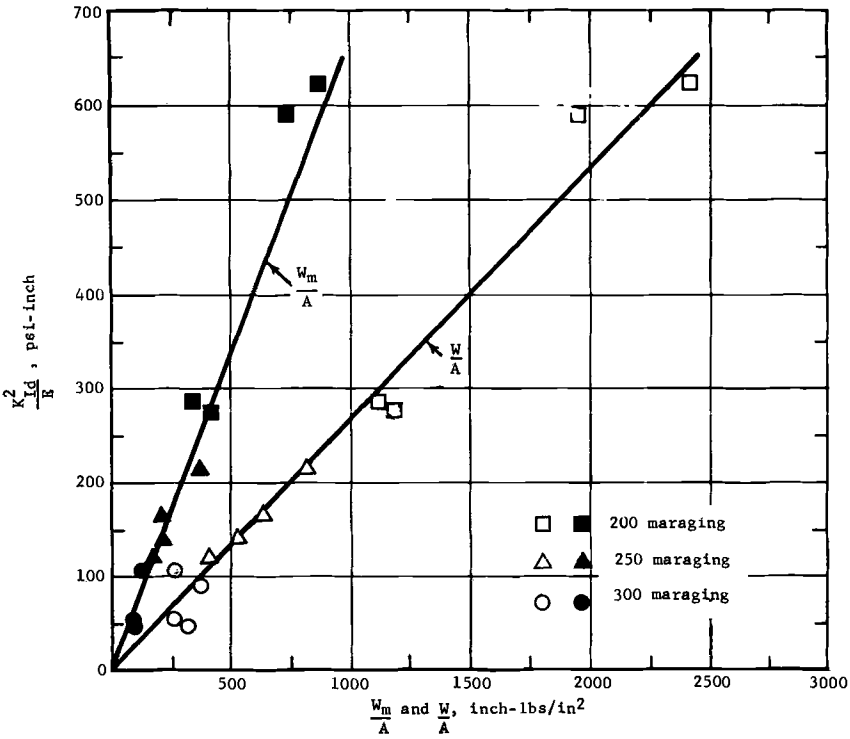

FIG. 13–K_{Id}^2/E *versus* W_m/A *and* W/A *for maraging steels.*

treatment. Values of K_{Id} were determined at −65 and 72°F (−54 and 22°C) in specimens aged at temperatures from 1025°F (552°C) to 1250°F (677°C), and the results are shown as a functon of the room temperature yield strength in Fig. 14. A normal type of strength-toughness behavior is observed for this age-hardened alloy. In the solution heat treated condition, a higher strength-toughness relationship exists than for the age-hardened structures.

Figure 15 shows K_{Id}^2/E as a function of W_m/A and W/A for Pyromet X-15 and the data can again be described by linear relationships. These results are especially interesting since the data represent specimens with a variety of microstructures, including a super-saturated martensitic solid solution, an age hardened structure with a martensitic matrix, and an overaged martensitic structure with about 30 percent reverted austenite. The relationship between K_{Id} and both W_m/A and W/A appears to be structure-insensitive.

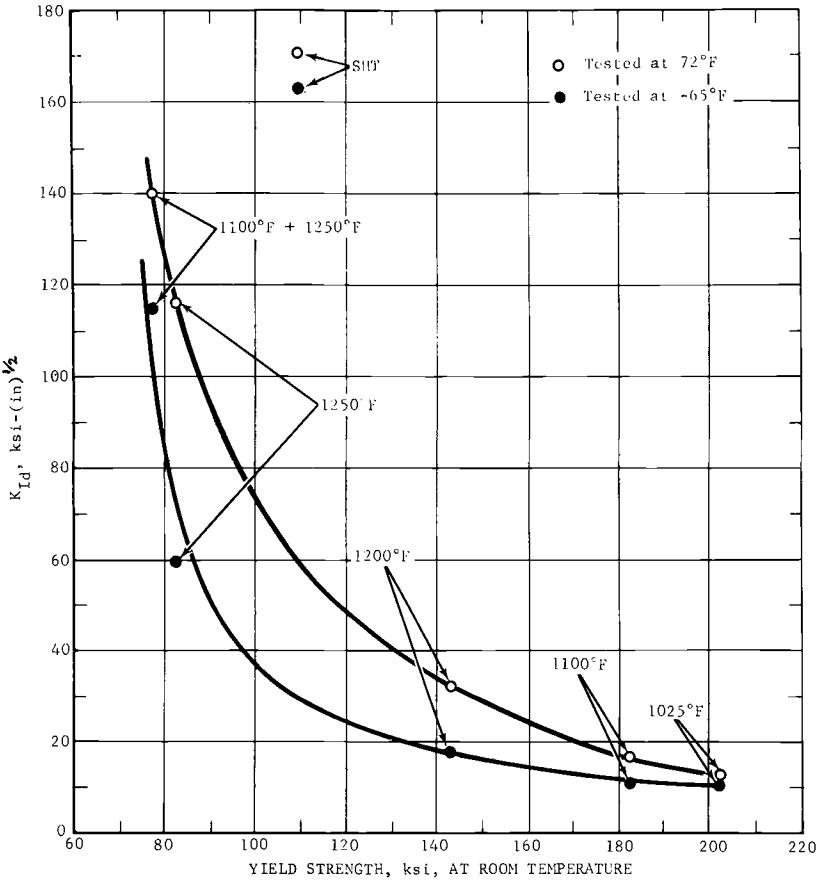

FIG. 14–K_{Id} *at 72°F (22°C) and −65°F (−54°C) versus room temperature static yield strength in Pyromet X-15. The elevated temperatures refer to the aging temperatures and SHT refers to the solution heat treated condition.*

Since both W_m/A and W/A can be expressed as linear functions of K_{Id}^2/E for a number of alloys (H-11, D6AC, 4340, Pyromet X-15, and 200, 250, and 300 maraging steel), the ratio of these energies, $(W_m/A) \div (W/A)$, should be some function of either K_{Id} or yield strength (or both). Figures 16 and 17 show this ratio as a function of K_{Id} and yield strength, respectively, for the seven alloys discussed thus far. Although considerable scatter in the data exists, the ratio (1) decreases with increasing values of K_{Id} and (2) increases with increasing values of yield strength. Therefore, as the fracture toughness decreases (yield strength increases), a larger ratio of the total fracture energy is required to initiate fracture (reach maximum load).

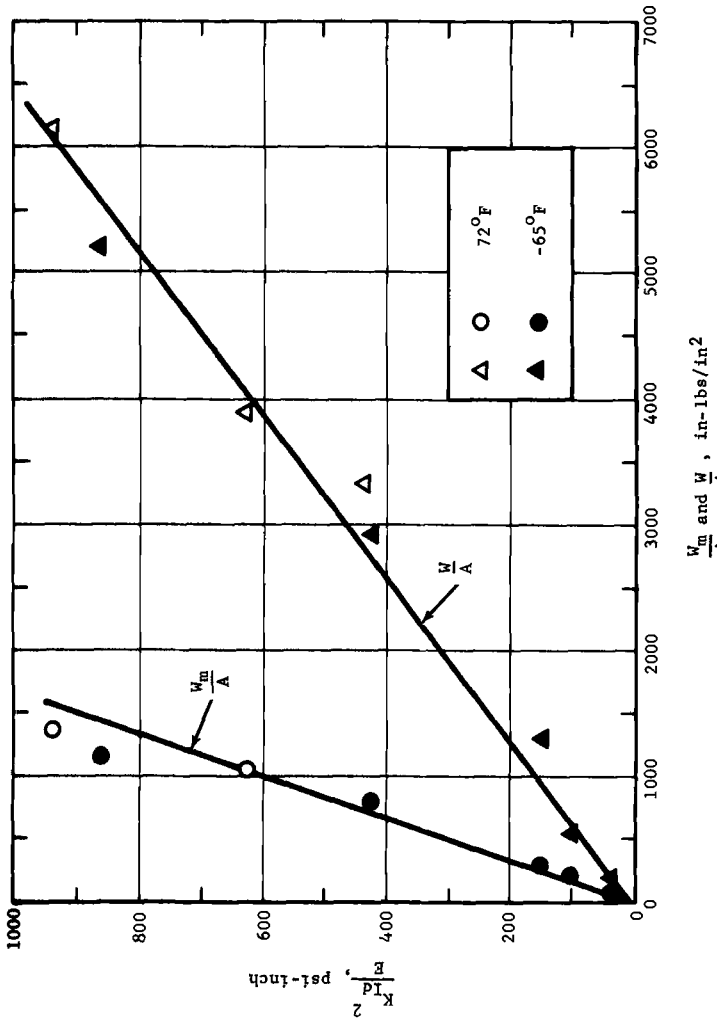

FIG. 15–K_{Id}^2/E *versus* W_m/A *and* W/A *for Pyromet X-15.*

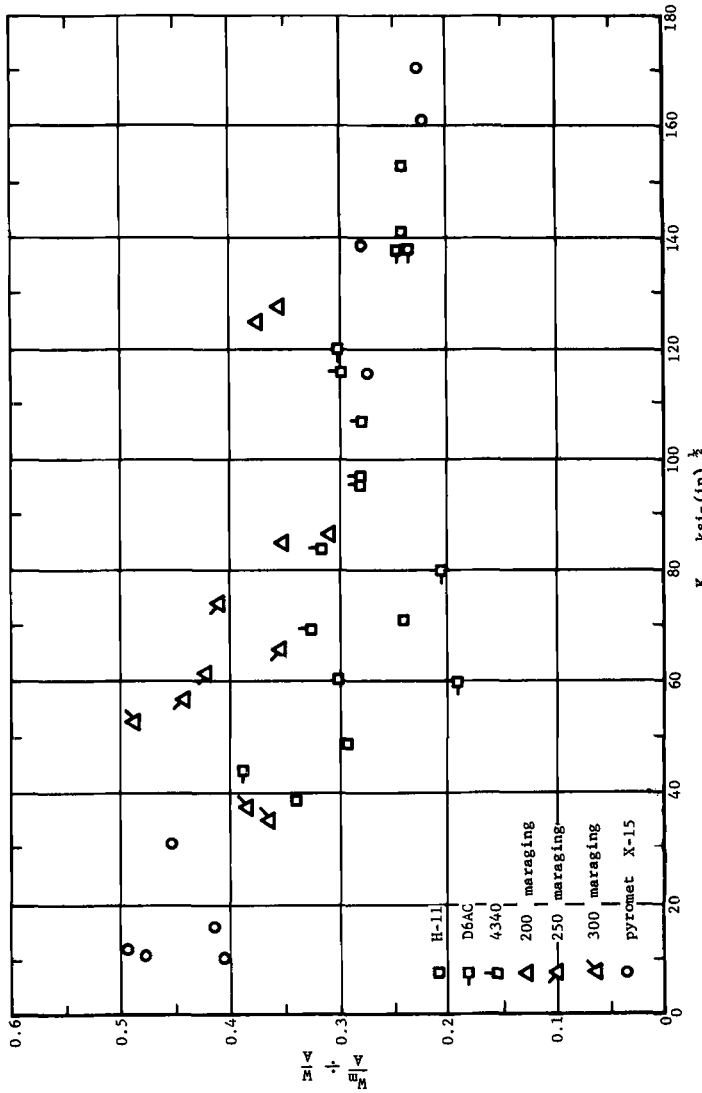

FIG. 16—*The ratio* $(W_m/A) \div (W/A)$ *as a function of* K_{Id} *for several alloys.*

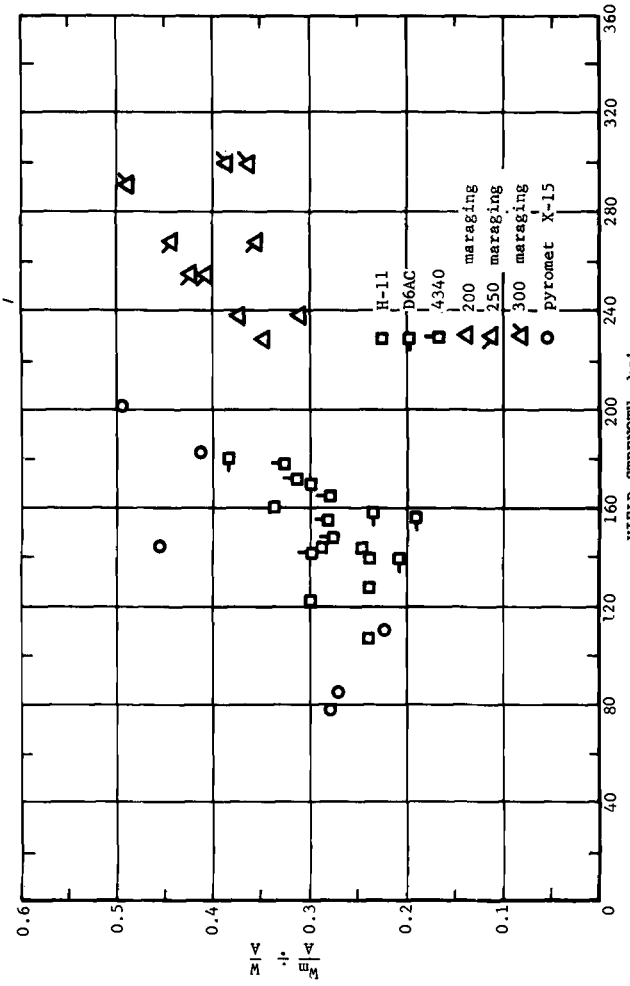

FIG. 17–*The ratio* $(W_m/A) \div (W/A)$ *as a function of static yield strength for several alloys.*

Discussion

The dynamic fracture toughness, K_{Id}, of a number of ferrous alloys has been measured using precracked Charpy specimens and an instrumented impact machine. In this section the observed relationship between K_{Id} and W/A (total energy per unit area for fracture) and W_m/A (energy per unit area to reach maximum load) is emphasized.

The similarity of the K_{Id} data obtained with the maraging steels shown in Fig. 11 and existing K_{Ic} static data appears to substantiate the testing procedure used in this investigation for those tests where fracture occurred prior to general yielding and linear elastic fracture mechanics could be applied. For those tests where K_{Id} was calculated on the basis of the equivalent energy concept (where plastic yielding occurs prior to initiation of fracture), reasonable values of K_{Id} were obtained based upon linear extrapolations of K_{Id} data calculated by linear elastic fracture mechanics. It therefore appears that the entire test procedure and the methods of analyses used here are applicable for measuring the dynamic fracture toughness of specimens with K_{Id} values up to (at least) $\simeq 150$ ksi-in.$^{1/2}$. As previously mentioned, values of K_{Id} calculated by the equivalent energy approach may be higher than would have been observed had plane-strain conditions existed.

In addition to demonstrating the general usefulness of the dynamic fracture toughness tests with precracked Charpy specimens, the investigation also established the experimental relationship between K_{Id} and both W/A and W_m/A. The method of presenting the data in Figs. 9, 10, 13, and 15 is based upon the general relationship [9]

$$\frac{K_{Ic}^2}{E} = \frac{G_{Ic}}{(1 - \nu^2)} \tag{7}$$

where G_{Ic} is the energy release at the point of unstable crack growth and ν is Poisson's ratio. Since unstable crack growth occurs at maximum load for tests conducted under plane-strain conditions, G_{Ic} can be associated with W_m/A and Eq 8 becomes (using the dynamic notation)

$$\frac{K_{Id}^2}{E} = \frac{1}{(1 - \nu^2)} \frac{W_m}{A} \tag{8}$$

The W_m/A data from Figs. 10, 13, and 15 are replotted together in Fig. 18 as a function of K_{Id}^2/E; Eq 8 is also plotted in this figure. The data can be described by a linear relationship, and the slope of the experimental line is about 65 percent of the predicted behavior. A couple of features may account for this difference. The use of the equivalent energy concept to calculate K_{Id} values where general yielding occurred prior to fracture produces upper values for both K_{Id} and W_m/A as already commented upon. In addition, the compliance be-

tween the test specimen and machine during initial loading may produce a recording for the tup (where the strain gages are located) that is not representative of the specimen. The compliance of the test machine was experimentally determined to be 2.26×10^{-6} in./lb using standard techniques [*10*]. Using this correction, the slope of the experimental curve in Fig. 18 becomes 83 percent of the predicted behavior.

The relationship between K_{Id} and W/A is also of interest in evaluating this type of testing. In Fig. 19 values of K_{Id}^2/E are shown as a function of W/A for a number of ferrous alloys tested to date in our laboratory. Some scatter is evident, but most of the data can be described by linear relationships having slopes between 0.25 and 0.15. This is appreciably different than predicted from Eq 8, and the relationship is therefore considered to be empirical. From a practical viewpoint, however, the correlation indicates that measurements of W/A alone on precracked specimens (that do not require an instrumented impact machine) could be used to measure *relative* toughness for screening and materials selection purposes. As more data relating K_{Id} and W/A for impact testing become available, it may be possible to use the W/A of precracked specimens to determine the value (or range of expected values) of K_{Id} by use of the behavior shown in Fig. 19.

Ronald, et al [*11*] measured K_{Ic} in slow bending using precracked Charpy specimens and established the relationship

$$\frac{K_{Ic}^2}{E} = \frac{1}{2(1-\nu^2)} \frac{W}{A} \tag{9}$$

In correlating the experimental results to Eq 7, the authors related W/A to G_{Ic} and explained the factor of 1/2 on the basis that two surfaces were being created during fracture. However, it appears that this feature was considered [*12*] in developing Eq 7, and the relationship shown by Ronald et al is, therefore, empirical. Using the data generated in the present investigation, this relationship can be explained. Figure 16 shows that for low values of K_{Id} (which was the range investigated by Ronald et al)

$$\frac{W_m}{A} \simeq \frac{1}{2} \frac{W}{A} \tag{10}$$

Substituting, Eq 9 becomes identical with Eq 8, and the static behavior is seen to be identical to the dynamic behavior.

Conclusions

On the basis of the experimental results observed in this investigation, three important conclusions can be made:

1. The instrumented, precracked Charpy test can be effectively used to determine relative fracture toughness.

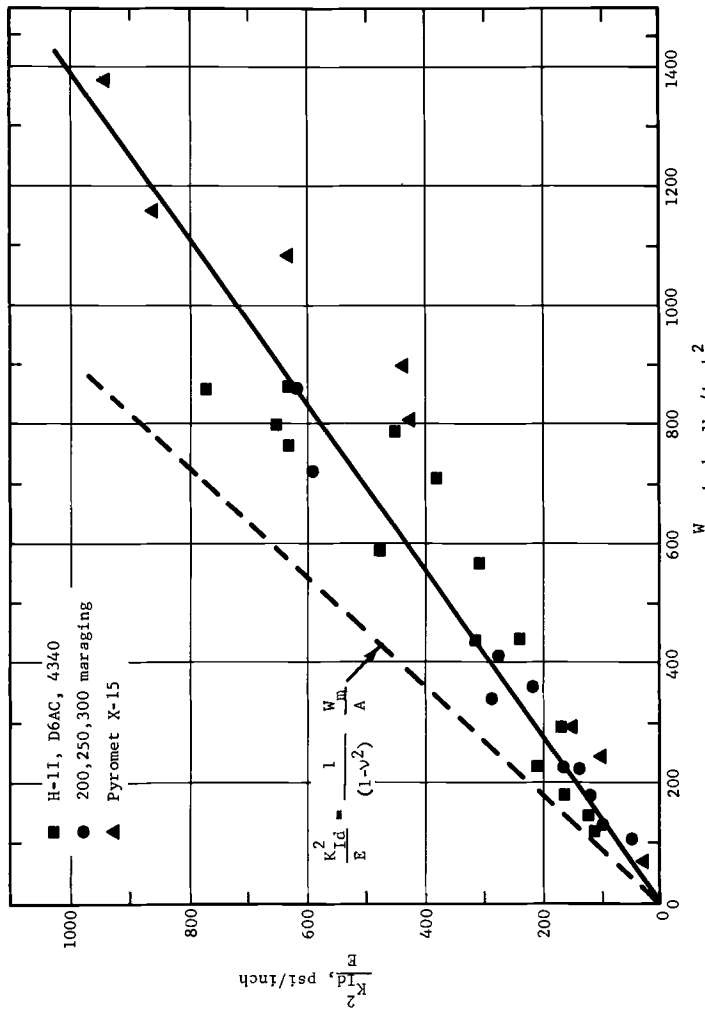

FIG. 18–K_{Id}^2/E *versus* W_m/A *for several alloys.*

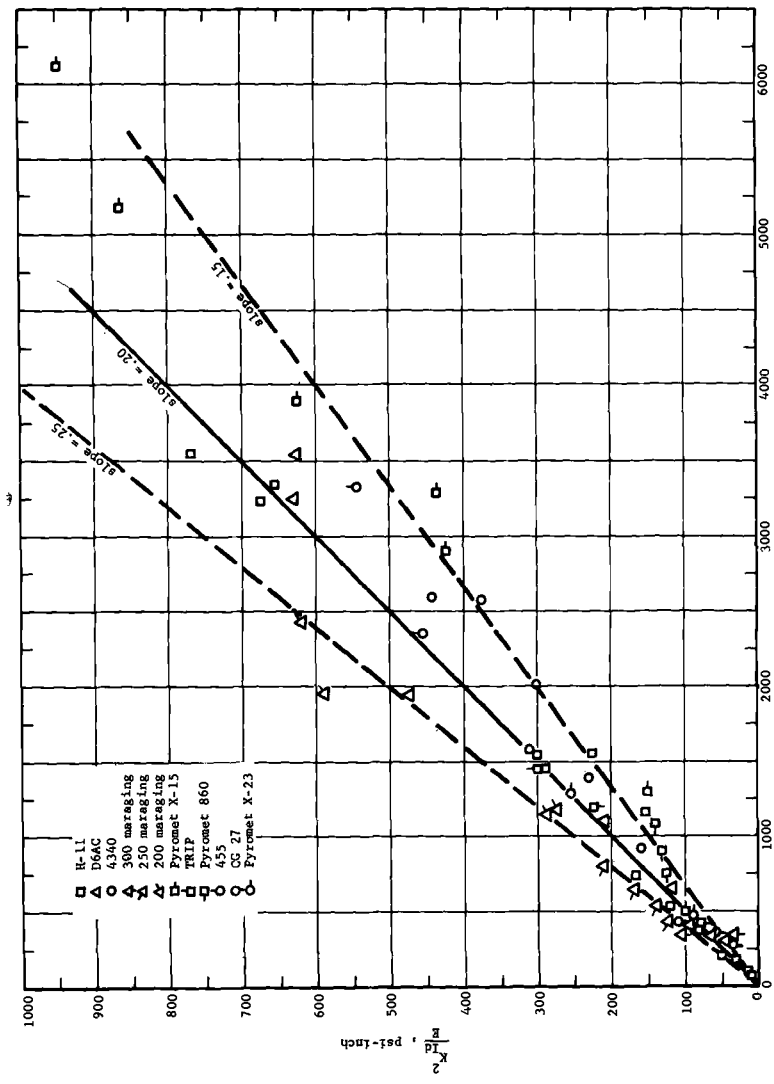

FIG. 19–$K_{Id}{}^2/E$ *versus* W/A *for several ferrous alloys.*

2. Under proper conditions the instrumented, precracked Charpy test can be used to determine dynamic *plane-strain* fracture toughness values.

3. The dynamic fracture toughness, K_{Id}, is related to both the energy to initiate fracture and the total energy of fracture.

Acknowledgments

The author would like to thank M. J. Harrigan, D. R. Ireland, R. P. Sernka, W. L. Server, A. S. Tetelman, and R. A. Wullaert for their helpful discussions during the course of this work. Most of the experimental work was performed by W. L. Holland and J. M. Seay.

This investigation was sponsored in part by the Air Force Armament Laboratory under Contract F33657-72-C-0020 and the Army Weapons Command under Contract DAAF03-72-C-0145.

References

[1] Wullaert, R. A., in *Impact Testing of Metals, ASTM STP 466*, American Society for Testing and Materials, 1970, p. 148.
[2] Server, W. L. and Tetelman, A. S., *Engineering Fracture Mechanics*, Vol. 2, 1972, p. 367.
[3] Srawley, J. and Brown, W. in *Plane Strain Fracture Toughness Testing, ASTM STP 410*, American Society for Testing and Materials, 1966.
[4] Server, W. L., M.S. thesis, University of California, Los Angeles, 1972.
[5] Witt, F. J., *Proceedings*, Fourth National Symposium Fracture Mechanics, Pittsburgh, Pa., 24-26 Aug., 1970.
[6] Tetelman, A. S., private communication.
[7] Carter, C. S., Technical Report AFML-TR-70-139, Air Force Materials Laboratory, June 1970.
[8] Kendall, D. P., *Materials Research and Standards*, Vol. 10, 1970, pp. 14, 32.
[9] Tetelman, A. S. and McEvily, A. J., *Fracture of Structural Materials*, Wiley, New York, 1967, p. 138.
[10] Priest, A. H. and May, M. J., BISRA Open Report MG/C/46/49, The Inter-Group Laboratories of the British Steel Corporation, London, England, 1969.
[11] Ronald, T. M. F., Hall, J. A., and Pierce, C. M., *Metallurgical Transactions*, 1972, Vol. 3, p. 813.
[12] Wullaert, R. A., Ireland, D. R., and Tetelman, A. S., presented at the WESTEC Conference, March 1972 (to be published).

J. W. Sheckherd,[1] *M. Kangilaski,*[2] *and A. A. Bauer*[1]

Impact Properties of Shock-Strengthened Type 316 Stainless Steel

REFERENCE: Sheckherd, J. W., Kangilaski, M., and Bauer, A. A., "Impact Properties of Shock-Strengthened Type 316 Stainless Steel," *Instrumented Impact Testing, ASTM STP 563*, American Society for Testing and Materials, 1974, pp. 118-132.

ABSTRACT: The effect of shock strengthening on impact properties of Type 316 stainless steel at temperatures ranging from room temperature to 650°C (1202°F) was established by utilizing the instrumented Charpy impact test. It was found that the total impact energy absorbed progressively decreases with increasing shocking pressure.

The dynamic yield strength (σ_{dy}) was increased by increasing the shocking pressures for all testing temperatures. This trend is expected because the static yield strength (σ_{sy}) was also found to increase with increasing shocking pressure. However, the ratio of dynamic-yield to static-yield strengths (measure of strain-rate sensitivity) was found to decrease with increasing shocking pressure.

KEY WORDS: impact tests, impact properties, explosive shocking, stainless steels

Explosive shock loading has been shown to change mechanical properties of metals [*1*].[3] Shock loading generally increases hardness, yield strength, and ultimate strength while decreasing ductility. However, the impact properties of shock-strengthened metals have not been thoroughly investigated. In this study the impact properties of shock-strengthened Type 316 stainless steel were investigated.

Experimental Procedures

Material

The material utilized in shock strengthening was hot rolled and annealed 316 stainless steel plates, 4 by 6 by 0.5 in. The chemical composition and grain size for the plates are given in Table 1.

[1] Senior research and research leader, respectively, Battelle Memorial Institute, Columbus Laboratories, Columbus, Ohio 43201.

[2] Researcher, General Electric Co., Nuclear Energy Division, Breeder Reactor Department, San Jose, Calif. 95125.

[3] The italic numbers in brackets refer to the list of references appended to this paper.

TABLE 1—*Composition and grain size of the Type 316 stainless steel plates utilized in the shock-strengthening experiments.*

Designation	Material	Grain Size, μm	Composition, weight %									
			Fe	Cr	Ni	Mo	Mn	Si	Cu	C	P	S
A	316SS	125	Bal	18.0	12.4	2.25	1.74	0.41	0.22	0.42	0.039	0.010
B	316SS	62	Bal	17.7	12.6	2.23	1.96	0.66	0.13	0.070	0.023	0.029

Shock-Strengthening Procedures

The shock strengthening was achieved by using the flyer plate impact technique [*2*]. In this technique an explosive charge is set off behind a flyer plate which then strikes the test plate, causing a planar shock wave in the test plate. The 316 stainless steel was shocked by an estimated pressure of 80 and 160 kilobar. Pressure estimates were based on the flyer plate impact velocity and the Hugoniot relation of the flyer plate and the test material. The shock wave produced a relatively uniform hardness throughout the test plate as shown by the Rockwell hardness values in Table 2.

TABLE 2–*Rockwell A hardness values for shocked and unshocked 316 stainless steel.*

	Unshocked	80 Kilobar	160 Kilobar
Plate Top	49	61	59
	49	58	61
Center	49	57	59
	48	57	59
Bottom	48	59	59

Testing Techniques

Impact tests were done on standard V-notch Charpy specimens at temperatures ranging from 25 to 650°C (77 to 1202°F) by using recommended test procedures (ASTM Notched Bar Impact Testing of Metallic Materials (E 23-66)). Elevated temperatures were obtained by radiant heating in an electric muffle furnace. Specimens were overheated 3 percent of the nominal centigrade test temperature to compensate for temperature loss incurred during the approximately five seconds needed to complete the test. This overheat percentage was established over the temperature range of interest by analyzing the time-temperature records of a standard Charpy specimen under normal testing conditions. Temperature measurements were made with a Chromel-Alumel thermocouple spot-welded at the Charpy notch root.

Tests were conducted on a conventional 240-ft·lb Satec impact machine. This machine has been certified with U. S. Army Materials and Mechanics Research Center standard Charpy V-notched specimens. The instrumented components of the system consist of a strain-gaged striker, a high-gain dynamic amplifier, and a fast-writing storage oscilloscope. The instrumented striker serves as a load measuring device (much like a tensile load cell), and through signal conditioning provides a load-time history of the test specimen. This information is recorded on film using an oscilloscope camera. The x-axis of this record was converted to deflection using the effective pendulum velocity. Deflection was not corrected

for elastic and plastic deformation occurring outside of the notched area; therefore, deflection is considered as an upper bound within the context of this study. The y-axis is dynamically calibrated for load in pounds [*3*].

Results and Discussion

The only measured parameter in conventional Charpy testing is total energy. However, with load measuring capabilities the Charpy test can be considered a dynamic notch-bar bend test, and the many well-developed notch-bar bending theories can be applied to the data analysis. These theories are based on sound metallurgical relations and have been experimentally evaluated by other investigators [*4-7*]. Failure in notch-bar bending has been classified into six distinctive types [*8*]; those observed in this work are shown in Fig. 1.

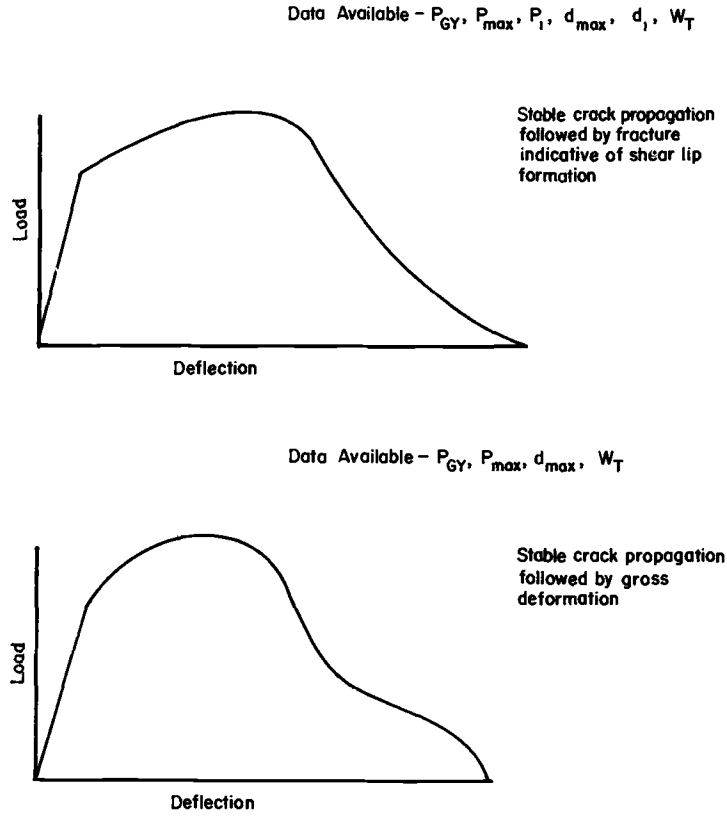

FIG. 1–*Fracture types observed in 316 stainless steel.*

Distinguishing features of the load-time oscillograph are used to analyze the fracture behavior of the material. These features are shown in the idealized load-deflection record of Fig. 2. The symbols used in this figure are:

P_{GY} = load at general yielding,
P_{max} = maximum load,
P_1 = load at the onset of fast fracture,
d_{max} = deflection at maximum load, and
d_1 = deflection at the onset of fast fracture.

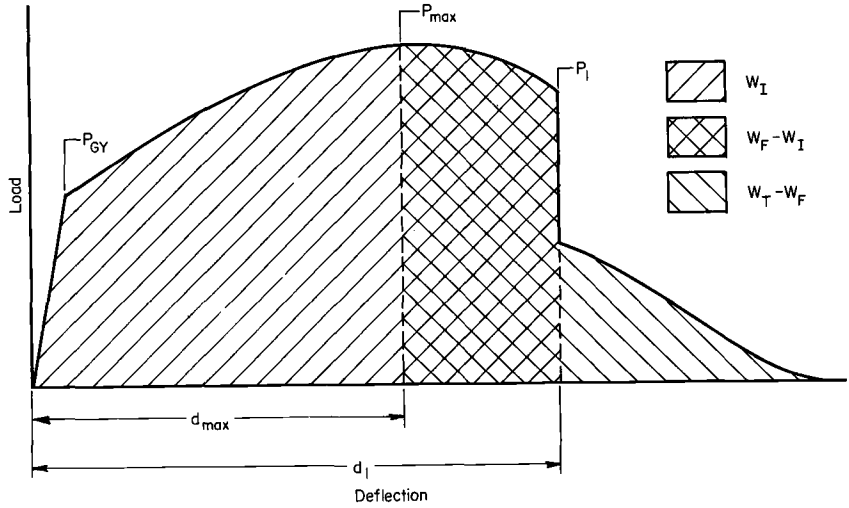

FIG. 2–*Idealized load-deflection record.*

Figure 2 also shows how total energy (W_T) can be subdivided into components of energy absorbed prior to crack initiation (W_I) and energy absorbed prior to unstable crack propagation (W_F). The energy, W_T, on the load-deflection curve is equivalent to that measured on the pendulum dial.

Data from the load-time record are used in calculating the dynamic yield stress and fracture toughness. The dynamic yield stress is calculated from the measured general yield load, P_{GY}, and is related to the uniaxial tensile yield stress, σ_{sy}, by

$$\sigma_{sy} = 33.3 P_{GY} \tag{1}$$

This factor is for a standard Charpy V-notch specimen, and is dependent upon the flank angle of the notch and assumed yield criterion (Tresca for this case) [9].

For the Type 316 stainless steel, all specimens contained a blunt notch (0.01 root radius), and fractures occurred beyond general yield. Therefore, linear elastic fracture mechanics was not directly applicable, and toughness values are limited to comparative use within this study. The crack opening displacement (COD) approach was considered a conservative method for approximating

fracture toughness. The relationship used to calculate the K_c fracture toughness is:

$$K_c = (G_c E)^{1/2} \tag{2}$$

where G_c is the critical strain energy release rate and E is the elastic modulus. The COD approach essentially uses the deflection measurements to calculate the strain at the root of the notch [*10*]. The COD is intended to represent this strain and can be calculated from the following [*8*]:

$$\text{COD} = 0.51\ (0.394\text{-}2)\ d_{max} \tag{3}$$

where a is the notch depth and d_{max} is the appropriate deflection. The generally accepted relation of COD to G_c is

$$G_c = \text{COD} \times \sigma_{sy} \tag{4}$$

and K_c is found by combining Eqs 2, 3, and 4:

$$K_c = (\text{COD} \times \sigma_{sy} \times E)^{1/2} \tag{5}$$

For these impact tests, σ_{sy} in Eq 5 is that determined by Eq 1.

The testing direction of specimens relative to the rolling and shocking directions of the plate is illustrated in Fig. 3. Testing temperatures were selected to overlap those used in uniaxial tension tests, thus allowing a direct comparison with static test data [*11,12*]. In the temperature range covered, the elastic constraint is reduced so much that plastic deformation occurs across the entire specimen cross section. Thus, fracture is initiated by fibrous tearing at, or close to, the root of the notch and maximum load is reached prior to fracture load. Under these conditions while standard Charpy tests provide little insight into dynamic material behavior, instrumentation furnishes load-time data which can be evaluated by notch-bar bend theory and provide useful information.

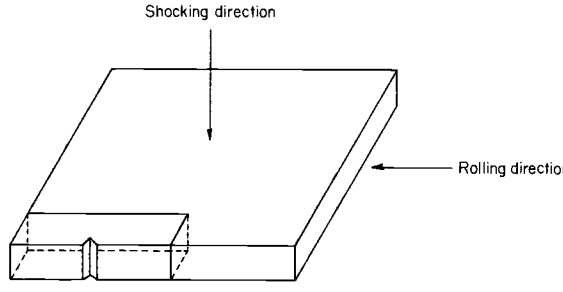

FIG. 3—*Testing direction of specimens relative to the rolling and shocking directions.*

TABLE 3—*Measurements obtained from time-load records for specimens tested in impact by instrumented Charpy tests.*

Material Condition	Test Temperature, °C	Energy, ft·lb			Deflections, in.		Yield Stress, ksi		Fracture Toughness, ksi$\sqrt{\text{in.}}$
		W_T	W_I	W_F	d_{max}	d_1	Static[a]	Dynamic	Approximated from COD_{max}
Unshocked	25	237.6	34.1	...	0.181	...	33.7	65.7	236.0
	300	229.7	52.3	...	0.363	...	22.8	35.9	231.0
	500	203.3	53.5	...	0.449	...	19.9	28.7	219.6
	600	196.0	53.3	...	0.468	...	19.9	27.9	215.3
	650	184.5	54.9	...	0.491	...	19.9	27.9	217.4
Shocked 80 kilobar	25	119.5	38.7	65.9	0.166	...	52.1	86.5	259.2
	500	110.0	28.1	...	0.196	...	37.1	52.6	192.7
	500	103.0	22.5	...	0.156	...	37.1	52.6	175.3
	600	109.0	21.9	...	0.157	...	33.9	50.6	167.9
	650	111.5	21.0	...	0.162	...	31.0	47.0	162.1
Shocked 160 kilobar	25	76.9	22.1	37.6	0.100	0.160	60.5	91.6	207.1
	500	77.0	17.5	36.7	0.105	0.204	51.7	68.5	164.1
	600	75.0	18.0	32.9	0.120	0.203	46.9	59.8	159.6
	650	74.0	17.2	...	0.120	...	43.5	56.6	153.1

[a] Data obtained from Refs *11* and *12*.

Figure 4 shows typical fracture surfaces and load-time records for material tested at room temperature. The load-time record for each specimen is converted to load-deflection data. These data are used for the previously described calculations of stress, and approximating fracture toughness, thus furnishing information for engineering analysis. The test results from this investigation are presented in Table 3. In general, it is observed that total energy, yield, and maximum load decrease as the temperature increases; however, some shocked materials show a minimum total energy absorbed at approximately 500°C (932°F) and then slight increases at 600°C (1112°F) or 650°C (1202°F) or both.

A comparative plot of the total energy absorbed during impact versus temperature for all materials is shown in Fig. 5. The shocked materials show a relatively small total energy (W_T) change over the entire temperature range. The unshocked material undergoes a continual decrease in W_T with increased temperature, but still exhibits a very high energy absorption (184.5 ft·lb) at 650°C (1202°F).

The overall trend is for a decrease in energy absorbed with an increase in shocking pressure or temperature.

The room-temperature fracture toughness of all shocked material is less than that of the control material except for the material shocked at the lowest pressure (Fig. 6). Significantly, an increase in toughness is indicated in static tension tests also, where increases in both ductility and yield strength were obtained. Fracture toughness (K_c) decreases as the temperature increases, with all elevated-temperature values of the shock material falling below those of the unshocked material.

Figure 7 shows how the dynamic yield stress increases with increased shocking pressure. This diagram also shows how the dynamic yield stress is affected by increasing the test temperature from 25 to 650°C (77 to 1202°F). The ratio of maximum load (P_{max}) to general yield load (P_{GY}) as a function of shocking pressure is shown in Fig. 8. The ratios for all elevated-temperature tests fall very near the same curve, thus indicating quite similar dynamic strain-hardening characteristics at 500, 600, and 650°C (932, 1112, and 1202°F). The unshocked material has an elevated-temperature P_{max}/P_{GY} ratio greater than 2, but the ratio rapidly approaches unity as the shocking pressure increases. At room temperature the unshocked material has a much lower initial ratio of 1.48 and it shows only a slight decrease as a function of increasing pressure.

The ratio of dynamic yield stress to static yield stress is plotted as a function of temperature in Fig. 9. The ratio exhibits a general decrease as the temperature increases, with a minimum being reached at 500 to 600°C (932 to 1112°F) and with a slight increase shown at 600 to 650°C (1112 to 1202°F). The ratio of dynamic to static yield stress at 25°C (77°F) decreases from 1.95 for unshocked material to approximately 1.5 at pressures of 160 kilobar. This indicates a decrease in strain-rate sensitivity as the shocking pressure increases. This difference decreases as the test temperature increases and, in fact, undergoes a

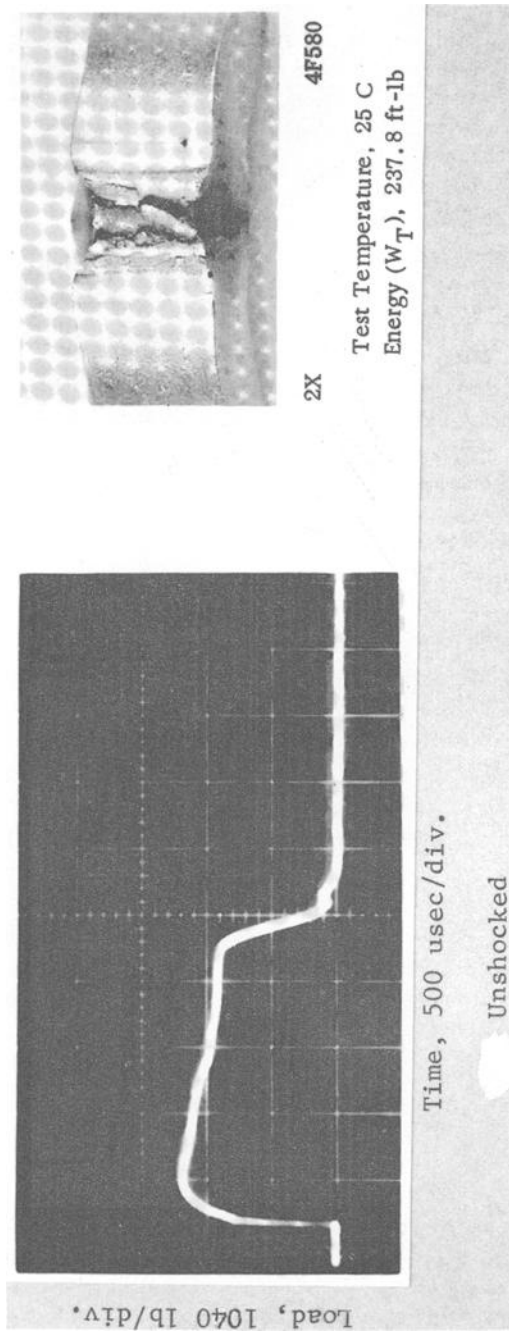

FIG. 4—*Typical load-time traces and fracture appearance of unshocked and shocked Type 316 stainless steel.*

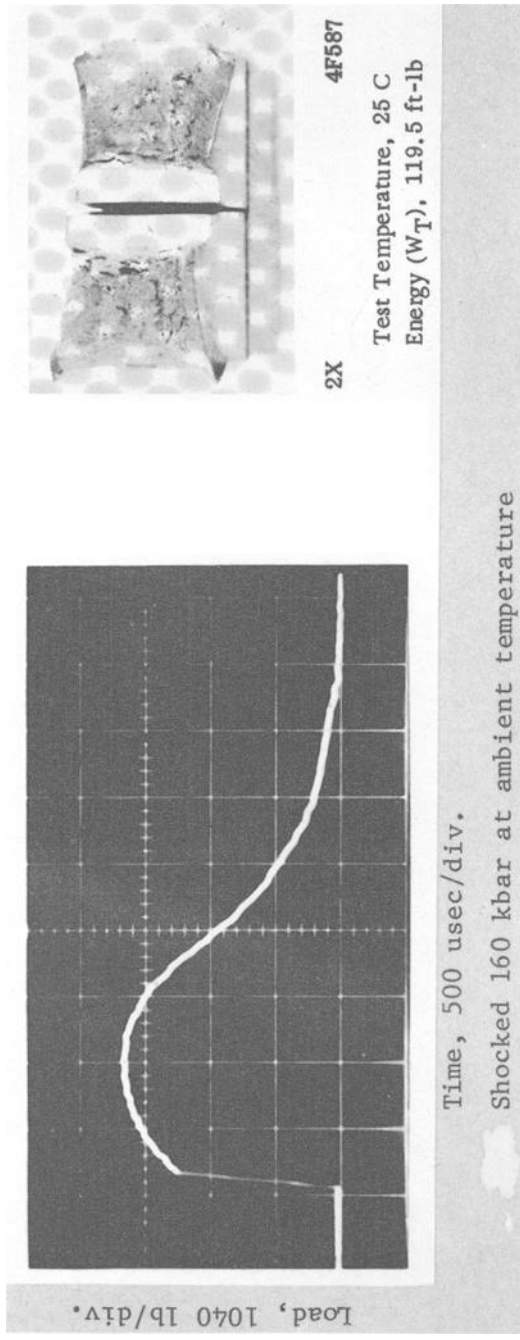

FIG. 4–*(Continued).*

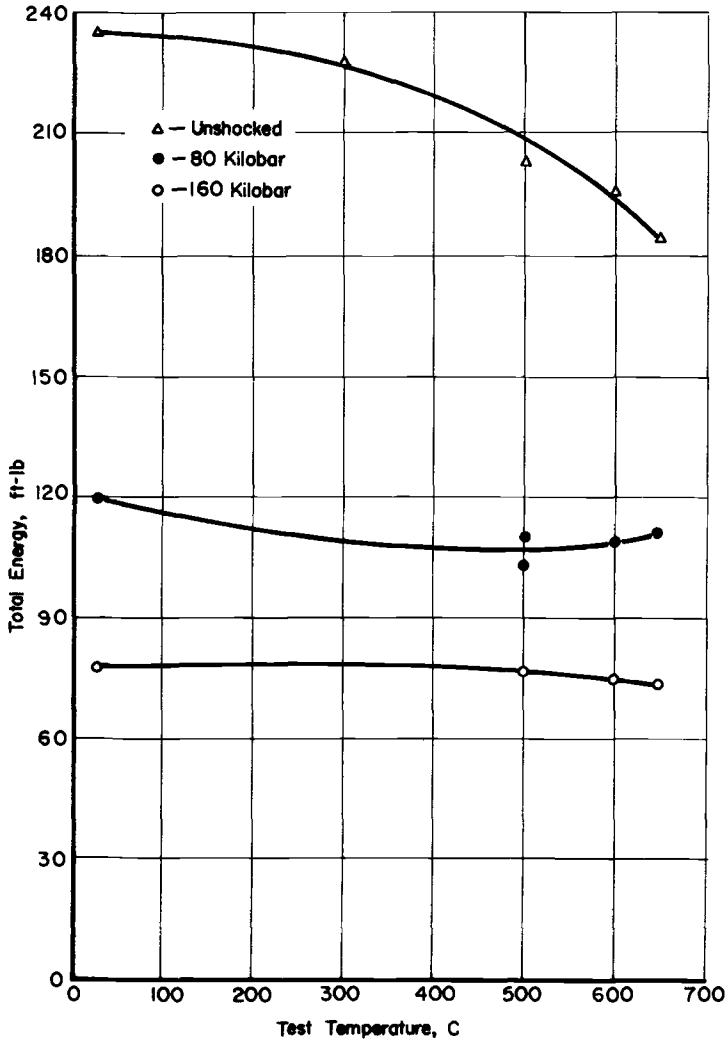

FIG. 5—*Temperature diagram for total energy absorbed during impact of unshocked and shock-strengthened Type 316 stainless steel.*

reversal at 600 and 650°C (1112 and 1202°F) for material shocked at the lowest (80 kilobar) pressure level as compared with unshocked material.

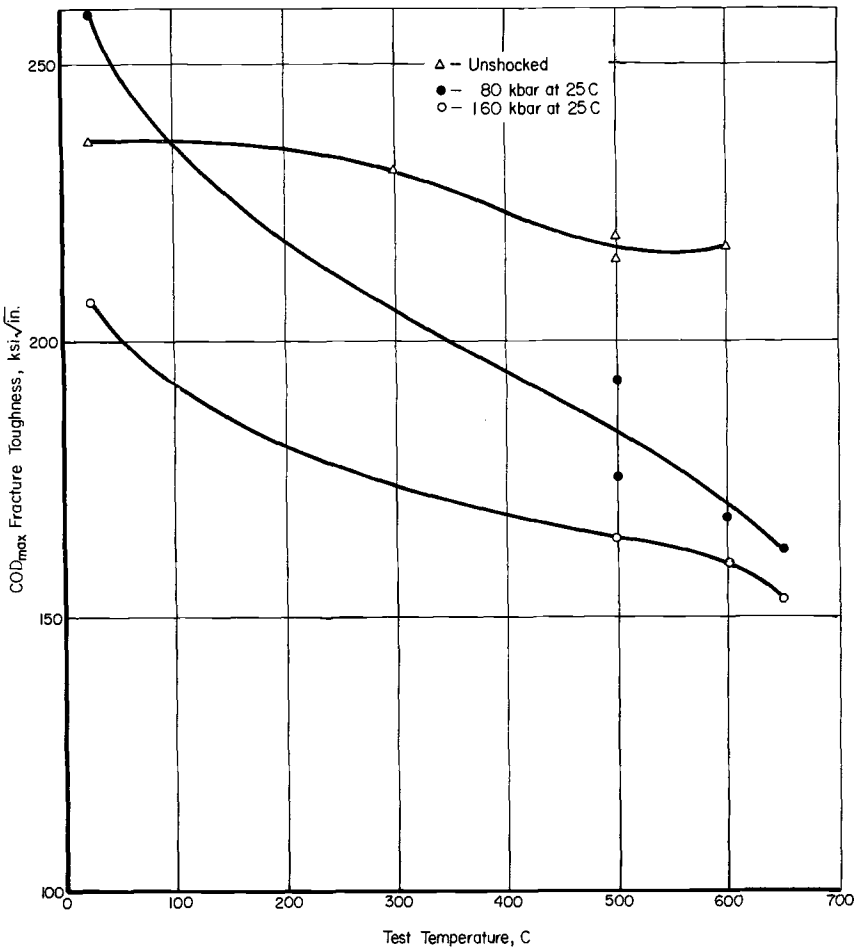

FIG. 6–*Temperature diagram for fracture toughness of unshocked and shocked Type 316 stainless steel.*

Conclusions

Instrumented impact testing of shock-strengthened Type 316 stainless steel resulted in the following conclusions:

1. The total Charpy impact energy is progressively decreased by increasing the shocking pressure.

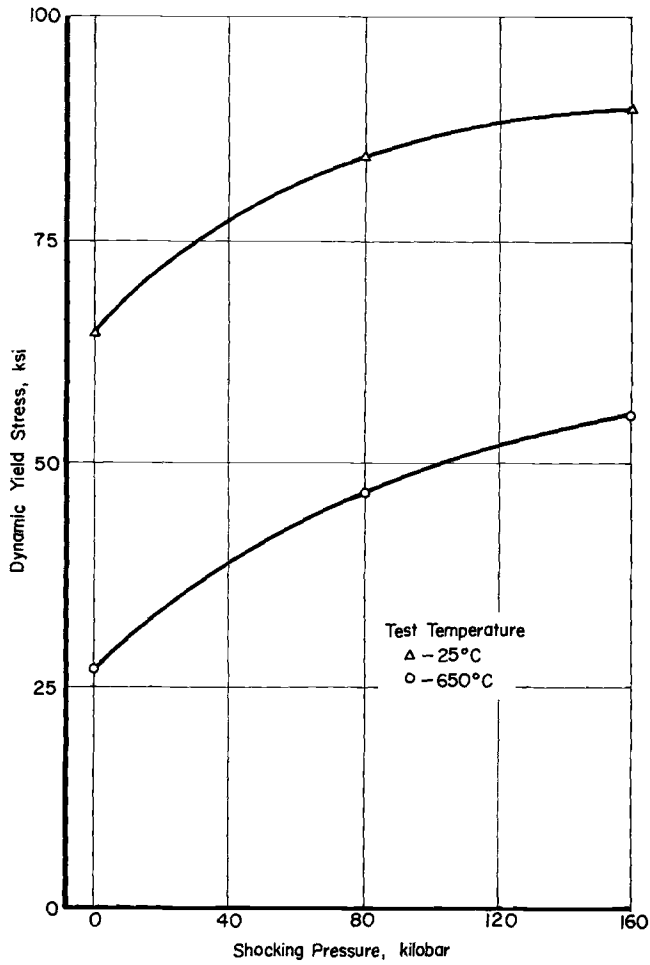

FIG. 7–*Dynamic yield stress of Type 316 stainless steel as a function of shocking pressure.*

2. The dynamic yield strength (σ_{dy}) is increased by increasing the shocking pressures for all testing temperatures. This trend is expected because the static yield strength (σ_{sy}) was also found to increase with increasing shocking pressure [*11-12*]. However, the ratio of dynamic yield to static yield strength (measure of strain-rate sensitivity) was found to decrease with increasing shocking pressure.

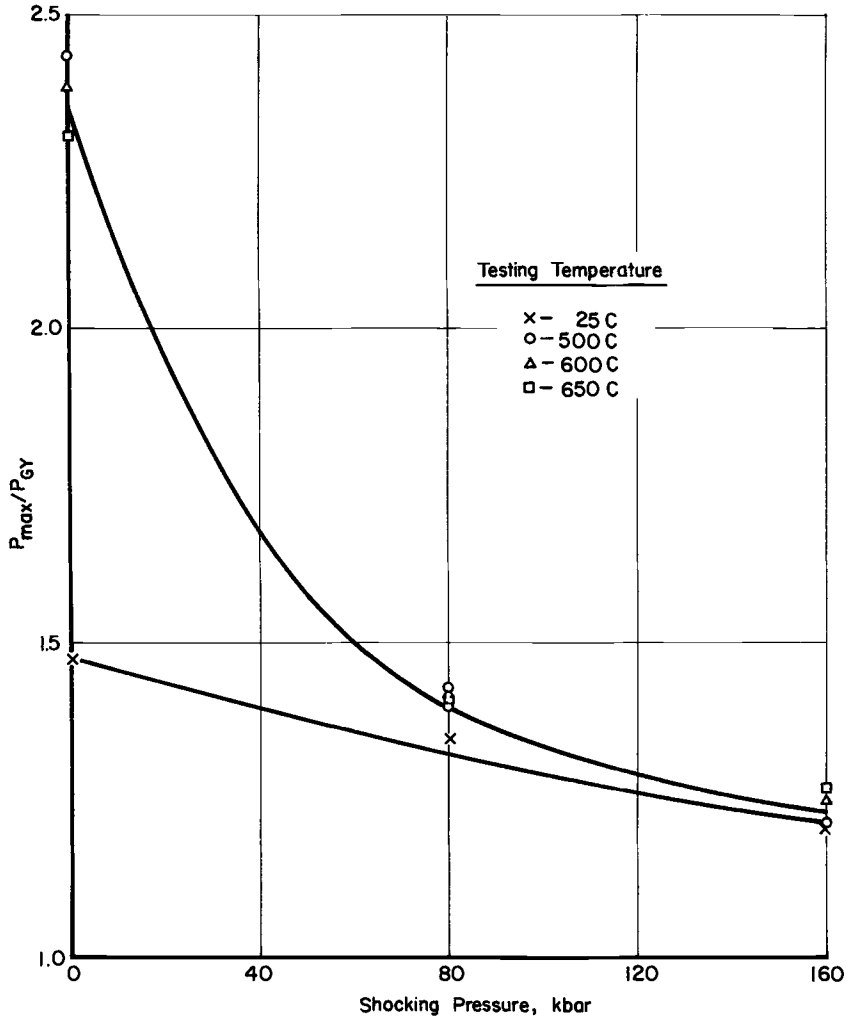

FIG. 8–*Ratio of maximum load to general yield load at various temperatures as a function of shocking pressure for Type 316 stainless steel.*

Acknowledgment

The work herein was performed under AEC Contract W-7405-eng-92.

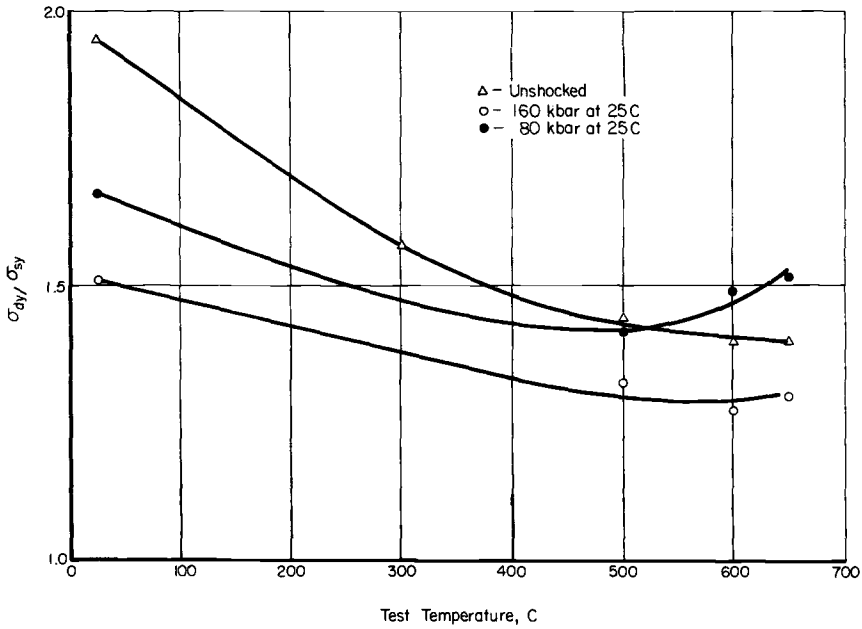

FIG. 9–*Ratio of dynamic yield stress to static yield stress for unshocked and shocked Type 316 stainless steel at various temperatures.*

References

[*1*] Kagilaski, M., Perrin, J. S., Wullaert, R. A., and Bauer, A. A., *Metallurgical Transactions*, Vol. 2, 1971, pp. 2607-2612.

[*2*] Trott, B. D., Jung, R. S., Goodard, S., and Stein, R. A., "Impact Sensitivity of Explosives," Battelle's Columbus Laboratories Report, 1971.

[*3*] Server, W. L. and Tetelman, A. S., "The Use of Pre-Cracked Charpy Specimens to Determine Dynamic Fracture Toughness," UCLA Report ENG-7153, University of California at Los Angeles, 1971, p. 4.

[*4*] Wullaert, R. A. in *Impact Testing of Metals, ASTM STP 466*, American Society for Testing and Materials, 1970, pp. 148-164.

[*5*] Wullaert, R. A., Ireland, D. R., and Tetelman, A. S. in *Irradiation Effects on Structural Alloys for Nuclear Reactor Applications, ASTM STP 484*, American Society for Testing and Materials, 1971, pp. 20-41.

[*6*] Tardiff, H. P. and Marquis, H., *Canadian Metallurgical Quarterly*, Vol. 2, 1963, pp. 373-398.

[*7*] Ireland, D. R., "Application of the Instrumented Charpy to Fracture Toughness," presented at the Fracture Toughness Symposium of the ASM 1971 Materials Engineering Congress, 18-21 Oct. 1971.

[*8*] Ireland, D. R., "Dynamic Properties of Superalloys at Elevated Temperatures," Battelle's Columbus Laboratories Report, 1971.

[*9*] Green, A. P. and Hundy, B. B., *Journal of the Mechanics and Physics of Solids*, Vol. 4, 1956, p. 128.

[*10*] Wells, A. A., Symposium on Crack Propagation, Paper No. B4, Cranfield, England, 1961.

[*11*] Kangilaski, M. and Bauer, A. A., "Mechanical Properties of Shock-Strengthened Austenitic Stainless Steel," Battelle's Columbus Laboratories Report BMI-1909, 1971.

[*12*] Kangilaski, M., Sheckherd, J. W., and Bauer, A. A., "Mechanical Properties of Shock-Strengthened Type 316 Stainless Steel" (to be published).

R. H. Toland[1]

Impact Testing of Carbon-Epoxy Composite Materials

REFERENCE: Toland, R. H., "Impact Testing of Carbon-Epoxy Composite Materials," *Instrumented Impact Testing, ASTM STP 563*, American Society for Testing and Materials, 1974, pp. 133-145.

ABSTRACT: Advanced fiber composite materials exhibit elastic properties and fracture mechanisms distinctive from metals. Consequently, the mechancis of impact resistance are also different for these materials. Carbon-epoxy and boron-epoxy composites can exhibit brittle modes of fracture. In studies to improve the impact resistance of carbon-epoxy materials, traditional impact tests provided very little understanding of the problems involved. However, instrumented Charpy-type tests provided considerable insight into the mechanisms associated with impact resistance. Load versus time response records can be partitioned into regions corresponding to events occuring sequentially in time. Energy absorbed by a composite specimen through the various fracture mechanisms is seen to be the distinguishing characteristic between composite systems. Two mechanisms to improve the carbon-epoxy system's impact resistance are shown to be the modification of the fiber-resin interfacial strength and hybridization with a second fiber of high strength and lower modulus.

KEY WORDS: composite materials, carbon, glass, fracturing, impact strength, epoxy resins, impact tests

Advanced composite materials have extended a promise of significant advances in many commercial and military structural applications. This results from such inherent properties as high specific modulus and strength, low creep, good fatigue resistance, and thermal stability. However, these materials can also exhibit elastic anisotropy and bending-extensional and in-plane shear coupling effects. Further, the fracture mechanisms associated with the three-phase (fiber, resin, and interface) constituency of the composite are unique to these materials. Both the elastic and fracture behaviors strongly influence the static, dynamic, and impact structural response characteristics. In part because of these effects, a basic understanding of the impact resistance phenomena of composites is not readily found through utilization of traditional impact tests. The instrumented impact test, however, greatly extends the capabilities of the traditional test methods. The load versus time oscilloscope trace generated by this technique results in considerable insight into the unique character of composite impact

[1] Assistant professor of mechanics, Drexel University, Philadelphia, Pa. 19104.

resistance. By separation of the response record and associated energy into those regions dominated by elastic and fracture behaviors, a quantitative description of each can be determined. In a consistent manner quasi-brittle and nonbrittle behavior are differentiated, mode of fracture and point of onset determined, notch sensitivity evaluated, and a more objective evaluation between two materials can be made. In addition, the influence on specimen response of such parameters as specimen geometry, fiber type, and interfacial bond strength can be studied for its relative importance [*1*].[2]

The composite materials of principal interest here are S-glass-epoxy (GRP) and high-strength carbon-epoxy (CFRP) unidirectional fiber systems. Table 1 presents typical values of static strengths, S, and moduli, E and G. Subscripts 1, 2 and 3 refer to the fiber, transverse to the fiber, and normal to the plane directions, respectively; see Fig. 1. Subscripts T and C refer to tension and compression.

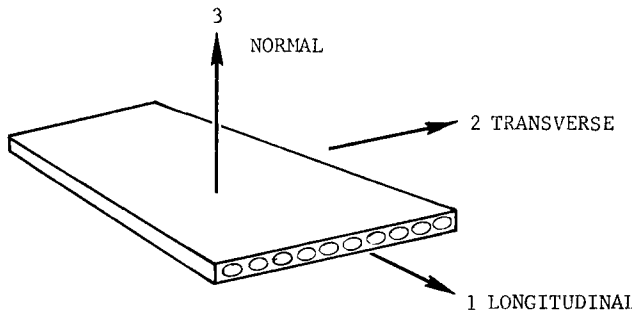

FIG. 1–*Idealized single-ply unidirectional composite lamina.*

TABLE 1–*Typical CFRP and GRP unidirectional composite properties (static).*

Material	E_1, msi	S_{1T}, ksi	S_{1C}, ksi	E_2, msi	S_{2T}, ksi	S_{2C}, ksi	G_{12}, msi	S_{12},[a] ksi
CFRP	22	200	200	1.4	12.0	35	0.6	12-18
GRP	9	275	60	2.0	6.5	24	0.8	6-13

[a] Interlaminar shear strengths S_{13} and S_{23} are approximately equivalent to S_{12}.

[2]The italic numbers in brackets refer to the list of references appended to this paper.

Rate dependency can be found in those properties governed by the resin matrix such as E_2 and S_2 while properties governed by the fiber are rate insensitive. The elastic anisotropy is evident upon examination of the E_1 and E_2 values. Also, note that the composite shear strengths S_{12}, S_{13}, S_{23} are of the order of 10 percent of the tensile strength for the fiber direction, S_{1T}. This becomes an important factor in beam impact loading. These two composite systems also exhibit approximately linear elastic behavior to fracture in the fiber-oriented direction.

The introduction of GRP composites in the late 1950's did not precipitate much interest in impact resistance because of apparent satisfactory Charpy and Izod impact energies. Around 1965, the carbon and boron fibers had been developed and formed the vanguard of new 'advanced,' higher-modulus fibers for aerospace and commerical use. While Charpy energies C_V were considerably lower, Fig. 2, and fractures were more brittle, research emphasis was concentrated in developing lamination and strength theories. By 1970, commercial and aerospace applications were being found which were design limited by an impact environment. Foreign object damage (FOD) encountered by jet fan blades is an operational hazard condition. Golf club shafts see impact as a design service load. These two specific applications generated great interest in the impact resistance 'problems' of these new materials.

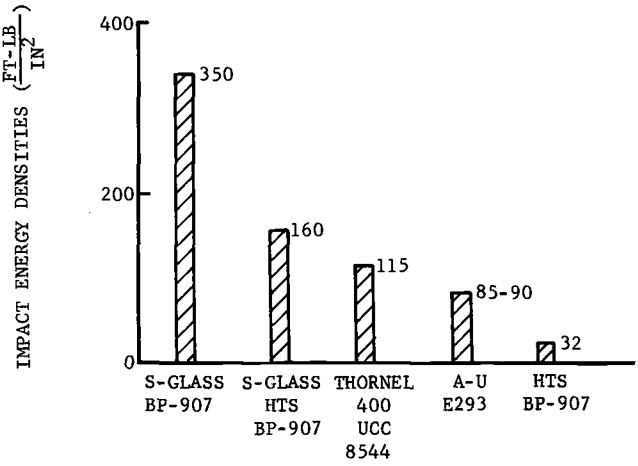

FIG. 2—*Typical Charpy data for several composite systems.*

The Impact Environment

Physical impact is the collision of two or more bodies in which the forces created are applied and removed in a very brief interval of time. Both bodies possess mass, material elastic and fracture properties, and physical dimensions.

Both short-time transient stresses and longer-time vibrations are induced in the bodies. Since penetration of a body is possible and because of the briefness of the event, the transient stresses are important in describing the short-time local events. The physical description of the impinging body and the dynamics of the impact event are needed to perform a wave propagation analysis. Also, as yielding or fracture may occur in either body, appropriate failure criteria are needed to supplement the elastic wave and vibrational analyses.

The response of the impacted object can be separated into regimes corresponding to time-elapsing events. In the first microseconds after initial contact, transient stress waves propagating from the impact region have not reached the boundaries of the specimen (or structure). During this interval the response is analyzed as a wave propagation problem and the material characteristics play a dominant role in the stress history. After these initial wave fronts have encountered the specimen boundary, the structural aspects of the impacted body become significant. After a time corresponding to multiple transversals of the specimen by the initial wave fronts, the wave propagation analysis can be superseded by a Timoshenko beam or similar vibration analysis. The impact reponse is equally a structural and material problem at this point in time. The role of geometry is also significant in a test specimen design.

The average engineer or materials scientist is well acquainted with the analytical models and experimental techniques available for describing the behavior of static and dynamic (rapid loading) events. Unfortunately, analysis and instrumentation have been too frequently omitted from impact studies, with a resulting loss in understanding of the phenomenon. Analytical tools are now available [*2,3*], and instrumentation can be intelligently applied. The application of instrumentation to the Charpy-type impact test of composite materials has been successful in providing greater insight into this phenomenon.

Instrumented Charpy Testing of Composite Materials

Figure 3 is a schematic of an instrumented Charpy impact response record. The equipment designed by Effects Technology, Inc. incorporates an instrumented tup whose strain response is calibrated to represent an analog of the impact contact force. Because the Charpy test almost always involves fracture in a composite specimen, the response deviates from the approximate half-sinusoid characteristic of impact on an elastic beam. As illustrated in Fig. 3, the response of the typical composite Charpy impact specimen corresponds to three distinct regions in the load versus time curve. They are regions of preinitial fracture, initial fracture, and postinitial fracture. The initial region corresponds to the elastic response of the composite beam. The initial fracture occurs in one of the modes discussed in the next section. The mode of this first fracture in large measure determines the subsequent specimen response. It is with regard to the two latter regions that the distinctive elastic and fracture characteristics of composite systems are manifested in the Charpy test.

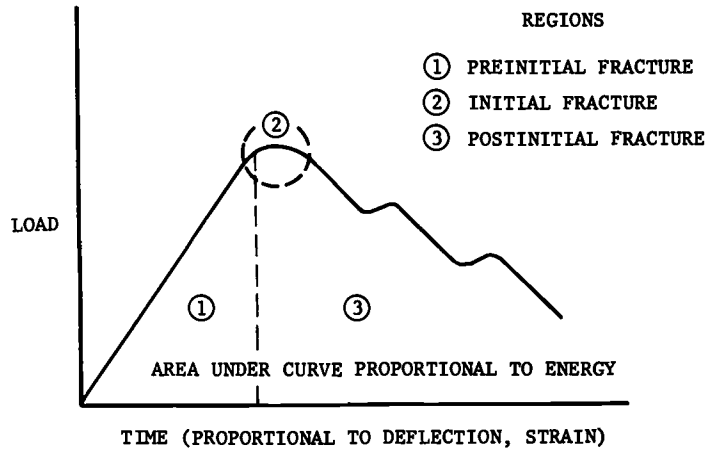

FIG. 3—*Characteristic response record of an impact-loaded composite laminate.*

The advantages of this test form are immediately apparent. Where the traditional test resulted only in a measurement of total absorbed energy and a fractured specimen, the instrumented test provides a measure of the specimen response which can be interpreted in terms of events. This approach, then, reinstates the same concern for information in the impact experiment as is commonly found in most other testing. It also draws in some of the analytical tools available to describe the mechanics of impact. These aspects plus the studies of fracture and reliability can elevate impact studies to a high plane of endeavor.

Figure 4 presents typical notched Charpy data for several composite systems where the total energies absorbed during impact are partitioned into elastic and fracture regions. This chart is informative since it shows the major distinction between the different systems to be the energetics of fracture. The role of fracture in the Charpy impact resistance phenomenon is a major factor to be considered for composite materials. In addition, the roles of damage tolerance and reliability are fundamental to the materials selection process for specific applications. Basic questions arise, such as: Can any form of fracture (damage) be permitted? If yes, what extent of damage in a structure is to be allowed in a given operational environment? The instrumented test methods are able to provide direction in the development of such criteria.

Figure 5 is a response record for a glass-epoxy Charpy specimen. Since the area under the curve is proportional to energy, the elastic energy to first fracture is seen to be considerably less than the subsequent fracture energies, as noted in Fig. 4. As will be discussed in the next section, the mode of initial fracture is an interply delamination due to interlaminar shear. It should be recalled at this point that this is a weaker-strength mode in resin matrix composites. Each

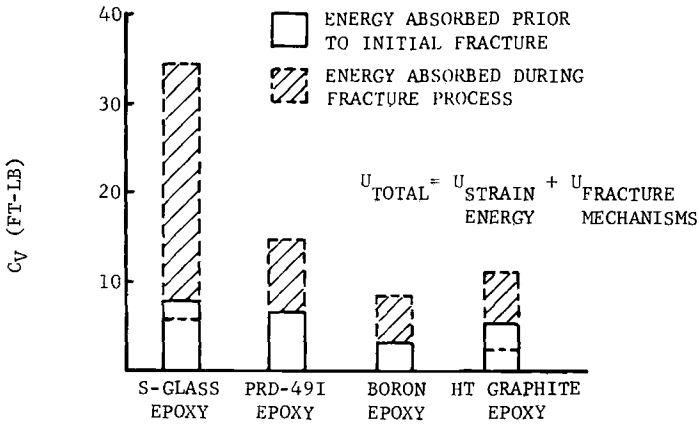

FIG. 4—*Representative notched Charpy impact energies for different composite materials.*

subsequent 'drop-off' in the load versus time trace can be correlated to a major delamination in the specimen, Fig. 6. This fracture mechanism is apparently an effective mode of impact resistance. If the same record were truncated at the onset of initial fracture, the record would be typical of a 'quasi-brittle' cleavage fracture seen in some carbon-epoxy systems. The fracture energy of this mode is minimal. Two carbon-epoxy Charpy specimens are shown in Fig. 7. The fracture on the left is a classical brittle cleavage. The fracture on the right shows sheets of

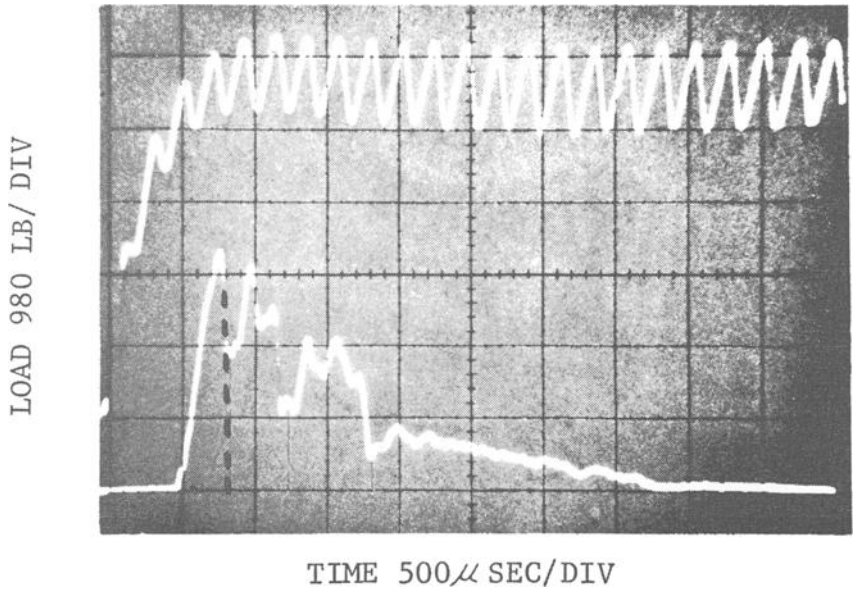

FIG. 5—*Response record for a glass-epoxy Charpy specimen.*

fibers pulled out of the other half of the specimen. This latter fracture is shown to be more energy consuming than the cleavage mode, and the load versus time response indicates effective postinitial fracture behavior. It is of interest to discuss briefly the fracture mechanisms experienced by composite systems, several of them unique to these materials, and to consider means of possible enhancement of the impact resistance of select materials.

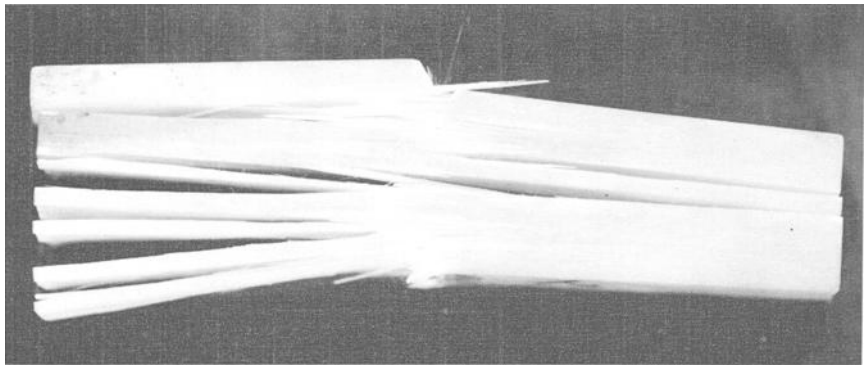

FIG. 6—*Fractured glass-epoxy Charpy specimen.*

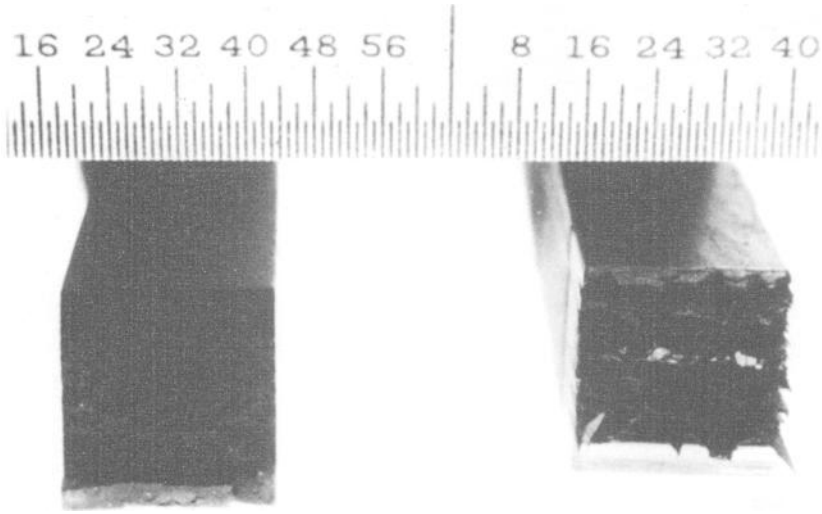

FIG. 7—*Fractured carbon-epoxy Charpy specimens.*

Fracture Mechanics

Since the advent of the advanced composite systems, considerable interest has been focused on the fracture mechanics of these materials. Several references [*4,5,6*] from the multitude available are listed. Also, recent works [*7,8*] summarize much of the current theories on fundamental composite fracture phenomena. Several aspects of these theories were summarized in Ref *1* and will be repeated here.

Fracture initiation in the bending specimen can be a tensile failure in the fiber reinforcement, a fiber compression failure in any one of the several possible modes such as microbuckling, and an interlaminar shear failure in the composite. Prior to a fiber tensile failure, debonding of the fiber and matrix at the interface may occur. The mode of this initial fracture is important in subsequent events.

When the fiber-resin bond is very strong, typical of graphite fiber composites with high surface treatment level for the fiber, a fiber tensile fracture will promote cleavage of the matrix normal to the fiber axis [*4*]. The strain energy released by the broken fiber must be absorbed locally to prevent propagating an unstable crack. The ability to do this in an assumed perfectly bonded composite is a function of the composite fiber volume, the elastic transfer length, and the surface energies to form fractures in resin and fiber. The numerical calculations in Ref *4* indicate that high-tensile-strength carbon fiber fractures result in a borderline situation between stable and unstable matrix cracks. For fiber volumes greater than 50 percent, as in the practical cases, an unstable crack process is predicted. If, in addition, the crack is being forced as in a dynamic impact environment, a "brittle" cleavage fracture through the specimen is highly probable. It can be concluded that CFRP composite systems exhibiting high composite interlaminar shear and high resin-matrix bond strengths will most probably experience brittle cleavage fractures.

The initial failure mode in the GRP Charpy specimen was found to be interlaminar shear as in a dynamic short-beam shear specimen. While the specimen loses its original structural integrity, the fibers experience little or no tensile fracture. While this response is, in part, mechanistic and a function of the particular specimen-loading interaction, it is representative of an efficient energy absorbing mechanism. This is particularly true since the fiber strain energy is not lost through fiber fracture. Reference *9* provides an analytical description for the associated energy of interlaminar shear delamination as:

$$U_{ILS} = \frac{1}{2} \frac{S^2_{12}}{G_{12}} (N_D A_D L_D)$$

where N_D, A_D, and L_D are the number, area, and length of delamination, respectively.

Two additional energy-absorbing mechanisms associated with fiber tensile fracture are fiber debonding and fiber pullout. The debonding phenomenon is fiber-matrix separation for some distance along the fiber in the vicinity of a microcrack. References *5* and *6* present the fracture surface energy due to debonding as:

$$\gamma_D = \frac{V_f \, \sigma_f^2 \, y}{4 E_f}$$

where y is the debonded length of fiber immediately prior to debonding and V_f, σ_f, and E_f are fiber volume, tensile strength, and modulus, respectively.

The fiber pullout mode required that the fibers pullout against a restraining force due to interfacial shear stresses on the fracture surfaces as they are being separated. References *5* and *6* provide the following expression for energy dissipated during fiber pullout:

$$\gamma_D = \frac{V_f \, \sigma_f \, \ell_c}{24}$$

where ℓ_c is the critical transfer length. Reference *6* indicates, from experimental fracture energies, that the debonding model is in closer agreement with GRP tensile fracture behavior, while the pullout model agrees better with CFRP tensile fractures. Reference *4* equates energy absorbed by debonding to energy released at fiber fracture, indicating that stable fractures will occur in the CFRP composite for this fracture mode. The energy absorbed by debonding is shown to be two orders of magnitude higher than the energy absorbed in cleavage, indicating the considerable improvement in composite efficiency when fiber tensile failures are coupled with either debonding or pullout. The problem is to control the failure process through either of these two mechanisms without sacrificing other composite properties such as longitudinal compression, interlaminar shear, and transverse tensile strength. The fiber matrix interfacial bond is the principal parameter involved in achieving less brittle carbon fiber composites.

In Ref *1* brief discussions on the effects of notching, specimen thickness, and multiple-ply orientation on Charpy-type specimens are presented.

Improving Composite Impact Resistance

Coupling a knowledge of composite fracture with instrumented impact test techniques permits more rapid development of improved impact resistance in composite systems. Two practical approaches to improving the impact resistance of carbon-epoxy systems are discussed.

As noted in the previous section, interfacial bond strength between the fiber and the resin is the dominant factor involved in fiber debonding and interply shear delamination. The surface energies of both of these fracture modes can be considerable. These modes, then, form the basis for very effective impact energy absorption mechanisms in composite materials and structures. Interlaminar shear strength of a composite system is regarded as one indirect measure of interfacial bond strength. The level of this bond can be rapidly modified on a fiber, especially the carbon fibers. The principal mechanism for altering the bond is through treatment of the fiber surface. Figure 8 presents notched Charpy data for several carbon-epoxy systems with varying interlaminar shear strengths. The brittle cleavage fractures characteristic of high interfacial bond strength exhibit little postinitial fracture behavior in the load versus time records. With decreasing bond strength, both interply delaminations and fiber pullout mechanisms can be observed in the specimens. The response records now indicate significant fracture energies, Fig. 9. Optimum levels of interfacial bond strength can be found for given fiber-resin systems such that improved impact resistance is not achieved at the expense of the static strengths of the system. As an example, Fig. 10 is the load versus time record for a carbon-epoxy system with a very high C_V energy value and low interfacial bond strength. The record indicates that this apparently good impact resistance is achieved entirely in the postinitial fracture region of the response. The load level and corresponding

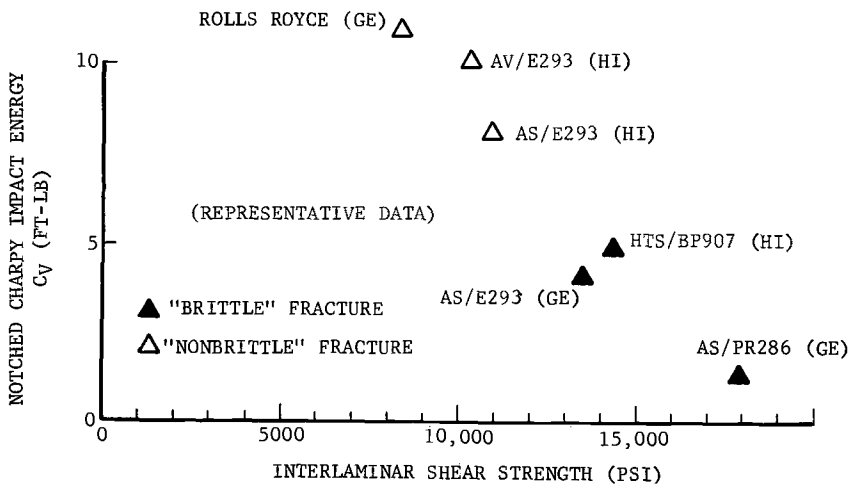

FIG. 8—*Notched Charpy impact data plotted against interlaminar shear strength.*

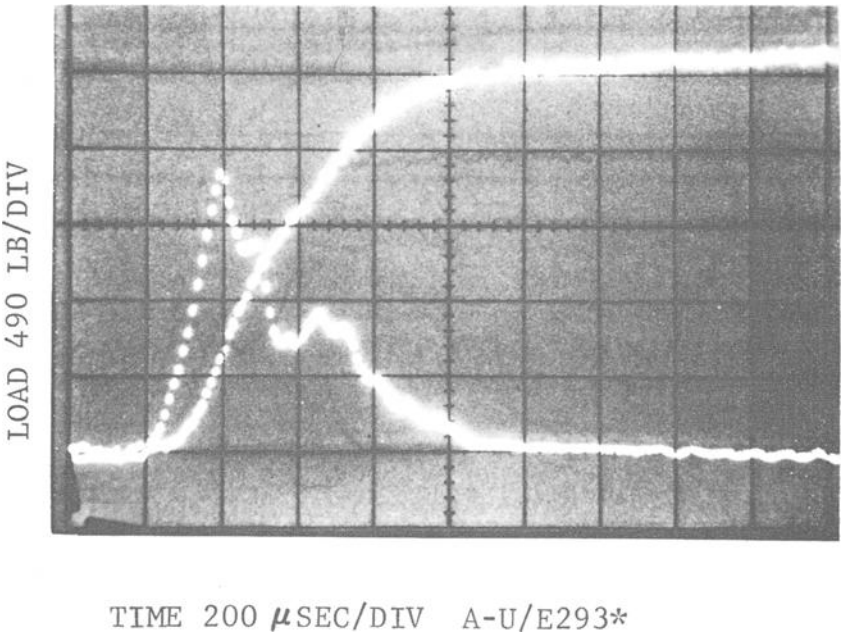

FIG. 9—*Response record for a "nonbrittle" carbon-epoxy Charpy specimen.*

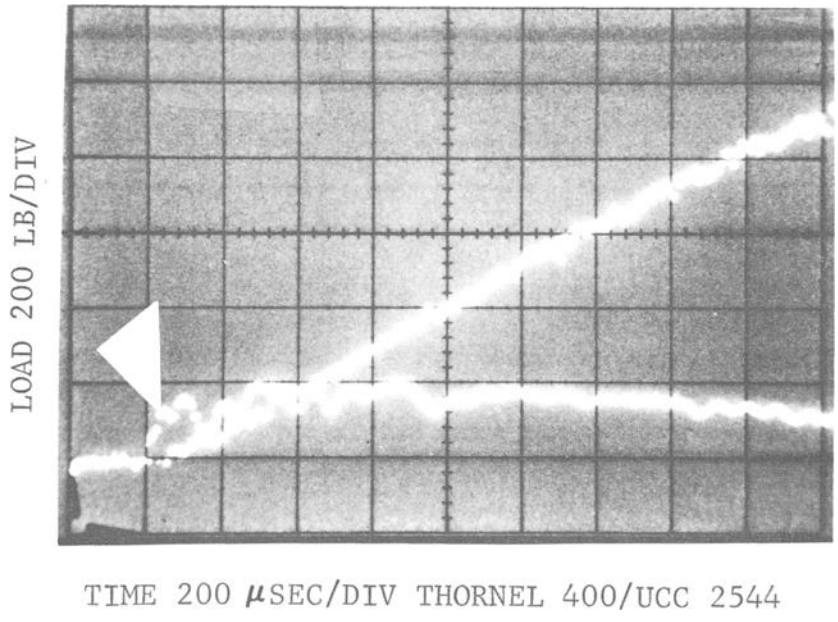

FIG. 10—*Response record for a carbon-epoxy system with a low damage threshold.*

energy to initial fracture are exceedingly low. Within a practical damage tolerance criterion, this material might prove unacceptable for many applications because of the low damage threshold.

A second practical mechanism for improving carbon-epoxy composite impact resistance is hybridization with a second fiber type. By including a high-strength, lower-modulus fiber such as S-glass or PRD-49, initiation of high-energy fracture modes associated with these fibrous systems can be induced in the hybrid system. The most frequently achieved mechanism when the fiber types are stratified in distinct layers is interply delamination. Either fiber debonding or delamination may be the dominant mechanism for hybrids with intraply dispersion of both fibers. Figure 11 is a representative instrumented Charpy response record for a glass-carbon epoxy hybrid specimen. The postinitial fracture energies are significant. The record also demonstrates a smoother profile perhaps representative of a better distribution in time of a greater number of smaller events. Reference *1* presents data on relative impact resistance improvement as a function of percent S-glass added to a carbon-epoxy system.

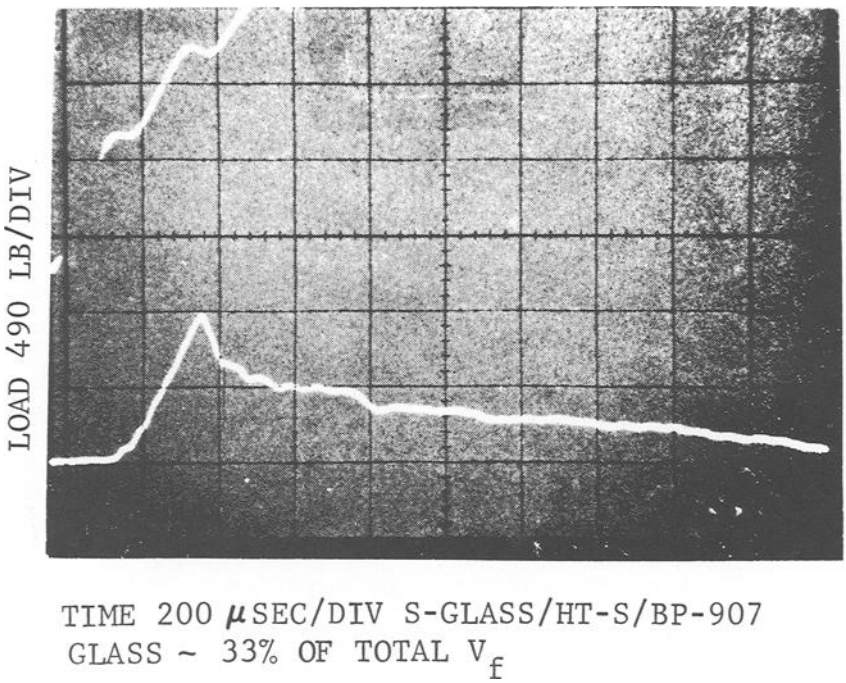

FIG. 11–*Response record for a carbon-glass epoxy hybrid composite system.*

Conclusions

Composite material systems exhibit unique elastic and fracture properties. Traditional impact tests developed for metals and plastics provide limited insight into the impact resistance phenomena of composite materials. However analytical and experimental techniques exist which can bring composite impact testing into better focus. The instrumented Charpy test is a good example. By this method it is possible to identify many time-dependent phenomena which occur during the impact loading of a specimen. Mode of fracture is found to be a dominant influence on composite impact resistance. Coupling a knowledge of composite fracture to instrumented test methods can result in the development of improved composite systems. It is shown that two techniques are readily available to improve the impact resistance of carbon fiber-epoxy systems. These are: (1) optimization of the interfacial bond strength between fiber and matrix; and (2) hybridization with a second fiber such as high-strength PRD-49 or S-glass. Nonbrittle modes of fracture are produced by these techniques and their effectiveness can be evaluated using instrumented test methods.

Acknowledgments

The data presented were generated by the author while in the employment of Hercules Incorporated, Salt Lake City, Utah, under internal research and development funding. Testing was performed by Effects Technology, Inc. of Santa Barbara, California.

References

[1] Toland, R. H., "Failure Modes in Impact-Loaded Composite Materials," American Institute of Mining, Metallurgical and Petroleum Engineers, Spring Meeting, Boston, Mass., 8-11 May 1972.

[2] Goldsmith, Werner, *Impact: The Theory and Physical Behavior of Colliding Solids*, Edward Arnold Ltd., London, 1960.

[3] Chou, P. C., "Introduction to Wave Propagation in Composite Materials," *Composite Materials Workshop*, Tsai, Halpin and Pagano, Eds., Technomic Publishing Co., Stamford, Conn., 1968.

[4] Mullin, J. V. and Mazzio, V. F., "Basic Failure Mechanisms in Advanced Composites, Final Report," NASA Contract NASW-2093, April 1971.

[5] Kelly, A., "Interface Effects and the Work of Fracture of a Fibrous Composite," *Proceedings* of the Royal Society, Series A. Vol. 319, 1970.

[6] Beaumont, P. W. R. and Phillips, D. C., "The Tensile Strengths of Notched Carbon Fiber and Glass Fiber Composites," Materials Development, School of Engineering and Applied Science, University of California at Los Angeles, Dec. 1971.

[7] Kelly, A., Reinforcement of Structural Materials by Long Strong Fibres, *Metallurgical Transactions*, Vol. 3, Sept. 1972.

[8] Murphy, M. C. and Outwater, J. O., "The Toughness of Reinforced Plastics," 28th Annual Technical Conference, The Society of the Plastics Industry, Inc., 1973.

[9] Chamis, C. C., Hanson, M. P., and Serafini, T. T., "Designing for Impact Resistance with Unidirectional Fiber Composites," NASA TN D-6463, Aug. 1971.

K. R. Iyer[1] *and R. B. Miclot*[1]

Instrumented Charpy Testing for Determination of the *J*-Integral

REFERENCE: Iyer, K. R. and Miclot, R. B., "**Instrumented Charpy Testing for Determination of the *J*-Integral,**" *Instrumented Impact Testing, ASTM STP 563,* American Society for Testing and Materials, 1974, pp. 146-165.

ABSTRACT: Rice's path-independent integral J of medium-strength alloys was determined under dynamic conditions by instrumented impact testing of precracked Charpy specimens. The viability of the instrumented Charpy technique for rapid and easy determination of useful fracture parameters is explained. Standard and side-notched Charpy specimens of Cr-Mo-V, H-11, and CG-27 alloys were precracked and tested. Load-displacement curves were generated for specimens with different fatigue precrack lengths. The energy for initiation of fracture in each case was determined by measuring the area under the load-displacement curve up to limit load. The value J at the onset of crack propagation, J_{ID}, was calculated from a plot of energy versus crack length. The value of J_{ID} is not affected by side notches. The slope of the energy versus crack length plot alters sufficiently to compensate for the reduction in thickness. Agreement is good between K_{ID} values calculated from J_{ID} measurements and by other methods.

KEY WORDS: impact tests, fracturing, crack propagation, mechanical properties, fracture properties

Nomenclature

B	Thickness of specimen
ℓ	Span length
W	Width of specimen
a	Crack length including depth of machined notch
U	Energy under corrected load-time curve up to limit load
E	Young's modulus
ν	Poisson's ratio
J_{ID}	Dynamic plane-strain J-integral
K_{ID}	Dynamic plane-strain fracture toughness
G_{ID}	Dynamic plane-strain critical strain energy release rate
P_F	Fracture load–limit load–load for initiation of fracture
Z	Factor to convert P_F to K_{ID} for precracked Charpy specimens (function of a)

[1] Research metallurgists, Research Directorate, General Thomas J. Rodman Laboratory, Rock Island Arsenal, Rock Island, Ill. 61201.

COD Crack opening displacement
LPD Load-point displacement
d Depth of axis of rotation from notch root

In recent years, linear elastic fracture mechanics has developed far enough to analyze actual and potential brittle failure problems. However, a large class of problems in fracture, involving low- and medium-strength materials where plastic deformation precedes fracture, cannot be treated by linear elastic fracture mechanics. The concept of J-integral, introduced by Rice [*1*],[2] provides an extension of linear elastic fracture mechanics to cases which sustain either small- or large-scale plasticity before fracture. The path-independent J-integral can be evaluated along any region enclosing the crack tip. Consequently, the path along which the integration is carried can be taken through regions where the elastic-plastic state is determined with sufficient accuracy. Rice's [*1*] interpretation of J, on the basis of energy comparisons of notches of neighboring sizes, leads to an equation of the form

$$J = -\lim_{\Delta a \to 0} \frac{U(a + \Delta a) - u(a)}{\Delta a} = -\frac{\delta U}{\delta a} \tag{1}$$

where $U(a)$ denotes the potential energy of an elastic body of unit thickness containing a flat surfaced notch of length a, and δU and δa are incremental quantities; $\delta U/\delta a$ is the rate of change of potential energy of the cracked elastic body with crack size. Thus, if two bodies containing cracks of neighboring sizes and identical geometries are loaded under the same conditions, the difference in the energy under the load/load-point displacement (*LPD*) curve up to a particular *LPD* will represent the difference in potential energies of the two bodies at identical states.

Such an approach was taken by Begley and Landes [*2*], who have successfully determined J-integral as a function of *LPD* from a series of load-*LPD* curves for specimens containing different initial crack sizes. Thin specimens of three-point bend, center notch, and compact tension configurations were tested by these authors at a slow strain rate. Agreement was good between the experimental J_{IC} values and the G_{IC} values (calculated from K_{IC} values of thick specimens), Kobayashi et al [*3*] have shown good correspondence between values of J computed by numerical analysis and experimentally determined crack opening displacement (*COD*) values. These results are of practical importance because a fundamental plane-strain fracture parameter can be determined from load-displacement curves. Also, the method is applicable to thin specimens of materials which experience small- or large-scale plasticity before fracture.

Service components which experience high rate loading demand that their

[2]The italic numbers in brackets refer to the list of references appended to this paper.

design be based on dynamic material properties. Also, the fabrication of large specimens for fracture testing is frequently impractical. A pertinent example is small- and medium-caliber gun barrels. Testing of precracked Charpy specimens is suitable under such circumstances. The Charpy impact test is essentially a high strain rate, three-point bend test of notched specimens. Load-time records can be obtained by instrumentation of the tup on the striking hammer. The load-time records can be translated to load-displacement curves by applying appropriate corrections. The feasibility of the instrumented Charpy test, when established, will offer a quick and easy method of testing for the determination of fracture parameters of materials under dynamic conditions. This paper presents the results and discussion of an investigation to determine J_{ID} of medium-strength alloys by instrumented Charpy testing.

Experimental

Material

The three medium-strength materials chosen for the investigation are H-11 steel, CG-27 alloy, and Cr-Mo-V steel. These alloys are current or potential ordnance materials. Their chemical compositions and heat treatments are given in Table 1. The two Cr-Mo-V steels (MIL-S-46047 and MIL-S-11595) differ slightly in composition.

Specimens

All specimens were made according to ASTM standards and machined after heat treatment of the materials. The side notches were machined such that the notch root geometry was the same as that of the Charpy V-notch. Transverse Cr-Mo-V steel specimens were machined from MIL-S-46047 material and longitudinal specimens from MIL-S-11595 material.

Precracking

All specimens were precracked in a ManLabs precracker (Model No. FCM-300). The stress setting in this machine is calculated from the desired outer fiber stress. The H-11 and Cr-Mo-V steel specimens were precracked at an outer fiber stress level of 65 000 psi and the CG-27 specimens were precracked at 45 000 psi. Average precracking time was four minutes. The precrack lengths were measured on broken specimens after the tests.

Testing

A 120-ft·lb capacity Tinius-Olsen impact testing machine was instrumented to record the load-time profile during a test. The record was displayed on an oscilloscope and the trace photographed. Locating tongs were used to accurately position the specimen for each test and all testing was done at room temperature. The fracture appearance of standard and side-notched Cr-Mo-V

TABLE 1—*Nominal chemical composition and heat treatment of selected alloys.*

Alloy	Weight %													Heat Treatment
	C	Mn	Si	P	S	Cr	Ni	Mo	V	Cb	Ti	Al	B	
Crucible CG-27	0.08	...	...	...	...	13	38	5.5	...	0.6	2.5	1.5	0.01	solution treat at 1875°F (1024°C) age at 1450°F (788°C) 16 h age at 1200°F (649°C) 16 h
H-11 steel	0.35	0.30	0.30	...	...	4	...	1.5	0.40	...	...	0.01	...	austenitize at 1825°F (996°C) temper at 1220°F (660°C) temper at 1220°F (660°C)
Cr-Mo-V steel														
(MIL-S-46047)	0.42	0.85	0.30	0.020	0.020	1.1	...	0.65	0.25	...	...	0.01	...	normalize at 1700°F (927°C) austenitize at 1550°F (843°C)
(MIL-S-11595)	0.45	0.75	0.30	0.020	0.020	0.95	...	0.35	0.25	...	...	0.01	...	temper at 1210°F (654°C) stress relieve at 1100°F (593°C)

steel (transverse) specimens is shown in Fig. 1. Typical load-time records for two series of specimens are shown in Fig. 2. The load-time records were corrected for the compliance of the testing machine. (See the Appendix.) Area measurements on load-time test records were made with a polar planimeter correct to a hundredth of a square inch. Measured areas were of the order of 1 to 1.5 $in.^2$. The area under the curve up to limit load was converted to energy based on the average velocity of the pendulum. (See Discussion.) The contribution of the area under the curve by inertial peaks does not change with crack length (Fig. 2 and Ref *4*). Since the addition or subtraction of the same amount of energy to all the data points in a U versus a graph will not change the slope, no attempt was made to correct for the inertial peaks.

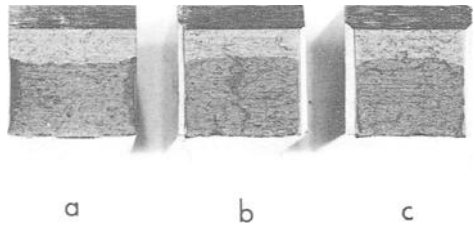

FIG. 1–*Fracture appearance of Cr-Mo-V steel (transverse) specimens: (a) standard; (b) side-notched 0.020 in.; (c) side-notched 0.030 in.*

Results

For the estimation of J_{ID}, areas under the curves up to limit load were measured, converted to energy, and plotted against crack length. For transverse specimens, fracture occurred before general yielding and sudden drop in load. For longitudinal Cr-Mo-V specimens, substantial yielding occurred before crack extension, and the drop in load was gradual. To arrive at a meaningful fracture criterion for such a material, Charpy-dimension specimens were tested under slow-bend conditions. At several post-yield stages the specimens were unloaded to check for crack extension. No crack extension was observed. Also, upon further loading, crack extension was always accompanied by a drop in load. This behavior is understandable for a non-work-hardening material like Cr-Mo-V steel. Attention must also be paid to the fact that a constraint is imposed by essentially elastic material above the crack tip and the compressive half of the specimen in bending. Noteworthily, Begley and Landes [*2*] did not notice any subcritical crack extension in bend specimens of ductile rotor steel. However, caution is warranted when dealing with specimens of other materials. The question of subcritical crack growth must be settled on an individual basis. For all materials in this investigation, 'limit load' is defined as the point in the load-time curve at which the load begins to decrease. Limit loads were not calculated but directly read from the load-time curves.

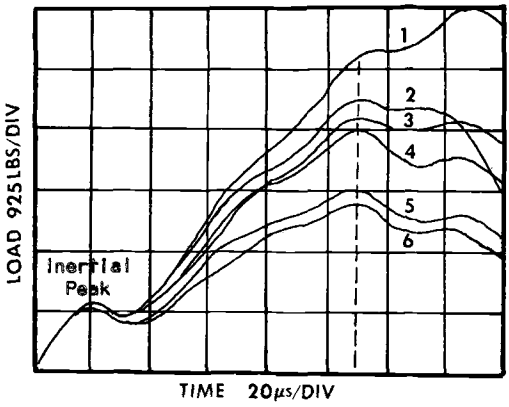

a - in.

1. 0.079 (Std. V-notch)
2. 0.093
3. 0.116
4. 0.139
5. 0.163
6. 0.176

(a)

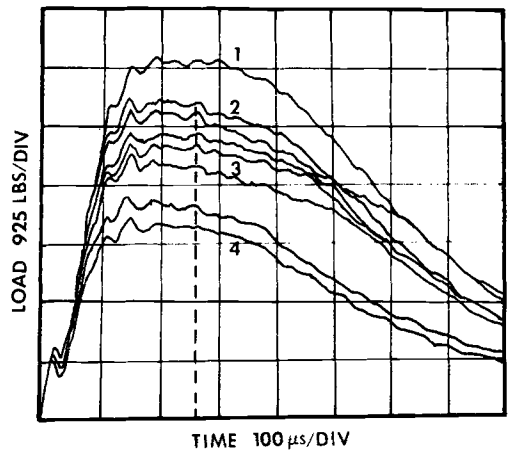

a - in.

1. 0.079 (Std. V-notch)
2. 0.110
3. 0.141
4. 0.175

(b)

FIG. 2—*Typical load-time oscilloscope traces of precracked Charpy specimens of Cr-Mo-V steel: (a) transverse specimens; (b) longitudinal specimens.*

Energy versus crack length plots for Cr-Mo-V steel (transverse) Charpy specimens containing different depths of side notches are shown in Fig. 3. The energy versus crack length plots for H-11 steel, CG-27 alloy, and Cr-Mo-V steel (longitudinal) specimens are shown in Fig. 4. Since all plots were linear, they were fit by the least-square method, and the slopes of the straight lines, du/da, were determined. The product moment correlation coefficients for the

least-square fits were between –0.94 and –0.99. The J_{ID} values were calculated from the relation

$$J_{ID} = \frac{-I}{B}\frac{dU}{da} \tag{2}$$

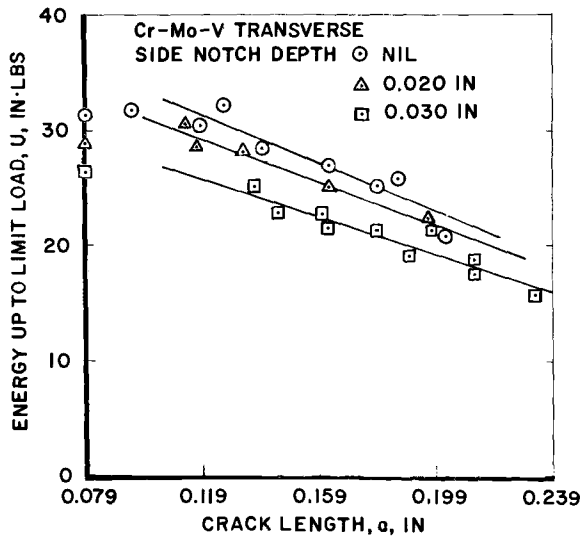

FIG. 3–*Energy up to limit load versus precrack length of side-notched Charpy specimens of Cr-Mo-V steel (transverse).*

A possible misconception due to the small differences in *LPD*'s for specimens of varying crack lengths could arise at this point. The *J*-integral is interpreted as the potential energy difference between identically loaded bodies having neighboring crack sizes. Crack extension is caused by a particular set of physical conditions in the body of the specimen at limit load. In that sense, the specimens containing cracks of neighboring sizes are under identical conditions at limit load. Hence, the limit load fracture criterion is considered to be consistent with the definition of the *J*-integral. The determined values of J_{ID}, the calculated values of K_{ID} from J_{ID}, maximum load, and *COD* values are given in Table 2.

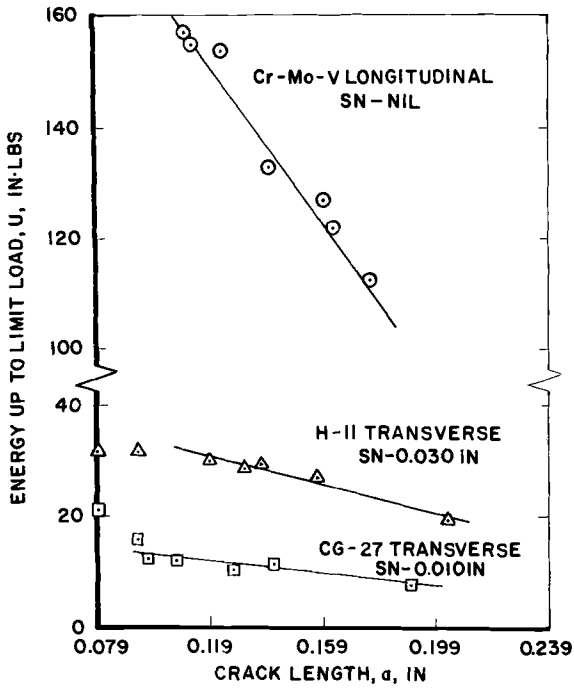

FIG. 4—*Energy up to limit versus precrack length of Charpy specimens of H-11 steel and CG-27 alloy (each transverse) and Cr-Mo-V steel (longitudinal).*

The K_{ID} values were calculated according to the following relations:

$$K_{ID} = Z \times P_F \tag{3}$$

$$= \left(\frac{G_{ID} \times E}{1 - \nu^2} \right)^{1/2} \tag{4}$$

$$= \left(\frac{J_{ID} \times E}{1 - \nu^2} \right)^{1/2} \tag{5}$$

$$G_{ID} = COD \times \text{yield strength} \tag{6}$$

Equation 3 is a simplified representation for the calculation of K_{ID} from fracture loads; Z is a function of (a/w) and its value can be obtained from compliance curves in Ref. *5*. Equation 4 is a standard fracture mechanics equation for plane-strain conditions. Equation 5 assumes the equivalence of J_{ID} and G_{ID}. Equation 6 contains an uncertainty since yielding in precracked Charpy specimens occurs under constraint. (See Discussion.)

TABLE 2–*Summary of results of this investigation.*

Material	Charpy, Impact Energy, ft·lb	Dynamic[a] Yield Strength, ksi	J_{ID}, in·lb/in.^{2}	K_{ID} ksi $\sqrt{\text{in.}}$ Calculated from P_F	K_{ID} ksi $\sqrt{\text{in.}}$ Calculated from *LPD*	K_{ID} ksi $\sqrt{\text{in.}}$ Calculated from J_{ID}	K_{ID} ksi $\sqrt{\text{in.}}$ Estimated (Ref 6)
Cr-Mo-V steel (transverse)							
SN depth nil	19	175	266.7	97.9	92	93	96
SN depth 0.020 in.	...	...	266.7	99.7	92	93	...
SN depth 0.030 in.	...	...	253.9	92	92	90	...
H-11 steel (transverse)							
SN depth 0.030 in.	18[b]	165	389.5	96.2	107.5	117	96
CG-27 alloy (transverse)							
SN depth 0.01 in.	5[b]	135	131	57.5	66.4	63	...
Cr-Mo-V steel (longitudinal)							
SN depth nil	65	175	1960	...	160	250	225

[a] Determined by instrumented Charpy tests.
[b] Values are for standard Charpy specimens.

Discussion

Two inherent features of the instrumented Charpy test warrant that correction procedures be employed before energy can be measured on the load-time records. First, the pendulum continuously loses energy as the specimen is being loaded. This loss is usually corrected by multiplying the time by the average velocity of the pendulum, instead of the initial velocity, to calculate load-point displacements.

In this investigation, since only energy under the curve up to limit load is considered, the average velocity of the pendulum was determined on the basis of loss of energy up to limit load. The correction factor averages –0.3 percent for the transverse specimens and –2.5 percent for the longitudinal specimens. Secondly, the multiplication of the elapsed time by the velocity of the pendulum measures the forward motion of the leading edge of the tup and not the load-point displacement directly on the specimen. The compliance of the testing system, therefore, must be independently determined and the load-time records must be individually corrected. This second correction could amount to as much as –30 percent and is strictly dependent on the 'hardness' of the machine. An example of the apparent load-time record and the corrected record are shown together in Fig. 5. The correction procedure (see the Appendix), when performed manually, is tedious, and some feature in the electronics of the system to correct the load-time record automatically would be highly desirable.

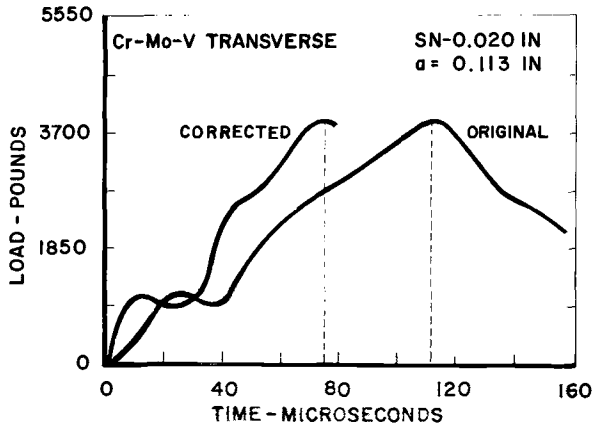

FIG. 5—*Original and corrected load-time oscilloscope traces of Charpy specimens of Cr-Mo-V steel (transverse).*

A series of corrected load-time records for transverse specimens of Cr-Mo-V steel containing different lengths of cracks is shown in Fig. 6. Comparison with Fig. 2*a* shows that the elapsed time to limit load in the apparent load-time

records does not change with crack length. Curves numbered '1' in Figs. 2*a* and 2*b* are for standard Charpy specimens. They have notches of 0.010 in. root radius. These curves should not be compared with the rest which have fatigue precracks. The elapsed time in the corrected set (the time to be used for computation of *LPD*) increases slightly with crack length. *COD*, which is a material property, is given by the relation

$$COD = \frac{LPD}{\ell/2} \times d \tag{7}$$

The value of d, for rigid-body rotation, decreases with increase in crack length. Therefore, *LPD* must increase with increasing crack length to give constant *COD*. This point is emphasized to show that the bending of precracked Charpy specimens can be treated as rigid-body rotation.

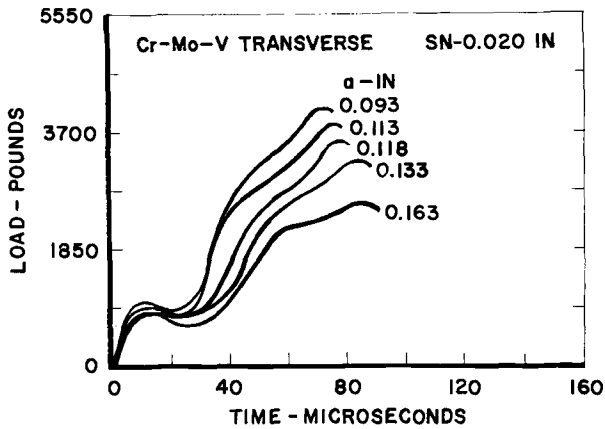

FIG. 6—*Corrected load-time oscilloscope traces of precracked Charpy specimens of Cr-Mo-V steel (transverse).*

By definition, J is the difference in potential energies of two identically loaded specimens at the same state containing neighboring crack sizes. Following this definition, the critical value of J, J_{ID}, was determined for initiation of fracture. Area measurements were made up to limit load instead of constant *LPD*. The limit load is a more meaningful fracture criterion since it represents an identifiable physical state of the specimen. This point has been clarified earlier.

The J_{ID} values calculated from the slopes of U versus a graphs were not affected by the presence of side notches. The slope of the U versus a graph is altered sufficiently to account for the change in the thickness. The value of *LPD* for P_F is also not affected by the side notches. The conclusion is that the side

notch does not introduce any additional constraint for the initiation of fracture. However, the post-limit load shape of the load-time curve is considerably altered by the presence of side notches.

The U versus a relationship for all materials was essentially linear for a values greater than a certain minimum. This minimum value depends on the material and the side notch depth. For values of a smaller than the minimum, the U value either did not significantly change with a (for Cr-Mo-V and H-11 steels) or dropped sharply with small increments in a (for CG-27 alloy). The difference in behavior during transition from a blunt to a sharp notch indicates the differences in the notch sensitivities of the materials and also the effect of the constraint imposed by the side notch on the notch sensitivity of a material. Because of the presence of such nonlinear effects close to the Charpy notch root, only specimens containing fairly long fatigue precracks $[0.25 < (a/w) < 0.55]$ are recommended to be tested for the estimation of J-integral. The minimum length of precrack will have to be decided for the test material and the depth of side notch to be introduced.

Table 2 summarizes the results of this investigation. As mentioned earlier, ASTM standard specimens for fracture toughness specimens could not be obtained from the representative bar stocks of the materials in this investigation. Fracture toughness values determined from precracked Charpy specimens based on other criteria (P_F and *COD*) and estimated from the data of Rolfe and Novak [6] for steels are incorporated in Table 2 for comparison. The agreement between values of K_{ID} calculated from J_{ID}, fracture load, and *COD*, is good for transverse specimens of H-11 steel, CG-27 alloy, and Cr-Mo-V steel. Interestingly, fracture precedes yielding and the load drops off sharply after limit load for each of these materials. The criterion for the limiting J value is initiation of crack propagation, which is identical to fast fracture in specimens where fracture precedes yielding. In Cr-Mo-V steel (longitudinal) the estimated J_{ID} value does not give the same K_{ID} value based on *COD* measurements (G_{ID} calculations) if displacement to limit load is chosen for the calculation of *COD*. As stated earlier, no subcritical crack extension was noticed before limit load; hence, other reasons must be sought to explain this discrepancy. The same type of results is obtained from the data published by Begley and Landes [2]. From their test results, assuming an average value of 0.0004-in. for *COD* of Ni-Cr-Mo-V steel and 135 ksi for its yield strength, the G_{IC} value is 540 in·lb/in.^{2}. For the same material at the same temperature the G_{IC} value, established from Westinghouse K_{IC} fracture toughness tests [7] for essentially elastic failure of 8-in.-thick compact tension specimens, was 1200 in·lb/in.^{2}. This disparity is to be expected since G_{ID} represents an unstable crack propagation criterion. The famous Griffith equation for fracture, which relates fracture stress to the Young's modulus, surface energy, and the crack length, is the basis for G_C, the critical strain energy release rate for crack propagation leading to complete rupture. The experimental procedures for K_{IC} utilize a 'pop-in' criterion which only reflects a crack extension. In a similar sense, J_{IC} also represents only crack

extension. Hence, crack instability criteria for J_{IC} and G_{IC} need not be identical for all materials.

Several factors of multiplication have been proposed for the estimation of G_{IC} from *COD* and yield strength values since yielding in precracked specimens occurs under constraint [*8*]. The *COD* criterion requires the accurate determination of either the displacement field or the stress field in the vicinity of the crack tip. Available theoretical solutions of elastic-plastic analysis are limited to the Mode 111 (antiplane strain) crack tip deformation [*9*]. The uncertainty in the use of *COD* criterion for G_{IC} estimation can be resolved only when explicit plane-strain solutions for the crack tip deformation are formulated.

Conclusions

1. Appropriate corrections for the compliance of the testing machine and the loss of velocity of pendulum must be applied to the load-time records of instrumented Charpy tests before J-integral can be determined.

2. The presence of side notch alters the slope of the U versus a line to account for the change in thickness of the specimen. The value of J is not affected.

3. For specimens which fracture before yielding, K_{ID} values calculated from maximum load, *COD*, and J_{ID} agree with one another. For specimens which yield considerably before initiation of fracture, the K_{ID} value calculated from *COD* is less than that calculated from J_{ID}. The disparity is due to the difference in the fracture criteria for K_{ID} (or J_{ID}) and G_{ID}.

4. Identical crack-tip geometries of the test specimens are a necessary requisite for the experimental determination of J. If precracked Charpy specimens are used for this purpose, the precracks should be long enough below the standard V-notch root to override the effects of the blunt V-notch.

APPENDIX

Compliance Correction for Instrumented Charpy Testing

The recent popularity of the 'instrumented Charpy testing' technique to determine dynamic properties is due to the simplicity in specimen requirements and method of testing. The test is a high-strain rate, three-point bend test of notched, rectangular bar specimens. The tup is strain-gaged to measure the applied load as a function of time while the specimen breaks. Besides the impact energy, the load to fracture, the time to fracture, and the energy up to any load or time can be obtained from the records. Dynamic plane strain fracture toughness (K_{ID}), crack opening displacement (*COD*), and J-integral values can be computed from the test records of suitably precracked specimens. The determination of fracture parameters, other than fracture load, is critically dependent on the ability to accurately translate the load-time records into load/load-point displacement curves.

Customarily, the elapsed time is multiplied by the average velocity of the pendulum during the test to obtain load-point displacement (*LPD*). This product measures the forward motion of the pendulum and not just the specimen deformation. The compliance of the testing machine must be determined to calculate *LPD*. The correction factor (hereinafter referred to as the compliance correction) depends on the 'stiffness' of the machine and does not necessarily have to be linear over a wide range of loads. This short note describes a procedure to determine the compliance correction and discusses the magnitude of error in results if the compliance correction is ignored.

The constructional and operational features of Charpy testing machines inhibit the measurement of *LPD* on the specimen directly. A loading system that will push the pendulum against the specimen at a constant known speed can be devised for calibration. This technique will entail the determination of the stiffness of the loading system by an independent method. The most expedient procedure uses the pendulum itself for loading. The testing conditions and the specimen material can be judiciously selected such that the forward displacement of the tup can be calculated as a function of time and compared against the elastic load-point displacement of a rectangular specimen.

The technique followed in our laboratory employs a low-blow test on an unnotched, Charpy-size bar of a material whose Young's modulus is known. The elastic load-point displacement of a three-point bend bar without a notch can be accurately calculated as a function of load from established relations. This value can be compared against the corresponding load-time record to obtain a compliance correction graph for the desired load range.

One feature of the instrumented Charpy test record is the ever-present inertial peaks. On impact, the specimen travels faster than the pendulum and the pendulum momentarily loses contact with the specimen. When the specimen slows down, the pendulum regains contact and the dynamic loading continues. This sequence of events may take place a few times before the specimen fractures. The heights of the inertial peaks are functions of the elastic modulus and the density of the specimen, the pendulum velocity, and the system frequency response.

Figure 7 shows the inertial peaks for a pendulum velocity of 16 ft/s, (4.88 m/s) on the load-time curves of a variety of materials whose densities and elastic moduli are given in Table 3. Figure 8 shows the inertial peaks for Cr-Mo-V steel and a series of pendulum velocities. Figure 8 indicates that the inertial peak on the load-time record decreases as the pendulum velocity is decreased, and becomes practically nonexistent at initial pendulum velocities of the order of 3 to 4 ft/s (0.91 to 1.22 m/s). Physically, this effect means that at low initial pendulum velocities the tup constantly contacts the specimen during a test. Continuous contact is ideal for compliance determination. While low velocity of the pendulum and light material with low modulus is the ideal combination, it may not be suitable for calibration over a wide range of loads. The judicious selection of pendulum velocity and the material of the specimen depend on the range of load over which compliance calibration is required. *The material must be sufficiently hard to resist brinelling from impact.*

Figure 9*a* is a low-blow test record for an initial pendulum velocity of 6.5 ft/s (1.98 m/s) and a specimen (unnotched Charpy bar, 55 by 10 by 10 mm) of Cr-Mo-V steel quenched from 1575°F (875°C) to a hardness of HRC 52. Figure 9*b* is a tracing of the same record divided into convenient segments. The areas A_1, A_2, A_3, A_4, and A_5 were measured correct to a hundredth of a square inch (6.5 mm^2). Area A_1 was converted to energy U_1 on the basis of initial velocity of the pendulum. Energy U_1 is lost by the pendulum and the velocity is reduced

TABLE 3–*Densities and elastic moduli of tested alloys.*

Alloy	Density, lb/in.^{3}	Elastic Modulus, 10^6 psi
6061	0.097	10
Ti-6A1-4V	0.158	18
Manganese bronze	0.284	15
Cr-Mo-V steel	0.284	30

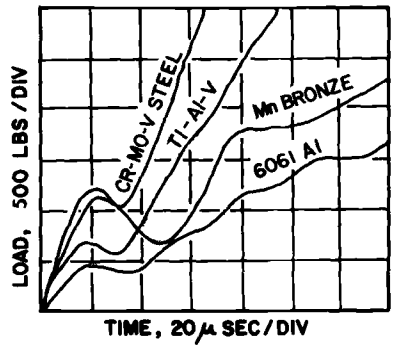

FIG. 7–*Inertial peaks for a variety of materials with different elastic moduli and densities.*

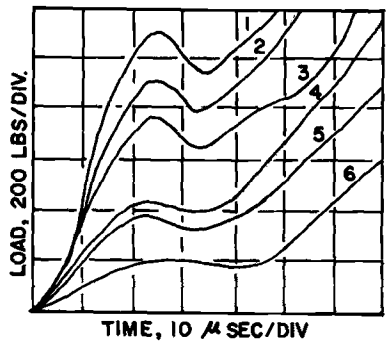

FIG. 8–*Inertial peaks for a series of pendulum velocities (ft/s): (1) 16, (2) 13.8, (3) 11.3, (4) 8.0, (5) 5.6, and (6) 4.6.*

correspondingly. The relation between the initial velocity, v_o, final velocity, v_f, initial energy, E_o, and energy loss, E_T, is given by the equation

$$\frac{v_f}{v_o} = \left(1 - \frac{E_T}{E_o}\right)^{1/2} \tag{8}$$

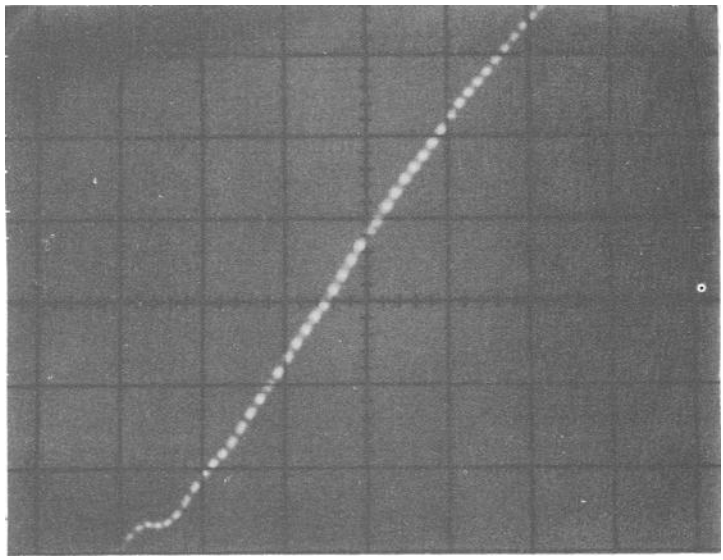

FIG. 9a—*Low-blow test record for an unnotched Charpy-size bar of hardened Cr-Mo-V steel. Scale: Abscissa, 50 μs/Div; Ordinate, 1000 lb/Div.*

An arithmetic average, $\bar{v} = (v_f + v_o)/2$, can be used to convert the time element in area A_1 to distance. For area A_2, the initial velocity will be the final velocity of the previous step, and a new v_f value, and hence $\bar{v}$, can again be calculated. The procedure was continued to convert each time element to distance values, the cumulation of which gives load-point displacements. Table 4 shows the step-by-step conversion of time to distance, and Fig. 9*b* shows the time and corresponding displacement on the abscissa. The load-point displacement, δ, for a three-point bending of an unnotched bar by a concentrated load at the middle is given by the relation [*10*]:

$$\delta = \frac{P\ell^3}{4EBW^3}\left[1 + 2.85\,\frac{W^2}{\ell^2} - 0.84\,\frac{W^3}{\ell^3}\right] \tag{9}$$

TABLE 4—*Conversion of load-time data to load/load-point displacement data.*

Area Under Curve in Fig. 9*b*, in.^{2}	Initial Energy, E_o ft·lb	Energy Lost, E, ft·lb	Initial Velocity, v_o, ft/s	Final Velocity, v_f, ft/s	Average Velocity, $\bar{v}$, ft/s	Displacement Equivalent to 50 μs, in.
(A_1) 0.05	20.0	0.0875	6.5	6.486	6.493	0.00389
(A_2) 0.22	19.9125	0.3842	6.486	6.423	6.455	0.00387
(A_3) 0.49	19.5283	0.8473	6.423	6.282	6.353	0.00381
(A_4) 0.79	18.6810	1.3361	6.282	6.053	6.168	0.00370
(A_5) 0.99	17.3449	1.6290	6.053	5.761	5.907	0.00354

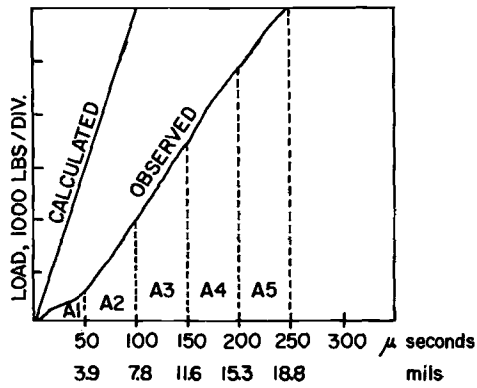

FIG. 9*b*—*Observed and calculated load-point displacements for unnotched Charpy-size bar of hardened Cr-Mo-V steel.*

where

P = load, lb;
ℓ = span length, 1.57 in. (40 mm);
E = Young's modulus;
B = thickness of bar specimen, 0.394 in. (10 mm); and
W = width of bar specimen, 0.394 in. (10 mm).

Figure 9*b* also shows the calculated *LPD* for the Cr-Mo-V steel bar as a function of applied load. The difference between the observed and the calculated *LPD* values is the compliance correction. Figure 10 is a graph between load and compliance correction. For the most part, this plot is linear, as would be expected. The initial nonlinearity could be due to friction, slack in the bearing, etc. Annual determination of compliance correction for a machine is highly desirable.

Application of the Compliance Correction to Charpy Records

1. To determine *LPD*: The elapsed time, t_c, to initiation of unstable crack propagation and the area under the curve up to that point are measured from the test records. The area is converted to energy from which the average velocity of the pendulum ($\bar{v}$) is calculated. The apparent *LPD* for fracture is given by $\bar{v} \times t_c$. Since the load for unstable crack propagation also can be read from the test records, the compliance corrections, C_c, can be determined from Fig. 10. The true *LPD* for unstable crack propagation is given by $(\bar{v} \times t_c - C_c)$.

2. To determine J_{ID}: The determination of J_{ID} from Charpy test records involves the accurate measurement of work done in deforming a precracked specimen up to the point of initiation of crack propagation (up to limit load). Figure 11 shows the test record and the corrected curve for a Cr-Mo-V steel specimen. For convenience, the abscissa is kept as time scale. Area $A_1B_1C_1$ measures the work done in deforming the specimen, the anvil, and the tup, and losses due to friction. Area $A_1B_2C_2$ measures the work done in deforming the specimen only. The line A_1B_2 is generated by applying the compliance

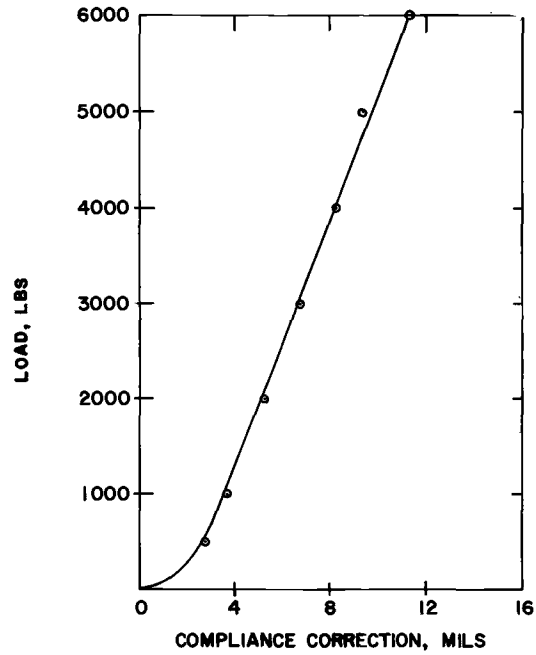

FIG. 10—*Compliance correction for the test machine as a function of load.*

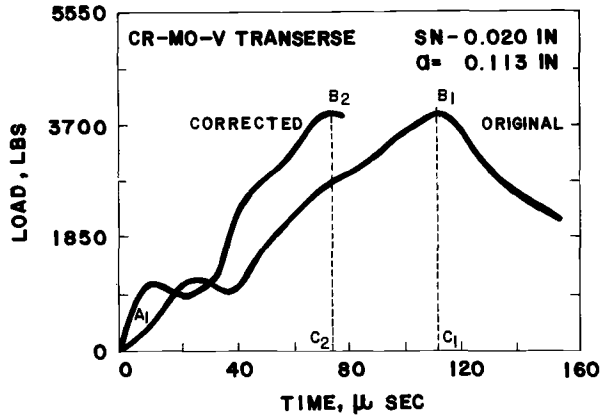

FIG. 11—*Original and corrected load-time curves for transverse Charpy specimen (Cr-Mo-V steel), side notched 0.020 in., and precracked 0.113 in.*

correction to as many points as possible on the line $A_1 B_1$. These two examples illustrate the magnitude of error which will be introduced in the results of instrumented Charpy testing if the compliance of the machine is not accounted for.

References

[1] Rice, J. R., *Journal of Applied Mechanics, Transactions*, American Society for Mechanical Engineers, June 1968, pp. 379-386.

[2] Begley, J. A. and Landes, J. D. in *Fracture Toughness, ASTM STP 514*, American Society for Testing and Materials, 1972, pp. 1-20.

[3] Kobayashi, A. S. et al, "A Numerical and Experimental Investigation on the Use of *J*-Integral," Technical Report No. 12, Department of Mechanical Engineering, University of Washington, Seattle, 1972.

[4] Server, W. L., "Dynamic Fracture Toughness Determined from Instrumented Precracked Charpy Tests," Technical Report, UCLA-ENG-7267, University of California at Los Angeles, 1972, p. 43.

[5] Brown, W. F. Jr., and Srawley, J. E. in *Plane Strain Crack Toughness Testing of High-Strength Metallic Materials, ASTM STP 410*, American Society for Testing and Materials, 1966, p. 13.

[6] Rolfe, S. T. and Novak, S. R. in *Review of Developments in Plane Strain Fracture Toughness Testing, ASTM STP 463*, American Society for Testing and Materials, 1970, p. 146.

[7] Begley, J. A. and Toolin, P. R., "Fracture Toughness and Fatigue Crack Growth Rate Properties of a Ni-Cr-Mo-V Steel Sensitive to Temper Embrittlement," presented at the Fourth National Symposium on Fracture Mechanics, Carnegie Mellon University, Pittsburgh, Pa., Aug. 1970.

[8] Begley, J. A., Westinghouse Research Laboratories, Pittsburgh, Pa. private communication.

[9] Rice, J. R. in *Fatigue Crack Propagation, ASTM STP 415*, American Society for Testing and Materials, 1967, pp. 247-311.

[10] Timoshenko, S., *Strength of Materials*, 2nd ed., Van Nostrand, New York, Part 1, p. 174.

R. C. Lueth[1]

An Analysis of Charpy Impact Testing as Applied to Cemented Carbide

REFERENCE: Lueth, R. C., "An Analysis of Charpy Impact Testing as Applied to Cemented Carbide," *Instrumented Impact Testing, ASTM STP 563*, American Society for Testing and Materials, 1974, pp. 166-179.

ABSTRACT: In an effort to better understand the nature and the limitations of impact testing, the Charpy impact test was studied in detail via instrumentation of both the tester and the specimen. It was found that the energy associated with the impact testing of cemented carbide consists mainly of elastic bending energy and absorption of energy by the testing machine. The vibrational and plastic components are insignificant. The toss energy and energy necessary to create new surfaces can be fairly well calculated from other considerations. The tests have shown no rate effects in cemented carbides, and the state of stress in the beam is uniaxial tension. Thus the test does not describe the material's propensity for cleavage or brittle failure, but rather describes mainly the modulus and strength of cemented carbides (which are routinely and more easily measured in other ways), and the stiffness of the testing machine–all of which have very little bearing on the toughness of the cemented carbide. The components which describe this are the energy of plastic work and the energy necessary to create two new surfaces, and these consist of only a few percent of the total measured energy. The amount of energy which the machine absorbs will vary with the modulus and strength of the material being tested. In the case of a hard low-strength grade like Carboloy[2] Grade 320, the anvil sees very little load before failure and thus the energy partitioning will be significantly different than that for a stronger grade.

The Charpy test conducted with the conditions in this study has little value in ascertaining the toughness of cemented carbide; in fact, results from it may be misleading. When cemented carbide is evaluated for toughness by impact testing of any kind, careful attention must be given to the aforementioned factors because they are encountered to a large extent in most, if not all, types of impact tests. Charpy impact-type tests on cemented carbide are essentially fast transverse-rupture strength tests on a "soft" test machine.

KEY WORDS: impact tests, toughness, cobalt containing alloys, evaluation, test equipment

For many years both users and producers have attempted to evaluate the relative resistance of various WC-Co alloys to impact loading in an effort to better predict the performance of these types of alloys in situations where normally they would receive such loadings during service. Several types of tests

[1] Research metallurgist, Materials Research and Development, Carboloy Systems Department, General Electric Company, Detroit, Mich. 48232.

[2] Carboloy is a trademark of the General Electric Company.

have been applied in this effort, including Charpy-type tests and drop weight tests.[3,4] In the final analysis, however, little in the way of guidance for selecting standard materials or developing improved materials has resulted from this approach.

The impact energy or impact strength of WC-Co alloys is currently determined at the Carboloy Systems Department of General Electric by loading an unnotched 1/4 by 1/4 by 2-in. specimen in three-point bending (span is 9/16 in.). This is done on a Charpy Impact Tester of 24 ft·lb capacity (Model CIM-24, Manlabs, Inc.). The results of these tests are generally considered to be an indication of the "toughness" of cemented carbide. However, much of the field experience where carbide is subjected to impact loading, such as in mining, does not correlate well with the Charpy impact values of the various grades of cemented carbides. In an effort to better understand the nature and the limitations of impact testing, the aforementioned test was studied in detail via instrumentation of both the tester and the specimen.

Energy Absorption During Impact Testing

Several factors are involved in the absorption of energy during an impact test.

(*a*) Energy due to elastic bending of the beam.

(*b*) Energy due to plastic work (gross yielding of this material).

(*c*) Energy needed to create two new surfaces.

(*d*) Energy used to accelerate the specimen to tup velocity (toss energy).

(*e*) Energy due to vibrations set up in the specimen or machine (due to impact).

(*f*) Energy absorbed by the machine itself.

The energy which is indicative of the "toughness" of the material is that indicated by factors (*b*) and (*c*) and these should be large relative to the rest if the test is to be of value. Factor (*a*) can be calculated from the strength and modulus of the material. Factors (*d*), (*e*), and (*f*) are not related to the material "toughness" but are peculiar to the test and should be relatively small in order for the test results to be considered a measure of the material's shock resistance.

Experimental

The tup of the Charpy machine was instrumented with strain gages such that the load on the sample could be studied throughout the duration of the test. The tup was statically calibrated and the signal fed to an Ellis BAM I amplifier and displayed on an oscilloscope. Figure 1 shows the experimental setup. The resultant load versus time curve (and a replot with units added) for a typical WC-Co alloy (namely, Carboloy Grade 55B) can be seen in Fig. 2. The total

[3] Spaeth, W., *Industrial Diamond Review*, Vol. 17, No. 197, 1957.

[4] Sacman, E. J., Tinklepaugh, J. R., and Curran, M. T., *Journal of the American Ceramic Society*, Vol. 39, 1956, p. 261.

energy measured or indicated for Grade 55B in this test was 26.9 in·lb. In Fig. 2 it is noted that:

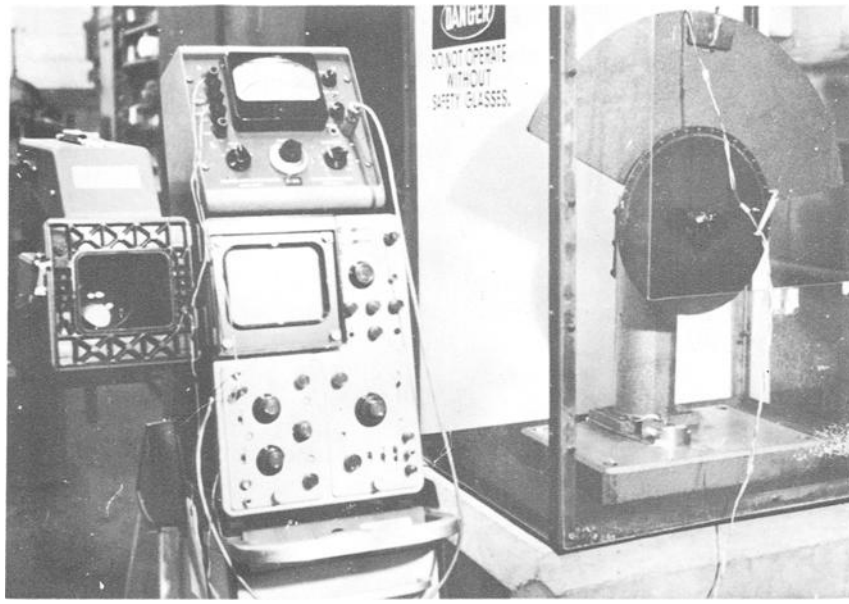

FIG. 1–*Experimental apparatus.*

1. In the latter part of the curve, there is a linear variation of load with time with some vibratory component superimposed on it.

2. The early part of the curve appears to have a different behavior than the latter.

This indicates that some different phenomenon is occurring in the early part of the test as opposed to the latter. To investigate this difference between the early and late part of the curve, several tests were run on specimens which were not held in place by anvil supports. Results are shown in Fig. 3. It was observed that the early part of the curve can be reproduced exactly with no constraint whatsoever. As further evidence, the load on the anvil was investigated (again by instrumenting it with strain gages) as a function of time during the test. It was observed that there was no load on the anvil for approximately the first 50 μs of the test (Fig. 4).

Since the anvil is not a factor in the early part of the test, the normal three-point bending is absent during this time period. The initial part of the

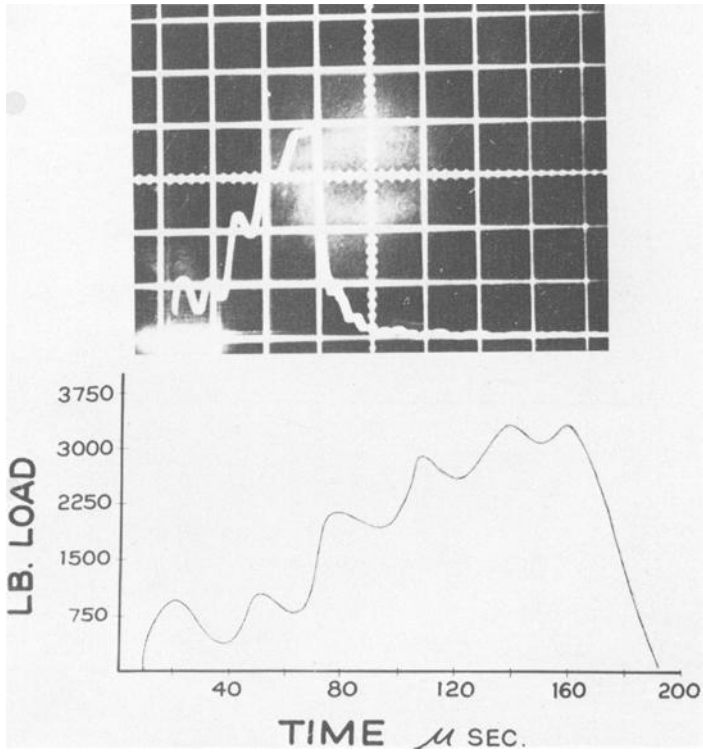

FIG. 2–*Time-load trace, Carboloy Grade 55B.*

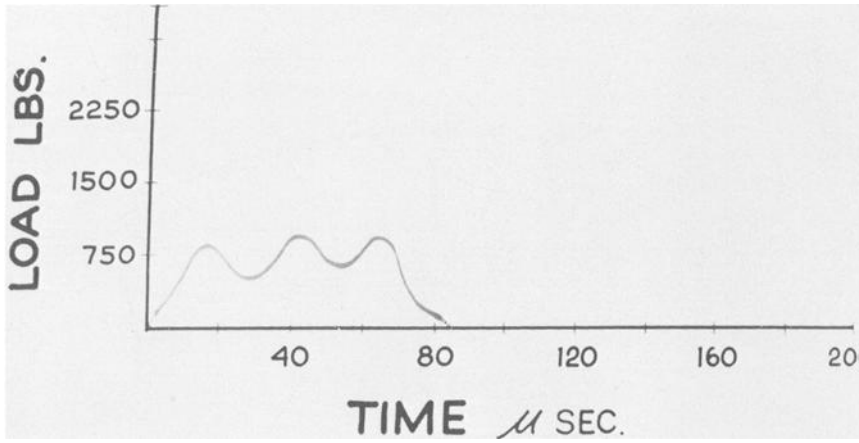

FIG. 3–*Time-load trace for unsupported specimen.*

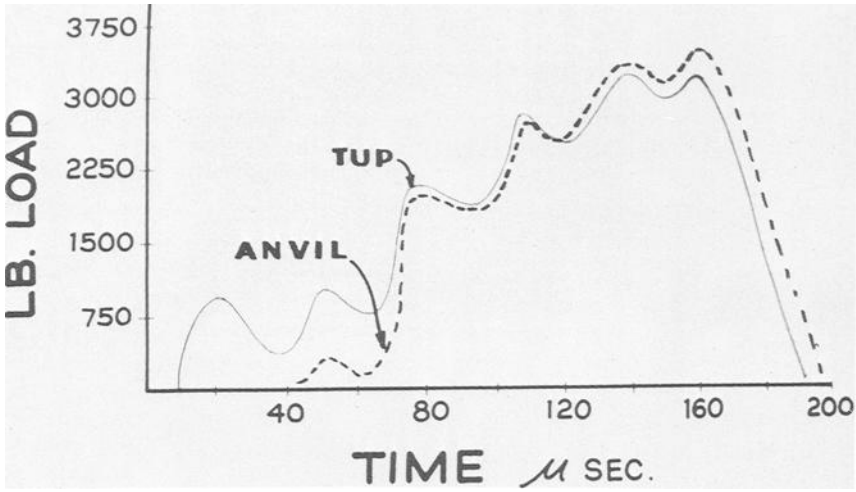

FIG. 4—*Time-load traces for anvil and tup.*

curve consists of an inertial acceleration with a strong vibrational component. This acceleration will also introduce a bending moment into the beam, for as the mass of the beam is accelerated, some kind of distributed load across the beam will be present (Fig. 5).

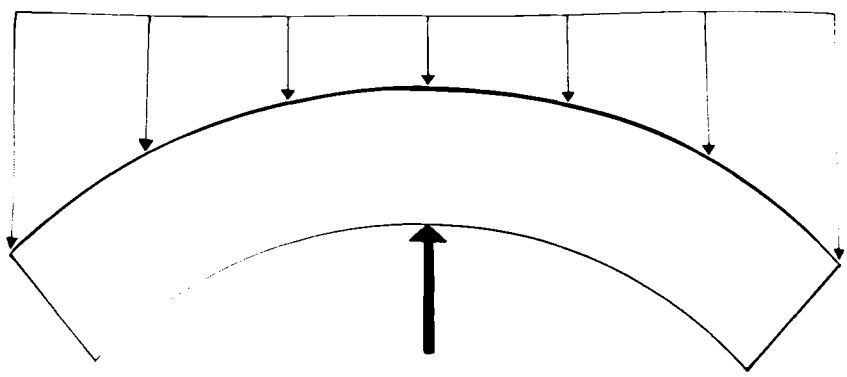

FIG. 5—*Load due to beam mass and acceleration.*

Since the force versus time curve has a sinusoidal component in this region, the neutral position of the wave was chosen as being representative of the force due to acceleration of the mass of the beam (Fig. 6).

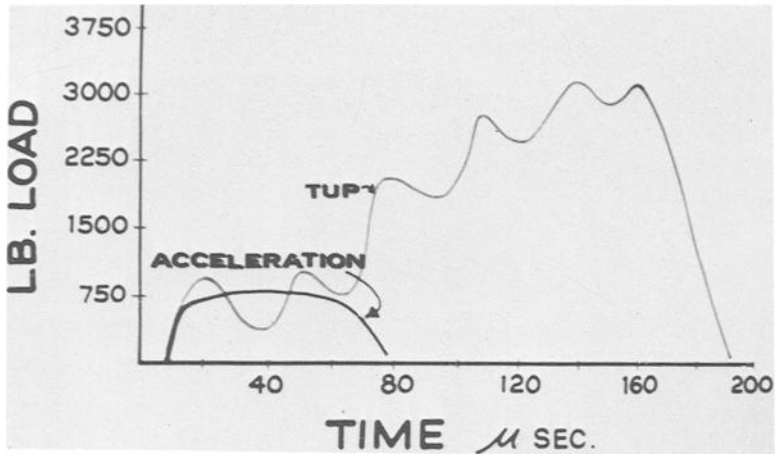

FIG. 6–*Force due to acceleration of beam.*

This acceleration force can be satisfactorily described as a ramp function for the first 5 μs and a constant up to the point of anvil contact. To ascertain the origin of the vibration the specimen was instrumented at critical positions (Fig. 7) such that the strain behavior during the test at these points would allow a deduction of the vibrational mode of the specimen. These readings indicate that, indeed, the vibrations were in the specimen and that the specimen was vibrating in a mode similar to the second mode of a cantilever beam with the center of the specimen acting at the zero-slope cantilever mount (Fig. 8). The calculated period of such a vibration is 26 μs, which is an excellent agreement with the measured period. If the nodal points of the vibration are near the anvil support location, this vibration can persist throughout the test. With this information, the test was modeled on a computer using the following scheme:

1. Ramp function for the first 5μ and then a constant up to the point of anvil contact to simulate the acceleration load.
2. Sinusoidal function to simulate the vibration.
3. Second ramp function to simulate the bending of the beam.

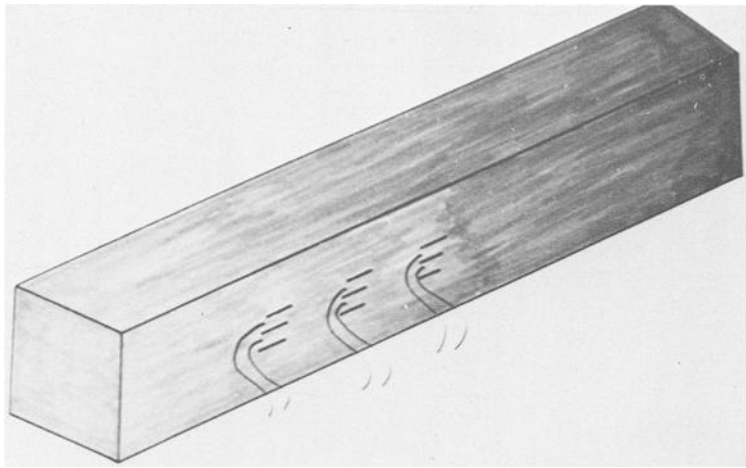

FIG. 7–*Instrumentation of specimen for vibration analysis.*

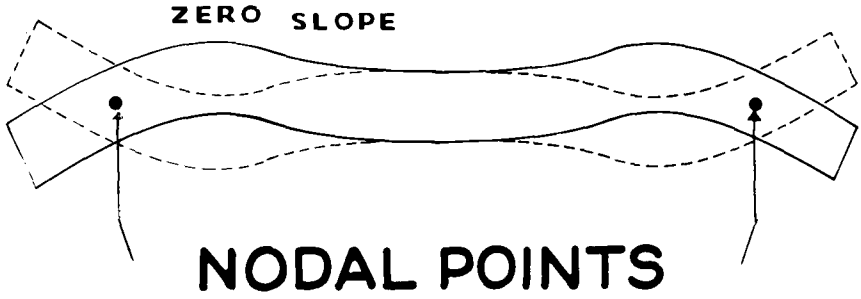

FIG. 8–*Vibrational mode of carbide impact specimen.*

The results are shown in Fig. 9. This indicates essentially no plastic component in the bending, as all functions used in the model are linear elastic and the model appears quite good. To facilitate the calculation of the magnitude of each of the energy components of the test, (*a*) through (*f*) given earlier, a computer procedure was set up to calculate the force-distance energy relationships from the force-time curves. With information on the tup speed in the critical area and effective pendulum mass, it was possible to calculate the

foregoing parameters through the use of Newton's laws and an incremental computer program, using data from the force-time curves. The method used to obtain the tup speed and the effective pendulum mass is given in the Appendix. A resultant force-displacement curve is shown in Fig. 10. Note here that the slope of the force versus distance curve is different than that expected from the bending of the carbide beam. From the difference between the expected versus actual slope, a machine stiffness coefficient can be calculated. The value of this coefficient is approximately 1.5×10^{-6} in./lb.

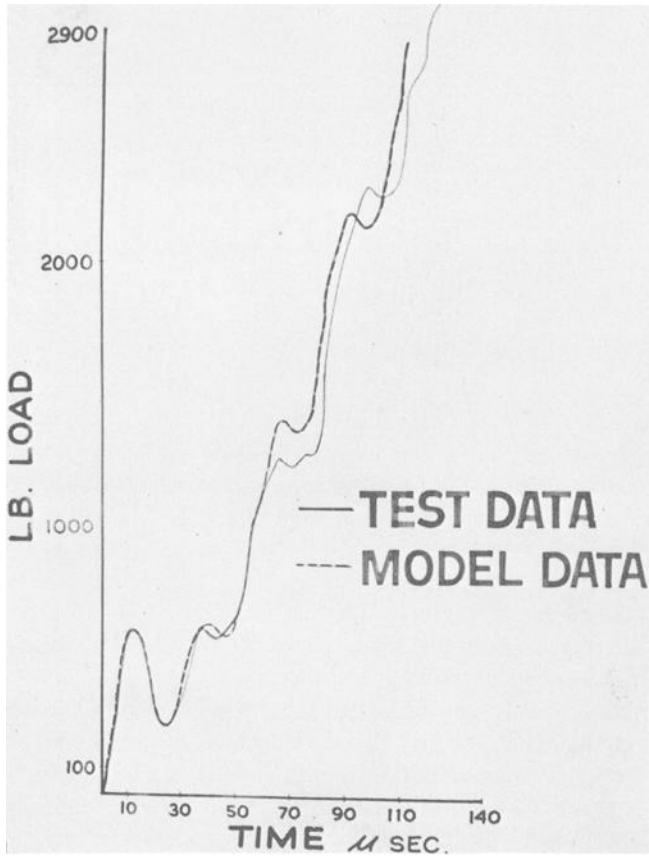

FIG. 9—*Time-load trace for actual test and computer model.*

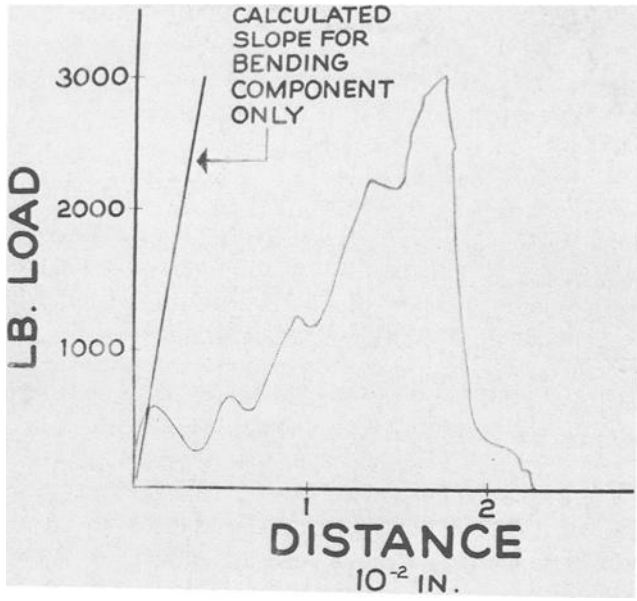

FIG. 10–*Force-displacement relationship for Charpy impact test.*

The magnitude of the various energy-absorbing mechanisms in the test can now be calculated. From the force-distance energy calculation the energy used up to the point of anvil contact is approximately 2.5 in·lbs. This can be accounted for by

1. Vibrational energy.
2. Inertial bending energy.
3. Kinetic energy of the specimen.
4. Energy absorbed by the tup.

The vibrational energy, as calculated using the force from the average line to maximum as the amplitude and the second mode of vibration of a cantilever beam as the mode of vibration, is approximately 0.0001 in·lb. The inertial bending energy calculated on the basis of a constant distributed load will give a minimum energy and calculated on the basis of concentrated loads on the ends of a maximum energy:

$$E_{Ib} \text{ min} = 0.2588 \text{ in·lb}$$

$$E_{Ib} \text{ max} = 0.776 \text{ in·lb}$$

Using the machine stiffness coefficient as 1×10^{-6} in./lb since the anvil is not in contact with the specimen, the machine-stored energy to this point is 0.125 in·lb and the kinetic energy due to specimen speed is approximately 1.64 in·lb. The total energy is then

2.5 max

2.0 min

The energy used in the first part can be well accounted for in this manner. The total elastic bending energy calculated from the standard strength of materials formulation is 15.6 in·lb.

The energy stored in the machine is $(P^2/2) \times 1.5 \times 10^{-6} = 6.75$ (where P is the loading).

The total energy to maximum load is then the sum of these three (15.6 + 6.8 + 2.3, or 24.7 lb·lb).

According to the energy distance program, the energy at maximum load is 24.6 in·lb. As stated in the foregoing, the total energy measured in the actual impact test on Grade 55B is 26.9 in·lb. Part of the 2.3 in·lb discrepancy can be accounted for by the energy required for crack propagation, which, according to Lueth,[5] is approximately 0.3 in·lb in a metastable condition. Since this is a high-speed fracture, the energy absorbed here may be greater but should not exceed 1 in·lb. The rest of the energy is due to the fact that once fracture has occurred (and this will occur in 1 to 2 μs), the tup will spring back, thus maintaining some load for a small extra time which accelerates the broken pieces to a speed greater than tup velocity. This can be seen in Fig. 10 as a noninfinite slope of the load distance trace after maximum load. In any case, the sum of the energies from the aforementioned sources is very close to the 27 in·lb measured by the machine.

The transverse rupture strength of the specimen was calculated from the maximum load observed in the impact test and was found to correlate well with transverse-rupture strength data as determined on the two halves of the impact sample. The data on the broken halves of the impact specimen were obtained in a normal three-point bend test with a 5/8-in. span. Both methods gave a value of 460 000 psi for Grade 55B. Thus, carbide shows no appreciable rate effects on strength up to the rates of loading exhibited by the unnotched Charpy test.

Discussion

The Charpy impact test was devised to determine the propensity of steel to brittle failure by subjecting it to

(*a*) a triaxial stress state (such as produced by a notch),

(*b*) high strain rates, and

(*c*) various temperatures.

When engineers applied the Charpy test to cemented carbide, probably few, if

[5] Lueth, R. C., *Fracture Mechanics of Ceramics*, Vol. 2, Plenum Publishing Corp., New York, 1974, p. 791.

any, were interested in the carbide's reaction to biaxial or triaxial stress (absence of notch) or to temperature (tests generally are conducted at room temperature). Most likely, they were interested in the energy required to break the specimens or in a strain-rate effect. Data presented here indicate that there is no appreciable rate effect. Moreover, the energy which is indicative of the "toughness" of the material, (*b*) and (*c*) in Table 1, is only about 3 percent of the total. This is not enough to differentiate between grades as a performance

TABLE 1—*Amount of energy absorbed by the various mechanisms, in·lb.*

(*a*)	Bending energy	15.57
(*b*)	Energy due to plastic work	0
(*c*)	Energy needed to create surfaces	1
(*d*)	Energy used to accelerate specimen to tup velocity	1.64
(*d*-1)	Energy due to acceleration bending	0.776
(*e*)	Energy due to vibration	1×10^{-4}
(*f*)	Energy absorbed by machine	6.75
(*f*-1)	Energy of final acceleration	1
	Total Energy	27

indicator. All of the data in Table 1 are on one material, namely, Carboloy Grade 55B. However, the same analysis was done on specimens of several different grades and the analysis has been found to hold for those alloys of less than 16 percent cobalt. The energy associated with the toughness of the material is a small part of the total energy measured by the test machine for those grades containing less than about 16 percent cobalt. For grades containing high cobalt content, such as 25 percent, the plastic component becomes more significant and the energy associated with the toughness of the material becomes a larger part of the total. Most grades contain less than about 16 percent cobalt and most applications are best satisfied by grades having less than about 16 percent cobalt.

Conclusions

The energy associated with the impact testing of cemented carbide consists mainly of elastic bending energy and absorption of energy by the testing machine. The vibrational and plastic components are insignificant. The toss energy and energy necessary to create new surfaces can be fairly well calculated

from other considerations. The tests have shown no rate effects in cemented carbides, and the state of stress in the beam is uniaxial tension. Thus the test does not describe the material's propensity for cleavage or brittle failure, but rather mainly describes the modulus and strength of cemented carbides (which are routinely and more easily measured in other ways), and the stiffness of the testing machine–all of which have very little bearing on the toughness of the cemented carbide. The components which describe this are the energy of plastic work and the energy necessary to create two new surfaces, and these consist of only a few percent of the total measured energy in the example described in the foregoing. The amount of energy which the machine absorbs will vary with the modulus and strength of the material being tested. In the case of a harder but lower strength grade like Carboloy Grade 320, the anvil sees very little load before failure and thus the energy partitioning will be significantly different than that for a stronger grade.

Thus the Charpy test conducted with the conditions in this study has little value in ascertaining the toughness of cemented carbide; in fact, results from it may be misleading. When cemented carbide is evaluated for toughness by impact testing of any kind, careful attention must be given to the aforementioned factors because they are encountered to a large extent in most, if not all, types of impact tests. Charpy impact-type tests on cemented carbide are essentially fast transverse-rupture strength tests on a "soft" test machine.

APPENDIX

Velocity of Charpy Impact Tup

Three copper wires known distances apart were attached to the side of the tup (Fig. 11). A metal contact was placed so that the wires on the tup brushed by the metal contacts and completed an electrical circuit (Fig. 12). This signal was recorded on an oscilloscope. The first wire triggered the oscilloscope and the last two recorded the time necessary for the tup to move by the contact (see Fig. 13). From the foregoing information, the speed of the tup was determined as 141 in./s.

Effective Mass of Pendulum

The pendulum was displaced 90 deg to the vertical and the force exerted by the tup in that position was measured via a load cell. The mass determined in this way was 5350 g (Fig. 4).

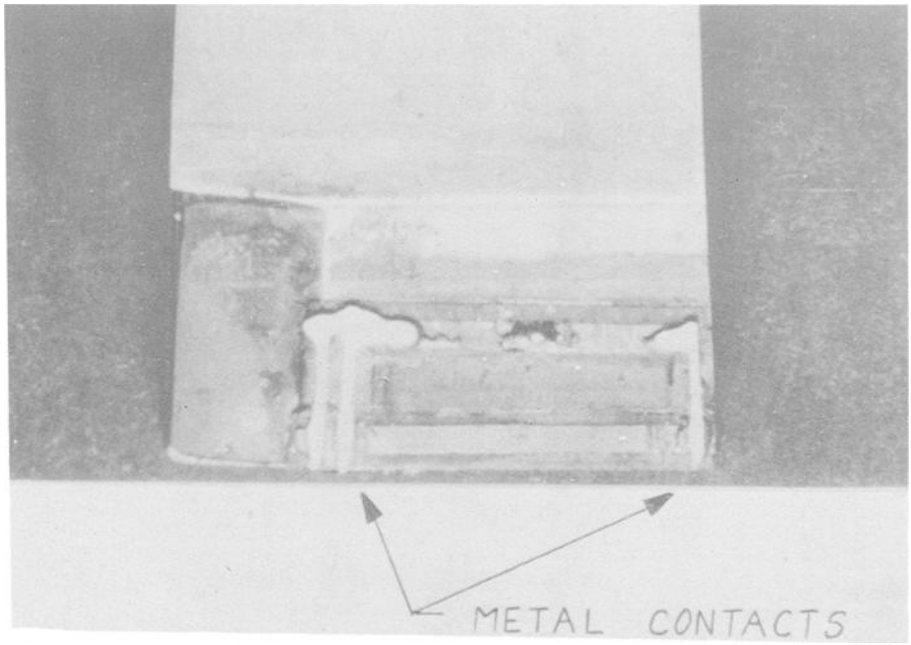

FIG. 11–*Tup with metal contacts.*

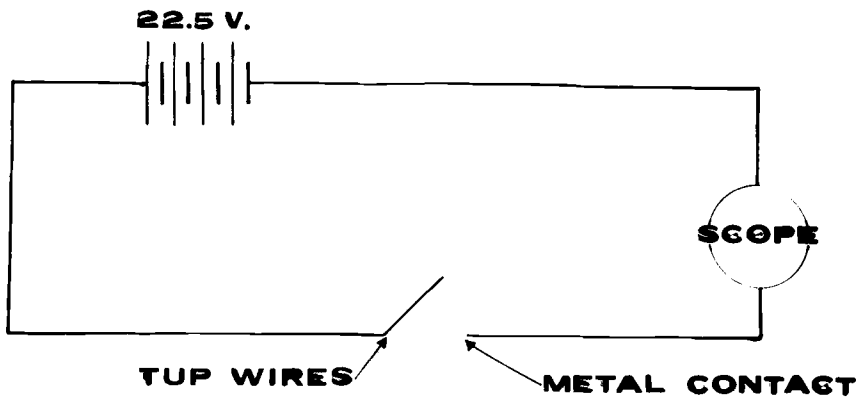

FIG. 12–*Schematic for velocity measurement.*

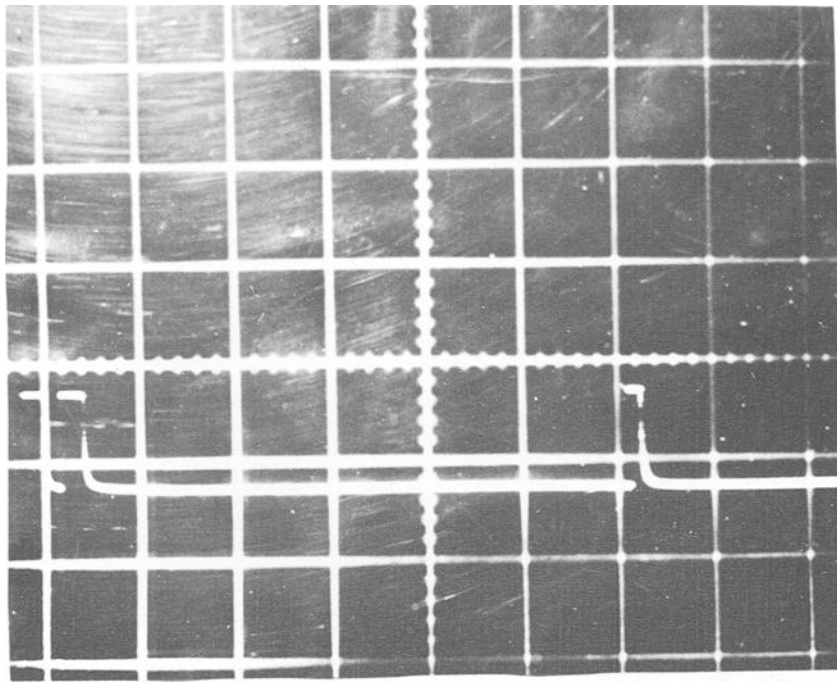

FIG. 13–*Oscilloscope trace from metal contacts.*

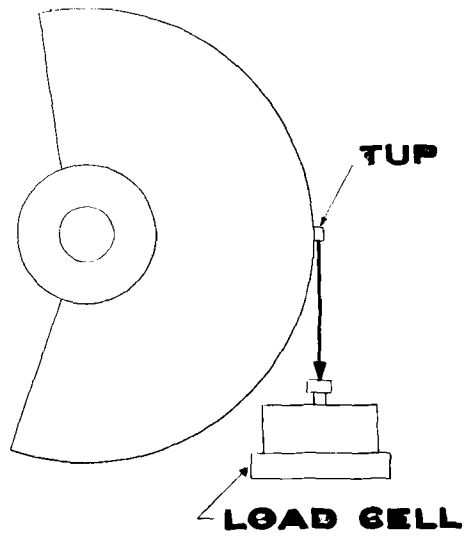

FIG. 14–*Effective mass measurement.*

A. Ewing[1] *and L. Raymond*[2]

Instrumented Impact Testing of Titanium Alloys

REFERENCE: Ewing, A. and Raymond, L., "Instrumented Impact Testing of Titanium Alloys," *Instrumented Impact Testing, ASTM STP 563,* American Society for Testing and Materials, 1974, pp. 180-202.

ABSTRACT: The dynamic fracture toughness was determined for two titanium alloys (Ti-6A1-4V and Ti-6A1-6V-2Sn) from different suppliers and in various heat-treated conditions. The strain-rate effect associated with the dynamic test is shown to increase the fracture toughness for all the alloys with the exception of mill-annealed and duplex-annealed Ti-6A1-6V-2Sn, where the fracture toughness was found to be independent of strain rate. Dial energy per unit specimen area $(W/A)_d$ for precracked Charpy specimens can be used to calculate K_{Id} as long as a relatively flat fracture appearance (small shear area) is obtained. Otherwise, when a large amount of shear is present, the energy to maximum load $(W/A)_m$ or P_{max} from the load-time trace must be used to calculate K_{Id}.

KEY WORDS: impact tests, strain rate, static fracture toughness, dynamic fracture toughness, inertia loads, instruments, dynamic calibration, dial energy, energy to maximum load

The purpose of this study is to evaluate the usefulness of instrumented impact testing for titanium alloys. The dynamic fracture toughness was determined for two high-strength titanium alloys. Three heats of Ti-6A1-4V from different suppliers were bought to the same specification and strength level. One heat of Ti-6A1-6V-2Sn was processed by three different methods to about the same strength level. These were then compared to second heat of Ti-6A1-6V-2Sn, which was beta-worked for comparison with other processing parameters.

Precracked Charpy test coupons were machined from contour double cantilever beam (CDCB) specimens (Fig. 1) that were used previously for fatigue crack growth rate studies. In the same study, the fracture toughness (K_{Ic}) was also measured with compact tension (CT) specimens according to ASTM Test for Plane-Strain Fracture Toughness of Metallic Materials (E 399-72). The compact tension specimens were machined from the CDCB specimen. Therefore, the crack growth rate, fracture toughness and the instrumented impact fracture data were from the same plate for each heat treatment.

[1]California State University, Long Beach, Calif.
[2]Head, Metallurgy Research, Materials Sciences Laboratory, The Aerospace Corporation, El Segundo, Calif. 90009.

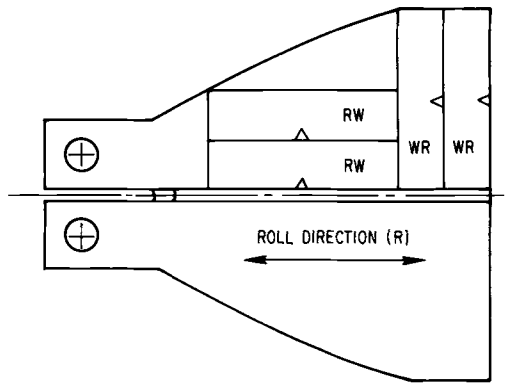

FIG. 1—*Specimen orientation showing the relationship of crack propagation and rolling direction of specimens taken from double cantilever beam specimens (CDCB).*

Background

The most extensive work on Ti-6A1-4V alloys was done by Hartbower et al [*2*].[3] Using precracked Charpy impact specimens, they demonstrated an empirical correlation between impact or dial energy per unit area, $(W/A)_d$, and static fracture toughness parameter $K_{Ic}{}^2/E$. The discrepancy is resolved because the data, $(W/A)_d$, which were correlated to static uniaxial tensile data and static plane stress and plane-strain fracture toughness.

More recently, Ronald et al [*3*] demonstrated that the energy absorbed by a precracked Charpy specimen, measured from the area under the slow-bend load-displacement trace, $(W/A)_s$, could be used to measure the static fracture toughness, K_{Ic}, which is normally calculated from the maximum load. They showed that the static toughness parameter, $(K_{Ic}{}^2/E)$, was related to the slow-bend energy, $(W/A)_s$, by the reciprocal of the proportionality constant of 2 $(1-\nu^2)$, which is one half of the theoretical value from the relationship

$$K_{Ic}{}^2/E = G_{Ic}/(1-\nu^2) = (W/A)_s/(1-\nu^2)$$

With a limited number of Ti-6A1-4V specimens, no correlation was observed when the dynamic energy $(W/A)_d$ measured from precracked Charpy specimens was compared with $K_{Ic}{}^2/E$, taken from slow-bend specimens.

The results of this work show that a relationship identical to that found by Ronald et al [*3*] does exist for titanium alloys when $(W/A)_d$ is plotted against the dynamic fracture toughness parameter $K_{Id}{}^2/E$ instead of the conventional fracture toughness parameter $K_{Ic}{}^2/E$. The discrepancy is resolved because the fracture toughness was found to be strain-rate sensitive for some of the alloys;

[3] The italic numbers in brackets refer to the list of references appended to this paper.

TABLE 1—*Chemical composition of the material used in program [1].*

Alloy Designation	Supplier[a]	Element, weight %								
		C	O	H	N	Al	V	Sn	Fe	Cu
Ti-6A1-4V	TMCA	0.038	0.16	0.0074	0.014	6.23	4.06	...	0.11	...
Ti-6A1-4V	CSA	0.049	0.15	0.0065	0.009	6.18	4.06	...	0.20	...
Ti-6A1-4V	RMI	0.042	0.18	0.0055	0.014	6.23	4.06	...	0.21	...
Ti-6A1-6V-2Sn	RMI-2[b]	0.023	0.15	0.0068	0.012	5.46	5.39	2.00	0.67	0.70
Ti-6A1-6V-2Sn	RMI-1	0.021	0.15	0.0054	0.011	5.46	5.46	2.00	0.60	0.70

[a] TMCA = Titanium Metals Corporation of America.
RMI = Reactive Metals Incorporation.
CSA = Crucible Steel Corporation of America.
[b] Beta-worked.

TABLE 2—*Heat treatment and processing of Ti-6A1-6V-2Sn alloys [1][supplied by RMI].*

Designation		Processing/Heat Treatment
Mill-anneal	RMI-1	mill annealed to MIL-H-81200A
Beta-anneal	RMI-1	1810°F (988°C) ± 10°F for 1 h in vacuum, argon cool to room temperature
Duplex-anneal	RMI-1	1700°F (927°C) ± 10°F for 1 h in vacuum, argon cool to room temperature, reheat 1400°F (760°C) for 1 h in vacuum, argon cool to room temperature
Beta-worked (STA)	RMI-2	beta-rolled at 1825°F (996°C), solution treated at 1675°F (913°C) for 15 min, water quenched, aged 1100°F (593°C) for 4 h

that is, $K_{Id} \geqslant K_{Ic}$, and correspondingly $(W/A)_d \geqslant (W/A)_s$.

Materials

The chemical compositions and suppliers for the Ti-6A1-4V and Ti-6A1-6V-2Sn alloys are listed in Table 1. All of the Ti-6A1-4V alloys were purchased and tested in the mill-annealed condition per MIL-H-81200A.

One heat of Ti-6A1-6V-2Sn was purchased in the mill annealed condition per MIL-H-81200A and then subsequently processed as described in Table 2. The second heat was beta-processed at the mill as described in Table 2.

Experimental Procedure

A 24-ft·lb-capacity Manlabs Charpy impact machine (Fig. 2) was instrumented to measure the dynamic properties. A Sonntag Model SI-I 240-ft·lb machine (Fig. 3) was also instrumented, but the smaller-capacity machine was found to be a better instrument for impact testing of the precracked Charpy specimens used in this report.

The tup of a 24-ft·lb Manlabs Charpy impact test machine, Model CIM-24A (Fig. 2), was instrumented to measure dynamic loads. A full 350-Ω strain-gage

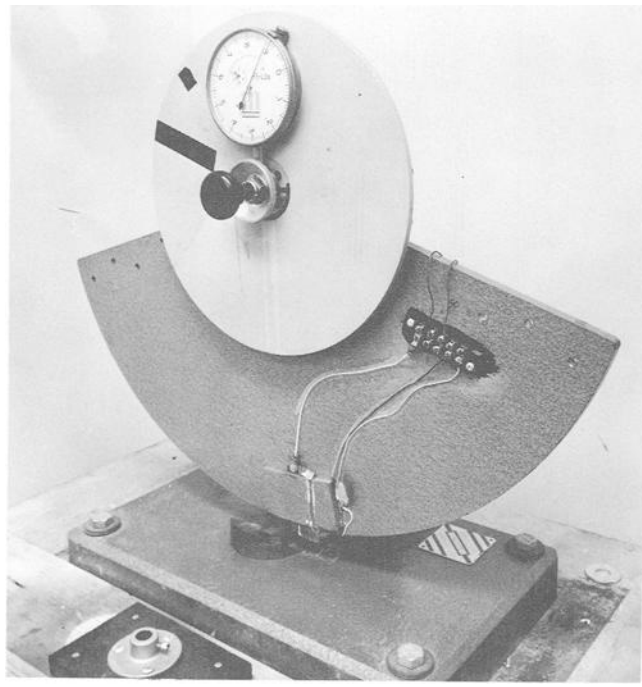

FIG. 2—*The 24-ft·lb-capacity Manlabs Charpy impact machine, Model CIM-24A, used to determine dynamic properties used in this experiment.*

bridge was used with 12 V d-c excitation and a Daytronics strain-gage conditioner-amplifier. The strain-gage load-output was displayed on an oscilloscope and recorded using a Polaroid camera. (Details of striker instrumentation are shown in Appendix I.) Standard-dimensioned Charpy impact specimens (according to ASTM Notched Bar Impact Testing of Metallic Materials (E23-72)) were machined from CDCB specimens as shown in Fig. 1 with some specimens reduced in thickness to approximately 0.30 in. All impact specimens were fatigue precracked using a Physmet Model FCM-300 Fatique Cracking Machine. The tup of the 240-ft·lb Sonntag Charpy machine was instrumented with the same 350-Ω strain gages and used similar excitation and recording equipment as that used for the 24-ft·lb machine.

All specimens were oriented either with the crack propagating in the rolling direction with the normal to the crack plane in the width direction (WR) or with the crack propagating in the width direction with the normal to the crack plane in the rolling direction (RW) (Fig. 1).

FIG. 3—*Sonntag Model SI-1 240-ft·lb-capacity Charpy impact machine initially instrumented to measure dynamic properties.*

Calibration

The instrumented impact test system was calibrated using both static and dynamic calibrations. Static calibration consisted of loading the tup, or impact striker, with a hydraulic jack while the tup was in contact with a standard

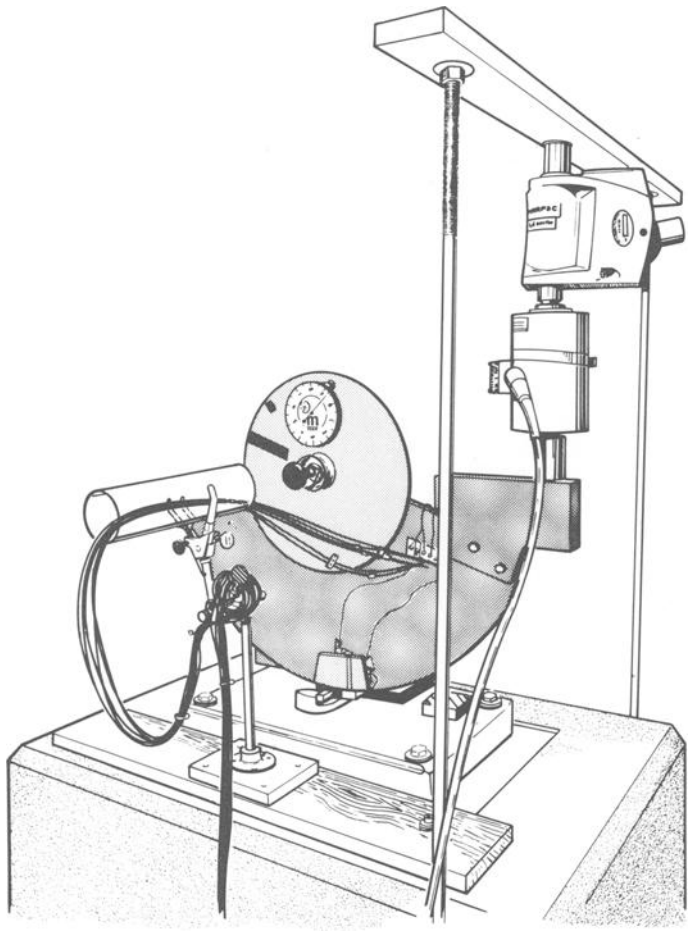

FIG. 4—*Schematic setup for static calibration on 24-ft·lb Charpy impact machine.*

Charpy dimensioned specimen (without a notch) as shown in Fig. 4. The loads applied to the tup were measured by means of a 10 000-lb-capacity BLH SR-4 load cell with an automatic digital readout. As the specimen-tup load was increased, the corresponding strain-gage outputs were recorded. The bridge outputs were linear with loading throughout the entire loading range (0 to 4500 lb). This static calibration provided a means of determining the dynamic loads from the oscilloscope traces (or pictures) of strain-gage outputs versus time.

The span setting on the strain gage conditioner-amplifier was adjusted to give a loading scale of 1000 lb per volt of amplified gage output. With this adjustment it was possible to use the oscilloscope preamp to obtain loading scales of 200, 500, and 1000 lb per centimeter of trace deflection. A shunt-type resistor was then selected to use as a calibration check during testing.

Dynamic calibration consisted of two parts. A high-strength, low strain-rate sensitive material (in this case, E4340 HR heat treated to 240 ksi yield strength and a hardness of HRC 48-52) was tested dynamically on both the 24 and 240-ft·lb-capacity machines. Its dynamic toughness was then compared with the static values obtained from contoured double cantilevered beam (CDCB) specimens of the same material and strength level.

The static toughness, K_{Ic}, was 79 ± 3 ksi $\sqrt{\text{in.}}$ [4] while the average dynamic toughness, K_{Id}, values were 75.8 ksi $\sqrt{\text{in.}}$ (75 ± 9 ksi $\sqrt{\text{in.}}$) for the 24-ft·lb-capacity machine and 75.3 ksi $\sqrt{\text{in.}}$ (76 ± 2 ksi $\sqrt{\text{in.}}$) for the 240-ft·lb machine.

The second method of dynamic calibration required using the area under the load-time curve to determine the energy absorbed by the specimen, and to compare this energy value with the dial energy obtained from the pendulum swings. (This method is explained in Appendix II.) The results of the energy calculations are shown in Fig. 5. Because the energy calculations were generally within only a few percent of the actual dial energy readings, the calculations were made only on the E4340 HR steel calibration specimens and 29 titanium test specimens. The calculated energy values were used only as a means of establishing the reliability of the system. The dial energies were then used for measuring the $(W/A)_d$ values.

Inertia Loads

The inertia loads (P_i) observed as a small initial peak on the load-time trace were recorded and compared with those obtained by other investigators [5]. The inertia loads for the 4340 steel calibration specimen fell within the limits as shown in Fig. 6. In addition to the inertia data provided for lucite and steel, an estimated inertia load range (or boundaries) for titanium has been superimposed using the data from this report. The loads that appear low at the 200-in./s velocity may be attributed to the relatively low response time (10 kHz minimum) of the instrumentation used. As shown in Fig. 6, the inertia loads can be quite high at the higher striker velocities associated with the 240-ft·lb-capacity machine. For some materials, this inertia load is more than enough to

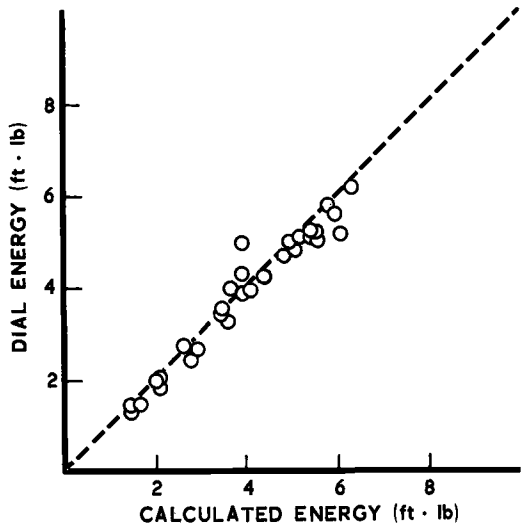

FIG. 5–*Comparison of energy measured from actual pendulum swing (dial energy) with the energy calculated from the load-time curve for 4340 steel and titanium specimens.*

break a specimen. Some materials, especially the high-strength steel, caused a great deal of noise (oscillations) or "ringing" to appear on the load-time traces when specimens were broken on the large 240-ft·lb-capacity machine.

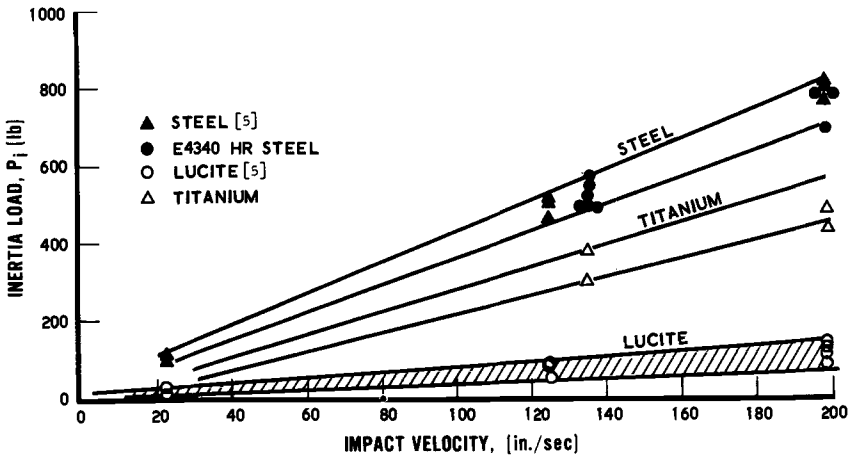

FIG. 6–*Comparison of inertia loads for lucite, steel, and titanium [5].*

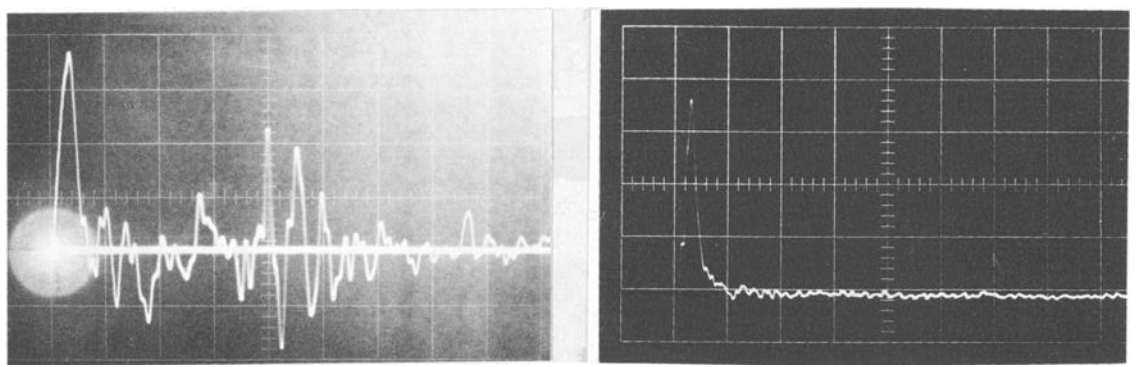

FIG. 7—*Actual load-time traces for E4340 HR showing how the problem of noise or "ringing" was eliminated by using the 24-ft·lb machine (*right*) instead of the 240-ft·lb machine (*left*).*

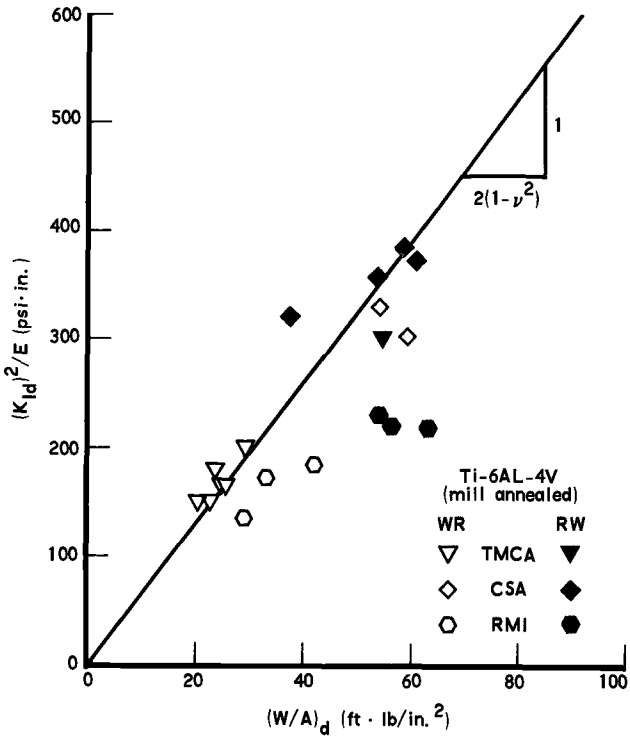

FIG. 8—*The relationship between dynamic stress intensity parameter* $(K_{Id}{}^2/E)$ *and the dial energy per unit specimen area* $(W/A)_d$ *for a precracked Charpy specimen tested in impact for mill-annealed Ti-6A1-4V.*

Both the effects on inertia load and especially the problem of ringing were eliminated by using the smaller-capacity Manlabs impact machine. The lower velocity of the 24-ft·lb-capacity Manlabs machine is primarily responsible for the decrease in the inertia loading. The elimination of the ringing (Fig. 7) is attributed in part to the decrease in velocity, but primarily it is due to the more rigid design of the Manlabs pendulum striker arm.

Calculations

Dynamic fracture toughness was calculated from the standard fracture toughness equation for a three-point bend specimen [*6*]:

$$K_{Id} = Y \frac{6M\ a^{1/2}}{bw^2} \tag{1}$$

where

M = applied bending moment, $PL/4$,
a = crack length, in.,
b = specimen thickness, in.,
w = specimen width = 0.394 in.,
Y = $1.93 - 3.07\ (a/w) + 14.53\ (a/w)^2, -25.11\ (a/w)^3 + 25.80\ (a/w)^4$,
P = applied load, lb, and
L = span length or anvil spacing = 1.574 in.

Results

The average values of the dynamic and the conventional or static results are presented in Table 3. The exact values of all of the data points obtained in this investigation are plotted in Figs. 8 and 9, where the dynamic stress intensity parameter $K_{Id}{}^2/E$ is plotted against $(W/A)_d$ for the Ti-6A1-4V and Ti-6A1-6V-2Sn alloys, respectively. The points are generally clustered except for the TMCA Ti-6A1-4V in the RW direction and for the duplex-annealed Ti-6A1-6V-2Sn in the RW direction.

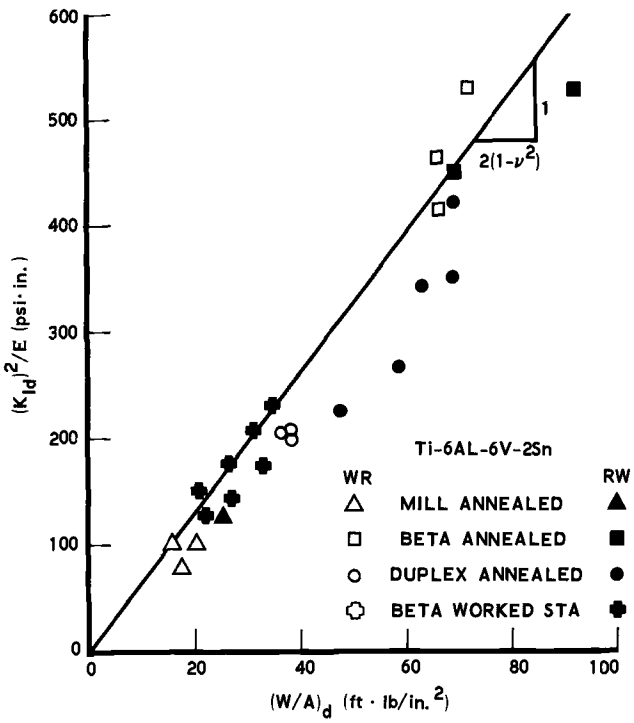

FIG. 9—*The relationship between the dynamic stress intensity parameter* $(K_{Id}{}^2/E)$ *and the dial energy per unit specimen area* $(W/A)_d$ *for a precracked Charpy specimen tested in impact for Ti-6A1-6V-2Sn.*

TABLE 3—*Average values of dynamic and static test results.*

Supplier	Orientation	Dynamic K_{Id} ksi $\sqrt{\text{in.}}$	Dynamic $(W/A)_d$ ft·lb/in.^{2}	Dynamic R_c	Static[a] E 10^6 psi	Static[a] K_{Id} ksi $\sqrt{\text{in.}}$	Static[a] σ_{ys} ksi	Static[a] σ_{uts} ksi
Ti-6A1-4V								
TMCA	[b] ▽ WR (6)[c]	50.2	23.4	36	16.1	...	150.0	152.8
	▼ RW (1)	67.4	54.3	36	...	36.8	...	...
CSA	◇ WR (2)	71.2	56.5	35	15.9	...	133.9	138.2
	◆ RW (3)	71.8	58.5	35	...	48.2	...	...
RMI	○ WR (3)	54.7	33.3	36	18.4	35.5	140.0	146.5
	● RW (3)	62.3	55.0	36	17.5	...	150.0	152.0
Ti-6A1-6V-2Sn								
Mill-annealed	△ WR (3)	39.0	18.9	39	17.0	35.6	163.3	170.2
RMI heat No. 2	▲ RW (1)	45.3	25.4	39	...	...	...	...
Beta-annealed	□ WR (3)	84.6	65.2	...	16.3	54.3	139.8	156.3
RMI heat No. 2	■ RW (2)	86.0	70.0	37	...	...	...	...
Duplex-annealed	○ WR (3)	58.1	38.2	37	16.6	65.2	150.5	161.1
RMI heat No. 2	● RW (5)	65.1	57.0	37	...	...	...	...
Beta-worked (STA)	⬡ WR (1)	...	21.8	42	16.3	34.1	173.3	182.5
RMI heat No. 1	⬢ RW (7)	56.6	22.5	42	16.9	...	173.7	180.4

[a] Titanium static data referenced from Amateau, Hanna, and Kendall [*1*].
[b] Symbol.
[c] Number of specimens tested.

Since the dial energy per unit specimen surface area is represented by the total energy under the load-time trace, a correlation would not be expected between the dynamic stress intensity parameter K_{Id}^2/E and the dial energy $(W/A)_d$ when shear lips are observed, as is indeed the case as shown in Figs. 8 and 9 (Ti-6A1-4V RMI-RW, for example). When the fracture is flat and the load-time trace is symmetrical, a good correlation is obtained. In fact, the agreement is equivalent to that of Ronald et al [*3*] where the slope of the line is $\frac{1}{2}(1 - \nu^2)$. Also, as expected, the RW direction has the highest toughness because the crack plane is perpendicular to the rolling direction.

The K_{Id} results with the two different thicknesses are summarized in Figs. 10 and 11, and compared with the K_{Ic} measurements obtained by Amateau et al [*1*]. Figure 10 identifies a strain-rate effect with K_{Id} greater than K_{Ic} for all of the mill-annealed Ti-6A1-4V alloys. Figure 11 demonstrated that beta-worked and beta-annealed Ti-6A1-6V-2Sn have a strain-rate effect similar to Ti-6A1-4V, that is, K_{Id} greater than K_{Ic}, but the mill-annealed and duplex-annealed exhibit no strain-rate sensitivity, that is, K_{Id} equals K_{Ic}. The thickness of 0.3 in. is shown to be adequate to K_{Id} values in excess of 80 ksi $\sqrt{\text{in.}}$ even with a large percentage of shear on the specimens.

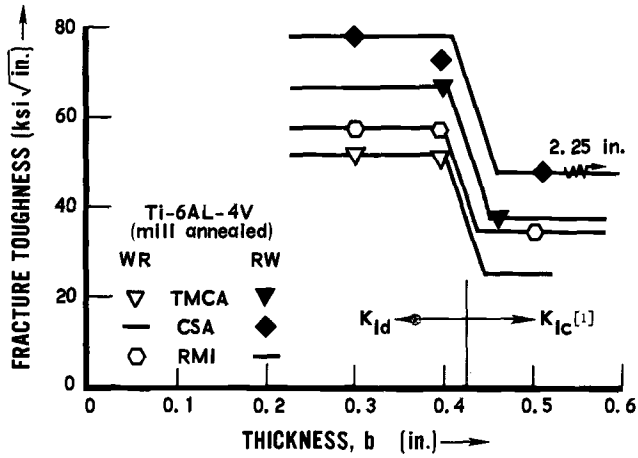

FIG. 10—*Toughness versus specimen thickness for Ti-6A1-4V in the mill-annealed condition from three suppliers.*

Both 0.3 and 0.394-in.-thick specimens exhibited a minimum of about 80 percent flat fracture for both the Ti-6A1-4V and Ti-6A1-6V-2Sn alloys. The only exception was the beta-annealed Ti-6A1-6V-2Sn where the percentage of shear lip increased from 20 percent for the 0.394-in. specimen to 45 percent shear lip for the 0.30-in. specimen. This change was accompanied by only a

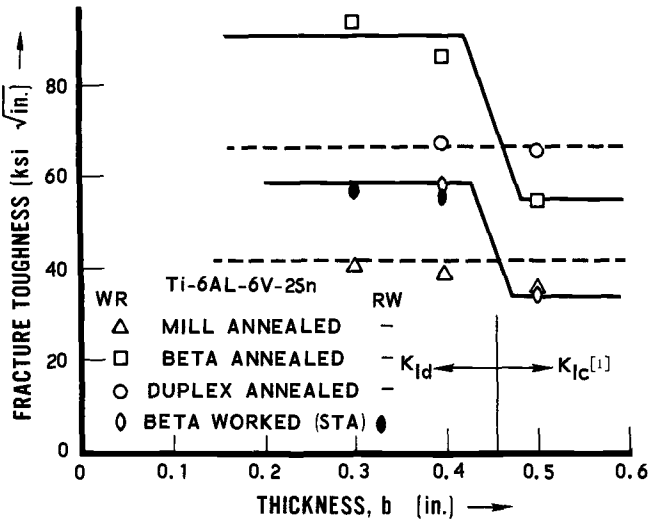

FIG. 11–*Toughness versus specimen thickness for Ti-6A1-6V-2Sn.*

slight increase in toughness. The reason for this observation is explained with Fig. 12.

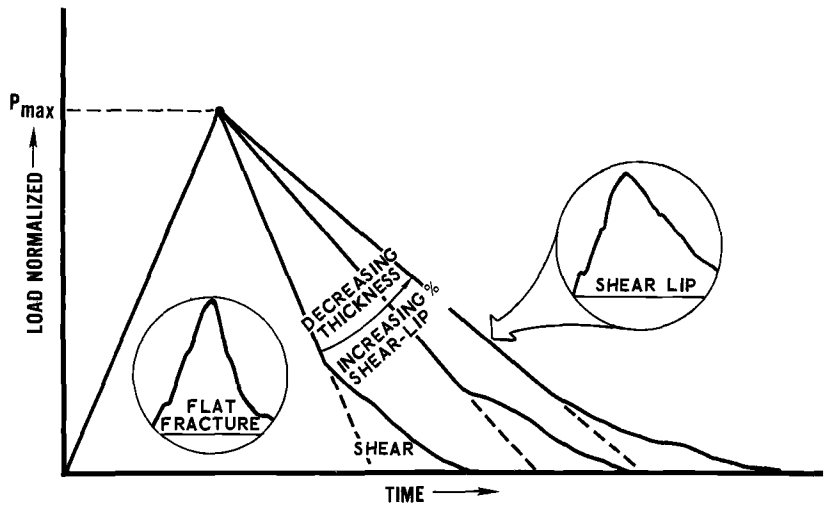

FIG. 12–*Typical slope change in the load-time/trace as the thickness is decreased or the percentage of shear increases.*

If the load was normalized for the various thickness specimens and the fracture surface was essentially flat, the load-time trace was symmetrical about the maximum load (note insert in Fig. 12). For specimens with a larger amount of shear lip caused by decreasing the thickness (beta-annealed Ti-6A1-6V-2Sn at 0.30 in.), the load-time traces were less symmetrical, as shown in Fig. 12. However, the calculated K_{Id} for both thickness was the same, suggesting that the maximum load in an instrumented Charpy provides a valid K_{Id} number even when large amounts of shear are present.

Conclusions

1. The dynamic fracture toughness versus energy correlations follow the same relationship as that obtained by Ronald et al [*3*] using slow-bend energy and slow strain-rate toughness measurements. If the fracture appearance of the specimen exhibits primarily a flat fracture with little shear area, an estimate of the dynamic toughness (K_{Id}) can be made using half the dial energy $(W/A)_d$ in the equation:

$$K_{Id} = \sqrt{\frac{E}{2(1-\nu^2)} \left(\frac{W}{A}\right)_d}$$

This estimate can be made without the aid of an instrumented impact test. If the fracture appearance of the specimen exhibits excessive shear lip, then the instrumented system will have to be used to obtain an accurate value of K_{Id}, which can be obtained because of the nature of the load-time trace.

2. Instrumenting the impact test allows for K_{Id} to be calculated directly from P_{max} using Eq 1 or from the energy to maximum load $(W/A)_m$ on the load-time trace by using the relationship:

$$K_{Id} = \sqrt{\frac{E}{(1-\nu^2)} \left(\frac{W}{A}\right)_m}$$

3. The toughness for the mill-annealed and duplex-annealed Ti-6A1-6V-2Sn showed no strain-rate dependence. However, the beta-annealed and beta-worked (STA) Ti-6A1-6V-2Sn as well as the mill-annealed Ti-6A1-4V from three different heats showed a definite strain-rate dependence (Figs. 10 and 11).

The relative strain-rate dependence of the Ti-6A1-6V-2Sn alloys seems to be a result of processing. The two strain-rate independent materials, mill-annealed and duplex-annealed Ti-6A1-6V-2Sn alloys, were purchased from the same heat in the same mill-annealed condition RMI-1 and both were heat treated below the beta transus temperature. But the beta-annealed RMI-1 heat showed a strain-rate dependence similar to the RMI-2 heat that was beta-worked.

The microstructures of the mill-annealed and duplex-annealed Ti-6A1-6V-2Sn (no strain-rate effect) were essentially equiaxed with the duplex anneal having a slightly larger grain size. The beta-annealed and beta-worked TI-6A1-6V-2Sn (strain-rate dependent) microstructures were very different. However, both of the strain-rate dependent materials had relatively large equiaxed grain size with a very noticeable or more pronounced segregation of alpha and alpha-plus-beta phases. At best, a study of the microstructural differences suggests that segregated beta phase accounts for favorable strain-rate sensitivity.

The foregoing conclusion based on microstructure would suggest that the mill-annealed Ti-6A1-4V would not be strain-rate sensitive, which is contrary to the experimental data (Fig. 12). All of the mill-annealed Ti-6A1-4V specimens showed a definite strain-rate dependence though their microstructures are similar to the strain-rate insensitive Ti-6A1-6V-2Sn materials. Therefore, based on these observations, no definite conclusion can be made about the relationship between microstructure and strain-rate sensitivity.

4. It is generally believed that no relationship exists between fracture toughness and fatigue crack growth rates. This appears valid if the K_{Ic} numbers of Fig. 11 are compared with the relative crack growth rate resistance curves of Fig. 13. However, a comparison of fatigue crack growth data [*1*] (Fig. 13) with the dynamic fracture toughness, K_{Id} (Fig. 11) seems to unscramble this relative order and suggests that a correlation does exist between these two parameters. For the Ti-6A1-6V-2Sn alloys (Fig. 13), the beta-annealed had the highest dynamic toughness and the highest resistance to fatigue crack growth while the mill-annealed Ti-6A1-6V-2Sn had the lowest dynamic toughness and the lowest resistance to crack growth, with duplex-annealed and the beta-worked (STA) bracketed between these values.

The relative order of increasing toughness did not change as a function of strain rate for the three heats of Ti-6A1-4V in the mill-annealed condition, though the resistance to fatigue crack growth (Fig. 14) does appear to follow the same relative ranking as the dynamic and the static increase in toughness (Fig. 10). These results suggest that dynamic fracture toughness may possibly be used as a relative measure of resistance to fatigue crack growth within a specific alloy group.

Acknowledgments

M. F. Amateau is acknowledged for providing the static data and the materials for the dynamic test specimens for both titanium alloys, and D. L. Dull for providing the E4340 HR steel used in the calibration of the instrumented impact machines.

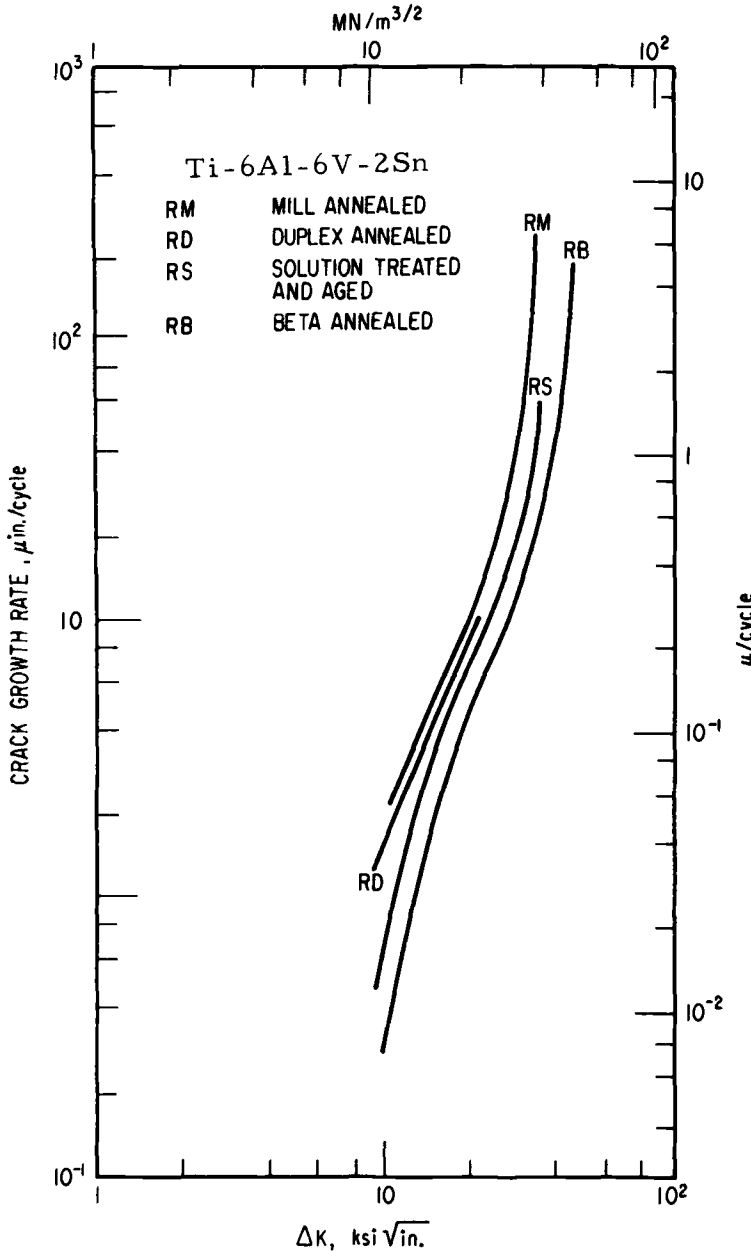

FIG. 13–*Fatigue crack growth data for Ti-6Al-6V-2Sn [1].*

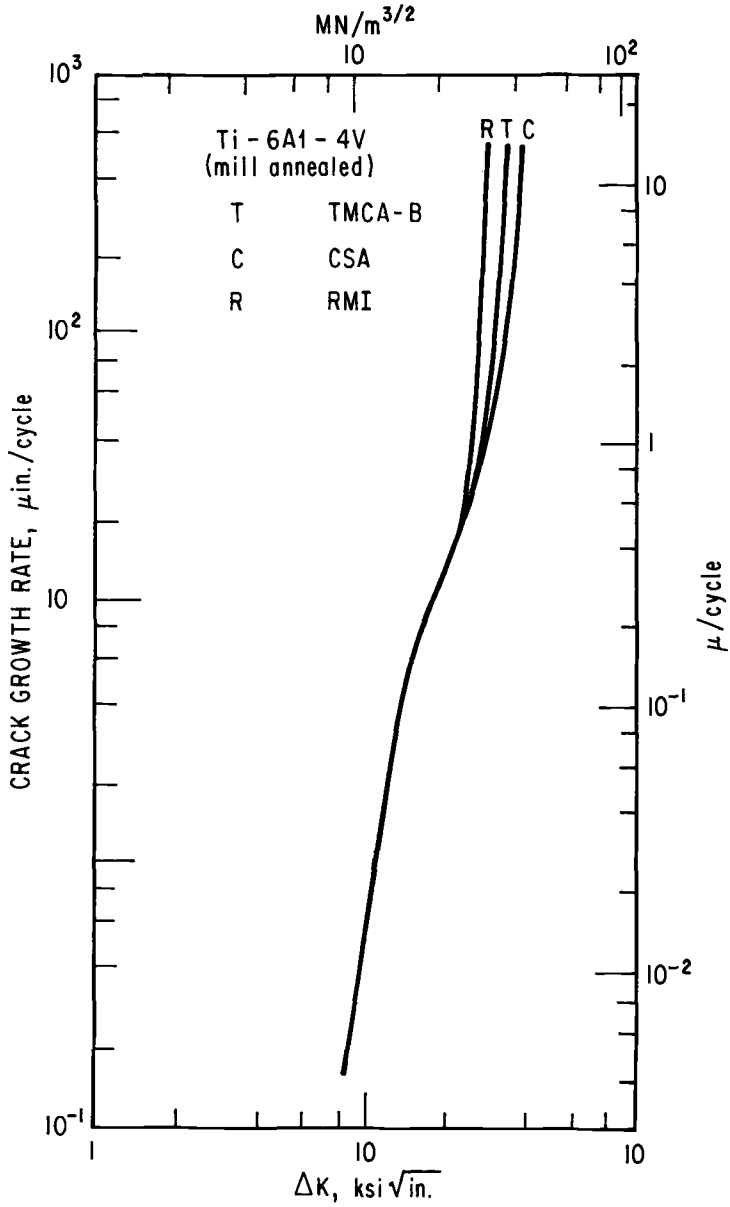

FIG. 14—*Fatigue crack growth data of mill-annealed Ti-6Al-4V [1].*

APPENDIX I

Striker Instrumentation

Instrumentation of the 24-ft·lb Charpy impact machine consisted of milling two slots on the side of the tup, or striker (Fig. 15) to accommodate the two active strain gages. The two slots should be sufficiently deep to allow complete protection of the lead wires as well as the gages (or transducers). They should also be approximately twice the width of the strain indicating device to aid in their placement. To ensure a linear output with loading, care should be taken to make sure that the gages are symmetrically located with respect to each other.

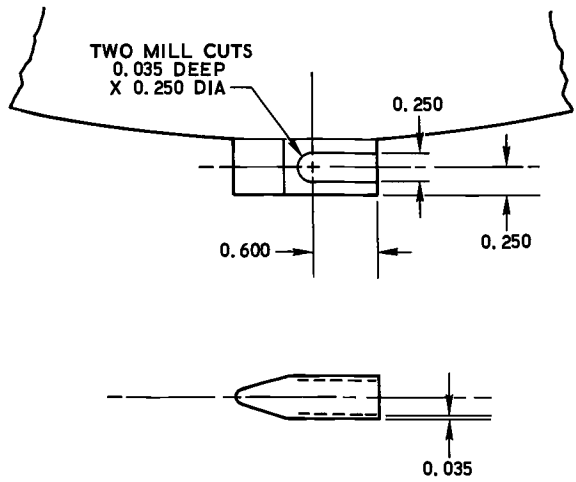

FIG. 15—*Modification of 24-ft·lb Charpy striker (all dimensions in inches).*

The two dummy gages were mounted on the striker arm in a convenient location. The strain gages (Micro-Measurement Type ED-DY-062AK-350) were wired in a full-bridge configuration as shown in Fig. 16. The gages were then covered with Micro-Measurement M-Coat G protective covering which was again covered with stainless steel shim stock to protect the gages from deflected specimen halves.

The strain-gage bridge was energized with a 12 V d-c excitation voltage using a Daytronics Model 870 strain-gage conditioner-amplifier module. The bridge output signal was displayed on a Tektronix Type 535A oscilloscope with a fast-rise preamp and recorded using a standard Polaroid oscilloscope camera. The oscilloscope sweep was triggered by externally triggering the sweep off the vertical output signal. This provided a very small loss in actual trace picture. The schematic layout is shown in Fig. 16.

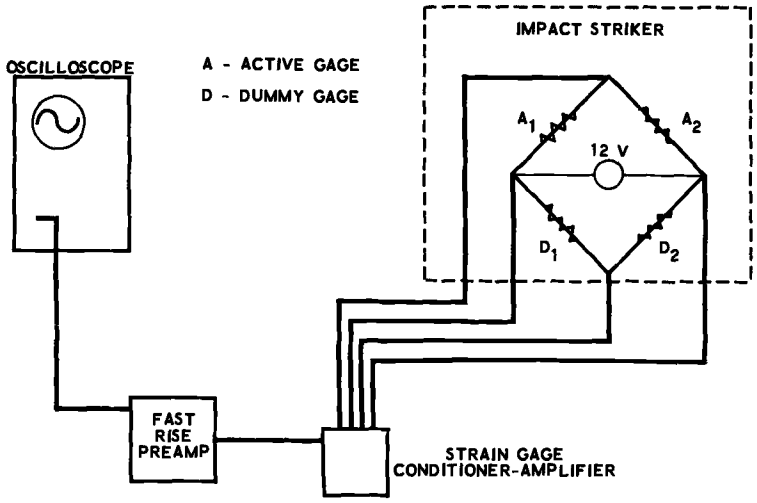

FIG. 16–*Schematic layout of instrumented impact test system including strain-gage bridge configuration.*

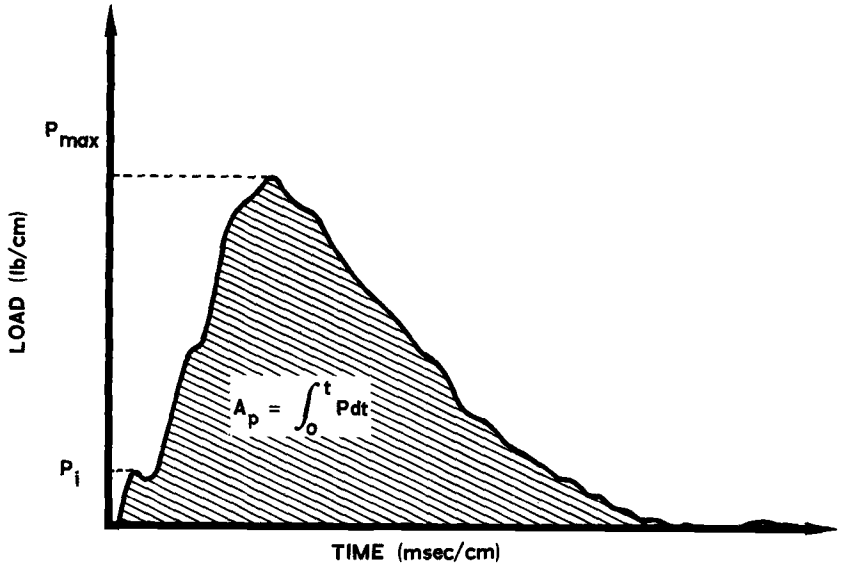

FIG. 17–*Typical load-time curve for a titanium specimen showing the area,* A_p, *used to determine the energy absorbed by the specimen for dynamic calibration.*

APPENDIX II

Dynamic Calibration

The second method of dynamic calibration requires using the area under the load-time curve, Fig. 17, to determine the energy absorbed by the specimen, and to compare this energy value with the dial energy obtained from the pendulum swing. The energy in ft·lb under the load-time curve is

$$E = \int_0^S Pds \tag{2}$$

$$E = \int_0^t P\,V\,dt \tag{3}$$

where

P = applied load,
S = distance the load acts,
V = velocity during loading, and
t = time when loading takes place.

The impact striker velocity is continuously decreasing during the impact, or loading, of the test specimen. However, for energy losses of 5 ft·lb or less for the 24-ft·lb-capacity machine and less than 20 ft·lb for the 240-ft·lb-capacity machine, the change in velocity of the impact striker is relatively small. During the relatively short time that the striker is in contact with the specimen, the velocity, V, can be assumed constant. Therefore, it is sufficient to use the average of the initial and the final impact or loading velocities in Eq 3.

$$E = \bar{V} \int_0^t Pdt \tag{4}$$

where

$$\bar{V} = \frac{V \text{ initial} + V \text{ final}}{2}$$

The initial velocity was obtained from measuring the free-swinging velocity of the pendulum without a specimen and confirmed from measuring the height that the pendulum falls and determining the velocity using Eq 5:

$$V = \sqrt{2gh} \tag{5}$$

where

g = acceleration due to gravity and
h = height that the pendulum falls.

The final velocity, V_f, was obtained from Eq 5 using the height that the pendulum rises after impacting the test specimen.

The area, A_p, under the load-time curve (Fig. 17) is determined from

$$A_p = \int_0^t Pdt \tag{6}$$

where

A_p = area in units of pound-seconds.

Standard planimeter techniques were used in the actual calculation or measurement of these areas.

The energy absorbed by the impact specimen (or dial energy) should be equal to the area, A_p, under the load-time curve multiplied by the average impact velocity, $\bar{V}$:

$$E = \bar{V} A_p \tag{7}$$

Because energy calculations were generally within only a few percent of the actual dial energy readings, the calculations were made only on the E4340 HR steel calibration specimens and some of the titanium specimens. The calculated energy values were used only as a means of determining the reliability of the system and, whenever possible, the dial energies were used.

References

[1] Amateau, M. A., Hanna, W. D., and Kendall, E. G., "F-15 Program Final Report: Ti-6A1-6V-2Sn and Ti-6A1-4V Fatigue Crack Propagation," ATR-72-(9990)-3, Material Science Laboratory, Aerospace Corp., El Segundo, Calif., 29 Sept. 1971.

[2] Hartbower, C. E., Reuter, W. G., and Crimmins, P. P., "Tensile Properties and Fracture Toughness of 6A1-4V Titanium," AFML-TR-68-163, Air Force Materials Laboratory, Wright-Patterson Air Force Base, Ohio, Vol. 1, Sept. 1968, and Vol. 2, March 1969.

[3] Ronald, T. M. F., Hall, J. A., and Pierce, C. M., "Some Observations Pertaining to Simple Fracture Toughness Screening Tests for Titanium," AFML-TR-311, Air Force Materials Laboratory, Wright-Patterson Air Force Base, Ohio, March 1971.

[4] Dull, D. L. and Raymond, L., *Metallurgical Transactions*, Vol. 3, Nov. 1972, pp. 2943-2947.

[5] Server, W. L., "Dynamic Fracture Toughness Determined From Instrumented Pre-Cracked Charpy Tests," TR 8 (UCLA-ENG-7267), Materials Dept., School of Engineering and Applied Science, University of California, Los Angeles, Aug. 1972.

[6] Brown, W. F., Jr. and Srawley, J. E. in *Plane Strain Crack Toughness Testing of High-Strength Metallic Materials, ASTM STP 410,* American Society for Testing and Materials, 1966, p. 13.

W. R. Hoover[1]

Effect of Test System Response Time on Instrumented Charpy Impact Data

REFERENCE: Hoover, W. R., "Effect of Test System Response Time on Instrumented Charpy Impact Data," *Instrumented Impact Testing, ASTM STP 563*, American Society for Testing and Materials, 1974, pp. 203-214.

ABSTRACT: The effect of response time on instrumented Charpy impact data obtained on unidirectional Borsic-aluminum composites has been examined. It has been shown that the use of filters to eliminate high-frequency noise in the load-time traces obtained can significantly increase the response time of the testing system and lead to grossly inaccurate data. The current results indicate that as the response time is increased, the load is attenuated, the time to fracture is increased, and the absorbed energy is unaffected. The attenuation characteristics of the testing system can be documented through the use of a sine wave generator. These characteristics can be used both as a guide to ensure the adequacy of the system response time for future testing and as a means of correcting attenuated data which were obtained on a testing system with excessive filtering (inadequate response times).

KEY WORDS: impact tests, electronic filtering, composite materials, response time

The increasing demand for characterization of the dynamic fracture process in structural materials has stimulated a rapid growth in instrumented impact testing [*1*][2] This testing technique retains the advantages of impact testing (high loading rates, simple testing procedures, and simple specimen configurations) while, in addition, providing the load-time response during the impact event. Although this technique is becoming widely used, instrumented impact testing is still in its infancy, and all of its limitations have not been adequately established and are worthy of further study.

Whether it be drop weight, Charpy impact, or Izod impact testing, an instrumented impact testing system consists of three major components [*2*], the dynamic load cell, the data display system, and signal conditioning unit. The dynamic load cell is the tup (or striker) which produces an electrical analog of the interaction force between the specimen and the machine. The data display

[1] Composite Materials Development Division, Sandia Laboratories, Albuquerque, N. Mex. 87115.

[2] The italic numbers in brackets refer to the list of references appended to this paper.

system is commonly an oscilloscope which records the force data as a function of time. The signal conditioning unit facilitates the balancing of the strain-gage bridge, amplification of the bridge output, filtering of the signal, and a calibration function for determination of the bridge amplification.

The output signal (the load signal) is, of course, inherently filtered to some degreee by the signal conditioning unit, but at times additional filtering is employed to eliminate high-frequency noise in the output signal which can make data interpretation difficult. This increased filtering increases the response time of the testing system.

Instrumented impact systems are normally calibrated by one or more of three methods [*2,3,4*]. First, the tup is statically loaded in a standard testing machine to determine its load-voltage characteristics. Secondly, an impact test is conducted and the energy absorbed is recorded by the machine dial and by the area under the voltage-time trace. Since the average hammer velocity is known, it is thus possible to equate the two energies and determine the tup calibration. The third calibration method involves conducting slow-bend tests and impact tests on a strain-rate insensitive material. The tup calibration is determined by setting the dynamic loads equal to the static loads.

After one or more of the calibration procedures are completed, the system is usually considered to be "calibrated" and is often used to test a wide variety of materials. Recent data [*5*], however, indicate that these calibration procedures are insufficient for tests of very short duration, that is, high hammer velocities or brittle materials, because of inadequate system response times. This potential problem has gone unnoticed for some time since the standard calibration procedures do not define the response of the system during very rapid tests, and since many users are unaware that the response time of the system is potentially inadequate.

Ireland [*6*] has recently suggested that an experimenter can guard against gathering severely attenuated data by electronically measuring the response time of his testing system. This is done by using a signal generator to superimpose a sine wave on the output of the strain-gage bridge. Then, by increasing the frequency of the sine wave, the attenuation versus frequency behavior of the system can be documented. If the effective rise time of the sine wave is defined to be 0.35 divided by the frequency, the attenuation versus rise-time characteristics can be determined. Ireland then suggests that a reasonable definition of response time, T_R, is the rise time at which the signal is attenuated 10 percent. In other words, the response time is defined to be that rise time which corresponds to a 0.915 dB attenuation. Ireland proposes that test data should be considered acceptable if the time to fracture, t_f, is greater than T_R, while if $t_f \leqslant T_R$, the data should be considered suspect due to excessive attenuation. He did not present evidence that this approach can actually predict the attenuation for a test of arbitrary t_f; he only suggested that T_R was useful as a guide to obtaining reliable instrumented impact data.

The purpose of this investigation is twofold: (1) to document the effects of

inadequate response time (excessive filtering) with fracture data obtained from strain-rate insensitive Borsic-aluminum composites, and (2) to determine if the electronically measured attenuations, as determined by Ireland's method, agree with those measured during impact testing.

Experimental Procedures

Impact Testing

Impact testing was conducted on a State Impact Tester (Model No. SI-1C) with a 240 ft·lb (325.4 J) capacity. A Dynatup (Model No. 371) instrumentation system manufactured by Effects Technology, Inc. was used to obtain the dynamic fracture data. The Dynatup system employs a semi-conductor strain-gage bridge mounted on the tup and is capable of recording data at four arbitrary frequency settings (or filtering levels) designated as: open (100), 40, 20, and 10. The output of the Dynatup system was recorded on a Tektronics No. 564B oscilloscope, or a Biomation Transient Signal Recorder (Model No. 802) or both, which was then used to drive the oscilloscope. The impact tests for this study were conducted using hammer velocities of 15, 130 and 203 in./s (38.1, 330.2 and 515.6 cm/s) and frequency settings of 100, 40, 20 and 10.

Response Time Determination

A sine wave was superimposed on the output of the strain-gage bridge with a signal generator, and the attenuation versus frequence response of the system was determined for all four frequency settings. Attenuation versus rise-time curves were calculated following Ireland's suggested procedures [*6*] of using:

$$\text{rise time} = \frac{0.35}{\text{frequency}}$$

The response time, T_R for each frequency setting was defined as the rise time at 10 percent of signal attenuation (0.915 dB).

Materials

The material tested during this study was unidirectional Borsic-aluminum composites which consisted of 25.4 volume percent, 4.2-mil-diameter (0.1067mm) Borsic in a matrix of 1100 aluminum. The composites were fabricated by diffusion-bonding monolayer composite tapes at 1000°F (538°C) and 10 ksi (68.9 MN/m^2) for 5 min. The specimens were nominally 0.394 in. (10 mm) wide and 0.250 in. (6.35 mm) thick. Each specimen was notched using electro-discharge machining (EDM) techniques so that a nominal crack length-to-width ratio of 0.35 and notch root radii of 0.001 to 0.005 in. (0.025 to 0.127 mm) were obtained. It should be noted that previous work [*7*] on composites of this type indicates that this thickness is sufficient to assure plane strain conditions at the notch tip.

Data Reduction

The load-time traces obtained for these composites (Fig. 1) were characterized by a nearly linear increase in load up to the maximum load, after which the load decayed gradually, indicating controlled crack propagation. For the purpose of subsequent discussions, the time to fracture, t_f has been defined as the time to reach maximum load, P_{max}, and the hammer velocity used to convert the load-time traces to load-deflection traces has been taken as the initial hammer velocity. [The initial hammer velocity was considered equal to the average hammer velocity since the total energy consumed during these tests was only about 1.5 ft·lb (2.034 J), which corresponds to a maximum hammer velocity change of less than 1 percent.]

Previous work [*7*] on Borsic-aluminum composites has shown that the dynamic fracture toughness, K_{ID} as calculated from P_{max} and the analytical expression given in ASTM specification E-399-70T [*8*], is independent of thickness, crack length-to-width ratio, and notch root radius over the ranges used in this study. Since K_{ID} accounts for minor changes in geometry, it was chosen as the most appropriate means of documenting the experimentally observed attenuations in the load signal when excessive filtering was employed.

Similarly, the energy absorbed during fracture should most appropriately be discussed in terms of the work-of-fracture [*9,10*] γ_f which also accounts for minor geometrical variations. The work-of-fracture was calculated by the relation

$$\gamma_f = \frac{U}{2B(W-a)}$$

where U is the energy consumed during the test as determined by integration of the load-deflection curves, B the specimen thickness, W the specimen width, and a the crack length.

Results

The attenuation versus rise-time response of the system for all four frequency settings is given in Fig. 2. From these data, T_R, the response time for each frequency setting, was defined as the rise time at a 10 percent attenuation. The response times for various frequency settings are given in Table 1.

The results which stimulated this study are given in Fig. 3, where the effect of hammer velocity on K_{ID} was determined for two response times. As expected, the data from the two response times were similar at the lower hammer velocity where t_f was relatively long (1000 μs). As the hammer velocity was increased and t_f became shorter, the T_R = 162 μs results were significantly attenuated.

In order to investigate the details of the attenuation process, a series of tests at all four frequency settings was conducted at a hammer velocity of 130 in./s (330.2 cm/s). The effects of T_R on K_{ID}, T_f, and γ_f are given in Figs. 4, 5, and 6.

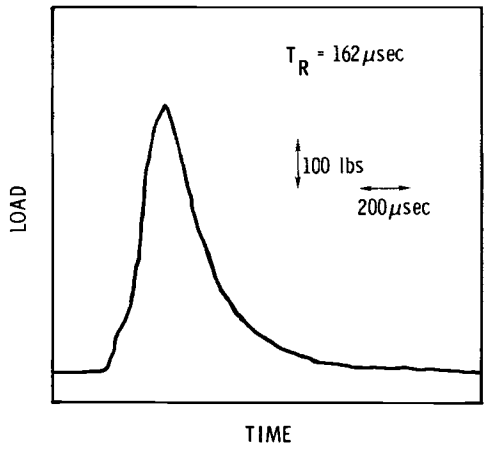

FIG. 1—*Typical load-time from an instrumented Charpy impact test on a Borsic-aluminum composite.*

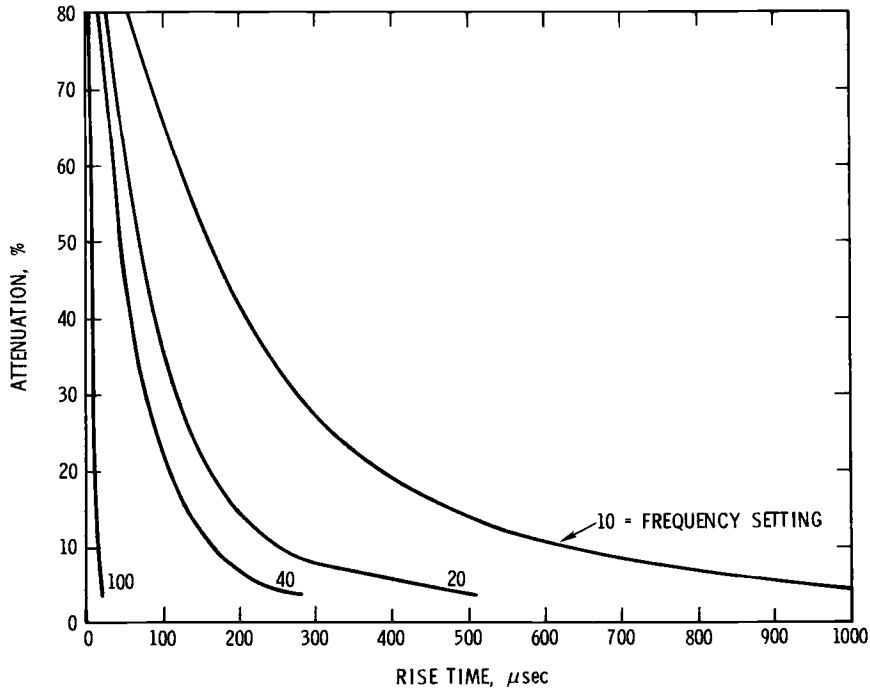

FIG. 2—*Effect of rise time on attenuation for various frequency settings as determined with a sine wave generator.*

TABLE 1—*Effect of frequency setting on system response time.*[a]

Frequency Setting	Response Time, μs
10	610
20	265
40	162
100 (unfiltered)	13.7

[a] Response time is defined as the rise time of the system when the load signal is attenuated 10 percent (0.915 dB attenuation).

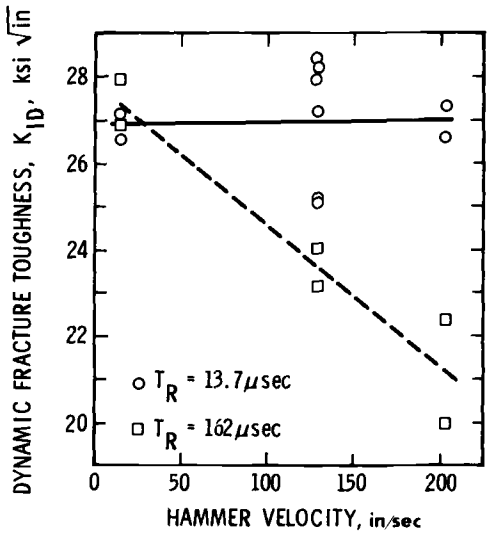

FIG. 3—*Effect of hammer velocity on the dynamic fracture toughness of a Borsic-aluminum composite with two different system response times,* T_R.

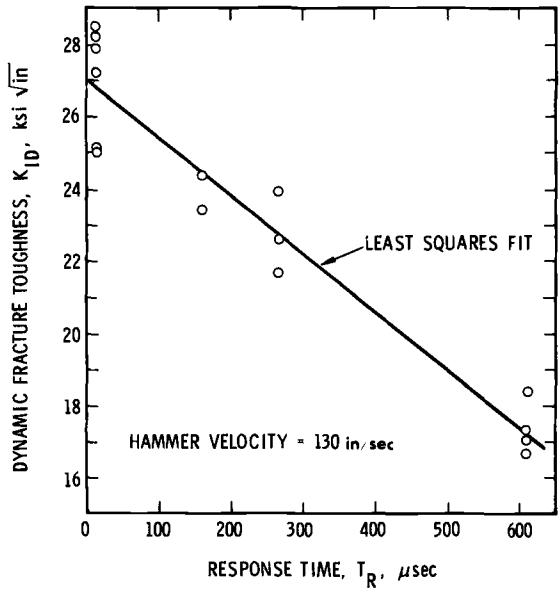

FIG. 4–*Effect of response time on the measured dynamic fracture toughness of a Borsic-aluminum composite.*

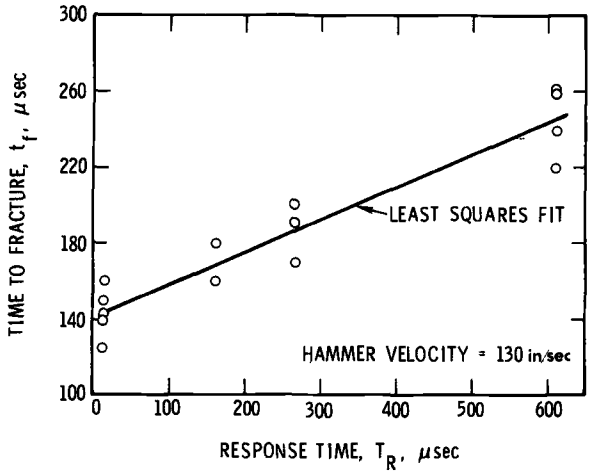

FIG. 5–*Effect of response time on the measured time to fracture of a Borsic-aluminum composite.*

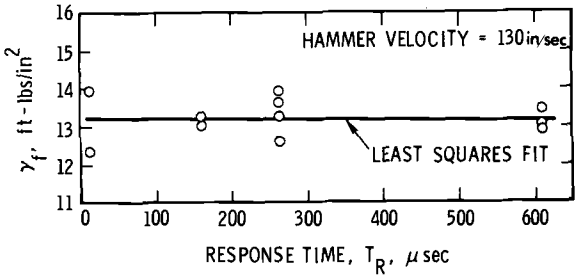

FIG. 6–*Effect of response time on the measured work-of-fracture of a Borsic-aluminum composite.*

As expected, K_{ID} decreased with increasing response time. In addition, t_f increased with increasing response time, indicating that excessive filtering not only attenuated the load signal but also distorted the load-time traces. Over the response time range investigated, γ_f was found to be essentially constant, implying that while the signal is attenuated and distorted, the area under the load-displacement curves remains constant.

In order to directly demonstrate the effects of inadequate response time, the Dynatup system was modified to facilitate simultaneous recording of both the unfiltered and the filtered traces from a given test. Figure 7 gives the results of this procedure and graphically illustrates that excessive filtering leads to a decrease in P_{max} and an increase in t_f while γ_f remains constant.

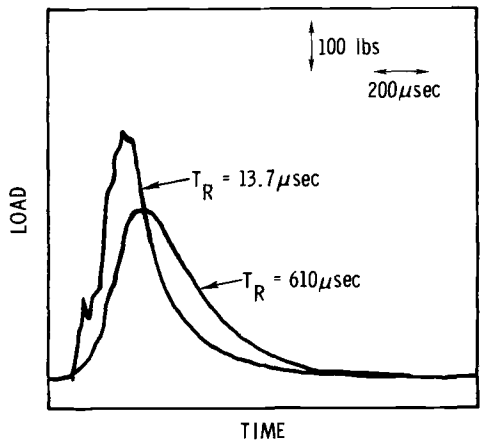

FIG. 7–*Results of an instrumented Charpy impact test of a Borsic-aluminum composite showing both the filtered* (T_R = 610 μs) *and the unfiltered* (T_R = 13.7 μs) *load-time traces.*

Discussion of Results

The attenuation versus rise-time data given in Fig. 2 illustrate two important points. First, the response time (T_R = 13.7 μs) of the open or unfiltered system (frequency setting = 100) is sufficiently short that it is reasonable to consider these data as being an accurate representation of the material's actual response. Second, the shapes of the attenuation versus rise-time curves indicate the importance of not allowing t_f to approach the value of T_R since small changes in t_f in this range can lead to large changes in attenuation. In view of the shapes of these curves, it may be desirable to define the system response time at the level of 5 percent attenuation (0.446 dB) to ensure more accurate results.

The data in Figs. 4, 5 and 6 indicate that K_{ID} decreases and t_f increases with increasing response time while γ_f remains constant. The relationship between the decrease in K_{ID} and increase in t_f can be rationalized if one assumes that the area under the attenuated trace up to P_{max} is the same as the area under the unattenuated trace up to P_{max}. This assumption is reasonable since the experimental data indicate that the total area under the two traces is constant (that is, γ_f is constant). If the traces up to P_{max} are approximated as triangles, then the equal-area assumption predicts that the product of K_{ID} and t_f will be constant over the range of response times tested. This product was found to be constant within ± 5 percent when the equations for the least-squares fits in Figs. 4 and 5 were multiplied together. Thus, the K_{ID} and t_f variation with response time can be approximated by the assumption that the areas under the traces are constant when excessive filtering is employed.

The significance of these results extends beyond illustration of the effects of inadequate response time and documentation of this Dynatup system's attenuation characteristics. This procedure, which is an extension of Ireland's [*6*] rise-time determination method, attempts to predict actual fracture behavior from attenuated data by assuming that the electronically measured attenuations correspond to those observed during impact testing. If accurate predictions of the actual fracture toughness can be obtained from attenuated data, results which have been gathered with excessive filtering can be salvaged.

The procedure, then, is to use the least-square values for K_{ID} and t_f at different response times (Figs. 4 and 5) to see if a K_{ID} of 26.8 ksi $\sqrt{\text{in.}}$ (29.7 MN/m$^{-3/2}$) can be predicted. The K_{ID} of 26.8 ksi $\sqrt{\text{in.}}$ (29.7 MN/m$^{-3/2}$) is the average value of all data obtained on tests conducted with T_R = 13.7 μs and is felt to be an accurate measure of the material's fracture toughness. For each value of T_R, the experimentally determined t_f values were used in Fig. 2 to determine the amount of attenuation, and then actual values of K_{ID} were predicted by:

$$K_{ID}\ (\text{actual}) = \frac{K_{ID}\ (\text{measured})\ \times\ 100}{(100 - \%\ \text{attenuation})}$$

The results of this procedure are given in Table 2 and it may be seen that the actual value of K_{ID} was predicted quite accurately.

Thus, the extension of Ireland's [6] approach to predict actual behavior works quite well when the actual t_f = 143 us. Using data from tests conducted at 203 in./s (515.6 cm/s) and T_R = 162 μs (Fig. 3), it may be shown (Table 3) that the prediction is also accurate to within 5 percent when the actual t_f is much shorter (100 μs). Obviously, additional testing is necessary in order to determine the limitations of this method of correcting attenuated data in the general case. These results suggest that this method will provide reasonably accurate fracture toughness values from attenuated, incorrect data gathered on a testing system with an inadequate response time, T_R.

Suggestions for Reliable Instrumented Impact Testing

This study suggests a number of methods of ensuring reliable dynamic fracture toughness data by means of instrumented impact testing:

1. Define a T_R for the system to be used at the 5 percent attenuation level or at least at the 10 percent attenuation level, and consider data suspect if $t_f \leqslant T_R$.
2. Use the lowest impact velocities allowed within the constraints of the testing program and thereby increase t_f.
3. Use no filtering when the adequacy of the system response time is in doubt.
4. If possible, make the simultaneous recording of both the unfiltered and filtered traces a standard testing procedure. This assures maximum accuracy and ease of data interpretation.
5. For data which are suspect from the standpoint of response time and cannot easily be reproduced, characterize the system attenuation and extract corrected data.

Conclusions

1. Inadequate system response times can lead to grossly inaccurate data during instrumented impact testing. The adequacy of the response time is most conveniently checked using Ireland's method of determining the attenuation versus rise-time characteristics of the system.
2. Inadequate response times arising from excessive filtering for Charpy tests on Borsic-aluminum composites produced attenuated maximum loads and increased times to fracture. The energy (work-of-fracture), however, was not strongly affected by the response times used in this study.
3. Use of attenuation versus rise-time curves to predict actual fracture toughness values from attenuated data gave reasonably accurate results for the materials and times-to-fracture investigated in this study.

TABLE 2—*Prediction of* K_{ID} *from attenuated data (Hammer velocity = 130 in./s*

Frequency setting	10	20	40
Response time, T_R, μs	610	265	162
Measured time to fracture, t_f, μs	245.3	186	169
Actual time to fracture,[a] μs	143	143	143
Measured fracture toughness, K_{ID}, ksi $\sqrt{\text{in.}}$ (MNm$^{-3/2}$)	17.22 (19.11)	22.79 (25.30)	24.45 (27.14)
Predicted attenuation, %	34.0	16.4	9.4
Corrected fracture toughness, ksi $\sqrt{\text{in.}}$ (MNm$^{-3/2}$)	26.09 (28.96)	27.26 (30.26)	26.99 (29.96)
Actual fracture toughness,[a] ksi $\sqrt{\text{in.}}$ (MNm$^{-3/2}$)	26.84 (29.79)	26.84 (29.79)	26.84 (29.79)
Difference between actual and corrected fracture toughness, %	−2.8	+1.6	+0.6

[a] As measured from unfiltered tests.

TABLE 3—*Prediction of* K_{ID} *from attenuated data (Hammer velocity = 203 in./s*[a]

Measured time to fracture, t_f, μs	120
Actual time to fracture, t_f,[b] μs	100
Measured fracture toughness, K_{ID}, ksi $\sqrt{\text{in.}}$ (MNm$^{-3/2}$)	21.19 (23.52)
Predicted attenuation, %	17
Corrected fracture toughness, ksi $\sqrt{\text{in.}}$ (MNm$^{-3/2}$)	25.53 (28.34)
Actual fracture toughness,[b] ksi $\sqrt{\text{in.}}$ (MNm$^{-3/2}$)	26.84 (29.79)
Difference between actual and corrected fracture toughness, %	−4.9

[a] T_R = 162 μs
[b] As measured from unfiltered tests.

References

[1] Wullaert, R. A., Panel Discussion on Instrumented Impact Testing, ASTM Annual Meeting, Philadelphia, Pa., American Society for Testing and Materials, June 1973.

[2] Wullaert, R. A., in *Impact Testing of Metals, ASTM STP 466,* American Society for Testing and Materials, 1970, pp. 148-164.

[3] Sever, W. L. and Tetelman, A. S., "The Use of Pre-cracked Charpy Specimens to Determine Dynamic Fracture Toughness," University of California at Los Angeles, DAH-04-68-C-008, 1971.

[4] Ireland, D. R., Effects Technology, Inc., private communication, 1972.

[5] Hoover, W. R. Panel Discussion on Instrumented Impact Testing, ASTM Annual Meeting, Philadelphia, Pa., American Society for Testing and Materials, June 1973.

[6] Ireland, D. R. "Procedure for Reliable Control of the Instrument Impact Test," Effects Technology Inc. Technical Report 73-25, July 1973, presented at the Instrumented Impact Testing Symposium, ASTM Annual Meeting, Philadelphia, Pa., American Society for Testing and Materials, June 1973.

[7] Hoover, W. R. and Allred, R. E., "The Dynamic Fracture Behavior of Borsic-Al Composites," Sandia Laboratories, SC-DC-721080, June 1972.

[8] "Tentative Method of Test for Plane Strain Fracture Toughness of Metallic Materials (ASTM designation E-399-70T)," *Review of Developments in Plane Strain Fracture Toughness Testing, ASTM STP 463*, W. F. Brown, Jr., ed., 1970, pp. 249-269.

[9] Tattersall, H. G. and Tappin, G., *Journal of Materials Science*, Vol. 1, 1966, pp. 296-301.

[10] Hoover, W. R. and Guess, T. R., "The Dynamic Fracture Toughness of Carbon-Carbon Composites," Sandia Laboratories, SLA-73-0499, April 1973, *Journal of Composite Materials*, Vol. 7, 1973, pp. 334-346.